IMPERIAL COLLEGE OF SCIENCE, TECHNOLOGY AND MEDICINE

UNIVERSITY OF LONDON

ROYAL SCHOOL OF MINES

T. H. HUXLEY SCHOOL OF ENVIRONMENT, EARTH SCIENCES
AND ENGINEERING

CENTRE FOR PETROLEUM STUDIES

Laboratory Investigation of Petrophysical Properties of Sandstone Rocks under True Triaxial Stress

by

Said Salim Al-Harthy

A thesis submitted in fulfilment of the requirements for
the degree of Doctor of Philosophy of the University of London
and the Diploma of Imperial College

March 1999

BIBL LONDON UNI

ABSTRACT

All producing petroleum reservoirs are subject to the dynamic behaviour of anisotropic stress fields in the rocks. Thus, experiments conducted under simulated *in situ* stress conditions are needed for understanding the storage and transport properties of reservoir rocks. Traditionally, however, experiments are conducted under hydrostatic conditions for convenience, but these do not accurately represent the *in situ* stress states which occur at depth.

An existing apparatus at Imperial College has been further developed to allow measurements of various important petrophysical and geophysical properties, such as permeability to single and multi-phase fluids (i.e. relative permeability), directional permeability and directional electrical conductivity (and therefore resistivity), capillary pressure and ultrasonic P-and polarised S-wave velocities, as well as mechanical parameters such as strength and deformability. This laboratory equipment has a capability to apply three boundary principal stresses independently, using cubic samples loaded in closed-loop control, achieving deviatoric stresses of 200 MPa and pore pressures to 145 MPa.

In this research, this equipment has been utilised to investigate permeability, capillary pressure and electrical properties in order to assess the significance of true triaxial stresses. In addition, transport properties such as permeability and electrical conductivity are also affected by changes during production and by anisotropy. This combined study of representative laboratory experiments will enable a more reliable interpretation of the behaviour of hydrocarbon reservoirs upon pressure depletion, and thus lead to improved reservoir management. This thesis reports results and discussion of the following aspects:

1. An investigation of the effect of dynamic permeability changes on reservoir performance forecasting during field production life of sandstone rocks under hydrostatic, triaxial and true triaxial stresses.
2. An investigation of permeability hysteresis of sandstone rocks under hydrostatic and true triaxial stresses during depletion or waterflooding.

3. An investigation of the effect of anisotropy on permeability and resistivity of sandstone rocks under hydrostatic and true triaxial stresses.
4. An investigation of the effect of stress on capillary pressure, resistivity index and pore volume deformation of sandstone rocks under hydrostatic and true triaxial stresses.
5. The evaluation of the consequences of using unrepresentative experimental data in reservoir performance predictions.

Initially, measurements of dynamic changes in permeability were carried out under hydrostatic, triaxial and true triaxial stresses, with elevated pore pressures. The measurements of permeability hysteresis on cubic rock samples under hydrostatic and true triaxial stresses were carried out to identify major effects. Reservoir and outcrop materials were used for measurement of permeability and electrical conductivity in the three principal directions, and for measurement of pore volume deformation under hydrostatic and true triaxial stresses. Cubes were also used in the measurements of capillary pressure and electrical properties under true triaxial stress, in order to provide a comparison with tests on cylindrical rock samples under hydrostatic stresses.

Reservoir engineering application studies using the Eclipse simulator provided by Schlumberger GeoQuest were carried out to show the significance of the effects of pore pressure, stress and anisotropy on the prediction of reservoir performance during production.

The results show that different stress states have significantly different effects on permeability hysteresis, pore volume deformation, directional permeability and electrical conductivity, capillary pressure and two-phase electrical properties. Pore pressure effects on permeability were also found to be influenced by stress states. The investigations of stress, pore pressure and anisotropy effects using the Eclipse simulator show a significant influence on oil production. The implications of the variations in these properties due to stress are discussed in the context of reservoir performance.

ACKNOWLEDGEMENTS

First I express my sincere gratitude to my supervisors Dr. X.D. Jing, leader of the petrophysics research group and Mr. J.R. Marsden, leader of the petroleum rock mechanics research group at the Centre for Petroleum Studies. Their supervision, stimulating discussions and valuable engineering guidance in many aspects have made this thesis possible. Many thanks to Dr. T.S. Daltaban for his advice during the initial stage of this thesis.

I would like to express my sincere thanks to Professor M.S. King for allowing the use of the true triaxial loading system and for help in many ways. Also, I would like to express my sincere thanks to Dr. R. Zimmerman for his friendship and help throughout my research.

Petroleum Development Oman (PDO) in Oman are gratefully acknowledged for their financial support and for providing the opportunity for this work. To my former lecturers at Sultan Qaboos University, their moral support throughout my studies is well appreciated.

Many thanks to Mr J. Dennis and Mr. L. Lombos (Laszlo Lombos Consultancy) for the technical modifications of the true triaxial loading system which have made this study possible. Their continuous technical assistance and encouragement throughout this work are highly appreciated.

Many thanks to Dr. A. Moss, Dr. C. Grattoni and Mr. G. Nash for their unlimited technical assistance throughout my research and the preparation of this thesis. Their helpful discussion, support and encouragement are acknowledged.

I would like to thank Geology department, Royal School of Mines, Imperial College for Petrographic (SEM and thin section) analyses.

My appreciation and sincere thanks to Dr. E. Syahrial, Dr. Q. Malik, Dr. W. Djatmiko, Dr. H. Purnomo, Dr. S. Al-Kafeef, Dr. L. Elysses, Dr. C. Coll, Dr. F. Al-Azri, Dr. N. Al-Yahyai, Mr. P. Denicol, Mr. N. Al-Marhoon, Mr. H. Al-Sharji, Mr. A. Al-Kindy, Mr. Q. Al-Riyamy, Mr. S. Al-Harthy, Mr. A. Al-Azri, Mr. Z. Al-Siyabi, Mr. R. Al-Mjeni, Ms. W. Al-Wardy, Mrs. Y. Al-Lawatiya, Mr. S. Al-Mahruqi, Mr. M. Al-Harthy, Mr. C. Romero, Mr. M. Ibrahim, Mr. S. Sisavath, Mr. C. Yang, Mr. P. Lock, Ms. J. Zambrano, Mr. J. Finol, Mr. H. Man and all my friends whose names I did not mention.

I would like to thanks my parents Mr. Salim Al-Harthy and Mrs. Jokha Al-Harthy, for their immense love, prayers and encouragement from class one until post graduate studies. Special thanks also go to my wonderful wife Amal, my son Salim and his Barney, my daughter Aya, brothers and sisters, especially cousin Rashid, and all my relatives and friends.

Finally I would like to express my appreciation to my family for their patience, direct or indirect support, and for the time taken from them for completion of this thesis.

DEDICATION

This work is dedicated to my parents, family (Amal, Salim and Aya), brothers and sisters, relatives and friends.

TABLE OF CONTENTS

ABSTRACT **1**

ACKNOWLEDGEMENTS **3**

DEDICATION **5**

TABLE OF CONTENTS **6**

LIST OF FIGURES **10**

LIST OF TABLES **14**

NOMENCLATURE **17**

1. INTRODUCTION **19**

1.1 Preamble 19

1.2 Objectives 20

1.3 Approaches 21

1.4 Outline of the Thesis 21

2. THEORY AND LITERATURE REVIEW **23**

2.1 Introduction 23

2.2 Stress 24

2.2.1 Basic Definitions 24

2.2.2 The Concept of Stress 25

2.2.3 Importance of *In Situ* Stress 27

2.2.4 *In Situ* Stress Measurements 27

2.2.5 Natural Stresses 29

2.2.6 Induced Stresses 29

2.2.7 Laboratory Measurements Under Stress 30

2.3 Permeability 32

2.3.1 Basic Definition 32

2.3.2 Importance of Permeability 32

2.3.3 Factors Affecting Permeability 33

2.3.4 Laboratory Determination of Permeability 33
2.3.5 Field Determination of Permeability 35
2.3.6 Effect of Pore Pressure on Permeability 36
2.3.7 Effect of Permeability Hysteresis 37
2.3.8 Effect of Stress on Permeability 38
2.3.9 Permeability Anisotropy 40
2.4 Capillary Pressure 42
2.4.1 Basic Definition 42
2.4.2 Importance of Capillary Pressure 43
2.4.3 Laboratory Determination of Capillary Pressure 44
2.4.4 Effect of Stress on Capillary Pressure 48
2.5 Electrical Properties 48
2.5.1 Basic Definition 48
2.5.2 Electrical Conduction in Porous Media 49
2.5.3 Archie Equations 50
2.5.4 Laboratory Determination of Electrical Properties 51
2.5.5 Field Determination of Electrical Properties 51
2.5.6 Effect of Stress on Electrical Properties 52
2.5.7 Electrical Conductivity Anisotropy 53
2.6 Summary 56

3. EXPERIMENTAL APPARATUS AND PROCEDURE 57
3.1 Introduction 57
3.2 Experimental Apparatus 57
3.2.1 Hydrostatic System 57
3.2.2 True Triaxial Stress Loading System 65
3.3 Description of Rock Samples 70
3.4 Selection of Rock Samples 70
3.5 Stress Paths for Tests 74
3.6 Procedure 77
3.6.1 Introduction 77
3.6.2 Sample Preparation and Characterisation 78

3.6.3 Single Phase Measurements Under Hydrostatic and True Triaxial Stresses 81
3.6.4 Two Phase Measurements under Hydrostatic Stress 83
3.6.5 Two Phase Measurements under True Triaxial Stress 87

4. EFFECTS OF PORE PRESSURE, HYSTERESIS AND TRUE TRIAXIAL STRESS ON PERMEABILITY 89
4.1 Introduction 89
4.2 Effect of Pore pressure on Permeability under Different Stress Paths 92
4.3 Permeability Hysteresis under Hydrostatic and True Triaxial Stresses 98
4.4 Effect of Stress on Permeability 105
4.5 Summary 108

5. PERMEABILITY AND RESISTIVITY ANISOTROPY, AND PORE VOLUME CHANGE 109
5.1 Introduction 109
5.2 Directional Permeability and Resistivity 111
5.2.1 Introduction 111
5.2.2 Directional Permeability 112
5.2.3 Directional Resistivity 119
5.3 Pore Volume Change 130
5.4 Summary 136

6. EFFECT OF TRUE TRIAXIAL STRESS ON CAPILLARY PRESSURE CURVES AND ELECTRICAL PROPERTIES 138
6.1 Introduction 138
6.2 Capillary Pressure 139
6.3 Electrical Properties of Oil/Brine/Rock Systems 145
6.4 Summary 150

7. RESERVOIR ENGINEERING APPLICATIONS 151
7.1 Introduction 151

7.2 Permeability 152
7.2.1 Description of the Base Model 152
7.2.2 Pore Pressure and Stress Effects 154
7.2.3 Dynamic Field Permeability Effect 161
7.2.4 Permeability Anisotropy Effect 163
7.3 Capillary Pressure and Electrical Properties 168
7.4 Summary 169

8. CONCLUSIONS AND RECOMMENDATIONS 171
8.1 Introduction 171
8.2 Conclusions 172
8.2.1 Experimental Techniques 172
8.2.2 Pore pressure, Hysteresis and Stress Effects on Permeability 172
8.2.3 Permeability and Resistivity Anisotropy, and Pore Volume Deformation 173
8.2.4 Capillary Pressure and Electrical Properties 173
8.2.5 Reservoir Engineering Applications 173
8.2.6 General Conclusion 174
8.3 Recommendations 174

REFERENCES AND BIBLIOGRAPHY 176

APPENDICES 193
Appendix-A 193
Appendix-B 207
Appendix-C 223

LIST OF FIGURES

Figure No.	Description	Page
Figure 2.1	Schematic of recommended procedures during laboratory measurements of rock properties for stress sensitive reservoirs	31
Figure 3.1	Schematic of the single sample cell for measuring capillary pressure, electrical properties and permeability of the rock samples at different confining pressure	62
Figure 3.2	Schematic of the multi-samples cell for measuring capillary pressure, electrical properties and permeability of the rock samples at different confining pressure	63
Figure 3.3	Core sample connected in series with precision resistor (R_r)	64
Figure 3.4	Multi-electrode core sleeve assembly with porous disks	64
Figure 3.5	Schematic of top and bottom view of the z axes platens of the true triaxial stress loading system	68
Figure 3.6	The true triaxial stress loading system	69
Figure 3.7	Isometric sketch of true triaxial stress loading system	69
Figure 3.8	Stress-strain curves for a Doddington sample	71
Figure 3.9	Stress-strain curves for a reservoir sample	71
Figure 3.10	Mercury capillary pressure curves for two adjacent reservoir samples	72
Figure 3.11	Mercury capillary pressure curves for two adjacent Doddington samples	72
Figure 3.12	Pore size distribution for two adjacent reservoir samples	73
Figure 3.13	Pore size distribution for two adjacent Doddington samples	73
Figure 3.14	Flow chart showing the experimental programme	77
Figure 3.15	Flow chart of the experimental programme under hydrostatic stress	83
Figure 4.1	Isometric representation of 3-D stress field and its representation in the laboratory experiments	90
Figure 4.2	Effect of pore pressure on permeability (Springwell)	96
Figure 4.3	Effect of pore pressure on permeability (Croslands Hill)	96

Figure 4.4	Effect of pore pressure on permeability (Stainton)	97
Figure 4.5	Effect of pore pressure on permeability (reservoir sample)	97
Figure 4.6	Schematic illustration showing pore space subjected to three principal stresses	99
Figure 4.7	Microscopic grain-grain contacts	99
Figure 4.8	Effect of hysteresis on permeability (Doddington)	102
Figure 4.9	Effect of hysteresis on permeability (Croslands Hill)	102
Figure 4.10	Effect of hysteresis on permeability (Springwell)	103
Figure 4.11	Effect of hysteresis on permeability (Stainton)	103
Figure 4.12	Effect of hysteresis on permeability (reservoir sample)	104
Figure 5.1	Pore volume deformation versus stress (reservoir sample)	131
Figure 5.2	Pore volume deformation versus stress (St. Bees)	131
Figure 5.3	Pore volume deformation versus stress (Springwell)	131
Figure 5.4	Normalised pore volume deformation versus stress (reservoir sample)	132
Figure 5.5	Normalised pore volume deformation versus stress (St. Bees)	132
Figure 5.6	Normalised pore volume deformation versus stress (Springwell)	132
Figure 5.7	Resistivity versus stress (reservoir sample)	133
Figure 5.8	Resistivity versus stress (St. Bees)	133
Figure 5.9	Resistivity versus stress (Springwell)	133
Figure 5.10	Formation factor versus stress (reservoir sample)	134
Figure 5.11	Formation factor versus stress (St. Bees)	134
Figure 5.12	Formation factor versus stress (Springwell)	134
Figure 5.13	Cementation factor versus stress (reservoir sample)	135
Figure 5.14	Cementation factor versus stress (St. Bees)	135
Figure 5.15	Cementation factor versus stress (Springwell)	135
Figure 6.1	Capillary pressure curves at ambient and hydrostatic stress (North Sea oil field 1L & 1M)	143
Figure 6.2	Capillary pressure curves under hydrostatic and true triaxial stresses (Clashach)	143

Figure 6.3	Capillary pressure curves at hydrostatic stress of 34.5 MPa (Clashach)	144
Figure 6.4	Capillary pressure curve at stress of 34.5 MPa (Croslands Hill)	144
Figure 6.5	Resistivity index versus brine saturation under hydrostatic and true triaxial stresses (Clashach)	148
Figure 6.6	Resistivity index versus brine saturation at stress of 34.5 MPa (Clashach)	148
Figure 6.7	Resistivity index versus brine saturation at stress of 34.5 MPa (Croslands Hill)	149
Figure 7.1	Base model used in natural depletion	153
Figure 7.2	Base model used in pressure maintenance	154
Figure 7.3	Field oil production versus time showing the effects of permeability reductions	157
Figure 7.4	Field pressure versus time showing the effects of permeability reductions	157
Figure 7.5	Field oil production versus time showing the effects of one step permeability reductions	158
Figure 7.6	Field pressure versus time showing the effects of one step permeability reductions	158
Figure 7.7	Field oil production versus time showing the effects of three steps permeability reductions	159
Figure 7.8	Field pressure versus time showing the effects of three steps permeability reductions	159
Figure 7.9	Field oil production versus time showing the effects of three steps permeability reductions at different stress states	160
Figure 7.10	Field pressure versus time showing the effects of three steps permeability reductions at different stress states	160
Figure 7.11	Field oil production versus time showing the effects of different regions with three steps permeability reductions	162
Figure 7.12	Field pressure versus time showing the effects of different regions with three steps permeability reductions	162

Figure 7.13a	Show the wellbore direction in x-direction	164
Figure 7.13b	Show the wellbore direction in y-direction	164
Figure 7.14	Field oil production versus time showing the effects of permeability anisotropy and wellbore orientation	165
Figure 7.15	Field pressure versus time showing the effects of permeability anisotropy and wellbore orientation	165
Figure 7.16	Field oil production versus time showing the effects of permeability anisotropy, wellbore orientation and regional permeability change	166
Figure 7.17	Field pressure versus time showing the effects of permeability anisotropy, wellbore orientation and regional permeability change	166
Figure 7.18	Field oil production versus time showing the effects of permeability anisotropy, wellbore orientation and regional permeability change with pressure maintenance	167
Figure 7.19	Field pressure versus time showing the effects of permeability anisotropy, wellbore orientation and regional permeability change with pressure maintenance	167
Figure B.1	Mercury capillary pressure curve (St. Bees)	219
Figure B.2	Pore size distribution (St. Bees)	219
Figure B.3	Mercury capillary pressure curve (Springwell)	220
Figure B.4	Pore size distribution (Springwell)	220
Figure B.5	Mercury capillary pressure curve (Stainton)	221
Figure B.6	Pore size distribution (Stainton)	221
Figure B.7	Mercury capillary pressure curve (Clashach)	222
Figure B.8	Pore size distribution (Clashach)	222

LIST OF TABLES

Table No.	Description	Page
Table 3.1	Pore pressure effect on permeability	74
Table 3.2	Hysteresis and stress effects on permeability	74
Table 3.3	Permeability and resistivity anisotropy	75
Table 3.4	Stress effect on capillary pressure and electrical properties	75
Table 3.5	Pore volume deformation and resistivity	75
Table 4.1	Values of normalised permeability under different stress states (Doddington)	106
Table 4.2	Values of normalised permeability under different stress states (Croslands Hill)	106
Table 4.3	Values of normalised permeability under different stress states (Springwell)	106
Table 4.4	Values of normalised permeability under different stress states (Stainton)	107
Table 4.5	Values of normalised permeability under different stress states (reservoir sample)	107
Table 5.1	Directional permeability and anisotropy under different stress states (reservoir sample)	115
Table 5.2	Directional permeability and anisotropy under different stress states (St. Bees)	116
Table 5.3	Directional permeability and anisotropy for under different stress states (Springwell)	117
Table 5.4	Directional permeability and anisotropy under hydrostatic stress (reservoir samples)	118
Table 5.5	Directional permeability and anisotropy at ambient (reservoir samples)	118
Table 5.6	Directional permeability and anisotropy at ambient (St. Bees)	118
Table 5.7	Directional resistivity, anisotropy and anisotropy coefficient under different stress states (reservoir sample)	123

Table 5.8	Directional resistivity, anisotropy and anisotropy coefficient for under different stress states (St. Bees)	124
Table 5.9	Directional resistivity, anisotropy and anisotropy coefficient under different stress states (Springwell)	125
Table 5.10	Directional resistivity, anisotropy and anisotropy coefficient under hydrostatic stress (reservoir sample)	126
Table 5.11	Directional resistivity, anisotropy and anisotropy coefficient at ambient (reservoir sample)	126
Table 5.12	Directional resistivity, anisotropy and anisotropy coefficient at ambient (St. Bees)	126
Table 5.13	Permeability and conductivity anisotropy of different samples under hydrostatic stress state	128
Table 5.14	Permeability and conductivity anisotropy of different samples under true triaxial stress state	128
Table 5.15	Permeability and square of formation factor anisotropy of different samples under hydrostatic stress state	129
Table 5.16	Permeability and square of formation factor anisotropy of different samples under true triaxial stress state	129
Table 6.1	Electrical properties under true triaxial and equivalent hydrostatic stresses (Clashach)	146
Table 7.1	Effect of stress on parameter n and computed brine saturation	168
Table 7.2	Effect of stress on irreducible brine saturation during OIP calculation	169
Table A.1	Basic rock characterisation	204
Table B.1	Effect of pore pressure on liquid permeability (Springwell)	207
Table B.2	Effect of pore pressure on liquid permeability (Croslands Hill)	207
Table B.3	Effect of pore pressure on liquid permeability (Stainton)	208
Table B.4	Effect of pore pressure on liquid permeability (reservoir sample)	208
Table B.5	Permeability under different stress states (Doddington)	209

Table B.6	Permeability under different stress states (Croslands Hill)	209
Table B.7	Permeability under different stress states (Springwell)	210
Table B.8	Permeability under different stress states (Stainton)	210
Table B.9	Permeability under different stress states (reservoir sample)	210
Table B.10	Pore volume deformation under different stress states (reservoir sample)	211
Table B.11	Pore volume deformation under different stress states (St. Bees)	211
Table B.12	Pore volume deformation under different stress states (Springwell)	212
Table B.13	Electrical properties under different stress states (reservoir sample)	213
Table B.14	Electrical properties under different stress states (St. Bees)	213
Table B.15	Electrical properties under different stress states (Springwell)	214
Table B.16	Capillary pressure versus saturation under different stress states (reservoir sample 1L & 1M)	215
Table B.17	Capillary pressure versus saturation under different stress states (Clashach)	215
Table B.18	Capillary pressure versus saturation under hydrostatic stress (Clashach and Croslands Hill)	216
Table B.19	Resistivity index versus saturation under different stress states (Clashach)	217
Table B.20	Resistivity index versus saturation different stress states (Clashach and Croslands Hill)	217

NOMENCLATURE

Symbol	Units	Meaning
σ	*MPa*	*normal stress*
τ	*MPa*	*shear stress*
F_n	*N*	*normal force*
F_p	*N*	*parallel force*
A	m^2 *or* cm^2	*cross sectional area*
q	cm^3/s	*volumetric flow rate*
k	*mD*	*absolute permeability*
μ	*cP*	*fluid viscosity*
p	*psi*	*pressure*
L	*cm*	*length*
K	*mD*	*permeability tensor*
P_c	*psi*	*capillary pressure*
P_w	*psi*	*wetting phase pressure*
P_{nw}	*psi*	*nonwetting phase pressure*
γ	*dynes/cm*	*interfacial tension between fluids*
ρ_w	g/cm^3	*wetting phase density*
ρ_{nw}	g/cm^3	*nonwetting phase density*
r_c	*cm*	*radius of capillary tube*
g	cm/s^2	*gravitational acceleration*
h	*cm*	*equilibrium height of the wetting phase*
θ	*degree*	*contact angle at oil water solid interface*
ω	*cm/s*	*angular velocity*
S_w	*fraction*	*brine saturation*
S_{wir}	*fraction*	*irreducible brine saturation*
r	*ohm*	*resistance*
V	*volts*	*voltage*
I	*amperes*	*current*
RI		*resistivity index*

R	*ohm-m*	*resistivity*
R_o	*ohm-m*	*resistivity of the rock when fully saturated*
R_t	*ohm-m*	*resistivity of the rock when partially saturated*
R_w	*ohm-m*	*resistivity of the brine*
R_v	*ohm-m*	*vertical resistivity*
R_h	*ohm-m*	*horizontal resistivity*
F		*formation resistivity factor*
ϕ	*fraction*	*porosity*
m		*cementation factor*
n		*saturation exponent*
C	*mho/m*	*electrical conductivity*
λ		*anisotropy coefficient*
N	*stb*	*oil in place*
B_o	*res bbl/stb*	*oil formation volume factor*
V_p	cm^3	*pore volume*
Vb	cm^3	*bulk volume*
Vs	cm^3	*grain volume*
P_e	*psi*	*effective stress*
P_p	*psi*	*pore pressure*
P_t	*psi*	*total stress*
α		*Biot constant*

CHAPTER 1

INTRODUCTION

1.1 Preamble

Representative laboratory testing using reservoir rock samples is essential if accurate reservoir studies and management are to be achieved (Nelson, 1987). Accurate knowledge of rock properties based on representative laboratory methods are essential for the modelling of fluid content, distribution and dynamic flow in reservoir rocks. In order to reduce uncertainty and provide more representative reservoir data, it is advisable to measure rock properties at elevated stresses, temperature and other conditions as close as possible to those encountered in reservoir environments. In this study a systematic laboratory investigation of stress effects on the petrophysical properties of hydrocarbon reservoir rock samples, namely permeability, electrical properties and capillary pressure, was carried out. If *in situ* stress, pore pressure and hysteresis effects are neglected, then serious errors in forecasting the performance of hydrocarbon reservoirs might be introduced. Specifically, this research addressed the following aspects of reservoir engineering :

- ***How do different states of stress affect the petrophysical properties ?*** In general, special core analyses for petrophysical properties are conducted under simplified stress conditions using hydrostatic or Hassler type loading cells. Since the state of stress in a reservoir is generally neither uniform nor biaxial, what state of stress should be applied in the laboratory to represent reservoir stresses?
- ***How does pressure decline due to production affect the transport properties of permeability?*** The effect of pore pressure change on permeability is often considered to be negligible, so that permeability is approximated to be a constant throughout production life of the reservoir. However, is this assumption reasonable?
- ***How does the permeability hysteresis under in situ stress affect hydrocarbon recovery during production or water flooding?***

- ***How do pore volume deformation, permeability and resistivity anisotropy vary under in situ stress?*** Traditional/routine laboratory measurements of permeability and electrical conductivity are carried out in one direction which does not take into account any anisotropy of rock properties. Although multiple plugs including both horizontal and vertical plugs, can be used such an approach couples anisotropy with heterogeneity. Information on pore volume deformation under appropriate stress paths leads to better predictions of the production performance of hydrocarbon reservoirs and of surface subsidence.
- ***How do capillary pressure and resistivity index differ when measured under hydrostatic and true triaxial stress?***

1.2 Objectives

The main objectives of this research were :

1. to assess the impact of dynamic permeability changes on reservoir performance forecasting during field production life (i.e., effect of pore pressure under hydrostatic, triaxial and true triaxial stresses),
2. to examine the permeability hysteresis under different stress states (i.e., hydrostatic and true triaxial stresses),
3. to investigate experimentally the pore volume deformation, directional permeability and electrical conductivity under different stress states (i.e., hydrostatic and true triaxial stresses),
4. to investigate experimentally the capillary pressure and electrical properties under different stress states (i.e., hydrostatic and true triaxial stresses),
5. to identify representative laboratory procedures for petrophysical studies under stress,
6. to evaluate the influence of stress-dependence in the petrophysical properties of reservoir rocks upon reservoir performance calculations,
7. to incorporate the experimental results into reservoir simulations of model reservoirs.

1.3 Approaches

In this work, outcrop and hydrocarbon reservoir rock samples were used and the following approaches were adopted :

1. A single-sample cell, capable of measuring permeability, electrical properties and capillary pressure under different confining pressures, was used to measure electrical properties and capillary pressure of cylindrical samples under constant hydrostatic stress.
2. An existing true triaxial stress loading system was modified to allow testing of fluid-saturated cubic samples in order to meet the specific requirements of this research, i.e., pore pressure and liquid saturations of 40mm samples, with the three principal stresses varying independently. The system was used to measure permeability, electrical properties and capillary pressure under conditions of representative stress and pore pressure.
3. Permeability hysteresis under hydrostatic and true triaxial stresses was investigated using the true triaxial stress loading system. Measurements of pore volume deformation, directional permeability and electrical conductivity in the rock sample cubes were also conducted using the true triaxial system.
4. Fluid flow simulator (Schlumberger GeoQuest Eclipse) for assessing implications of representative petrophysical experimental data.

1.4 Outline of the Thesis

Chapter 2 provides a review of theory and previous studies on permeability, capillary pressure and electrical properties of reservoirs rocks. Effects of stress, pore pressure and hysteresis on permeability, pore volume deformation, permeability and electrical conductivity anisotropy, and the effect of stress on capillary pressure and electrical properties, are discussed.

Chapter 3 describes the experimental techniques and procedures. Modifications and improvements made to the experimental apparatus are discussed.

Chapter 4 presents the results on the effects of pore pressure, hysteresis and different stress states on permeability.

Chapter 5 presents the results of pore volume deformation, directional permeability and electrical conductivity under hydrostatic and true triaxial stress. Also highlighted is the importance of anisotropy with regards to transport properties during production at various stress states.

Chapter 6 focuses on the effects of stress on capillary pressure and electrical properties. It also addresses parameters such as irreducible water saturation from capillary pressure curves, and Archie parameters from electrical properties, taking into account different stress states.

Chapter 7 describes applications of the experimental data for predicting reservoir performance and, in particular, the impact of accurate and representative input data for simulation models.

Chapter 8 presents conclusions of this research and recommendations for further study.

CHAPTER 2

THEORY AND LITERATURE REVIEW

2.1 Introduction

Petrophysical properties such as porosity, permeability, capillary pressure, resistivity and relative permeability are influenced by the state of stress acting on a rock. These properties should be measured at stress states which are representative of the *in situ* conditions. For stress-sensitive reservoirs (e.g., fractured, very low permeability reservoirs or weak and poorly cemented porous materials), there is a need to carry out petrophysical measurements on core samples subjected to realistic (often anisotropic and true triaxial) stress states and elevated pore pressure.

In general, special core analyses for petrophysical properties are conducted under elevated confining pressures which are usually generated by hydrostatic or Hassler-type loading cells (with mechanically loaded ends and variable horizontal confining pressure), at very low pore pressures (Core Lab. Manual, 1992). Previous researchers (Gray and Fatt, 1963; Zoback and Byerlee, 1976; Teufel *et al.,* 1991; Rhett and Tuefel, 1992; Holt, 1990) have investigated experimentally these petrophysical properties under simplified stress conditions which are quite different from those found in hydrocarbon reservoirs.

In many laboratories, these quantities are measured under hydrostatic (isotropic) stresses that do not truly reflect the deviatoric stress or true triaxial stress states that exist *in situ* (Crawford and Smart, 1994). In addition, routine experiments do not simulate the changes of stress or pore pressure which occur as a reservoir is being produced. Thus the question remains whether the subsequent laboratory data are representative of the actual parameters in the reservoir and, if they are not, how can one correct those laboratory measurements to reservoir conditions? Reliable and accurate petrophysical properties are essential in order to undertake successful planning and management of petroleum reservoirs.

The main purpose of this research was to provide an insight of the rock properties, and the appropriate experimental procedures for determining them under simulated *in situ* conditions. In addition, the research aimed to investigate the benefits and limitations of the representative laboratory measurements techniques, and the impact of laboratory data on reservoir performance predictions.

2.2 Stress

2.2.1 Basic Definitions

1. *In situ* rock stress means the representation of all stress components existing in the earth's crust prior to any engineering activity, due to tectonic loading, overlying rock masses and other natural processes.
2. *Stress* is the force acting across a given surface element divided by the area of the element over which it acts.
3. *Uniaxial stress* is the application of normal stress in a single direction only.
4. *Hydrostatic stress* is the state of stress in which all of the principal stresses are equal. It is sometimes termed pressure.
5. *Triaxial stress* is the state of stress in which three principal stresses are applied but where two of the principal stresses can be equal. It is also termed biaxial stress.
6. *True triaxial stress* is the state of stress in which none of the principal stresses (σ_1, σ_2, or σ_3) are equal.
7. *Stress state* is the stress configuration acting at the boundary of an element of rock i.e., hydrostatic, triaxial or true triaxial.
8. *Stress path* is the path, in a σ_1, σ_2, σ_3 or some similar space, which defines the way the stresses are applied.
9. *A deviatoric stress* is the difference between two principal stresses (i.e., σ_1-σ_2, or σ_1-σ_3).
10. *Creep* is time dependent deformation which can occur under constant stress, and which is irrecoverable.
11. *Hysteresis* is the incomplete recovery of strain or any parameter during unloading cycles, due to irrecoverable work.

12. *Elasticity* is the behaviour of a material which returns to its original form or condition after applied forces are removed. If the material recovers completely and immediately it is called perfectly elastic. If the material does not recover completely, the strains remain and the material is termed anelastic.
13. *Plasticity* is the behaviour of a material which undergoes continuous and permanent deformation under a stress exceeding its yield condition. The plastic deformation of a material is the permanent deformation after complete unloading of the material.

2.2.2 The Concept of Stress

The stress in two dimension can be expressed by considering the face of a cubic element subjected to an applied force. If the force F is acting normal to the surface area A then stress is termed normal, and is given by the general equation :

$$\sigma = \frac{F_n}{A}, \text{ normal stress} \tag{2.1}$$

When the force is acting parallel to the cross section area, the stress is termed a shear stress :

$$\tau = \frac{F_p}{A}, \text{ shear stress} \tag{2.2}$$

Before defining the three dimensional stress field, it is desirable to define scalars, vectors and tensors. They are all part of the tensor family depending on the order (Herget, 1988 and Hudson *et al.*, 1993). Scalar is a tensor of zero order with magnitude independent of orientation (i.e., temperature in a room, energy, work, pressure). Vector is a tensor of first order with magnitude and direction (i.e., normal force, velocity). Tensor is a tensor of second order with magnitude, direction and orientation (i.e., stress, permeability).

Stress is a tensor property, represented in three dimensions by nine components, of which six are independent. Consider a cube with its edges parallel to the axes x, y, z of a rectangular co-ordinate system. The stresses acting on the faces of the cube are described by three normal stress components (σ_{xx}, σ_{yy}, σ_{zz}) and six shear stress

components (τ_{xy}, τ_{yx}, τ_{yz}, τ_{zy}, τ_{zx}, τ_{xz}). Therefore the state of stress is completely defined by symmetric matrix with six independent components.

$$\sigma = \begin{bmatrix} \sigma_{xx} & \tau_{xy} & \tau_{xz} \\ \tau_{yx} & \sigma_{yy} & \tau_{yz} \\ \tau_{zx} & \tau_{zy} & \sigma_{zz} \end{bmatrix}, \text{the stress tensor} \tag{2.3}$$

The first subscript for the shear stress indicates direction of normal to plane on which the stress is acting, and the second subscript indicates the direction in which the shearing stress is acting. For example, τ_{xy} means a stress acting in the y direction on a plane normal to the x axis. The stress tensor on an elementary cube element is represented by the above expression.

Due to symmetry $\tau_{xy} = \tau_{yx}$, $\tau_{yz} = \tau_{zy}$, $\tau_{xz} = \tau_{zx}$, only six out of the nine quantities are unique. Accurate determination of these quantities represents a challenge in data collection due to practical difficulties in quantifying them. A principal direction is defined as the normal to a plane in which all shear stresses are zero, such that only the normal stress remains. When normal stresses act parallel to the principal directions they are called principal stresses. Hudson and Cooling (1988) suggested that *in situ* stress is conventionally characterised by the magnitudes and directions of the three principal stresses, thus

$$\sigma = \begin{bmatrix} \sigma_1 & 0 & 0 \\ 0 & \sigma_2 & 0 \\ 0 & 0 & \sigma_3 \end{bmatrix} \tag{2.4}$$

Jaeger and Cook (1979) classified the three basic internal stress conditions, namely compressive stress which occurs when external forces are directed toward each other along the same plane, tensile stress which occurs when external forces are parallel and directed in opposite directions along the same plane, and shear stress which occurs when external forces are directed in opposite directions but in a plane lying parallel to the axes of the stresses.

2.2.3 Importance of *In Situ* Stress

Knowledge of *in situ* stresses is very important to many problems dealing with rocks in civil, mining, and petroleum engineering and energy development, as well as in geology and geophysics (Amadei and Stephansson, 1997). In petroleum engineering the design of wells especially horizontal and deviated wells, or programming a massive hydraulic fracturing treatment, requires a knowledge of the magnitude and direction of the *in situ* stresses. In addition, stress is very important in the simulation of reservoir conditions during laboratory measurements, and especially during the measurement of transport properties for forecasting production and designing waterflooding schemes.

Knowledge of the *in situ* stress magnitude and direction can impact on decisions and designs throughout the drilling and completion of a well (Amadei and Stephansson, 1997). Some of the specific areas that need detailed knowledge of *in situ* stresses are as follows (Widarsono, 1997) :

- Establishing the most stable direction for horizontal wells
- Injection/production well patterns for Enhanced Oil Recovery (EOR).
- Stability of vertical and deviated wells.
- Hydraulic fracturing stimulation.
- Hot dry rock geothermal exploitation.

Thus success in drilling, production and reservoir engineering depends not only on good quality reservoir characterisation but also on having information on stress orientation and magnitude, and storage and transport properties of reservoir rocks under representative in situ stress.

2.2.4 *In Situ* Stress Measurements

Even today, the determination of *in situ* stress presents a challenge in the oil industry, and there remains a lack of adequate methods for the large variety of rock types. In most cases *in situ* stress orientation and magnitude determination are based upon the utilisation of several techniques rather than only on one method. Breakout analysis has proved to be a very powerful indicator for vertical wells of the horizontal stress

direction, since it is caused by *in situ* stress contrasts. Hydraulic fracturing seems to be the best option for determining the minimum horizontal *in situ* stress magnitude. The methods commonly used can be divided into four categories :

- core-based methods,
- borehole-based techniques,
- near-wellbore techniques and regional geological indicators.

For any new area, the most accurate stress profile will be based on the multiple measurements of *in situ* stresses from stress tests (Hopkins, 1997). Most of the measuring techniques intentionally disturb the state of stress in the rock and then measure the subsequent deformations, but it is usually assumed that the rock behaves ideally, i.e., homogeneous, isotropic, continuous, and linearly elastic. The strains and failures recorded during testing are then related to the rock stresses.

There are a wide range of stress determination techniques (Bloch *et al.,* 1997): anelastic strain recovery (ASR) or anelastic strain relaxation, borehole breakout analysis, borehole deformation gauges, borehole imaging, circumferential velocity anisotropy (CVA), differential strain curve analysis (DSCA or DSA), direct observation of recovered open-hole microfractures, directional gamma ray logging, drilling induced fractures in core, earth tilt surveys, extended leak off tests, microfracture pressure analysis, microseismic logging, overcoring of retrieved core and petrographic examination of microcracks.

Each technique has its advantages and disadvantages, but a commonly used core based method in the oil industry is DSA (Differential Strain Analysis), which involves measuring strain in a cubic rock specimen as a function of reinstated hydrostatic pressure (Bloch *et al.,* 1997 and Widarsono, 1997). A set of DSA data provides a set of strain data, which are then used to calculate a principal stress tensor by assuming the ratios of the principal strains magnitudes represent the ratios of the effective principal *in situ* stresses. Analysis of experimental data can lead to magnitudes and directions of the *in situ* stresses.

2.2.5 Natural Stresses

Stresses found in rock are grouped according to origin, (i.e., natural stresses are found in the rock before excavation and exist prior to any disturbance), and induced stresses are result of stress changes brought about by man's intervention and artificial disturbance (i.e., excavation, drilling, pumping, loading etc.).

Herget (1988) classified natural stresses as gravitational stresses, tectonic stresses, residual stresses and thermal stresses :

- Gravitational stresses result from the weight of the overlying rock, and include the vertical overburden stress and the lateral stresses caused by the Poisson effect (Jaeger and Cook 1979).
- Tectonic stresses result from the continuous movements of the earth's crust, and the horizontal tectonic stresses are usually higher than any vertical ones.
- Residual stresses are the results of self-equilibrating stresses within a mass of rock. The stresses are detected in rock fabric when the boundaries of a rock sample are free of stress.
- Thermal stresses are the result of heating and cooling in a rock. They can occur close to the earth's surface due to exposure to the sun.

2.2.6 Induced Stress

Induced stress may occur due to removal or additional of material, and hence stress distributions around an excavation are different from those existing in the undisturbed rock. Thus, there is a stress concentration around the wellbore compared to the far-field. During production a pressure gradient is induced through the formation adjacent to the wellbore and, depending upon the magnitudes of this pressure gradient and the strength of the rock, the induced stresses, may induce rock failure near the wellbore and in the far field. This can result in wellbore stability problems during drilling, resulting in massive sand production or reservoir compaction (Tiab and Donaldson, 1996). In addition, fluid production and pressure drawdown lead to an increase of the effective stresses, which in turn result in a substantial reduction in permeability and pore volume compressibility, and leads to

reservoir compaction. The phenomenon may result in unequal reduction of components of principal permeabilities, thus introducing permeability anisotropy. Hydrocarbon reservoirs may change considerably throughout their production history due to induced stresses (Buchsteiner *et al.,* 1993).

Fracturing can also occur due to thermally induced stress, which can provide a tool for water flood operations. If rock deformation results in a noticeable closure of the wellbore due to induced stresses, the motion of the drill bit may be restricted. If the stresses are tensile and there is an expansion in the wellbore, the rock formation may fracture and lost circulation may result (Tiab and Donaldson, 1996). Reliable prediction of stable borehole and perforation conditions are therefore dependent on an understanding of the natural and induced stresses.

2.2.7 Laboratory Measurements Under Stress

Understanding the effects of stress on reservoir rock properties is important to petroleum engineers. For example, being able to predict the mechanical behaviour of underground formations is key to the avoidance of borehole instabilities during drilling, and for well completion and stimulation design. Reservoir compaction, which may lead to surface subsidence, is important with respect to design of casings, platforms, and to overall reservoir performance (Tiab and Donaldson, 1996).

Petrophysical properties, such as permeability, resistivity, compressibility, capillary pressure and acoustic velocity, are influenced by stress state in rock. Due to the dynamic behaviour of the earth's stress associated with production of hydrocarbon, water flooding and tectonic movements, *in situ* stress continues to be important for the determination of storage and transport properties of reservoir rocks. Different stress states cause different degrees of pore deformation, and hence cause the petrophysical properties to change according to the state of stress.

The main objectives of the measurements of petrophysical properties under *in situ* stress are as follows :

- To provide representative values of the petrophysical properties at the same or very similar conditions as found in the reservoir.
- To predict future changes in a property due to changes occurring in the *in situ* stress states, either through production of hydrocarbons or by injection of water or gas during pressure maintenance. This is very important in mature reservoirs due to a higher degree of disturbance in the *in situ* stress.
- To find an approximation factor or correction factor which can be used to correct routine core data for stress effects in stress sensitive reservoirs.

Hence there is a need to perform petrophysical measurements under realistic, anisotropic and true triaxial stress states. Recommended procedures for stress-sensitive reservoirs are illustrated in the following flow diagram :

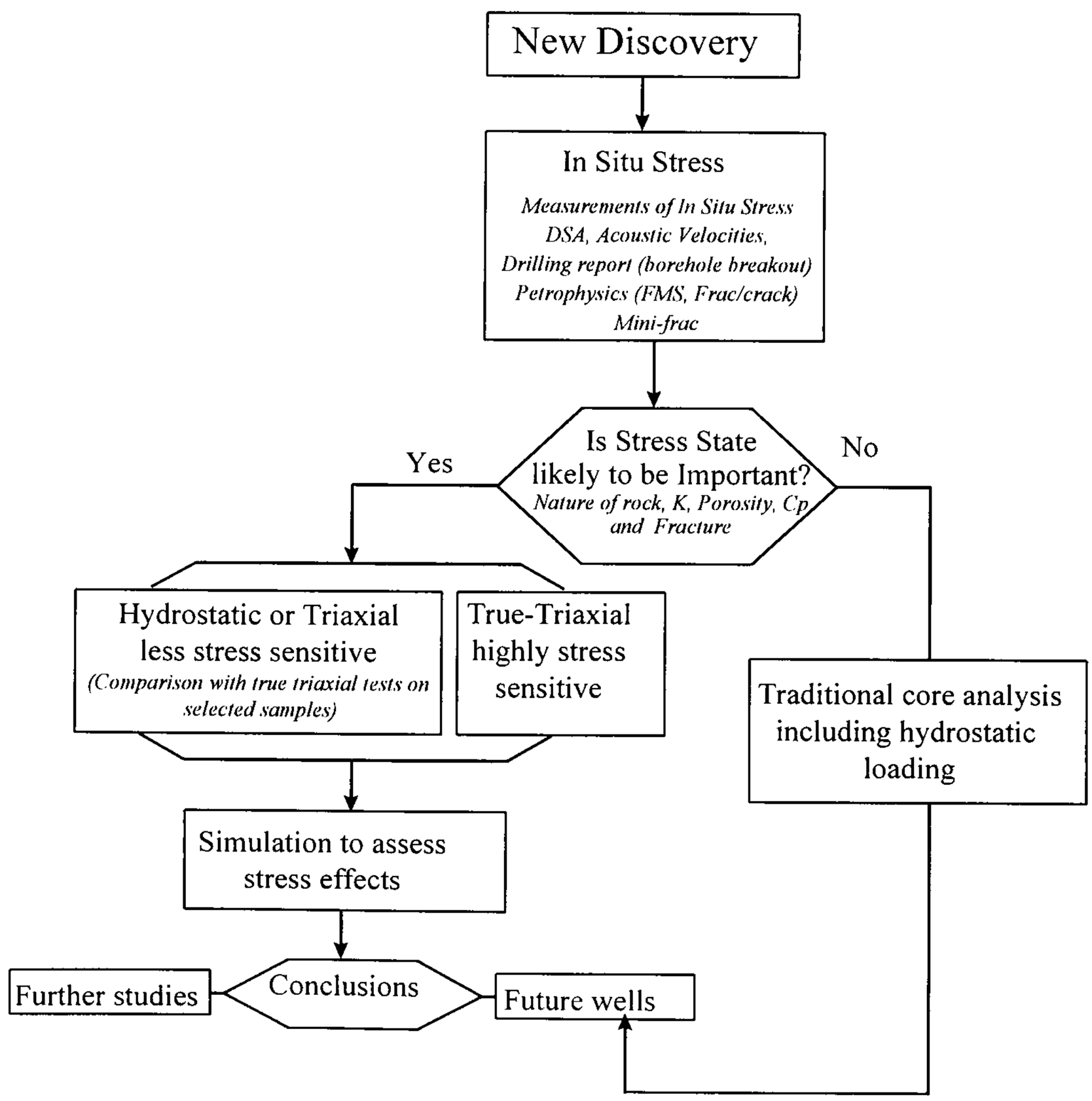

Figure 2.1 Schematic of recommended procedures during laboratory measurements of rock properties for stress sensitive reservoirs.

2.3 Permeability

2.3.1 Basic Definition

Permeability is the ability of the formation to conduct fluid through its interconnected pore spaces. It is defined through Darcy's law. For a horizontal, homogeneous system, with laminar flow of single phase incompressible fluid, Darcy's law can be expressed as (Archer and Wall, 1986) :

$$q = -\frac{kA}{\mu}\frac{dp}{dx} \tag{2.5}$$

where :

q = volumetric flow rate, cm^3/s

k = absolute permeability of the rock, Darcy

A = cross sectional area in the flow direction, cm^2

μ = fluid viscosity, cP

$\frac{dp}{dx}$ = fluid pressure gradient, atm/cm

The term *absolute* is used to define permeability when the rock is 100% saturated with one fluid phase. When two or more fluids present in the rock, the permeability of the rock to the flowing fluid is called *effective permeability.*

2.3.2 Importance of Permeability

Of all formation parameters used in petroleum engineering, permeability is one of the most important. Its direct link to formation flow potential is a prime factor governing how a well should be completed and deciding how many wells are required. Therefore, permeability is a fundamental parameter controlling the behaviour of hydrocarbon reservoirs, and is essential for reservoir engineering calculations. For example :

- It is important in overall reservoir management and development (i.e., for choosing the optimum drainage points and production rate, optimising completion and perforation design, and devising EOR patterns and injection conditions).

- It dictates the number of wells necessary to economically drain a reservoir, and controls production mechanisms during the life of a field.
- It impacts greatly on hydrocarbon recovery estimates, and hence determines project economics and guides investments decisions.
- It impacts on abandonment pressure (i.e., the higher the permeability the lower abandonment pressure).

2.3.3 Factors Affecting Permeability

The following factors affect permeability :

- Shape and size of grains in sandstone rocks control the variation of the permeability. If the reservoir rock is composed of large grains uniformly arranged its permeability will be high. If the grains are small and of irregular shape then the permeability will be low.
- Sorting (grain size distribution) of grains also influences permeability. Poor sorting reduces the pore size and consequently reduces permeability of the medium.
- Cementation reduces the pore size and results in the reduction of permeability.
- Fracturing and solution increase the permeability of rocks; features are common to carbonate reservoirs.
- Permeability tends to decrease with depth of burial, due to compaction.
- Layering in sedimentary rocks causes the horizontal permeability to be higher than the vertical one. Permeability of reservoir rocks often shows anisotropy. This directional dependency is due to, at the microscopic scale, grain alignment. At the continuum scale the presence of tight laminae, such as shales, is important.
- The presence of clay minerals can greatly reduce the permeability of sandstones.

2.3.4 Laboratory Determination of Permeability

Permeability measurements can be conducted directly on core plugs or cubes by measuring flow and pressures, based on Darcy's law. Permeability is usually measured in the laboratory using dry gas (air, nitrogen or helium) as the flowing fluid for convenience and in order to minimise rock-fluid reactions. Careful sample

cleaning and drying procedures must be followed. During drying there could be shrinkage or damage of delicate clay minerals in the rock. Humidity drying (for example, 40% relative humidity) (Worthington *et al.,* 1990) is often used for drying samples containing clays in order to prevent clay dehydration. Critical point drying may be necessary if hairy illite clay is present (Worthington *et al.,* 1990).

For steady state flow of an ideal gas, a modification to Darcy's law must be used to take into account gas compressibility :

$$q_{sc} = \frac{kA}{2\mu P_{sc}} \frac{(P_1^2 - P_2^2)}{L} \tag{2.6}$$

where :

q_{sc} = volumetric flow rate measured at base pressure and standard flowing temperature, cm^3/s

k = absolute permeability of the rock, Darcy

A = cross sectional area in the flow direction, cm^2

μ = fluid viscosity, cP

P_1 = absolute inlet pressure, atm

P_2 = absolute outlet pressure, atm

P_{sc} = absolute base pressure, atm

L = length of the rock, cm

During laboratory measurements using a gas as the flow medium, a gas slippage effect known as the Klinkenberg effect occurs. This slippage effect causes permeability to gas to vary depending on the pore pressure of the flowing gas. At low pressures and in small pores approaching mean free path of the gas molecules collide with pore walls and results in non zero boundary velocity and an increase in permeability. This is particularly significant for low permeability formations which contain a large percentage of small pores (Amyx *et al.,* 1960).

Gas permeability correction is obtained by measuring gas permeability at a series of different mean pore pressures. The plot of gas permeability versus reciprocal mean pore pressure yields a straight line with an intercept equal to equivalent liquid

permeability. This equivalent value represents the permeability of the porous medium to a non-reactive homogeneous single phase liquid (Amyx *et al.,* 1960).

The permeability of core samples under laboratory conditions is only representative of a very small part of the whole reservoir. Measurement conditions, scale and heterogeneity must be considered in order to relate laboratory measurements to formation permeability at reservoir conditions. Thus, permeability of core samples should be measured as close to the reservoir conditions as possible. Upscaling then needs to be applied carefully, taking into account the measurement conditions and any reservoir geological heterogeneities (Duquerroix *et al.,* 1993).

2.3.5 Field Determination of Permeability

Permeability can be determined directly in the field by well testing or indirectly by wireline log analysis (Cosse, 1993). In well testing, pressure transient tests are used to derive permeability in the field. The transient pressure test consists of recording the bottom hole pressure response as a function of time, while changing the flow rate of a well. There are essentially three ways by which permeability can be obtained from well testing (Lee, 1982). Firstly, short term tests include drill stem test (DST), impulse tests, transient rate tests and pressure tests. Secondly, conventional tests include pressure drawdown or injection tests, and pressure buildup or falloff tests involving single or multiple step rates. Thirdly, there is the family of advanced tests, which include layered reservoir testing, vertical interference testing and multiwell interference testing.

In wireline log measurements there are established methods for estimating permeability. Measurements of producible formation fluids are undertaken with nuclear magnetic resonance (NMR) logs. Permeability estimates are obtained from measurement of mineral abundances, using a geomechanical logging tool (GLT) (Schlumberger, 1989). Correlation of permeability with Stoneley wave velocity is possible with acoustic logging tools (Worthington, 1995). Pressure/time measurement of formation fluids can be obtained using repeat formation tester (RFT) tools (Schlumberger, 1989). The empirical correlation of permeability with porosity

and intergranular surface area based on Kozeny-Carman equation is also possible (Tiab and Donaldson, 1996).

2.3.6 Effect of Pore Pressure on Permeability

Pore pressure and stress changes affect permeability. Teufel *et al.* (1991a) investigated the effect of reservoir depletion and pore pressure drawdown of the Ekofisk field in the North Sea, and suggested that effective stresses increase linearly during reservoir depletion as pore pressure drawdown occurs. Shear failure during depletion can have a positive effect on production because it can increase fracture density and reduce matrix dimensions, thereby maintaining reservoir permeability. Teufel *et al.* (1991b) were able to observe that increases in effective stresses were larger than expected during primary production, which led to positive effect on production as a result of compaction drive.

Rhett and Tuefel (1992) reported that a period of 20 years of production from Ekofisk field resulted in pore pressure reductions of 21-24 MPa, and they also suggested that the permeability changes during production were due largely to these pore pressure changes. Jones and Mathiesen (1993) observed the pore pressure changes and compaction of a North Sea chalk hydrocarbon reservoir (Ekofisk field) and suggested that, due to production, there may be a change in mean reservoir pressure as time increases. Teufel *et al.* (1993) suggested that, during production of oil and gas, pore pressure decreases, which causes increases to the effective stresses and hence causes the fracture permeability to be stress-sensitive. They recommended that the prediction of permeability anisotropy in naturally fractured reservoirs must not only involve fracture characterisation but also must include stress measurements.

Khan and Teufel (1996) developed a model which incorporates geological and geomechanical parameters to predict reservoir stress paths, and they suggested that pore pressure reduction during primary hydrocarbon production will increase the effective stress and thus change the three dimensional effective stress field. They also suggested that a knowledge of total horizontal stress as a function of pore pressure drawdown can be used to provide an understanding of production by taking into

account the stress path and boundary conditions of the reservoir. Berumen and Tiab (1996) investigated the effect of pore pressure on permeability in artificially fractured rocks by using numerical modelling, and suggested that the permeability of a fractured reservoir does depend on pore pressure.

Osorio *et al.* (1997) developed a stress-sensitive model which couples the motion of pore fluid and the deformation of the rock solids. They further suggested that pore pressure behaviour in a hydrocarbon reservoir coupled with flow/geomechanical process is different to the typical behaviour predicted by conventional models, in which the effect of pore pressure change in permeability is not considered. Hettema *et al.* (1998) reported that, during production, changes in the pore pressures cause significant changes in horizontal stresses and, to a much lesser extent, changes in the total vertical stress of laterally extensive sandstone reservoirs. They also suggested that stress paths have strong influences on the depletion-induced compaction behaviour in laboratory measurements, and were able to report a reduction in pore pressure from 36 MPa to 14 MPa over 36 years in the Groningen gas field situated in the Netherlands.

2.3.7 Effect of Permeability Hysteresis

Reservoirs are dynamic systems that are constantly changing during production. The production of oil and gas from hydrocarbon reservoirs reduces the reservoir pore pressure and increases the net confining stress. The injection of water into a reservoir can alter the rock stresses again by increasing the pore pressure. In such circumstances, permeability hysteresis can have a significant effect, and may become important in reservoir management decisions.

Zoback and Byerlee (1976) reported hysteresis effects on permeabilities of Ottawa sand with complete cycles of increasing and decreasing confining pressure, and they concluded that samples irreversibly lost 20-80% of their permeabilities at effective confining pressures greater than 60 MPa. Dey (1986) investigated the effects of hydrostatic stress cycling on permeability, and observed that liquid permeability decreased during unloading from 31.5 to 3.5 MPa. Gobran *et al.* (1987) investigated

permeability hysteresis using Ottawa sand, and observed that during pressurisation (loading) and depressurisation (unloading) cycles the permeability reduced due to rearrangement of the grains into tighter structures.

Holt (1990) investigated the effect of loading and unloading on permeability, and concluded that a significant decrease in permeability occurs with increasing stress. He also suggested that permeability decrease is more pronounced when non-hydrostatic stress is used. Elashahab (1990) observed that permeability during unloading cycles of sandstones did not return to their initial values as seen in the loading cycles, but instead showed decreases of 3 to 7 %.

A direct application of permeability hysteresis is for the design and evaluation of water flood projects. Permeabilities from loading cycles can be used to predict behaviour when the reservoir rock is producing, whilst unloading data can be used to predict how the reservoir rock would respond if there is pressure maintenance.

2.3.8 Effect of Stress on Permeability

Core measurements are a main source of data, and they are normally performed at confining pressures somewhat lower than the effective stress levels experienced by rocks in reservoirs. Most commercial laboratories do provide routine petrophysical tests under hydrostatic or Hassler loading which has to be converted to more representative *in situ* stress conditions. The Teeuw correction factor based on Poisson's ratio and assuming isotropic and linearly elastic rock behaviour is often applied (Teeuw, 1971). Because most reservoir rocks are not linearly elastic simple conversion may not be valid, and laboratory measurements under true triaxial stresses are necessary especially for reservoirs regarded as stress sensitive. Routine laboratory measurements can be considered reliable only in cases where permeability is relatively insensitive to stress or where stress dependence is known and can be corrected (Holt, 1990). In many oil fields the influence of stress has been observed and has been seen to have a significant impact on reservoir performance (Osorio *et al.*, 1997). A number of investigators have determined the effects of hydrostatic

stress on sandstones, and have measured a wide range of permeability changes with increased effective stresses on various sandstones.

Dey (1986) observed 5-90% decreases for a 30 MPa increase of confining stress, whilst Gray and Fatt (1963) observed that reductions of permeability under non-uniform stresses used in their experiments were less than those under uniform stress. This means permeability measurements carried out under hydrostatic loading give the greatest reduction in permeability. Wilhelmi and Somerton (1967) observed a reduction of permeability with hydrostatic stress increase, and also suggested that the reduction of permeability was substantial when deviatoric stresses were increased.

Gobran *et al.* (1987) observed a reduction of permeability when confining pressure was increased on both consolidated and unconsolidated sands. Holt (1990) found experimentally that Red Wildmoor sandstone under hydrostatic and non-hydrostatic underwent a permeability reduction that was gradual prior to yield. He also noticed a sharp permeability decrease post-yield. Bruno *et al.* (1991) showed the importance of stress anisotropy on permeability in a series of flow-through experiments in which they compared permeability measured under increasing axial stress with permeability under increasing radial stress. They reported that permeability reduction is relatively small when stress is applied parallel to flow, but is more significant when the stress is perpendicular to flow.

Rhett and Tuefel (1992) observed that matrix permeability can be highly stress-dependent and that matrix permeability may either decrease or increase depending on how the *in situ* stress evolves as the reservoir is produced. Hence, permeability may not remain constant during production but may vary significantly with changes in pore pressure and effective stresses imposed within the reservoir. Crawford and Smart (1994) investigated the effect of stress anisotropy on permeability and concluded that with increases in mean stress, permeability variation can be non-systematic and may depend instead on heterogeneity.

Azeemuddin *et al.* (1995) investigated the permeability variation of Indiana limestone under hydrostatic, triaxial and uniaxial stress. Their results showed that, under hydrostatic stress, permeability decreases continuously with increasing mean effective stress, whereas under triaxial stress permeability decreases most significantly at relatively low confining pressures. Under uniaxial strain tests there was a sudden decrease in the permeability values at a particular axial stress level, corresponding to the yield stress of the material. Takahashi *et al.* (1995) investigated the effect of three principal stresses on permeability of cylindrical plugs of Shirahama sandstone. They observed that permeability decreased as the three principal stresses were increased due primarily to closure of pre-existing pores with low aspect ratios.

2.3.9 Permeability Anisotropy

Heterogeneity and/or anisotropy can affect the production of hydrocarbon in many reservoirs (Ayan *et al.,* 1994). Sedimentary rocks exhibit layering from the kilometre scale down to grain scale size. Petroleum engineers have often indicated the importance of small scale stratification on the permeability and, hence on producibility of a reservoir (Auzerais *et al.,* 1990).

Small scale stratification is the major contributor to anisotropy (Ayan *et al.,* 1994). Anisotropy or directional dependence of transport properties cause fluids to flow at different rates in different directions for a given potential. The direction of greatest interest in hydrocarbon reservoir sample is generally that parallel to the bedding planes, which are often horizontal. Darcy's law for anisotropic porous media in the three principal directions is given as follows :

$$q = -\frac{A}{\mu} K \begin{bmatrix} \frac{dp}{dx} \\ \frac{dp}{dy} \\ \frac{dp}{dz} \end{bmatrix} \qquad \text{where :} \qquad K = \begin{bmatrix} k_{xx} & 0 & 0 \\ 0 & k_{yy} & 0 \\ 0 & 0 & k_{zz} \end{bmatrix}, \tag{2.7}$$

where k_{xx}, k_{yy} and k_{zz} are three principal directional permeabilities (i.e., maximum horizontal, minimum horizontal which are perpendicular to each other, and vertical).

Due to the difficulty of quantifying all components of the permeability tensor only three principal components are used to represent fully the permeability tensor, by assuming that the chosen grid axes are aligned with the principal directions of permeability. Scheidegger (1957) showed that permeability measured in an anisotropic porous medium at different angles using whole cores results in an ellipsoid if the square root of permeability is plotted. Landrum and Crawford (1960) measured the permeability of whole core by rotating the core through several degrees and re-measuring the permeability, and they also investigated the effects of directional permeability on sweep efficiency and production capacity. Their work suggested that, in the early stages of the field development and certainly before the initiation of any fluid-injection program, measurements should be made to determine the possible magnitude and extent of any directional permeability. Carnes (1960) reported that directional movement of injected water can occur in many oil reservoirs, and this directional movement is caused by either natural fracture systems in the reservoirs or due to natural directional permeability orientation created by depositional features such as stream bed deposits.

Greenkorn *et al.* (1961) investigated the air permeability of 142 plugs oriented in eight directions spaced around the plugs at 45°, and reported that there was significant local anisotropy (variation within individual beds) more than half of the core plugs studied. Parsons (1972) reported that lateral directional permeability, or anisotropy, can be seriously detrimental to fluid injection operations if anisotropy is present but is neglected, since it leads to erroneous interpretation and prediction of pilot patterns and field behaviour. Guppy *et al.* (1978) investigated directional permeability by using spherical rock samples and concluded that there can be three dimensional variations in permeability.

Leung (1986) classified permeability anisotropy in two categories :

- Simple permeability anisotropy
  - (a) anisotropy and homogeneous and
  - (b) anisotropy and heterogeneous
- Full/general permeability anisotropy

In the first category, the simulation co-ordinates axes can be aligned with the principal axes of permeability. In case (a) the principal permeability does not change along the fixed direction, while in case (b) it does. In the second category, the simulation co-ordinates axes can not be aligned with the principal axes of permeability. This represents most general situations. The orientation and magnitude of the permeability may vary randomly, and the accurate determination of these quantities represents a challenge in data collection.

Lake (1988) reported that permeability is anisotropic and varies with direction, and that it should be represented by a second order tensor. Wang *et al.* (1992a) reported that in highly anisotropic media where there is a large variation of permeability, it is essential to include the full permeability tensor for accurate flow description. The fully permeability is also needed for the prediction of parameters such as water breakthrough time in water flood operations. Wang *et al.* (1992b) suggested that, in the case of complex bed geometries or fractures oriented in varying direction, the use of the non-diagonal permeability (also known as cross flow terms) gives better results than other averaging techniques in reservoir characterisation. Aasum *et al.* (1993) presented an analytical method for calculating effective permeability as a full tensor, and proposed that the method yields better predictions of flood front locations.

2.4 Capillary Pressure

2.4.1 Basic Definition

Capillary pressure is the pressure difference existing across a curved interface between immiscible fluids at equilibrium. The Laplace equation describes in general the pressure difference between non-spherical curved surfaces :

$$P_c = \left(P_{nw} - P_w\right) = \gamma\left(\frac{1}{r_1} + \frac{1}{r_2}\right) \tag{2.8}$$

where :

r_1 and r_2 are the principal radii of the curvature of the interface, cm

γ is the interfacial tension between the two immiscible fluids, dynes/cm

P_{nw} and P_w are the pressures in the nonwetting and wetting phases respectively, dynes/cm^2.

Since it is, in practice, impossible to measure the values of these radii, it was suggested by Leveret (1941) that the mean radius of curvature $\frac{1}{r_m} = \frac{1}{r_1} + \frac{1}{r_2}$ be used.

In reality the mean radius of the porous media is determined from the capillary pressure data obtained by the mercury injection method (Ritter and Drake, 1945). The capillary pressure can also be defined as the pressure differential that must be applied in order for a nonwetting fluid to displace a wetting fluid from the capillary tube. It is given by the following equation :

$$P_c = \left(P_{nw} - P_w\right) = \frac{2\gamma \cos\theta}{r_c} = \left(\rho_w - \rho_{nw}\right)gh \qquad (2.9)$$

where :

P_c is the capillary pressure, dynes/cm^2

P_{nw} is the pressure in the nonwetting phase, dynes/cm^2

P_w is the pressure in the wetting phase, dynes/cm^2

r_c is the radius of the capillary tube, cm

γ is the interfacial tension between wetting phase and non wetting phase, dynes/cm

θ is the contact angle,

h is the equilibrium height of the wetting phase, cm

ρ_w is the density of the wetting phase and ρ_{nw} is the density of the non wetting phase, gm/cm^2

g is the gravitational acceleration, cm/s^2

2.4.2 Importance of Capillary Pressure

Capillary pressure characteristics of reservoir rocks influence the flow and distribution of fluids in the reservoir. The drainage (oil displacing brine) capillary pressure curve can provide important information about the reservoir (i.e., whether the grains are sorted) and indications of permeability. For instance, if the capillary pressure versus brine saturation curve has low displacement pressure (entry pressure)

then large pores are connected to the point of entry. If the curve remains flat as the non wetting phase saturation increases, then many pores are invaded at the same pressure. This indicates uniform pores or a well sorted material. If the curve shows small irreducible wetting phase saturation (defined as fraction of pore volume which is occupied by formation water either adsorbed on grain surfaces or held in capillaries by capillary forces) then there is indication of large and uniform grains or pores. Irreducible wetting phase saturation can be obtained at a high capillary pressure approaching the asymptotic value. This can provide data needed to calculate the amount of oil in place, and give an indication of reservoir wettability. Since permeability is related to pore size, a rock with higher capillary pressure indicates a smaller set of pores and hence a lower permeability (Tiab and Donaldson, 1996).

From the imbibition (brine displacing oil) capillary pressure curve, irreducible nonwetting phase saturation can be obtained, and the size and distribution of the pore throats can be derived from the magnitude of the capillary pressure. This defines the initial fluid distribution in a reservoir, controlling the flood movements under influences of viscous, gravitational, and capillary forces. Capillary pressure curves are essential input data needed in reservoir simulations in order to define initial static fluid distribution, and for simulation of saturation front movement in reservoirs. Initialisation of reservoir simulation models requires capillary pressure data for fluid distributions, and location of transition zones, irreducible water saturations, oil- or gas-water contact and free water levels can be defined by the capillary pressure curve. Capillary pressure can be converted to height versus saturation curves and initial static fluid distribution in homogeneous reservoirs can be clearly defined (Archer and Wall, 1986).

2.4.3 Laboratory Determination of Capillary Pressure

Three methods are commonly used to measure capillary pressure curves, i.e., the porous plate/membrane method, mercury injection method and centrifuge method (Tiab and Donaldson, 1996).

Porous Plate Method

The diaphragm method is very accurate, reliable and so far the only method that may give the full loop of the capillary pressure curves including drainage and imbibition. However, the method is extremely time consuming. The important requirement of the method is a semi-permeable membrane or ceramic porous disk of uniform pore size distribution and, most importantly a high entry pressure for nonwetting phase. The pore sizes of the porous disks should be small enough to prevent penetration of the displacing fluid until the water saturation in the core has reached its irreducible value. In addition, it should have a displacing pressure that is higher than the largest capillary pressure to be measured. This limits the capillary pressure to around 200 psi. The following is a general procedure for the determination of capillary pressure curve (Tiab and Donaldson, 1996) :

1. Capillary pressure is measured by placing the sample, initially saturated with a wetting fluid, in a sleeve. Oil- and water- wet porous disks are placed against the inlet and outlet faces of the sample. These semi-permeable disks allow the respective wetting phase to be displaced from the sample, whilst blocking the passage of the nonwetting phase.
2. With the sample in place, the pressure of the non-wetting fluid is increased in steps and the system is allowed to equilibrate after each pressure change.
3. The volume of wetting phase displaced at each pressure is measured.
4. The capillary pressure is the non-wetting phase pressure minus the wetting phase pressure at each step.
5. The wetting phase saturation is determined from the volume of the wetting phase displaced at each pressure.

The advantages of the porous plate method include the estimation of the irreducible wetting phase and the determination of the full capillary pressure curves. However, there are limitations in that there is a restriction of the semi-permeable membrane pressure and a long duration is needed to obtain the entire capillary pressure curve. If thin micropore membranes are used instead of porous disks for the drainage capillary pressure then there is significant reduction in experimental time required. The porous plate method has been used in this research because it has the advantage of

minimising the capillary end effect, and it helps establish even saturation distributions in the rock when the system is equilibrated at fixed capillary pressures.

Mercury Injection Method

The capillary pressure is measured by injecting mercury, which is a non-wetting phase, into the sample. The system consists of a sample cell and a mercury injection pump. The following is a general procedure followed during measurements of capillary pressure curve (Wardlaw and Taylor, 1976) :

1. The dry sample is placed in the cell and the cell is evacuated. The mercury is injected into the system to a graduated level measured on the high pressure glass capillary above the sample chamber.
2. Nitrogen pressure is then applied in successive increments and, at each step, mercury is injected to maintain the mercury level with the graduation on the capillary.
3. The volume injected at each pressure determines the non wetting phase saturation.
4. From the volume of mercury forced into the sample pore spaces at each applied pressure, the mercury-air capillary pressure versus saturation can be obtained.

The method is very quick, taking only few hours, but it is destructive, requires strict safety precautions due to the presence of the mercury and the high pressures involved (40,000 psi), and it cannot be used to determine the irreducible wetting phase saturation. This technique has been used in this study in order to characterise pore size distributions and find nonwetting phase entry capillary pressures.

Centrifuge Method

The following section gives a general procedure used during air/brine drainage determinations of capillary pressure curve (Donaldson *et al.,* 1980) :

1. The core is cleaned and saturated with the wetting phase (usually brine). The sample is placed in the drainage centrifuge cell.
2. The core is placed in the core holder, which is then filled with oil to cover the core. The core holder is placed in the centrifuge shield and then attached to the centrifuge arm.

3. The rotor is balanced with core holders containing cores placed on opposing sides, the centrifuge cover is locked, and the rotational speed (revolutions per minute, rpm) is increased in increments. At each increment speed, the amount of fluid displaced is measured at successive intervals until fluid displacement stops. This process is continued until no more is displaced when the rotational velocity is increased. The data obtained can generate the drainage part of the capillary pressure curve.
4. The core containing oil and water at irreducible saturation is removed from the core holder and placed in another similar core holder. This is filled with brine until the core is completely submerged. The core holders are then assembled on the centrifuge rotor and the cores are again centrifuged at incremental rotational velocities until oil can no longer be displaced from the core. The data obtained can generate the forced imbibition part of capillary pressure curve.
5. The capillary pressure is obtained by using the following relation

$$Pc = \frac{\Delta\rho\omega^2}{2}\left(r_2^2 - r_1^2\right) \tag{2.10}$$

where :

P_c = capillary pressure at the core inlet, dynes/cm^2

r_1 = radius of the core inlet face measured from the centre of rotation, cm

r_2 = radius of the core outlet face measured from the centre of rotation, cm

ω = angular velocity (= $2\pi N/60$), N = centrifuge speed in revolutions per minute), radians/s

$\Delta\rho$ = density of water minus density of oil, gm/cm^3

The saturation at the inlet is given by the following equation (Hassler and Brunner 1945) :

$$S_w = S_{wav} + P_c\left(\frac{dS_{wav}}{dP_c}\right) \tag{2.11}$$

The centrifuge method is very fast (within a day per sample), and irreducible wetting saturation can be determined. It is also a preferred method for determining residual oil saturation and near end point relative permeability. However its limitations are its

inability to measure the displacement pressure, since the water saturation of the core inlet is always less than the average water saturation at the core. Also the Hassler-Brunner boundary condition at the core outlet may be violated at the high centrifuge speeds and the calculated water saturation at the core inlet is only an approximation. Also, spontaneous drainage and imbibition cannot be determined.

2.4.4 Effect of Stress on Capillary Pressure

Compaction of rocks under a confining stress results in the reduction of pore dimensions, as pore throats close-up and the channels narrow. Since the capillary pressure is a function of pore size, then as the rock compacts the pore size must decrease, and the capillary pressure must increase. For relatively tight cores having permeabilities less than 10 mD (i.e., small pore sizes), the capillary pressure is strongly dependent on stress. Dabbous *et al.* (1976) showed a strong relation between capillary pressure of Pittsburgh and Pocahontas Coals and their overburden pressures.

Sondenaa *et al.* (1989) and Ajufo *et al.* (1993) observed that at reservoir conditions the irreducible water saturation and capillary pressure are higher than those obtained at ambient conditions. Elashahab (1995) investigated the effect of confining pressure on capillary pressure as a function of saturation and concluded that there are noticeable increases in capillary pressure when the confining pressure is increased, due primarily to changes in pore size distributions in the rock. However, all these investigators used hydrostatic loading during their measurements, and data on capillary pressures at stress are limited due to the experimental difficulties involved.

2.5 Electrical Properties

2.5.1 Basic Definition

Electrical conductivity relates the movement of electrons (metallic conduction) or ions (solution conduction) through the conducting system. It is defined by Ohm's law which states that, for a given circuit at a particular temperature, the ratio of the

applied voltage to current is a constant. This constant of proportionality is the property of the circuit and is called the resistance, r.

$$r = \frac{V}{I} \tag{2.12}$$

where :

r = resistance, Ohms

V = voltage across the resistance, Volts

I = current across the resistance, Amperes

The inverse of r is the electrical conductance of that system. The resistance of an electrical conductor is directly proportional to its length, and inversely proportional to its cross-sectional area. It changes with temperature and depends on the conductor material, thus

$$r = R\frac{L}{A} \tag{2.13}$$

where :

R = resistivity of the conductor material, Ohms-m

L = length of the electrical conductor, m

A = cross-sectional area of the electrical conductor, m^2

2.5.2 Electrical Conduction in Porous Media

The most well known application of electrical resistivity in petrophysics is the evaluation of water saturation from electrical logs for use in the calculation of initial oil in place. In porous media the electrical conduction is through the ions in the aqueous solution. The fluids of interest in petroleum reservoirs are oil, gas and water. Water with certain concentrations of ions will conduct electricity, while oil and gas are considered as perfect insulators.

The electrical conduction in porous media depends on the geometry of the voids and the fluids that fill these voids. If the porosity is low then the electrical flow through the porous media is restricted due to constricted pore paths. In addition, when hydrocarbon is present, a greater restriction to electrical flow occurs. The greater the salt concentration, the greater the conductivity through the porous media.

2.5.3 Archie Equations

Archie (1942) proposed two empirical relationships between porous rocks and fluid parameters. Initially he calculated the resistivities of a large number of brine saturated cores from different formations having different porosities and salinities. The general Archie equation is expressed as :

$$F = \frac{R_o}{R_w} = \frac{a}{\phi^m} \tag{2.14}$$

where :

F is defined as the formation resistivity factor

R_o = resistivity of the rock when fully saturated with brine, Ohms-m

R_w = resistivity of the brine, Ohms-m

m = 'cementation factor' and changes with porosity of rock

a = emperical constant often assumed to be 1

Deviation of Archie's relationship was documented by Winsauer *et al* (1952) for a series of brine-saturated sands. When F is plotted versus ϕ on a logarithmic paper, the slope of the line is equal to m and is found to range from 1.08 to 2.0 for consolidated sandstones. However, the range is wider for clayey rock samples. Archie also found that for partially saturated porous rocks :

$$RI = \frac{R_t}{R_o} = \frac{1}{Sw^n} \tag{2.15}$$

where :

RI is defined as the resistivity index

R_t = resistivity of the rock when partially saturated with brine, Ohms-m

R_o = resistivity of the rock when fully saturated with brine, Ohms-m

S_w = brine saturation, (fraction)

n = saturation exponent which may not always be a constant for a given rock

Combining the above equations gives the well known Archie saturation equation as follows :

$$S_w = \left[\frac{R_o}{R_t}\right]^{\frac{1}{n}} = \left[\frac{FR_w}{R_t}\right]^{\frac{1}{n}} = \left[\left(\frac{a}{\phi^m}\right)\left(\frac{R_w}{R_t}\right)\right]^{\frac{1}{n}} \tag{2.16}$$

This equation is the base for all resistivity log interpretation.

2.5.4 Laboratory Determination of Electrical Properties

Electrical resistivity measurements are made in the laboratory, using either the two or four electrode method under static and flowing conditions. Routinely, for measurements of electrical properties at known frequencies (e.g., 2 kHz), the resistance across the sample is measured. The interpretation of data is based on the empirical relationships found from the above Archie's equations. Alternating current with a frequency of typically 2 kHz is used in the resistivity measurements in order to avoid electrolysis and polarisation.

Many studies have been reported on different methods to measure the electrical resistivities of fluid saturated cores. Lewis *et al.* (1988) reported that methods for measuring electrical resistivity can be separated into two general categories; two-electrode and four-electrode measurements. They also emphasised that monitoring fluid distribution along the core can be done using either multi-electrodes or X-ray scanning. Two electrode arrangements are relatively simple and allow resistivity measurements of entire plug sample. However, bad rock-electrode contacts can give rise to significant polarisation and contact resistance. Four electrode measurements provides a means of avoiding inclusion of rock-electrode coupling resistances in the measured signal. Saturation distribution along sample length can be monitored. However, potential electrodes are needed either to encircle the sample or consist of a series of point-contact electrodes around the sample circumference (Worthington *et al.*, 1990).

2.5.5 Field Determination of Electrical Properties

Borehole electrical resistivity measurements was first introduced to the oil industry by Schlumberger brothers in 1927 for identifying the presence of oil and/or gas in porous rock formations. Following the publications of Archie equations in 1942, it became possible to quantitatively interpret such measurements. Electrical well logs are used to characterise the rock/fluid system along the wellbore and resistivity data is used to estimate hydrocarbon saturation and porosity of formations. These also provide continuous measurements along the formation. However, logs do not

measure directly petrophysical parameters and their interpretation is based on the empirical relations suggested by Archie (1942).

2.5.6 Effect of Stress on Electrical Properties

Electrical resistivity measurements can be significantly influenced by variability in experimental conditions, i.e., by stress applied during the measurements. After drilling and coring, rock samples tend to relax when brought to the surface. At atmospheric conditions their properties may be considerably different to those at depth, and damage may have occurred. Compaction and thermal expansion may have affected the pore structures especially pore throats.

Fatt (1957) investigated the effect of pressure on electrical properties, and concluded that both F and m (see Equation 2.16) increased with confining pressure due to compaction of the rock. Brace and Orange (1966) investigated electrical resistivity changes in saturated sandstones under stress, and suggested that an increase in confining pressure resulted in changes in resistivity by as much as three orders of magnitudes. Brace *et al.* (1965) investigated the effect of pressure on electrical resistivity of water-saturated crystalline rocks, and concluded that resistivity increased with increasing pressure due to the reduction of pore dimensions and increase in tortuosity of the current flow path.

Sondenaa *et al.* (1989) suggested that resistivity indices obtained at reservoir conditions are higher than the resistivity indices obtained at ambient conditions at the same water saturation, primarily due to constriction of the pores as pressure is increased. Mahmood *et al.* (1991) suggested that resistivity, formation factor, cementation exponent and saturation exponent all increase with stress. The increase of resistivity is the result of both decreasing porosity and increasing tortuosity. The increase of n (see Equation 2.16) is due to changes in the mechanical properties and pore structure of the rock.

Jing *et al.* (1992) reported that for both clean and shaly rocks F and m increase significantly with an increase in confining pressure due to the reduction of the pore

sizes, and they also showed that less porous and less permeable rocks are more sensitive to changes of confining pressure than the more porous and permeable rocks. Elashahab *et al.* (1993) reported an increase of n (Archie saturation exponent) of up to 6% when confining pressure was increased from 400 to 4500 psi, due to a reduction of pore sizes and an increase in tortuosity.

Other factors such as wettability, stress hysteresis, presence of clay minerals and the roughness of the grain surfaces may influence the redistribution of the fluids within the pore space when confining pressure is changed. Jing *et al.* (1993) reported the effect of confining pressure on n for both outcrop and reservoir rocks, and found that n increases by up to 15% when confining pressure is increased from 400 to 4500 for less porous and permeable rocks. This was explained by the stress-induced change in pore geometry and pore size distribution. They also explained that at a given saturation, confining stress leads to a more tortuous brine phase distribution and, therefore, a higher electrical resistivity.

2.5.7 Electrical Conductivity Anisotropy

Porous geological media consist of minerals, rock fragments and void spaces. Schlumberger *et al.* (1934) suggested there are two types of anisotropy :

- Microscopic anisotropy, caused by a preferred orientation or alignment of the fabric of the rock itself; for instance, as occurs during deposition and compaction, cementation and diagenesis, or due to stress from tectonic forces after deposition.
- Macroscopic anisotropy, caused by a sequence of parallel, homogeneous rock layers, each with different electrical properties.

Thus total anisotropy is a combination of both macroscopic anisotropy (discrete beds of differing electrical properties) and microscopic anisotropy (anisotropy within individual beds).

Hill (1969) suggested that the conductivity of a porous medium is a symmetric second order tensor, and that it can be defined mathematically by a 3x3 symmetric matrix and geometrically by a triaxial ellipsoidal surface.

$$C = \begin{bmatrix} c_{xx} & c_{xy} & c_{xz} \\ c_{yx} & c_{yy} & c_{yz} \\ c_{zx} & c_{zy} & c_{zz} \end{bmatrix}, \text{ the conductivity tensor} \tag{2.17}$$

This tensor requires that directional measurements of resistivity be made in six or more different directions. However tensor principal direction can be estimated by measuring resistivity in three directions and by approximating the total resistivity. The assumption of cylindrical symmetry (where two principal values are equal) of the resistivity tensor has, for simplicity, been used extensively (Hill, 1969). This assumption is however only valid for certain cases. With this assumption the resistivity anisotropy is usually defined by the anisotropy coefficient given by :

$$\lambda = \sqrt{\frac{R_v}{R_h}} \tag{2.18}$$

where :

λ = anisotropy coefficient

R_v = vertical resistivity, Ohms-m

R_h = horizontal resistivity, Ohms-m

Zaafran (1981) investigated formation factors of horizontal and vertical oriented sandstones and concluded that there is distinct anisotropy of formation factor, probably as a result of characteristic orientations of the specific conducting minerals. Bonnie (1993) observed that significant differences in resistivities can be recorded in vertical and horizontal wells. He concluded that the differences are probably due to variations in reservoir quality, layering, resistivity anisotropy or borehole and invasion effects. He recommended that directional resistivity measurements should be carried out to quantify the effects of resistivity anisotropy, otherwise estimations of fluid saturations from horizontal well logging data must be treated with great care. This is especially true in calculations of oil in place and reserves.

Klein (1993) reported that resistivity anisotropy λ, from the Kuparuk river formation, North Slope, Alaska, was 2.7. He postulated that there is significant resistivity anisotropy in deviated wells, or when the beds are not perpendicular to the well bore. He concluded that electrical anisotropy should not be ignored because logs not

corrected for anisotropy will give erroneous estimations of hydrocarbon in place. Thus resistivities from highly deviated wells should always be corrected with reference to the bedding plane.

Anderson *et al.* (1994) suggested that electrical resistivity anisotropy depends on the direction that the current flows in the rock, and that any anisotropy will affect resistivity logs depending on the angle between the borehole and the formation. They recommended that in dipping formations where there is pronounced anisotropy, vertical and horizontal resistivities should be measured and a correction should be made. Hagiwara (1994) suggested that if the formation is of a thinly laminated sand/shale sequence having a layered structure, then its resistivity in the vertical direction can be different from that in the horizontal direction. Sharma (1995) suggested that there are two major factors which influence the resistivity :

- Rock texture, which includes microscopic structure of the pores, their sizes and shapes, interconnectivity, tortuosity, microscopic inhomogeneneity, shale laminations, vugs, macroscopic inhomogeneneities, fractures and anisotropy.
- Rock composition, which includes mineralogical composition of the rock, amount and distribution of saline water, porosity and saturations.

If rock resistivity depends on the direction the current flows then this is termed electrical anisotropy. If the wellbore is not perpendicular to the bedding plane, then the average resistivity measured will be too high since measured resistivity depends on the coefficient of anisotropy and the dip angle of the formation relative to the well. Grattoni and Dawe (1995) have investigated experimentally electrical anisotropy using packs of spheres, and have found that there is microscopic anisotropy even if a system is macroscopically homogeneous primarily due to the internal pore structure. They concluded that porous media can have a pore structure which is anisotropic, even though the packing is homogeneous, and thus the physical parameters will have directional qualities.

2.6 Summary

The following points summarise the previous studies :

1. As pore pressure declines there are changes in permeability.
2. During cycles of loading and unloading the permeability does not return to its original value (permeability hysteresis) either because of frictional sliding inside the rock, opening of cracks, uneven distribution of stress, failure of internal textures, rearranging of pore structures, mobilisation of fine grains, and/or an increase of tortuosity due to collapse of pore spaces.
3. Reduction of permeability occurs as hydrostatic stress increases, and reduction of permeability is substantial when deviatoric stress is increased.
4. As stress increases there is an increase in capillary pressure due to the reduction of pore radii.
5. There can be significant anisotropy in permeability and electrical conductivity.

However the majority of experiments reported in the literature were conducted at hydrostatic stresses, which generally do not represent the true stress fields in reservoirs. Therefore, realistic stress states and pore pressures encountered in reservoirs were not simulated during the previous experiments. Laboratory measurements of permeability and electrical conductivity were often carried out unidirectionaly in the past, and did not take into account anisotropy. In order to simulate the reservoir behaviour and the effects of stress, anisotropy, hysteresis or pore pressure, more representative stress configurations are required, with directional properties being measured in three principal directions.

CHAPTER 3

EXPERIMENTAL APPARATUS AND PROCEDURE

3.1 Introduction

Petrophysical properties such as permeability, capillary pressure, resistivity and relative permeability are influenced by the state of stress acting on a rock. Hence, these properties should be measured at a stress state that represents the *in situ* conditions. This research focuses on petrophysical measurements on rock samples subjected to realistic, anisotropic and true triaxial stress states. Cylindrical rock samples were used for measurements of permeability, capillary pressure and electrical properties to provide baseline data for comparison. In addition, measurements of permeability hysteresis on rock cubic samples under hydrostatic and true triaxial stresses, and measurements of changes in permeability with pore pressure were carried out. Measurements of permeability and electrical conductivity were then conducted in the three principal directions. Pore volume deformations were also measured under hydrostatic and true triaxial stresses and, finally, two phase tests were conducted to measure capillary pressure and electrical properties under hydrostatic and true triaxial stresses.

3.2 Experimental Apparatus

3.2.1 Hydrostatic System

Two hydrostatic rigs were used for measuring capillary pressure and electrical properties under hydrostatic stress, namely, a single cell and a multi-sample rig. The rigs have the capability to apply up to 69 MPa hydrostatic stress. The multi-sample petrophysics rig has the capability of measuring five core samples simultaneously at reservoir conditions of pressure and temperature. Both rigs are detailed in Figures 3.1 and 3.2. The multi-sample rig was built by Laszlo Lombos Consultancy to a specification from Imperial College, and was set up in the Earth Resources

Engineering Department at Imperial College in 1987. An upgraded version of the multi-sample rig was installed in 1998. The maximum working confining pressure is 69 MPa and maximum testing temperature is 200°C. However, the effect of temperature is beyond scope of this work. The apparatus consists of coreholder, pressure vessel, pressure maintainer or hand pump, QuadTech model 7600 RLC meter, pore pressure system, transducers, pressure indicator and regulators. In this research the apparatus has been used to investigate the effect of stress on two phase flow measurements, i.e., capillary pressure and electrical properties. The hydrostatic system is described in detail as follows :

Single-sample and Multi-sample Coreholder (Pressure Vessel)

The coreholder is constructed from stainless steel alloy to withstand a working pressure of 69 MPa and temperature of 200 °C. The wide bore cell allows easy access to each sample. The rock samples are enclosed in specially designed multi-electrode Viton sample sleeves with flow of fluids or electrical current through five separated inlet and outlet stainless steel ports for multi-sample rig and one pair of separated inlet and outlet stainless steel ports for single sample cell. These ports are insulated in the top and bottom from the cell body using insulated pressure and electrical feedthroughs. The multi-electrode Viton sample sleeves inside the cell body are connected electrically to the outside of the cell body through these ports. The cell is mounted in its own sturdy frame allowing easy access to all process control components (see Figures 3.1 and 3.2).

Pressure Maintainer

This is a hydraulic assembly module, i.e., stepper motor, gear box, ballscrew unit assembly, piston and pressure cylinder which sits on a purpose designed base module. It has a compact box with demountable side panels for accessing controls, i.e., stepper motor power pack and driver and maintainer control printed circuit. Load is developed by hydraulic pressure applied to the piston. The piston is directly mounted on the ballscrew which travels within the pressure cylinder. It has accuracy of 1% between 6.9 MPa and 69 MPa, pumping at a rate of 3.2 ml/min. The hand pump is used as a pressure maintainer or supply to a single cell. It is connected to the

cell body through a high rated pressure line and valve. Once the desired pressure is reached then the high rated pressure valve is closed in order to maintain the pressure.

Pore Pressure System

The pore pressure system consists of two gas/oil interface units, one connected to the bottom of the coreholder and the other to the top. The top gas/oil interface unit is connected at its top to a controllable gas pressure supply and from its bottom to an oil/brine interface unit. The oil/brine interface unit contains five calibrated glass burettes, partially filled with oil and partially with brine. All five burettes are connected individually to the top of the core samples, and are used for volume displacement measurement during application of stress (squeeze out) and drainage/imbibition cycles. A maximum pore pressure of 1.38 MPa (200 psi) can be supplied and pore fluid displacement volumes can be measured with an accuracy better than 0.02 cc. The oil pressure is applied through the five gas/oil interface units on the bottom of the pressure vessel, with one connected to each sample, oil pressure is varied by a very fine controllable regulators. The pressure can be accurately controlled to 0 - 1.38 MPa (0 - 200 psi). Both bottom and top interface units can be interchanged as either a supply or a collection and measurement unit. The pressure difference applied between gas/oil and oil/brine interface units is the capillary pressure.

Electrical Circuit

The electrical resistivity circuit is designed to measure in both two-electrode and four-electrode configurations. The sample is placed inside a multi-electrode Viton sleeve which contains six potential electrodes positioned at equal spacing along the sample length. Current is supplied into the sample by two silver covered stainless steel platens positioned at the top and bottom of the sample. In the two-electrodes configuration platens serve as both current and potential electrodes. In the four electrodes configuration, the platens are only used to introduce a current into the rock sample while the voltage is measured across any two potential electrodes along the sleeve. These electrodes are in contact with the sample via wires inserted in circular grooves made at the rock surface (see Figures 3.3 and 3.4).

Due to the high resistance of ceramic porous disk, especially in the oil wet side, a fine mesh bridge is positioned between the sample and the platen in order to ensure good electrical contact. At very low saturation this method ensures the continuity of flow of the electrical current between the metal end pieces and the rock sample faces. In addition, the method also enables resistivity measurements using a two-electrode configuration.

The rock sample is encircled within six wire electrodes positioned at fixed distances along its length, which provide electrical contacts to the sample circumference and resistance measurements in the four-electrode configuration. The wire electrodes are wrapped with a very fine porous stainless steel mesh in order to ensure good electrical contact. The idea of using the mesh is to increase the surface area of contact and improve the capillary contact between the potential electrodes and pore fluids.

The sample resistance is calculated by Ohm's law. The sample and the circuit precision resistor are connected in series. An AC multi-frequency power generator, which is usually set at 2 KHz during all the experiments, is used to generate a potential difference across the core sample and the circuit precision resistor. Since the sample is connected in series with the circuit precision resistor then the same current flows in both elements. Figures 3.3 and 3.4 illustrate circuit of the electrical measurements and multi-electrode core sleeve assembly and porous disks.

$$I = \frac{V_r}{R_r} = \frac{V_s}{R_s} \Rightarrow R_s = \frac{V_s R_r}{V_r} \tag{3.1}$$

where :

V_r = Voltage across the precision circuit resistor, Volts

R_r = Resistance across the precision circuit resistor, Ohms

V_s = Voltage across the sample, Volts

R_s = Resistance across the sample, Ohms

I = Current, Amperes

The electrical circuit described above is suitable for low frequency range (10 Hz to 10 kHz). The QuadTech model 7600 RLC meter can be used for complex resistivity measurements with high frequency range (10 Hz to 2 MHz). The meter has special four coaxial BNC terminals on its front panel which locate its calibration plane. It also allows for frequency-dependence corrections of cable capacitance.

Ceramic Porous Disks

Ceramic porous disks, both water-wet and oil-wet, have been used in this research. During the measurements of capillary pressure and electrical properties these disks (0.3 cm thick and 0.483 MPa (70 psi) entry pressure) were used to maintain capillary continuity across the sample and to allow only one phase to pass through. The water wet ceramic porous disk is positioned at the top of the sample while the oil wet ceramic porous disk is positioned at the bottom of the sample. The displacement of brine by mineral oil is performed from bottom to the top at various equilibrium capillary pressure steps. The continuity of the wetting phase should be maintained during the desaturation process by improving the capillary contact between the porous plate and the sample. The ends of the samples must be made flat to ensure good capillary and electrical contact. In addition, materials such as tissue papers, capillary contact mat and cellulose filters are used to improve the capillary contact. If capillary contact is not good then the non wetting phase may penetrate the contact region and the desaturation process may stop prematurely.

Transducers and Pressure Indicators

In each sample the pressure is measured using electronic pressure transducers supplied by Druck Limited. All measurements are digitally displayed using pressure indicators. The calibration of the transducers is performed frequently using a dead weight tester. The transducers are calibrated to an accuracy of ± 6.9E-5 MPa (0.01 psi)

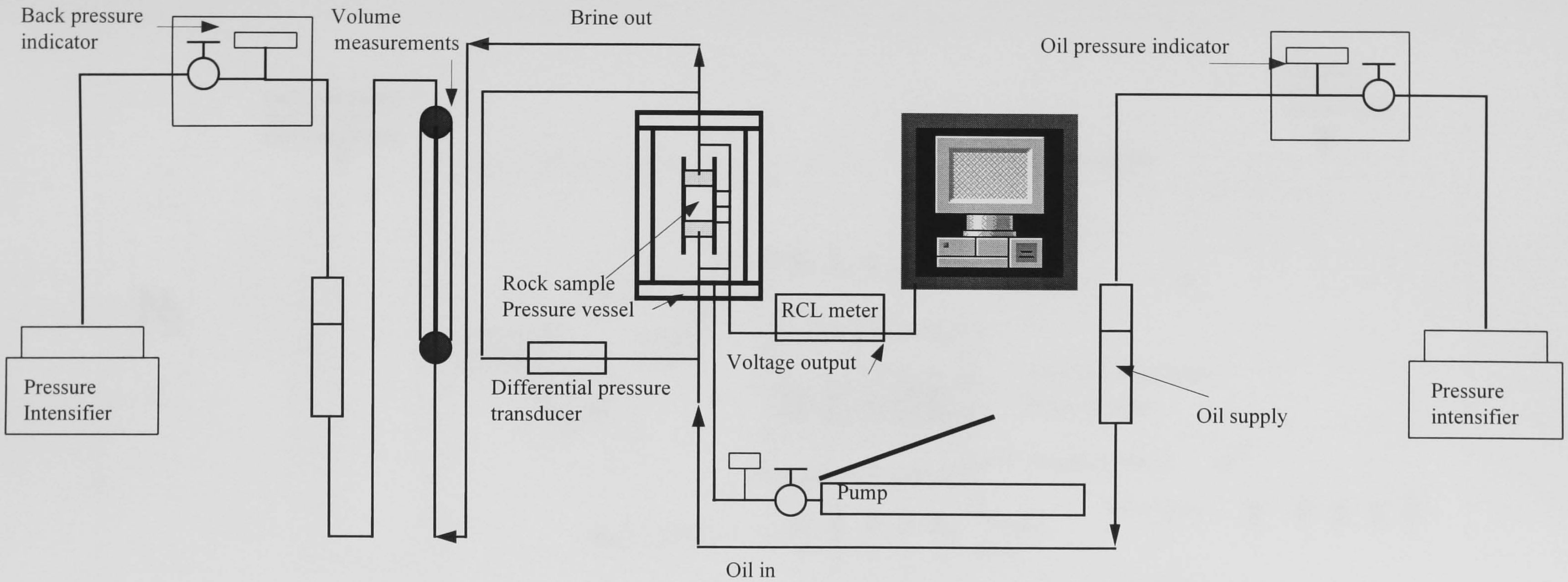

Figure 3.1 Schematic of the single sample cell for measuring capillary pressure, electrical properties and permeability of the rock samples at different confining pressures

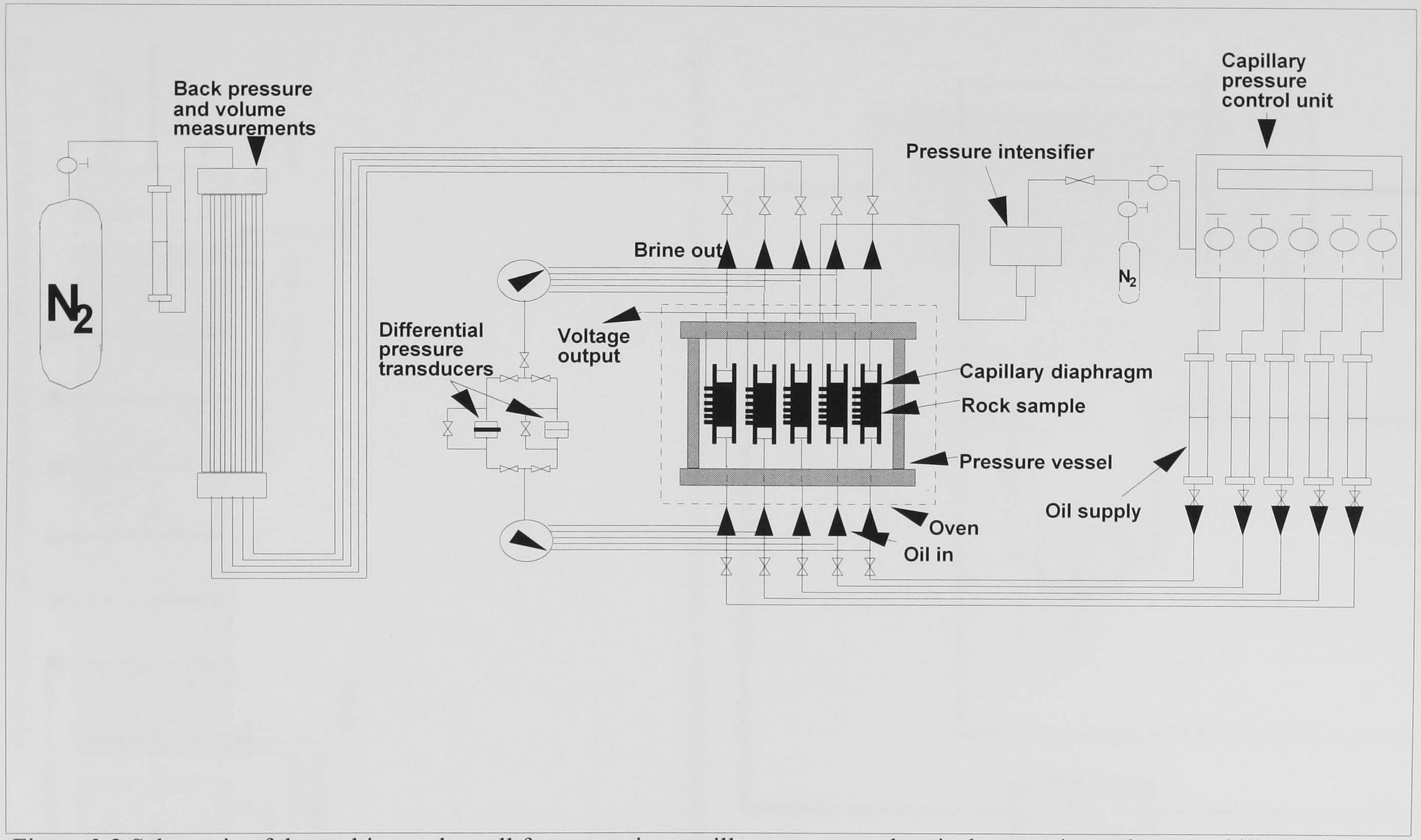

Figure 3.2 Schematic of the multi-samples cell for measuring capillary pressure, electrical properties and permeability of the rock samples at different confining pressures (after Elashahab 1995)

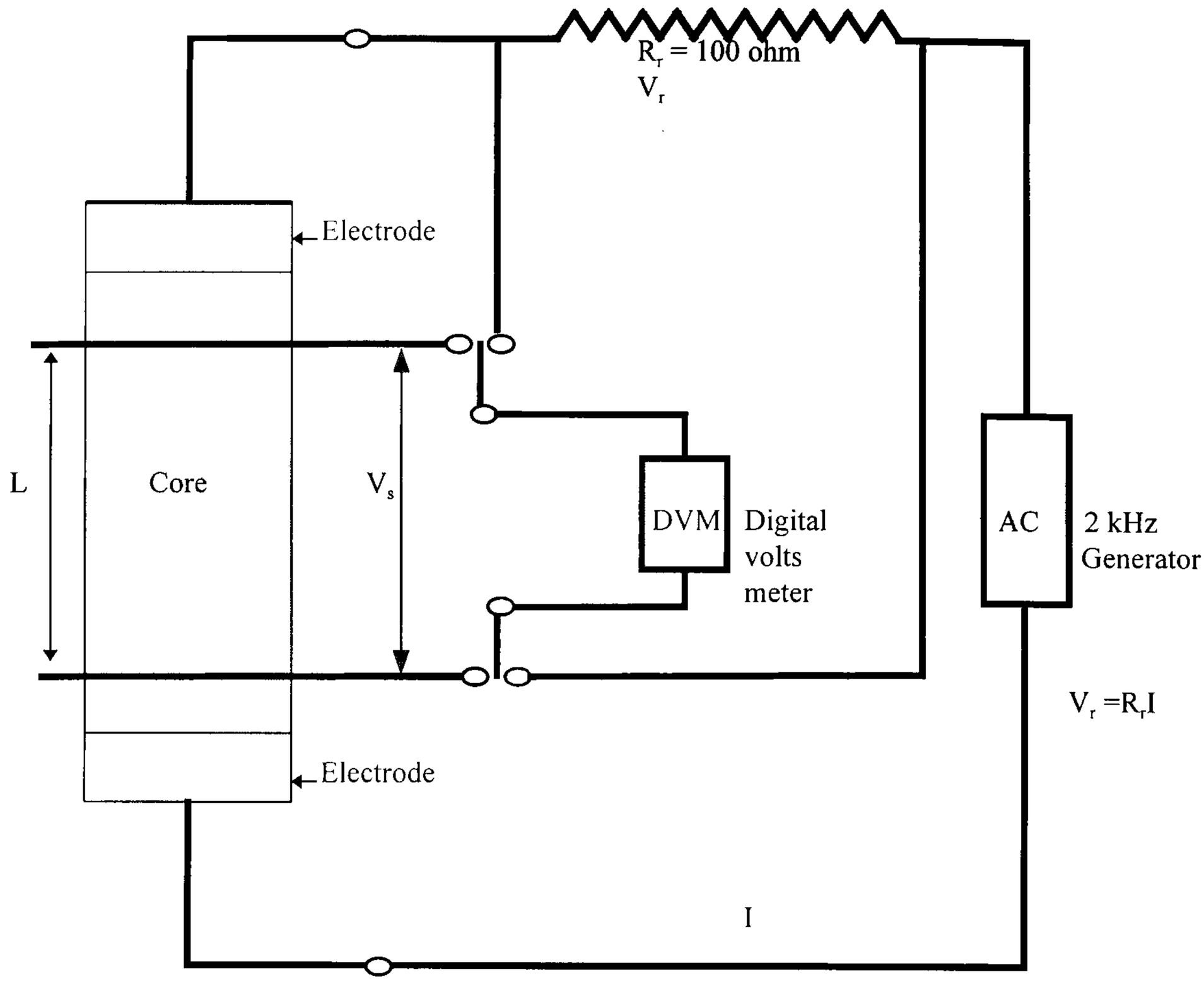

Figure 3.3 Core sample connected in series with a precision circuit resistor (R_r)

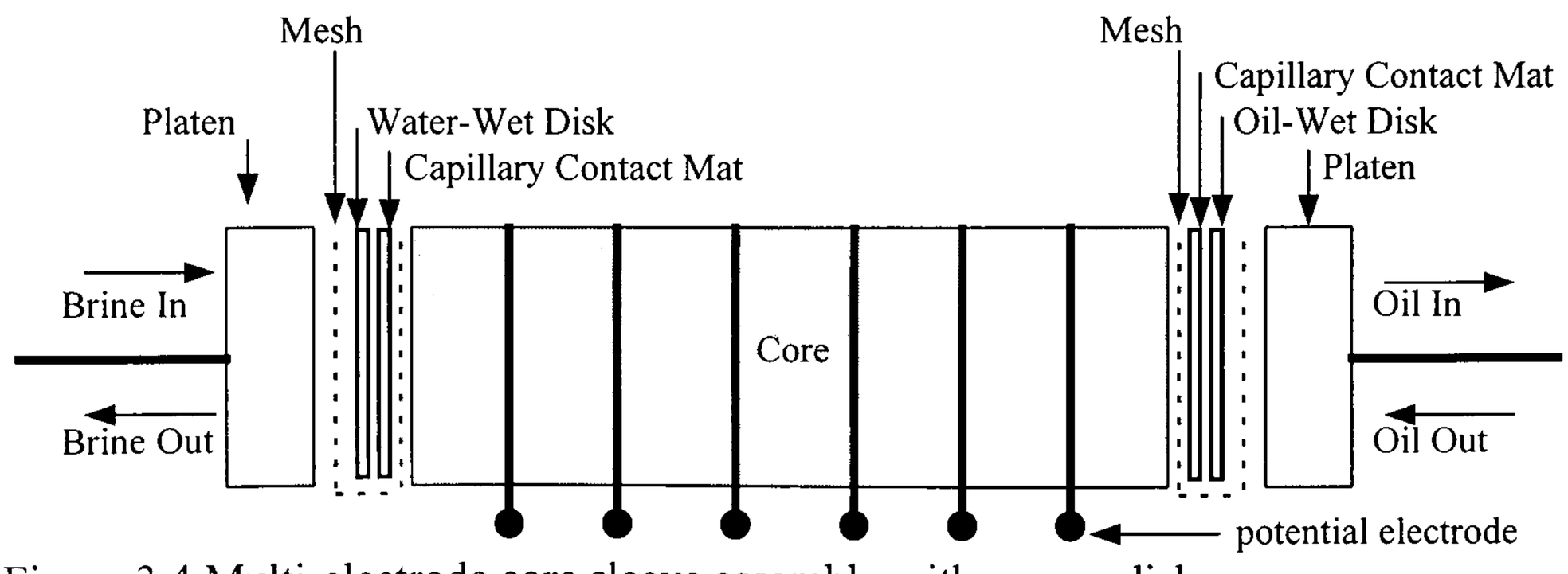

Figure 3.4 Multi-electrode core sleeve assembly with porous disks

3.2.2 True Triaxial Stress Loading System

Conventional triaxial testing systems are used routinely on core plugs during petrophysical measurements under stress. In such experiments horizontal stress is applied by a uniform radial stress to the curved surface of the rock cylinder. Simultaneously the vertical stress is applied axially to the prepared flat and parallel sample ends. However, in this type of tests the minor and intermediate principal stresses are equal.

A true triaxial stress loading system for testing 50 mm side cubic rock sample was reported by Sayers *et al.* (1990). The rig has the capability of applying a maximum compressive stress of 120 MPa in each of the principal directions. It was initially used for measuring P- and polarised S-wave velocities, and mechanical parameters of dry samples. Smart (1995) described a true-triaxial cell for testing cylindrical rock specimens, in which a number of flexible tubes located between the cell wall and specimen jacket are used to apply minor and intermediate stresses in the radial directions. A differential radial confining stress around the specimen is provided by maintaining these tubes at different pressures. The vertical stress is applied axially to the prepared flat and parallel sample ends. However, in this type of test geometry the minor and intermediate principal stresses are limited (typically to a maximum stress difference of 15 MPa).

A true-triaxial stress loading system (King *et al.*, 1995) was developed at Imperial College for testing 51 mm cubic rock samples, with the capability to vary each of the three principal stresses independently in the range of zero to 115 MPa in the horizontal principal directions, and to over 750 MPa in the vertical direction. The system was successfully employed to introduce sets of fractures and microcracks oriented perpendicular to the minimum principal stress, and to determine permeability, ultrasonic P- and polarised S-wave velocities, and mechanical parameters such as strength and deformability. This true-triaxial system has been modified by Imperial College and Laszlo Lombos Consultancy for this research to accommodate 40 mm cubic samples with single- and two-phase pore fluids at elevated pressures. The modified system is servo-controlled, and in the configuration

used in this investigation can achieve deviatoric stresses in excess of 200 MPa and pore pressures up to 145 MPa. The equipment now permits measurements of various petrophysical characteristics, such as directional permeability, acoustic velocity and electrical conductivity for single- and multi-phase situations. Compliance matching and a high degree of parallelism between sample and platens enables the boundary stresses to be distributed uniformly such that end- and edge-effects are minimised. In order to define the principal stresses with respect to the axes of the cubic sample, the z-direction has been defined as the major principal stress (σ_1), the y-direction has been defined as intermediate principal stress (σ_2), and the x-direction has been defined as the minor principal stress (σ_3). Figures 3.6 and 3.7 show a schematic diagram and photo of the experimental set up of a true triaxial loading system in the Rock Mechanics Laboratory at Imperial College.

The main experimental system used for this work is described in detail as follows :

1. *A dedicated loading frame*, in which a hydraulic ram provides the major stress (z-direction), which also houses an aluminium alloy reaction ring within which four horizontal hydraulic rams are mounted to provide the two orthogonal stresses in the horizontal plane. The three principal stresses are controlled by closed-loop servo-hydraulics. Deformation of the samples is measured by pairs of LVDTs mounted in each principal direction, and the boundary stresses are transmitted to the samples via engineering plastic/ceramic composite platens which match the geometry of the 40mm cubes.
2. *A gas volume accumulator, with pressure regulators*, to generate and maintain pressure in the pore fluid. A pre-moulded rubber jacket, captured in place by the loading platens, isolates the sample from atmosphere and enables elevated pore pressure to be applied.
3. *Capillary pressure and electrical measurements units*, including two gas-oil interface units for accurate measurements of pore volume change and fluid movements.
4. *A gas/liquid flow system*, for measuring permeability in the rock sample in the z-direction. This consists of a flow meter, and two pressure transducers and digital

displays for upstream and downstream pressures. The upstream pressure is generated and maintained using a gas volume accumulator.

5. *A data logger* is used to log continuously the applied loads, pore pressures and displacements during the experiments.

Figure 3.5 shows the schematic of top and bottom view of z-axes platens in the true triaxial loading system. The figure shows water-wet side, oil-wet side, flow lines, current and potential electrodes, burette for volumetric measurements, gas-oil interfaces and gas pressure supply.

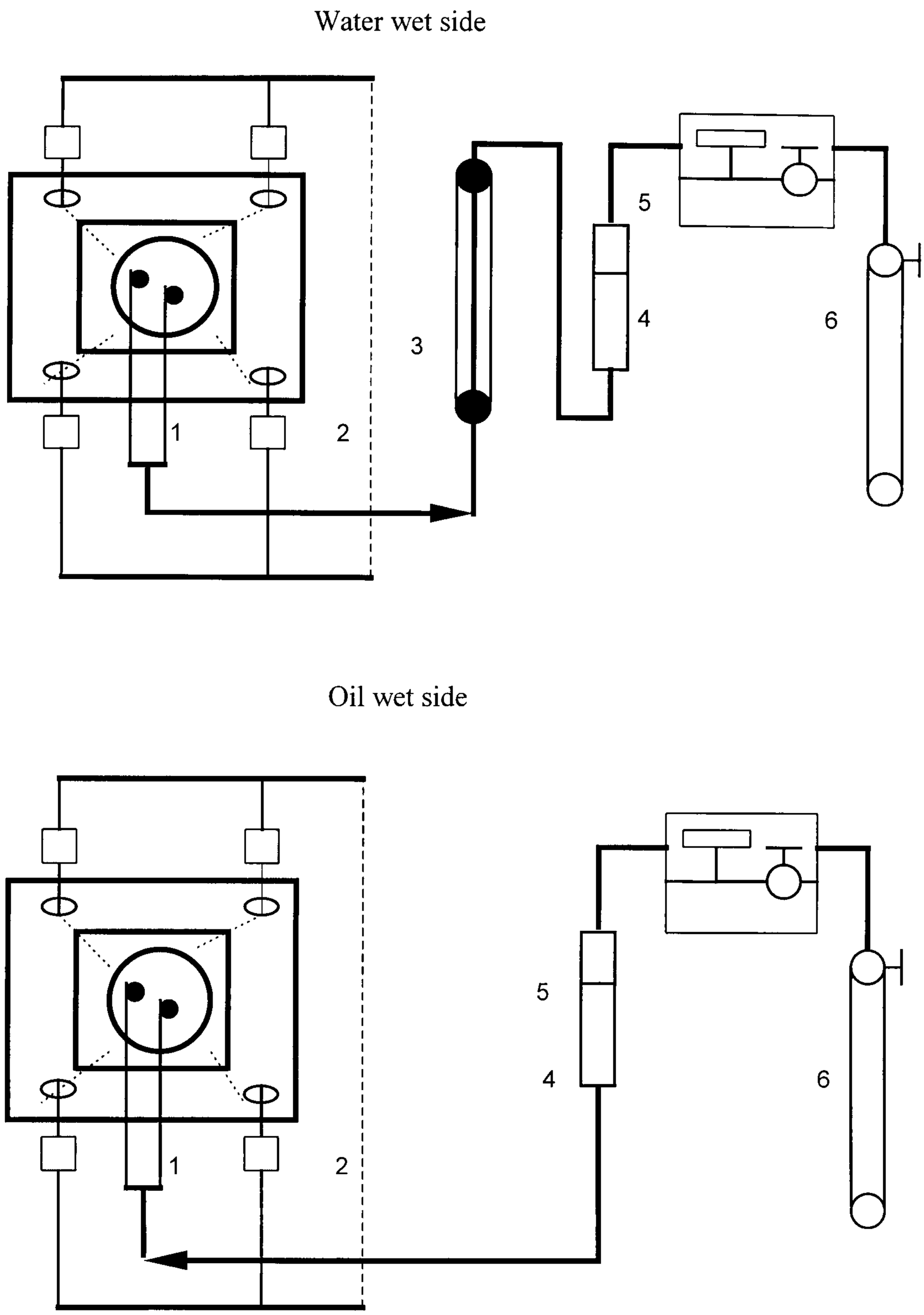

1. Pressure transducer, also used as brine flow line
2. Fluid flow lines, also used as current and potential electrodes
3. Calibrated brine volumetric measurements
4. Gas-oil interface
5. Regulator, brine pressure transducers and display
6. Gas supplier for air permeability and for gas-oil interface

Figure 3.5 Schematics of top and bottom view of the z-axes platens in the true triaxial stress loading system

Figure 3.6 The true triaxial stress loading system

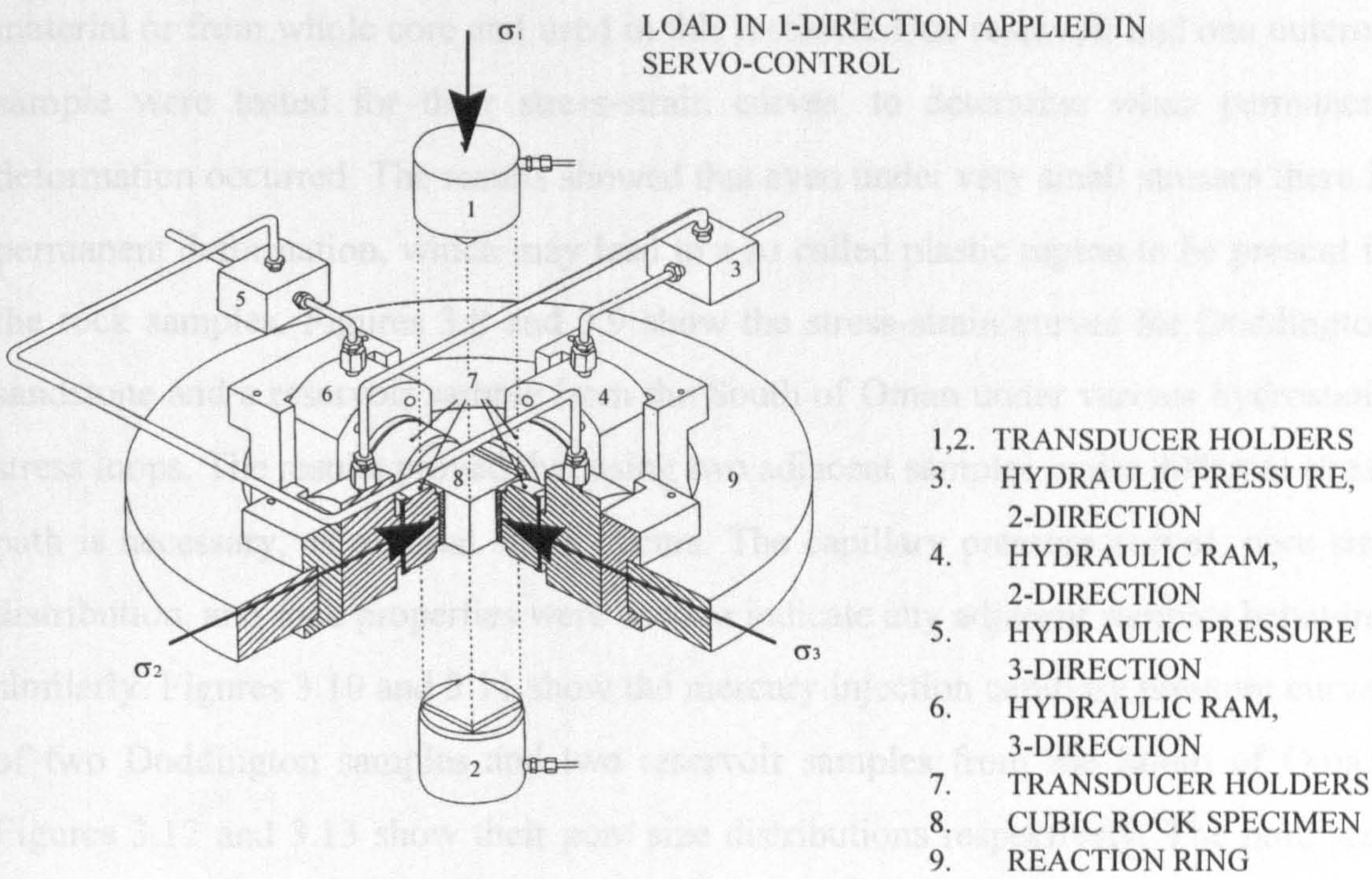

Figure 3.7 Isometric sketch of true triaxial stress loading system (King *et al.,* 1997)

3.3 Description of Rock Samples

Rock samples used in this research include six outcrop sandstone rocks and two hydrocarbon reservoir sandstones. The selected outcrop sandstone rocks are Doddington, Croslands Hill, Springwell, Clashach, St. Bees, and Stainton all from British quarries. The reservoir samples are from oil fields in the North Sea (1L & 1M) and the South of Oman (MM220). Not all rocks listed above were subjected to the same tests, depending on availability and suitability in order to illustrate specific effects. The samples selected cover a wide range of porosity and permeability. Two or three adjacent samples were used in order avoid repeating the same petrophysical measurements on the same cores under different stresses. The petrophysical, geological descriptions and SEM and thin section photos of each sample are given in appendix A. The sources of the outcrop samples are discussed by Jones *et al.,* (1991).

3.4 Selection of Rock Samples

Pre-stressing sample or using samples for two different stress paths was avoided, since these processes may create more deformation and damage in the sample. Therefore, two or three adjacent samples were cut from the same block of outcrop material or from whole core and used in this research. One reservoir and one outcrop sample were tested for their stress-strain curves, to determine when permanent deformation occurred. The results showed that even under very small stresses there is permanent deformation, which may lead to a so called plastic region to be present in the rock samples. Figures 3.8 and 3.9 show the stress-strain curves for Doddington sandstone and a reservoir sample from the South of Oman under various hydrostatic stress loops. The results proved that using two adjacent samples under different stress path is necessary, as residual strain occurs. The capillary pressure curves, pore size distribution, and rock properties were used to indicate any adjacent samples behaving similarly. Figures 3.10 and 3.11 show the mercury injection capillary pressure curves of two Doddington samples and two reservoir samples from the South of Oman. Figures 3.12 and 3.13 show their pore size distributions respectively. The pore size distributions for adjacent samples are almost identical indicating that two samples have almost identical petrophysical properties.

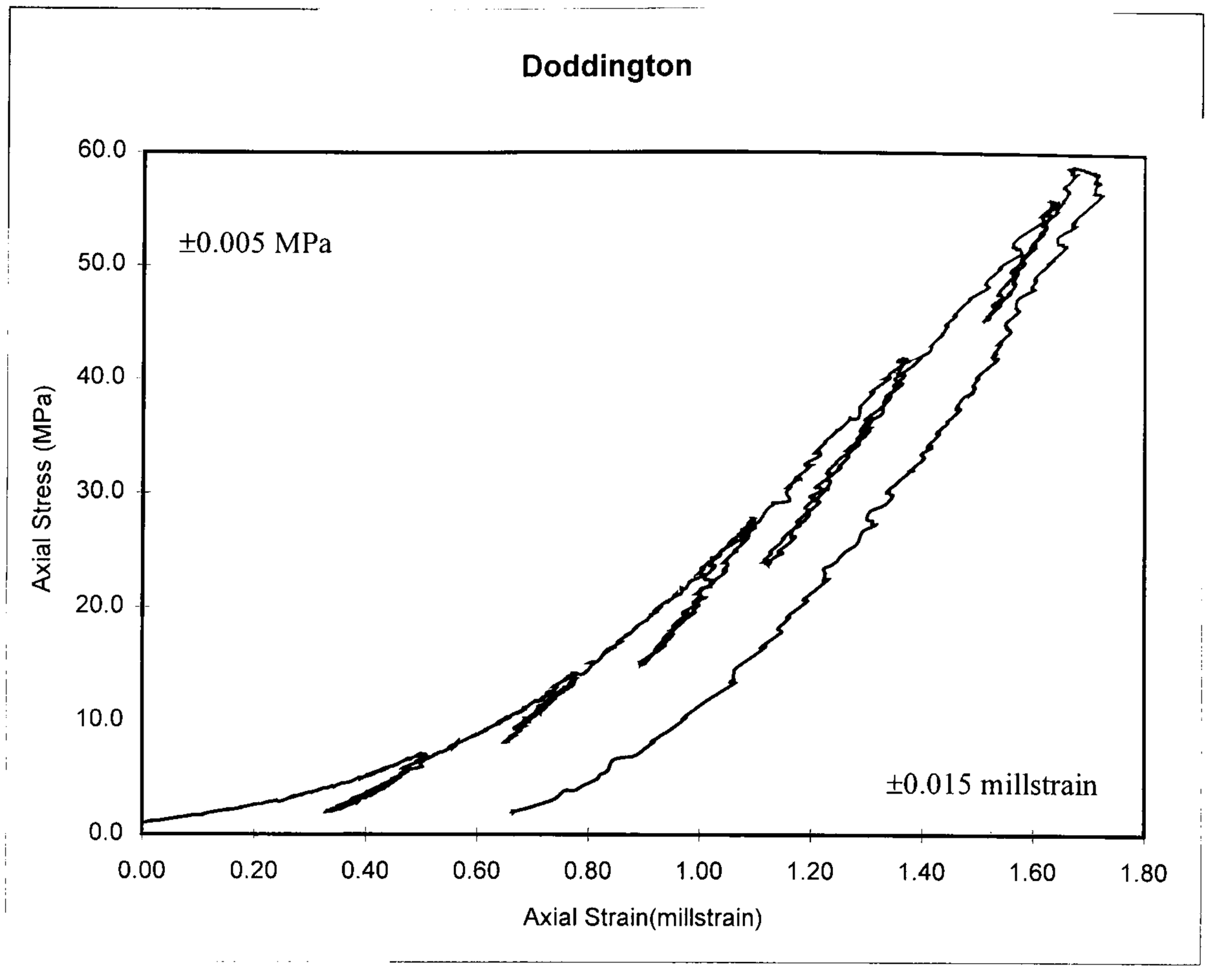

Figure 3.8 Stress-strain curve for a Doddington sample

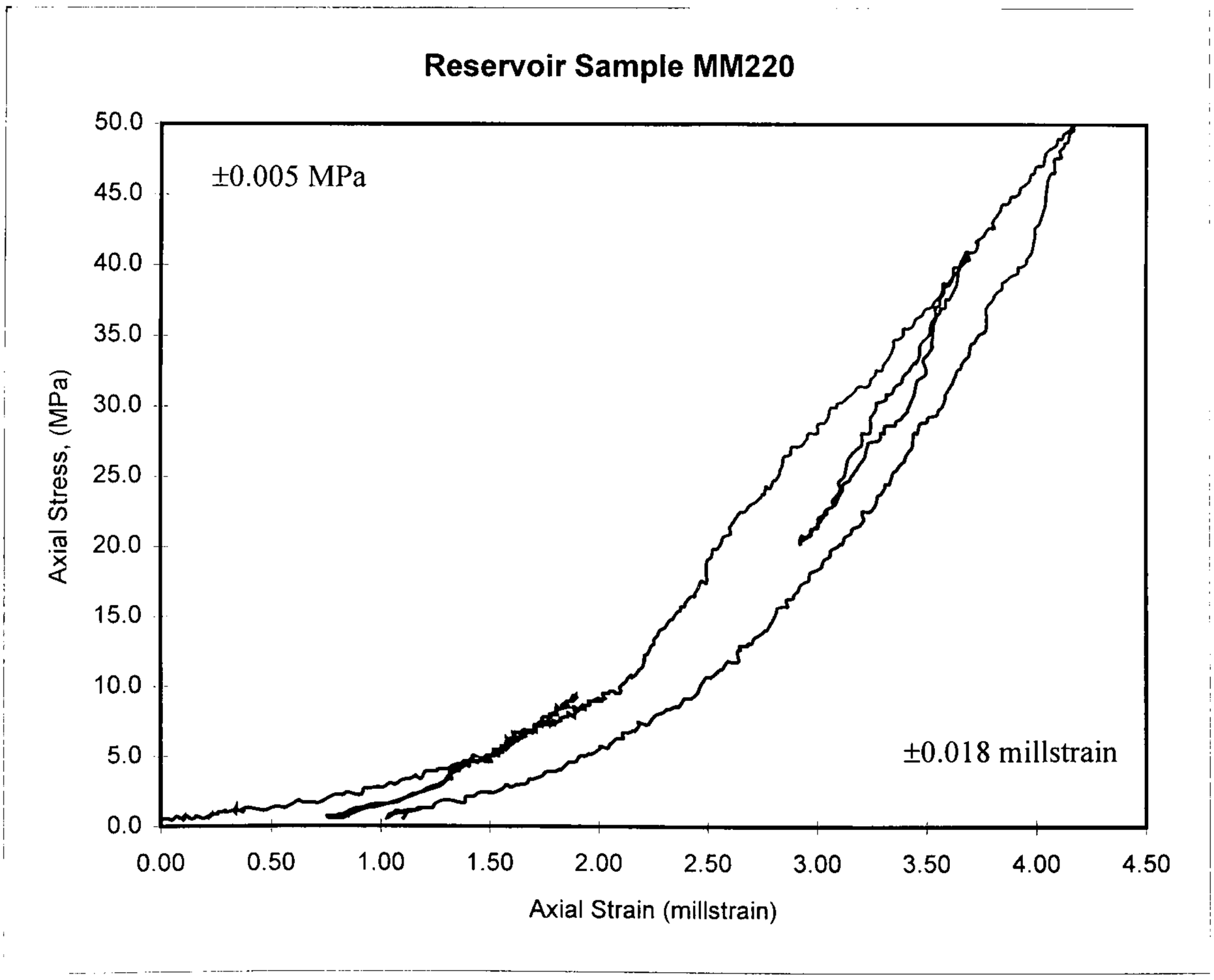

Figure 3.9 Stress-strain curve for a reservoir sample

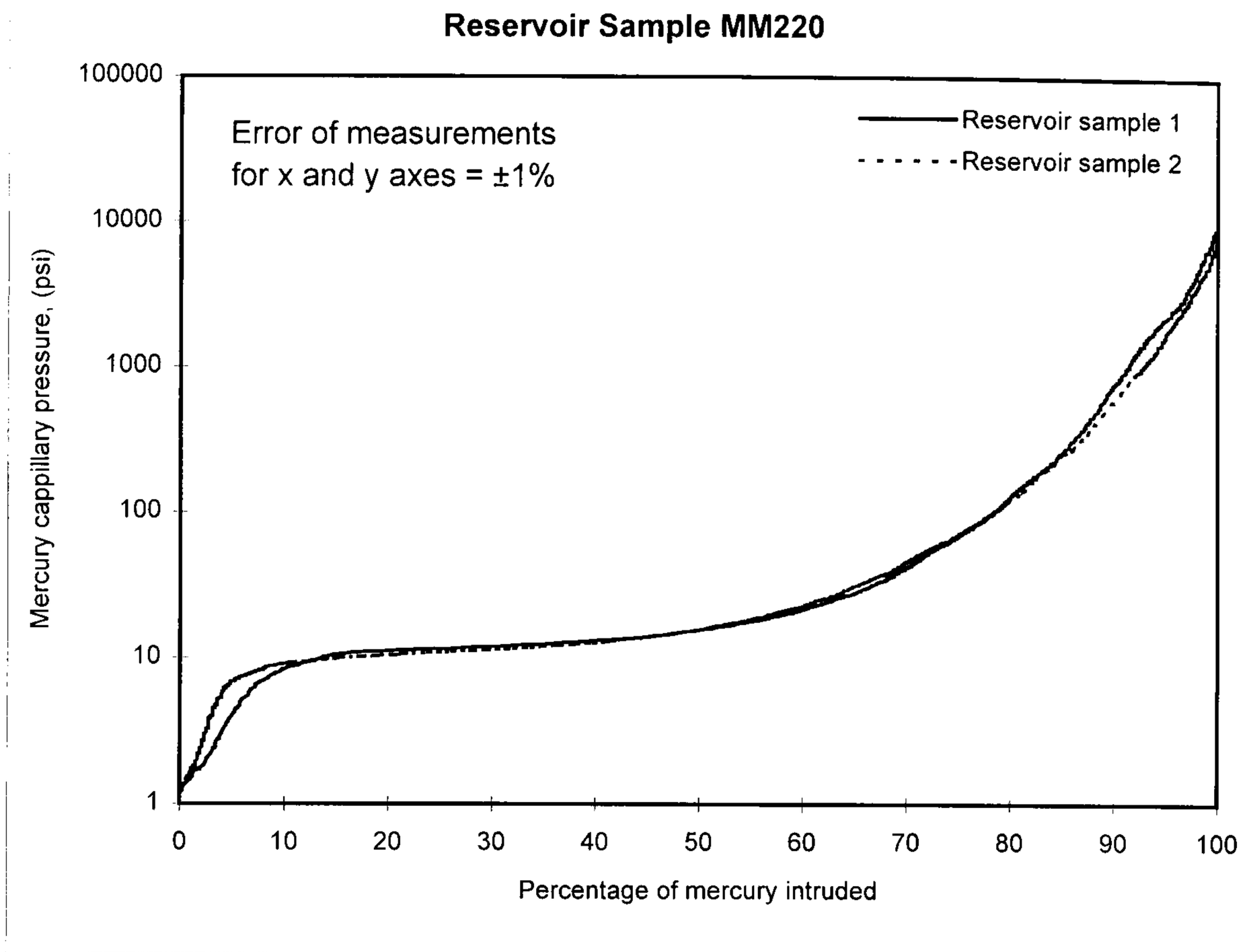

Figure 3.10 Mercury capillary pressure curves for two adjacent reservoir samples

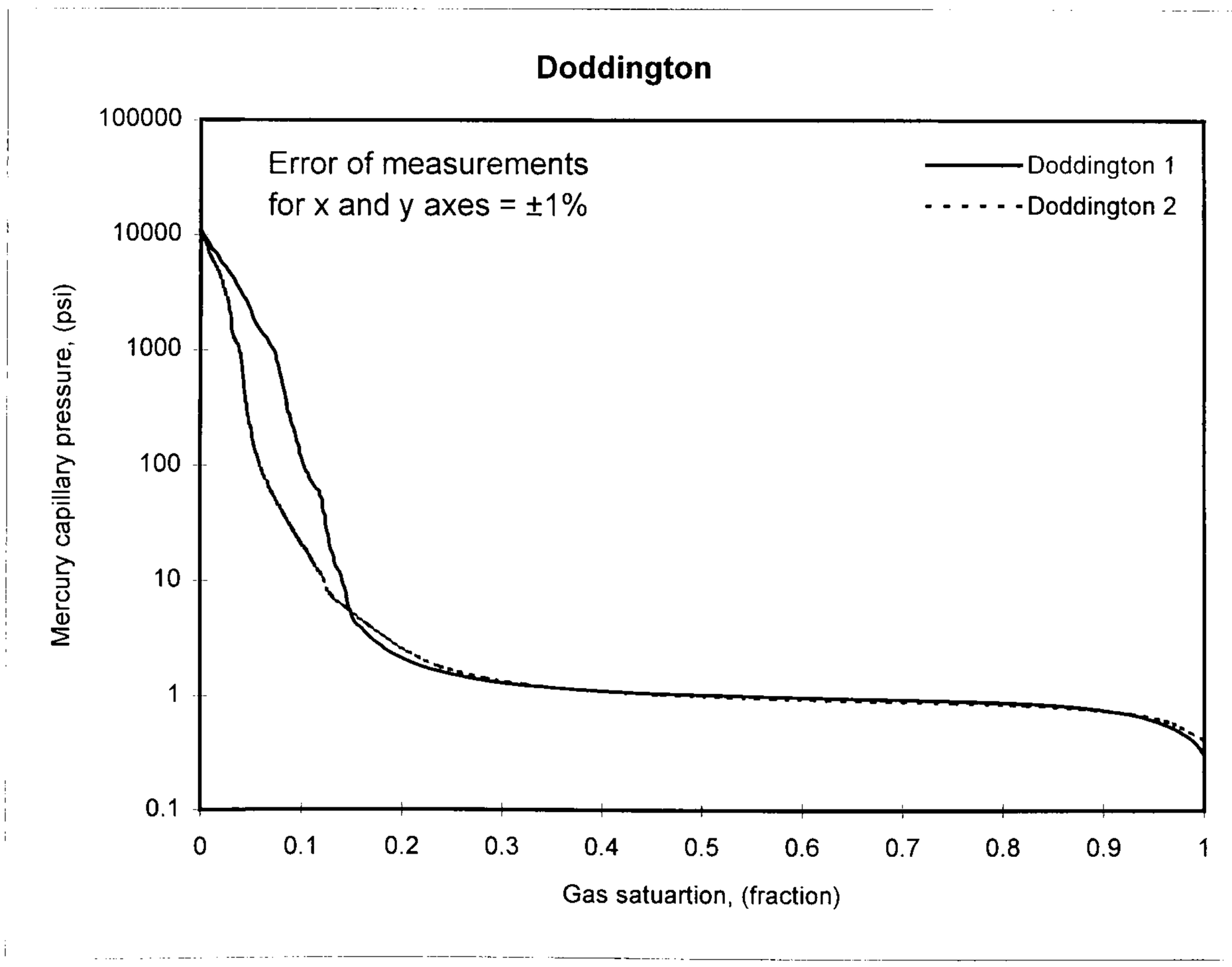

Figure 3.11 Mercury capillary pressure curves for two adjacent Doddington samples

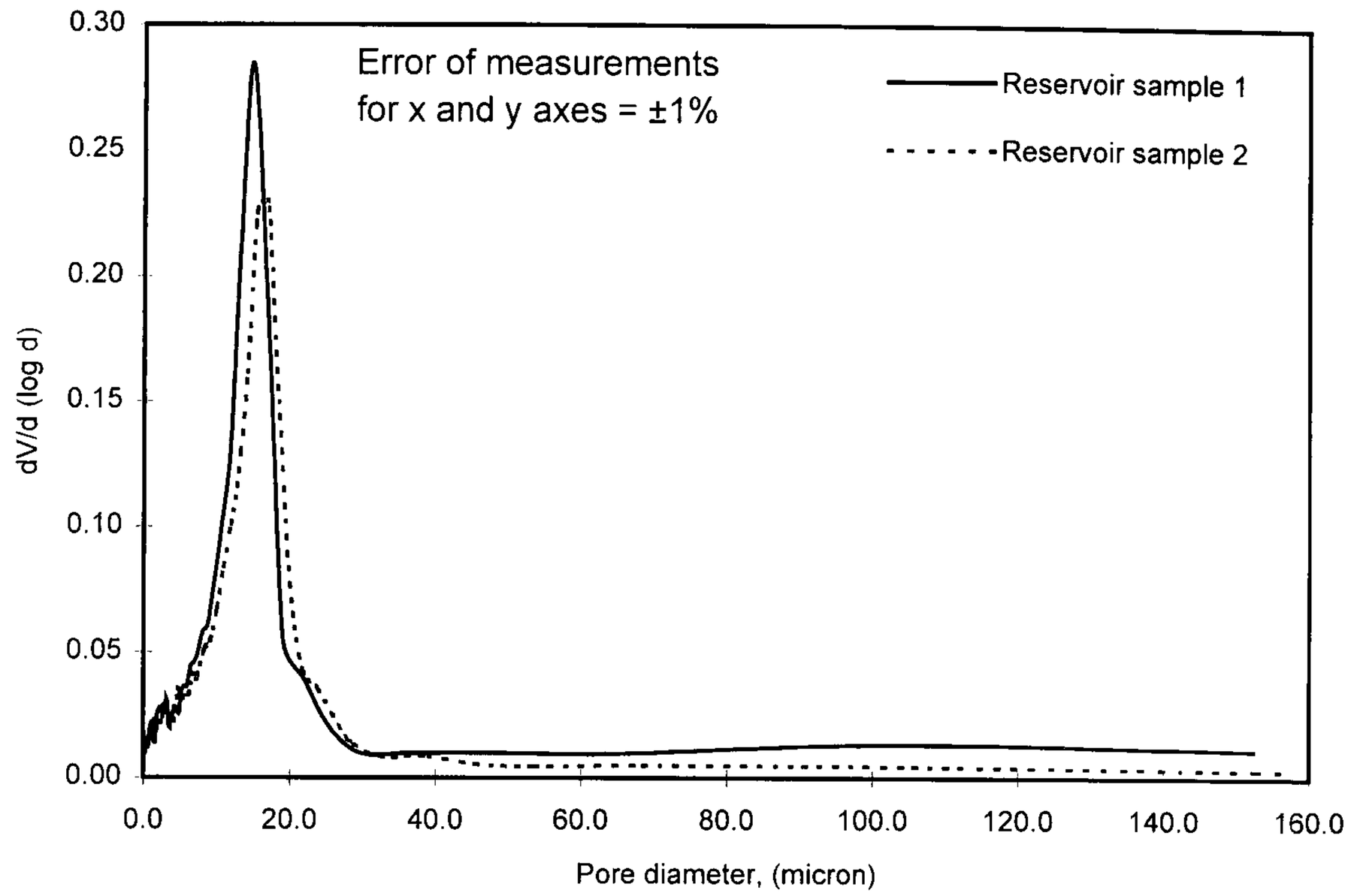

Figure 3.12 Pore size distribution for two adjacent reservoir samples

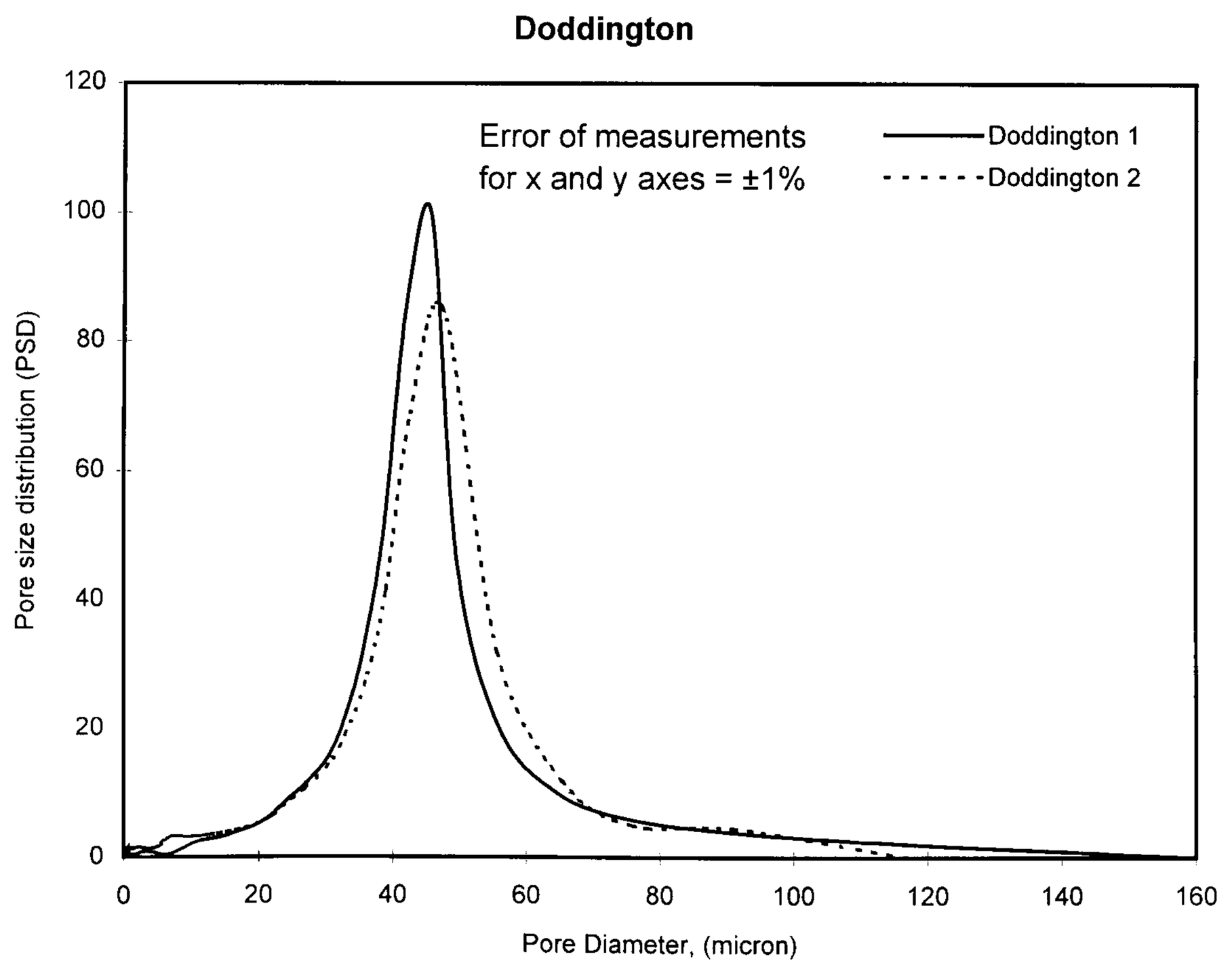

Figure 3.13 Pore size distribution for two adjacent Doddington samples

3.5 Stress Paths for Tests

The experiments conducted in this research are divided into five major categories: effect of pore pressures on permeability, effect of hysteresis and stress on permeability, effect of anisotropy on permeability and resistivity, pore volume deformation, and effect of stress on capillary pressure and electrical properties. The following stress states and stress paths were followed during the experiments in order to study each effect. The highest stress and ratios were selected based on the North Sea oil field experience (Marsden, 1996). Equivalent hydrostatic stress for true triaxial stresses means average of three principal stresses (i.e., $\sigma = (\sigma_1+\sigma_2+\sigma_3)/3$)

Table 3.1 Pore Pressure Effect on Permeability

Stress States	σ_1 **(MPa)**	σ_2 **(MPa)**	σ_3 **(MPa)**
True Triaxial	34.5	27.6	20.7
Triaxial	34.5	27.6	27.6
Equivalent Hydrostatic	27.6	27.6	27.6
Hydrostatic	34.5	34.5	34.5

Table 3.2 Hysteresis and Stress Effects on Permeability

Stress States	σ_1 **(MPa)**	σ_2 **(MPa)**	σ_3 **(MPa)**
True Triaxial	8.60	6.90	5.20
	17.3	13.8	10.4
	34.5	27.6	20.7
	51.8	41.4	31.1
	69.0	55.2	41.4
	86.1	68.9	51.7
Equivalent Hydrostatic	6.90	6.90	6.90
	13.8	13.8	13.8
	27.6	27.6	27.6

	41.4 55.2 68.9	41.4 55.2 68.9	41.4 55.2 68.9

Table 3.3 Permeability and Resistivity Anisotropy

Stress States	σ_1 **(MPa)**	σ_2 **(MPa)**	σ_3 **(MPa)**
True Triaxial	8.60 43.1	6.90 34.5	5.20 25.9
Equivalent Hydrostatic	6.90 34.50	6.90 34.50	6.90 34.50

Table 3.4 Stress Effect on Capillary Pressure and Electrical Properties

Stress States	σ_1 **(MPa)**	σ_2 **(MPa)**	σ_3 **(MPa)**
True Triaxial	43.1	34.5	25.9
Equivalent Hydrostatic	34.5	34.5	34.5

Table 3.5 Pore Volume Change and Resistivity

Stress States	σ_1 **(MPa)**	σ_2 **(MPa)**	σ_3 **(MPa)**
True Triaxial	0.86 1.73 2.59 3.45 4.31 5.18 6.04 6.90 7.80	0.69 1.38 2.07 2.76 3.45 4.14 4.83 5.52 6.20	0.52 1.04 1.55 2.07 2.58 3.11 3.62 4.14 4.66

	8.60	6.90	5.18
	13.0	10.4	7.80
	17.3	13.8	10.4
	21.5	17.2	12.9
	25.9	20.7	15.5
	30.1	24.1	18.2
	34.5	27.6	20.7
	43.1	34.5	25.9
Equivalent Hydrostatic	0.69	0.69	0.69
	1.38	1.38	1.38
	2.07	2.07	2.07
	2.76	2.76	2.76
	3.45	3.45	3.45
	4.14	4.14	4.14
	4.83	4.83	4.83
	5.52	5.52	5.52
	6.21	6.21	6.21
	6.90	6.90	6.90
	10.4	10.4	10.4
	13.8	13.8	13.8
	17.2	17.2	17.2
	20.7	20.7	20.7
	24.1	24.1	24.1
	27.6	27.6	27.6
	34.5	34.5	34.5

3.6 Procedure

3.6.1 Introduction

The following experimental procedures were followed during the experiments (see Figure 3.14) and single and two phase measurements were conducted under hydrostatic, triaxial and true triaxial stresses.

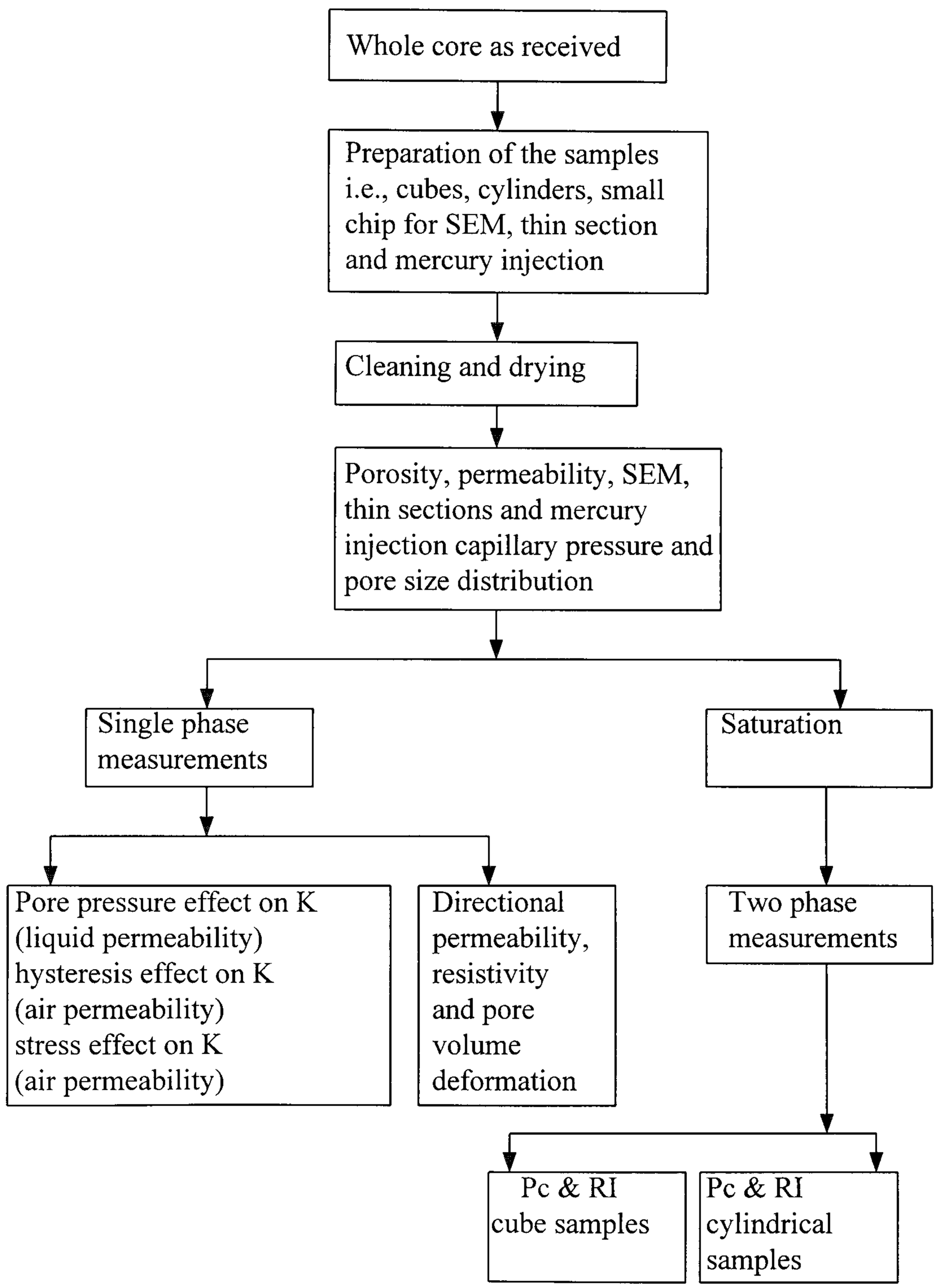

Figure 3.14 Flow chart showing the experimental programme

3.6.2 Sample Preparations and Characterisation

Preparation of rock samples

Cubic rock samples were cut from whole core or large blocks, using diamond saws, to a size slightly larger than 40 mm. The cubic samples were finally prepared to a size of 40.5 mm using a precision tool room diamond wheel grinder. The cylindrical plugs were diamond cored to 38 mm diameter and approximately 70 mm in length. All samples were carefully prepared with well defined dimensions. The end faces of the cubes and cylindrical samples were finished using the diamond wheel grinder to achieve good contacts between platens and rock samples and, between the rocks and current electrodes. For outcrop cores and reservoir samples, a 2% brine was used for coring. The table listing basic rock properties is included in appendix A.

Cleaning and Drying

The cleaning and drying procedures were as suggested by the Society of Core Analysts (Worthington *et al.,* 1990). After coring the plug samples were loaded into a Hassler cell and, cubic samples in true triaxial rig. Confining pressure of 250 psi in Hassler cell and approximately 400 psi in true triaxial rig was applied and a pump was connected to the inlet of the core holder. Approximately 20 pore volumes of methanol were pumped at a low flowrate in order to clean the core. Once enough pore volumes had been flushed through the core, air was flushed to displace the methanol. The above procedure was repeated with the flow reversed in order to ensure complete cleaning.

For the reservoirs sample, a 2% brine was used for flushing at a very low rate to reduce the concentration of the formation brine. A Soxhlet extractor was used for cleaning. Toluene was used first to remove any oil, then flushing fluid was then changed to Methanol to remove the brine in the sample and the effluent was continuously spot-tested with Silver Nitrate until no white precipitate was observed. The samples were then placed in a vacuum oven for 48 hours at a temperature of 80° C, and were then stored in a vacuum desicator until needed for testing. Special cleaning and drying procedures need to be followed if the reservoir cores contain delicate (sensitive) clays. Full procedure is well documented by Lerner *et al.* (1990).

Porosity and Permeability Measurements

There are various methods for determining porosity (Amyx, *et al.,* 1960). In this research, the Boyle's law Helium gas expansion porosimeter was used for grain volume measurement. The bulk volume was determined by measuring the dimensions of the core with a digital vernier.

The Helium gas expansion method porosity was calculated by :

$$\phi = \frac{V_p}{V_b} = \frac{V_b - V_s}{V_b} \tag{3.2}$$

where :

ϕ = porosity, fraction

V_p = pore volume, cm^3

V_b= bulk volume, cm^3

V_s = grain or solid volume, cm^3

However, for cubic samples, porosity was calculated by the using the difference between saturated and dry weight. The porosity of cubic samples was compared with duplicate adjacent cylindrical samples, and porosity was calculated by :

$$\phi = \frac{\text{(saturated weight - dry weight) / fluid density}}{\text{Bulk volume}} \tag{3.3}$$

Permeability can be measured using either gas or liquid as the flowing phase, based on Darcy's law. When gas is used to measure permeability a correction for the gas slippage (Klinkenberg correction) must be applied especially for low permeability cores.

If liquid is the flowing phase then

$$k = \frac{q\mu}{A\frac{dp}{dl}} \tag{3.3}$$

where :

q = flow rate, cm^3/s

A = cross sectional area, cm^2

μ = viscosity, cP

k = permeability, Darcy

$\frac{dp}{dl}$ = potential gradient, atm/cm

If gas is the flowing phase then

$$k_g = k_l\left[1 + \frac{b}{p_m}\right] \tag{3.4}$$

where :

k_g = gas permeability

k_l = liquid permeability

P_m = mean pressure at which the gas is flowing

b = constant for a given gas in a medium

Klinkenberg (1941) suggested that a plot k_g versus $1/P_m$ should yield a straight line with an intercept of k_l, which is the permeability of the medium to a single liquid phase.

In the experiments of hysteresis effect on permeability, permeability was measured during loading and unloading cycles. In the experiments of pore pressure effect on permeability, the stress was kept constant and the pore pressure was varied. At each pore pressure point the permeability was measured. A Hassler cell permeameter was used to measure permeabilities of the cylindrical samples, using nitrogen as flowing medium.

SEM (Scanning Electron Microscope), Thin section and Mercury Injection

For detailed investigation of the rock fabrics SEM, thin section and mercury injection were carried out. SEM at different magnifications were conducted to understand the pore scale characteristics. Thin section analysis was performed in order to provide geological description of the samples. Mercury injection tests were performed to characterise the pore size distribution of the samples. In addition, the mercury injection was used to estimate the entry pressures for the adapted porous plate capillary pressure measurements.

3.6.3 Single Phase Measurements Under Hydrostatic and True Triaxial Stresses

Pore Pressure Effect on Permeability

The clean dry cubic samples were saturated with a 5% brine solution. A pre-moulded rubber jacket was inserted between the edges of the platens to isolate the cubic sample from atmosphere so that pore pressure could be applied. The cube was then inserted between the loading platens. An initial stress of 2 MPa was applied all round the sample, then the flow lines were connected and the sample was flushed with brine to remove the air in the system. The stress was applied gradually until the desired stress of 34.5 MPa (see Table 3.1) was reached. If the stress state was hydrostatic then all three principal stresses were increased equally, otherwise the ratios of 1:0.8:0.6 for major:intermediate:minor were maintained for true triaxial stress tests.

Equilibrium at the desired stress was reached when there was no measurable change to brine volume and resistance. A gas volume accumulator with pressure regulators was used to generate and maintain pore pressure in the fluid. The pore pressure was increased to the desired value and the sample was left to reach steady state flow. The time of equilibrium depended on permeability of the sample. The upstream and downstream pressures were recorded using pressure transducers and digital indicators. A flow rate was obtained using a volumetric burette. Darcy's law was used to calculate liquid permeability, and the pore pressure was then increased to the next value and the test repeated for a new permeability value.

Hysteresis and Stress Effects on Permeability

A similar procedure to above was followed during the loading of the cubic sample. In these experiments, Nitrogen gas was used as the flowing fluid at a low pore pressure of around 0.69MPa. The stress was increased gradually in steps of around 6.9 MPa until 69 MPa was reached (see Table 3.2). The experiments were conducted during loading and unloading cycles. At each stress, the upstream and downstream pressures were recorded using pressure transducers and digital indicators. A volumetric flow meter was used to record flow rate, and Darcy's law was again used to calculate gas permeability. The experiments were performed under hydrostatic and true triaxial stresses.

Pore Volume Change

Pore volume change was measured by recording the volume of brine displaced when stress was applied. Both volume and resistance were recorded at every stress increase on the cubic sample until a desired level was reached. A small stress of around 3 MPa all round the sample was applied, then all the flow lines were connected and the sample was flushed with brine to remove the air in the system. The stress was increased gradually in steps of around 0.69 MPa until 6.9 MPa, then in steps of 6.9 MPa until 34.5 MPa was reached (see Table 3.5). At each stress step, the volume and resistance were recorded. The experiments were performed under hydrostatic and true triaxial stresses.

Permeability and Resistivity Anisotropy

Permeability and resistivity measurements were conducted in three principal directions. The cubic sample was rotated and the directional properties were measured. The cubic sample was designated with three principal directions x, y and z. The sample was loaded, flushed to remove air, and the stresses were applied gradually to 34.5 MPa (see Table 3.3). In these experiments 5% brine solution was used as flowing fluid, with a low pore pressure of around 0.69 MPa. The permeability was calculated in a similar manner as above, and resistance was recorded. Once one directional measurement had been performed the stresses were reduced gradually. The sample was unloaded, rotated and reloaded again. The stresses were also rotated and applied gradually again. Once the equilibrium was reached, the permeability was calculated for another direction in a similar manner, and resistance was again recorded. For the third principal direction, the procedure was repeated.

The experiments were performed under hydrostatic and true triaxial stresses. The measurements of directional permeability and directional resistivity in the cylindrical samples in the two directions x, z were conducted using a Hassler cell, the samples having been cored horizontally and vertically from the whole core.

3.6.4 Two Phase Measurements Under Hydrostatic Stress

The following steps were followed during the capillary pressure and resistivity measurements under hydrostatic stress (see Figure 3.15). The multi-sample rig and cylindrical samples were used during the measurements.

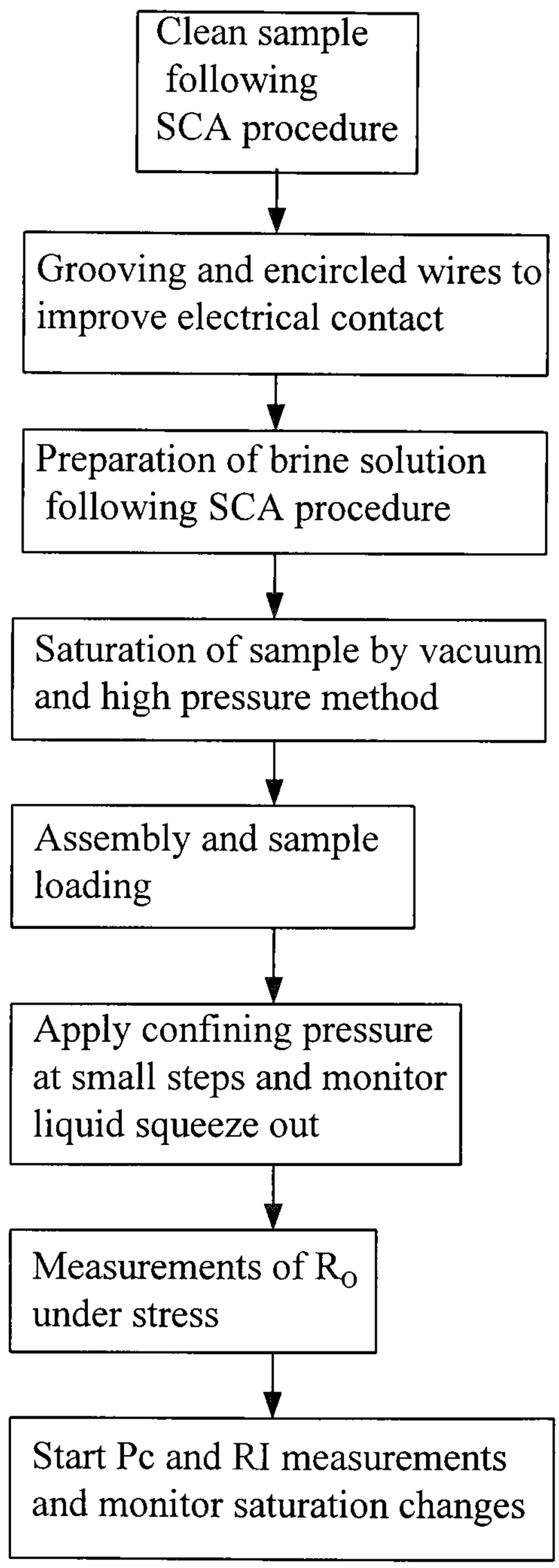

Figure 3.15 Flow chart of the experimental programme under hydrostatic stress

Grooving and encircled wires

The cylindrical rock sample was grooved around its circumference using a centre lathe, and a diamond cutting wheel. The grooves were about 0.25 mm in depth, so that half of the 0.5 mm wire would touch the pin of the Viton sleeve, the grooves were spaced at 12.5 mm along the core. The wire electrodes were wrapped firmly with very fine porous stainless steel mesh in order to increase the surface area of the contact.

Preparation of brine solution

The brine solutions (NaCl brine solution) were prepared using measured masses or volumes of the components as suggested by the Society of Core Analysis (Worthington *et al.,* 1990).

Saturation

For two phase measurements of capillary pressure and resistivity index, vacuum saturation and high pressure techniques were used as recommended by Society of Core Analyst (SCA) (Maerefat *et al.,* 1990). The sample saturation was checked by weighing the sample after saturation, and if the sample was not fully saturated then the high pressure saturation cell was again used.

Assembly and Loading

The following procedures were followed during loading of the sample under hydrostatic stress. Once routine measurements had been completed and the sample had been fully saturated and wires placed into its grooves, it was loaded into the multi-electrode Viton sleeve. Filter papers were placed at the end faces of the core sample, both saturated with brine. Resistance measurements were performed to check contacts between electrodes and wires along the core sample, and adjustments were made until satisfactory contact was established. The end platens were removed and saturated porous ceramic discs were put in place. The oil wet disc had been saturated with oil, and the water wet disc with an appropriate brine. The discs were tested in the Hassler cell to observe if there was any flow at a differential pressure of 1 psi. The water wet disc was placed on the top of the rock sample, labelled as A. The

stems and platens were filled with the appropriate fluid and clamped off. Later, a small tube was inserted inside stem with appropriate fluid to displace air. The disks were treated with care, avoiding forcing oil through the water wet side and water through the oil wet side. Two stainless steel inlet and outlet end platens were located into the multi-electrode Viton sleeve, then the sleeve, discs, platens and core were loaded into the cell body (i.e., the pressure vessel).

The bottom side was closed with an end cap, and the cell was filled with confining oil. Once the vessel was almost full the top cap was closed. The valve at the top was closed and the pressure vessel was connected to the hand pump at the bottom. Oil was pumped into the cell until all the air was displaced out, and the pore pressure unit was connected to both ends of the sample. The resistance measurements were taken for a reference. The bottom side of the cell (oil wet side) was closed and the top side (water wet side) was fully opened to allow brine to squeeze out. This procedure was reversed when the core contained mobile oil only.

Confining pressure was applied to a base line of around 2.76 MPa (400 psi). Resistance measurements and phase angle ($\theta < 2\text{-}3^{\circ}$) measurements were taken as base line data. The confining pressure was increased to the required level in small pressure steps to allow squeeze out, and resistance and volume measurements were taken at each pressure step. The measurements of resistance and volume at the final confining pressure were used as the base line data for the analysis, and the squeeze out data were used for pore volume corrections.

Measurements of R_o

Both the two and four electrode measurements of R_o were carried out on the sample at various confining pressures during squeeze out. The measurements were performed before the first point of capillary pressure was applied. In the two electrode measurement method the platens were used both as current and potential electrodes, and in the four electrodes method the platens were used to introduce the current into the core with the potential difference being measured across any two potential electrodes along the sleeve. By using Archie equations the formation factor

(F), cementation factor (m) and resistivity of the fully saturated sample (R_o) was calculated.

First Sw-decreasing test

The displacement test commenced with zero back pressure. The oil phase at 1-3 psi (depending on sample k) was increased, and fluid movement both in and out was monitored. If flow was observed, a back pressure was applied gradually through the interface unit connected to the brine side while maintaining a constant capillary pressure at a pre-selected level. The maximum pore pressure applied was 0.21 MPa (30 psi). The fluid movement and resistance changes were monitored, and when flow continued this was taken as the start of the drainage cycle.

The resistance and volumetric equilibrium was monitored usually daily for every capillary pressure point over 4 to 5 days to a maximum of few weeks. Once the fluid movement and resistance changes were observed then this was taken as the first Sw-decreasing test. The pressure in the oil side was gradually increased in steps from 0.21 MPa (30 psi) to 0.48 MPa (70 psi) while keeping the back pressure of 0.21 MPa (30 psi) in the outlet side. The resistance, capillary pressure and volume measurements were monitored and recorded at each equilibrium point. The equilibrium point was taken to be when there was no change in the resistance or volume. The average brine saturation was determined volumetrically from the displaced brine entering the glass burettes between one capillary pressure point to another. The capillary pressure and resistivity saturation curves were determined for the drainage cycle.

First Sw-Increasing test

When the capillary pressure curve approaches the asymptotic value (i.e., there was no change of saturation for every capillary pressure increase) then this was taken as the end of first Sw-decreasing test. The brine was then re-introduced into the sample by reducing the oil phase pressure in steps (i.e., spontaneous imbibition). The oil phase pressure was reduced until capillary pressure was zero, whilst keeping the back pressure at 0.21 MPa (30 psi). The brine phase pressure were gradually increased in

steps from 0.21 MPa (30 psi) to 0.48 MPa (70 psi) (i.e., forced imbibition). The capillary pressure and resistivity saturation data were monitored at each capillary pressure equilibrium, and average water saturation was calculated as before. The capillary pressure and resistivity saturation curve were generated for the imbibition.

Second Sw-decreasing test

When the brine phase pressure reached the irreducible oil saturation, Sor (i.e., residual oil saturation) this was taken to be the end of the first Sw-increasing test. The brine phase pressure was reduced in steps and the oil was re-introduced into the sample. Firstly, the brine phase pressure was reduced until zero capillary pressure was achieved whilst keeping a back pressure of 0.21 MPa (30 psi) and, secondly, the oil phase pressure was gradually increased in steps from 0.21 MPa (30 psi) to 0.48 MPa (70 psi) (i.e., forced drainage). The capillary pressure and resistivity saturation curve were generated for the forced drainage.

Monitor brine saturation distribution

Six potential electrodes positioned at equal distances along the rock sample were used to monitor the saturation distribution along the core. This was necessary for determination of the reliable saturation exponents from the electrical resistivity measurements. The interval saturation was plotted against resistivity index, and from this plot it could be seen if there was an uneven saturation distribution or an end effect. If a correction for local saturation levels is necessary, this was determined from the resistivities measured at each potential electrode following the procedure described by Elashahab (1995).

3.6.5 Two Phase Measurements Under True Triaxial Stress

The following steps were followed during the capillary pressure and resistivity measurements under true triaxial stress. The sample was cleaned and saturated by following SCA recommended procedure. The sample was assembled and loaded into the true triaxial stress loading system.

Assembly and Loading

The top and bottom platens were loaded with the water wet and oil wet ceramic disks respectively. Rubber/plastic epoxy was used to seal the ceramic disks and wires were inserted into selected flow lines to establish electrical contact between the sample and the electrodes. On the surface of the sample a porous metallic mat was used to increase flow distribution and create large surface area for the current to flow. The procedure for loading the sample was the same as that for the permeability measurements. All the flow lines were connected and any air was displaced from the system. The stress was increased to the required level in small steps to allow squeeze out, and the resistance and volume measurements were taken at each stage. The measurements of resistance and volume at the last confining pressure were used as the base line for analysis of the data and the squeeze out data, were used in pore volume corrections.

The three principal stresses were applied at small increment and squeeze out of liquid was monitored (see Table 3.4). The resistivity of the fully saturated sample was measured at stress. Capillary pressure and resistivity measurements were started, and saturation changes were monitored.

Measurements of R_o

Only two electrode measurements of R_o were carried out on each sample in this part of experiments. The measurements were performed before the first point of capillary pressure was applied. The Archie equations were used to obtain values for formation factor (F), cementation factor (m) and fully saturated resistivity (R_o).

Capillary Pressure and Resistivity Index

For capillary pressure and electrical properties measurements, similar procedures to those used in the hydrostatic tests were followed, but true triaxial stresses were applied.

CHAPTER 4

EFFECTS OF PORE PRESSURE, HYSTERESIS AND TRUE TRIAXIAL STRESS ON PERMEABILITY

4.1 Introduction

All producing hydrocarbon reservoirs are subject to the earth's stress field and to any regional tectonic movements. In addition, the production of fluids from a reservoir formation reduces its pore pressure such that there is an increase in its effective stresses, and dynamic changes can also occur to the horizontal field stresses as a consequence of partial or total lateral restraint to the rock mass. Similarly, the injection of water into a reservoir during water flooding, or gas injection during pressure maintenance, can alter the rock stresses in a similar dynamic manner. Thus reservoirs are dynamic systems that are constantly changing during their geological evolution and later during their production history. Production from a reservoir can reduce the pore pressure, increasing the effective stresses, and changing the three dimensional effective stress field. Since such changes can lead to hysteresis and permeability modification throughout the life of the reservoir, an understanding of such phenomena are of fundamental importance to reservoir performance prediction and reservoir management.

Conventional laboratory methods for studying permeability under simulated reservoir conditions involve hydrostatic stresses, or sometimes anisotropic triaxial loading in which two of the principal stresses are equal. However, such hydrostatic and triaxial conditions are very rarely encountered in hydrocarbon reservoirs, and true triaxial stresses are more representative of actual behaviour encountered in the field. This limitation not only affects significantly the strength and deformation characteristics of reservoir rocks, it can also be of significance when considering transport characteristics such as permeability, electrical permeability and ultrasonic wave propagation. Although previous investigators have utilised true triaxial stresses on cylindrical and prismatic samples, such studies have been somewhat restricted by the

limited deviatoric stress magnitudes which could be achieved with these test systems. This is a major limitation when one needs to consider the highly deviatoric polyaxial stresses in proximity to a wellbore, or where significant changes to horizontal field stresses occur as pore pressures change. In this investigation, laboratory equipment was developed which can apply the three principal boundary stresses independently using cubic samples, loaded in closed-loop control, and which can achieve deviatoric stresses in excess of 200MPa and pore pressures to 145MPa. Under such conditions, the equipment permits measurements of various petrophysical and geophysical properties such as permeability to single- and multi-phase fluids (i.e., relative permeability), electrical conductivity, capillary pressure, as well as mechanical parameters such as strength and deformability. Figures 4.1 shows a schematic diagram of an anisotropic stress field in the reservoir and its representation during laboratory measurements of petrophysical properties.

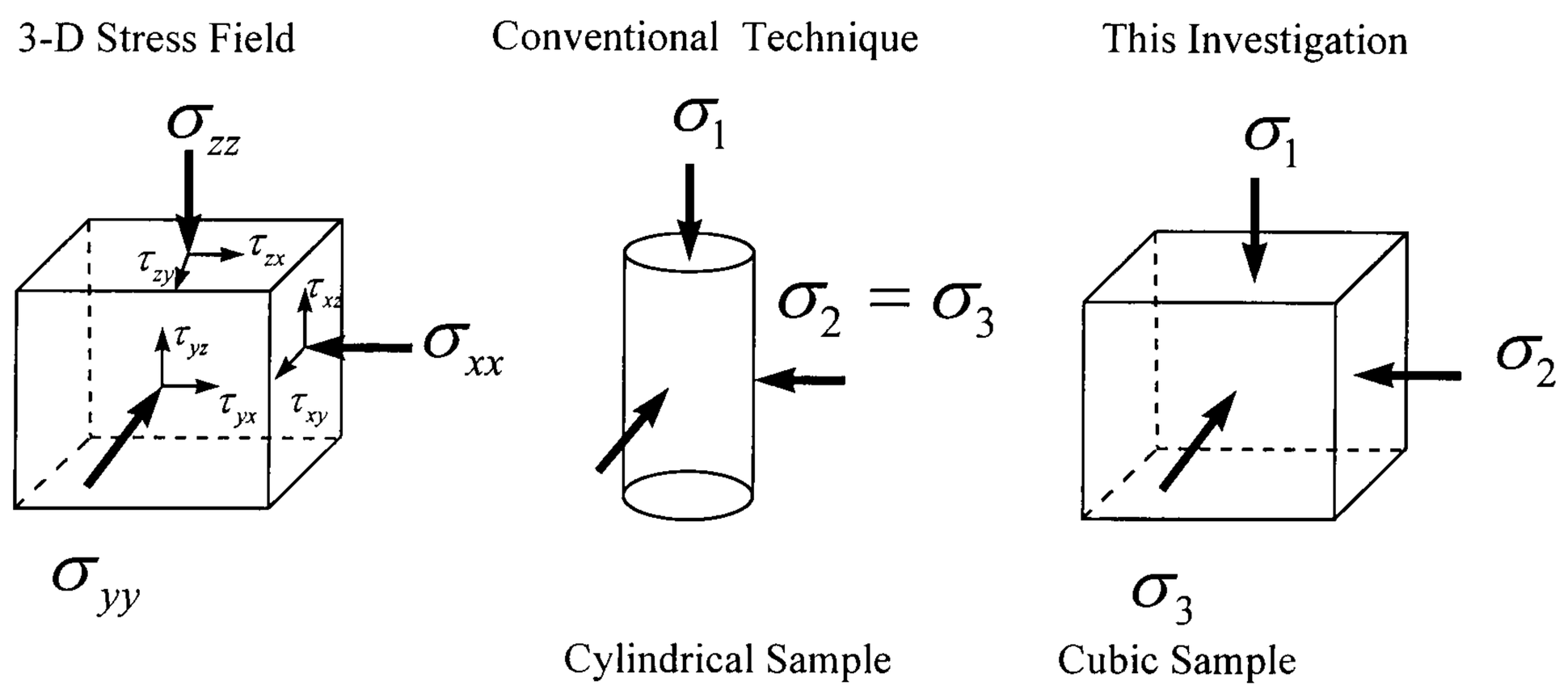

Figure 4.1 Isometric representation of 3-D stress field and its representation in the laboratory experiments

This chapter reports on the new experimental set-up and the work carried out to examine the effects of pore pressure changes under hydrostatic, triaxial and true triaxial stress conditions. The study has also investigated hysteresis and compression effects on permeability under hydrostatic and true triaxial stress conditions. In particular, the main objectives of the experimental work were to investigate how anisotropic stresses and pore pressures might influence permeability and the prediction of production-induced changes to the reservoir (i.e., to simulate the

reservoir depletion under different stress-paths), to investigate permeability hysteresis under *in situ* stress conditions, to integrate rock mechanics with the important petrophysical property of permeability, and to compare data obtained under different stress conditions (i.e., routine laboratory tests at hydrostatic stresses versus tests undertaken at true triaxial stresses).

The results have shown the importance of petrophysical measurements under true triaxial stress conditions and have highlighted some important implications with regard to the management of stress-sensitive reservoirs.

Pores in reservoir rocks are always subjected to two types of stresses; internal and external. The internal stresses are caused by fluid pressures and the external are the result of the overlying and surrounding formations. The production of fluids from a reservoir results in reductions to the internal pressures in the formations, causing the rocks to compact as a consequence of the increased effective stresses. Transport properties, such as permeability and electrical conductivity, are therefore modified during production. Studying combined effects of pore pressure, hysteresis and true triaxial stress in representative laboratory experiments will enable a more reliable interpretation of the behaviour of hydrocarbon reservoirs during depletion or repressuring.

The main focus of this chapter is to assess the impact of dynamic permeability changes on the reservoir performance forecasting during field production life (i.e., how the permeability changes with reservoir depletion). Stress-paths that a reservoir may experience during depletion have been simulated in laboratory experiments. Initially, measurements of permeability with pore pressure were carried out, after which permeability hysteresis in analogue sandstones from outcrops was then investigated under true triaxial stresses in order to identify major effects associated with loading and unloading cycles. Analogue sandstones from four Carboniferous outcrops and reservoir samples from the South of Oman were tested. Oriented cubic samples were prepared adjacent to each other, from single blocks of each material, in order to minimise any effects associated with heterogeneity and anisotropy.

A series of experiments were conducted on analogue sandstones from four Carboniferous outcrops as well as reservoir samples, i.e., Croslands Hill, Springwell, Stainton, Doddington and MM220 sandstones. The details of the samples can be found in the appendix A. Samples of each material were subjected to hydrostatic boundary stresses (35 MPa), triaxial stress ratios of 1.0:0.8:0.8 (35:28:28 MPa), and true triaxial principal stresses in the ratio of 1.0:0.8:0.6 (35:28:21 MPa) for the major:intermediate:minor stresses. The true triaxial ratios are based on North Sea field experience (Marsden, 1996). Initially, the pore pressure was varied and permeabilities to a 5% aqueous solution of NaCl were measured at different stress conditions, using the pressure accumulator to deliver and maintain the desired pore pressure. A pressure regulator was used to change the upstream pore pressure, and a back pressure regulator was used to control flow rate and to maintain the required pressure differential across the sample. Measurements of gas permeability were then made on matching samples, again under the hydrostatic (6.8 to 68 MPa) and true triaxial stress ratios of 1.0:0.8:0.6 (6.8 to 68 MPa). These tests included loading and unloading cycles with constant pore pressures.

4.2 Effect of Pore Pressure on Permeability under Different Stress Paths

Pore pressure is the pressure of the fluids in the pore space. In hydrocarbon reservoirs the effective stress is the difference between total stress and some fraction of the pore pressure. The ordinary effective stress is given by

$$P_e = P_t - \alpha P_p ,$$

where

P_e = effective stress, P_t = total stress, P_p = pore pressure, and α = Biot constant, often assumed to be near-unity and it depends on compressibility (Biot, 1955).

The mechanisms causing the dependency of permeability on the pore pressure and the stress state are as follows (Osorio *et al.,* 1997) :

1. fluid production/injection causes changes in the pore pressure,
2. during production, pore pressure changes cause variations in the *in situ* stresses and rock deformations,

3. *in situ* stress changes and rock deformations cause variations in the reservoir permeability.

The effect of pore pressure change on permeability is often considered to be negligible so that permeability is approximated to be a constant throughout production life of the reservoir, but is this assumption reasonable? How does pressure decline due to production affect the transport properties of permeability and electrical conductivity? All the above questions relate to the influence of pore pressure on permeability and electrical conduction during life of hydrocarbon reservoir. A series of experiments were conducted on Springwell, Croslands Hill, Stainton and reservoir sample sandstones. Samples of each material were subjected to hydrostatic boundary stresses (35 MPa), triaxial stress ratios of 1.0:0.8:0.8 (35:28:28 MPa), and true triaxial principal stresses in the ratio of 1.0:0.8:0.6 (35:28:21 MPa) for the major:intermediate:minor stresses based on the North Sea experience.

The effect of pore pressure on permeability is illustrated in Figures 4.2 through 4.5, which show normalised permeability (with respect to the highest permeability measured for the sample, at highest pore pressure) versus pore pressure for different stress states. Note that horizontal axes of these figures show a decrease in pore pressure in order to indicate the mechanisms of reservoir depletion. The results show similar trends, as pore pressure decreases the permeability decreases for all the rocks tested. Al-Harthy *et al.,* (1998a) observed similar behaviour as the pore pressure decreases the permeability decreases under different stress states. The following observations were made from the samples tested :

1. The tests indicate that there is a reduction of normalised permeability as the pore pressure decreases, corresponding to the increasing effective stresses. This behaviour is consistent with all test results. Under hydrostatic loading (i.e., conventional test procedure followed by the petroleum industry) the permeabilities of the sandstone rocks decrease with increasing effective stress. However, under corresponding true triaxial stress the permeability is higher. For Croslands Hill, Springwell, Stainton and reservoir sample MM220 sandstones the

reduction is around 35% to 60% when pore pressure was varied from 13.8 MPa to 0.69 MPa depending on the sample permeability. This is due to reduction in pore size and closure of pores caused by the increased stress.

2. The results also indicate that for all the rock samples tested there is less of a reduction in permeability when the samples are subjected to true triaxial stresses than when they are subjected to comparable hydrostatic or triaxial stresses. This indicates that the effect of pore pressure on permeability is stress-states dependent. As the stress states change from hydrostatic to true triaxial stress, the reduction in permeability with reduction in pore pressure became less and less. The maximum difference at the lowest pore pressure was around 10%. Despite the slight aberration in the decreasing trend, seen at around 6.9 MPa pore pressure in Figure 4.2 for the Springwell sandstone, a gradual decrease was seen in the normalised permeability for all the sandstones tested. Note that the experiments were repeated for two samples of the Springwell sandstone, both yielding the same behaviour at about 6.9 MPa and thus indicating that the behaviour is an intrinsic characteristic of the rock and is not an attribute of the testing system. It is believed that the behaviour may be a result of microcracks within the material, which open when the effective stress is low and close when it is high. Hence, the experimental data have so far confirmed the variations of permeability with pore pressure and effective stress, and that stress-path dependency has been observed. This could be explained by the argument that grain-grain contacts were strong and little compression occurred in the pores and connected passages under true triaxial stress. Hence the change of permeability was smaller in an anisotropic stress field than in an equivalent hydrostatic stress field.
3. The laboratory results simulating reservoir depletion for different stress states conditions (see Figures 4.2 through 4.5) demonstrated that dynamic permeability changes evolve during pore pressure drawdown. This should be considered in reservoir flow simulation where permeability is considered to remain constant with time and production.
4. There is correlation between air permeability and the degree of permeability reduction. A greater degree of reduction occurs in low permeability samples than

in high permeability samples. The reduction is around 60% for Springwell and Croslands Hill, and 35% in the reservoir sample and Stainton.

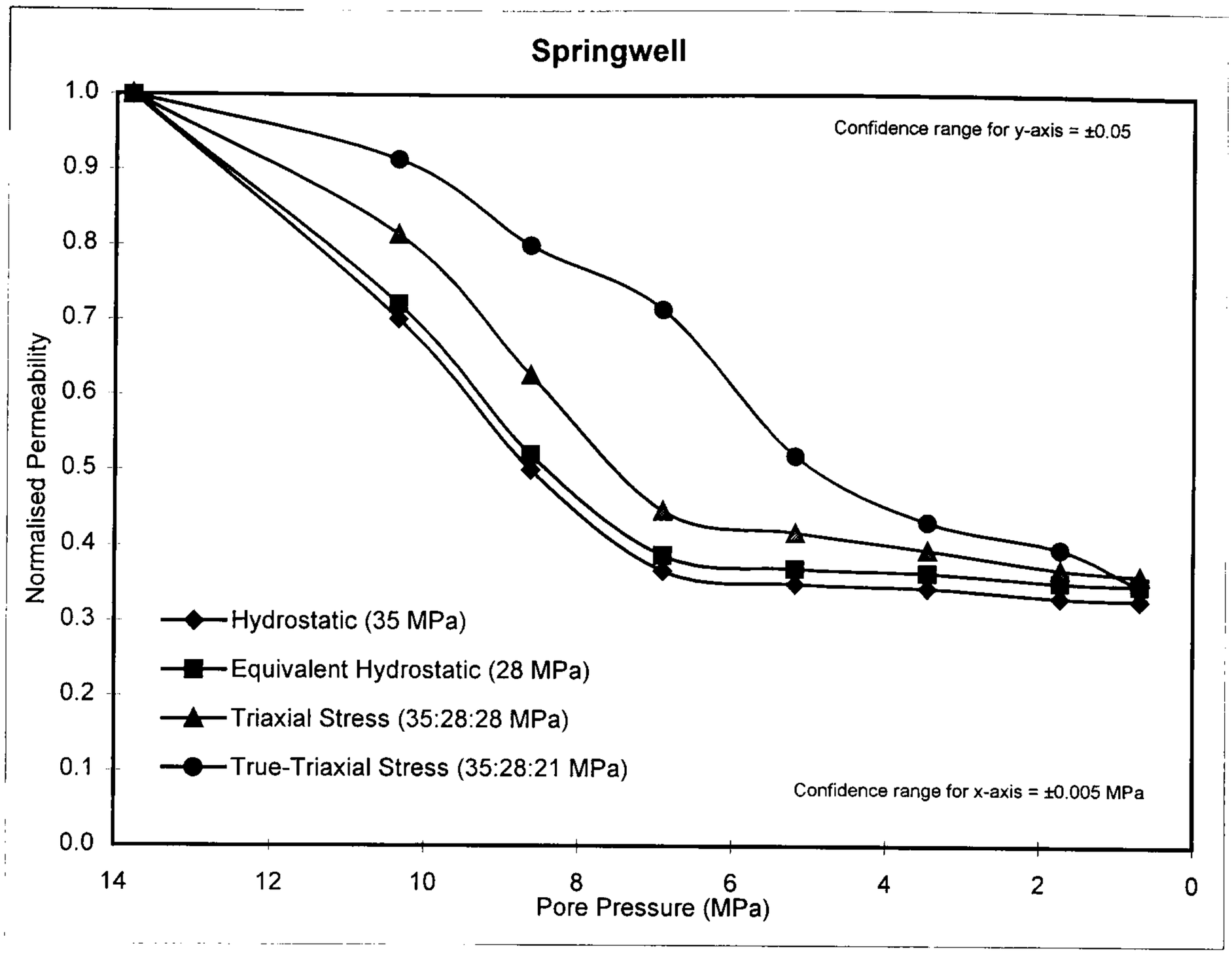

Figure 4.2 Effect of pore pressure on permeability (Springwell)

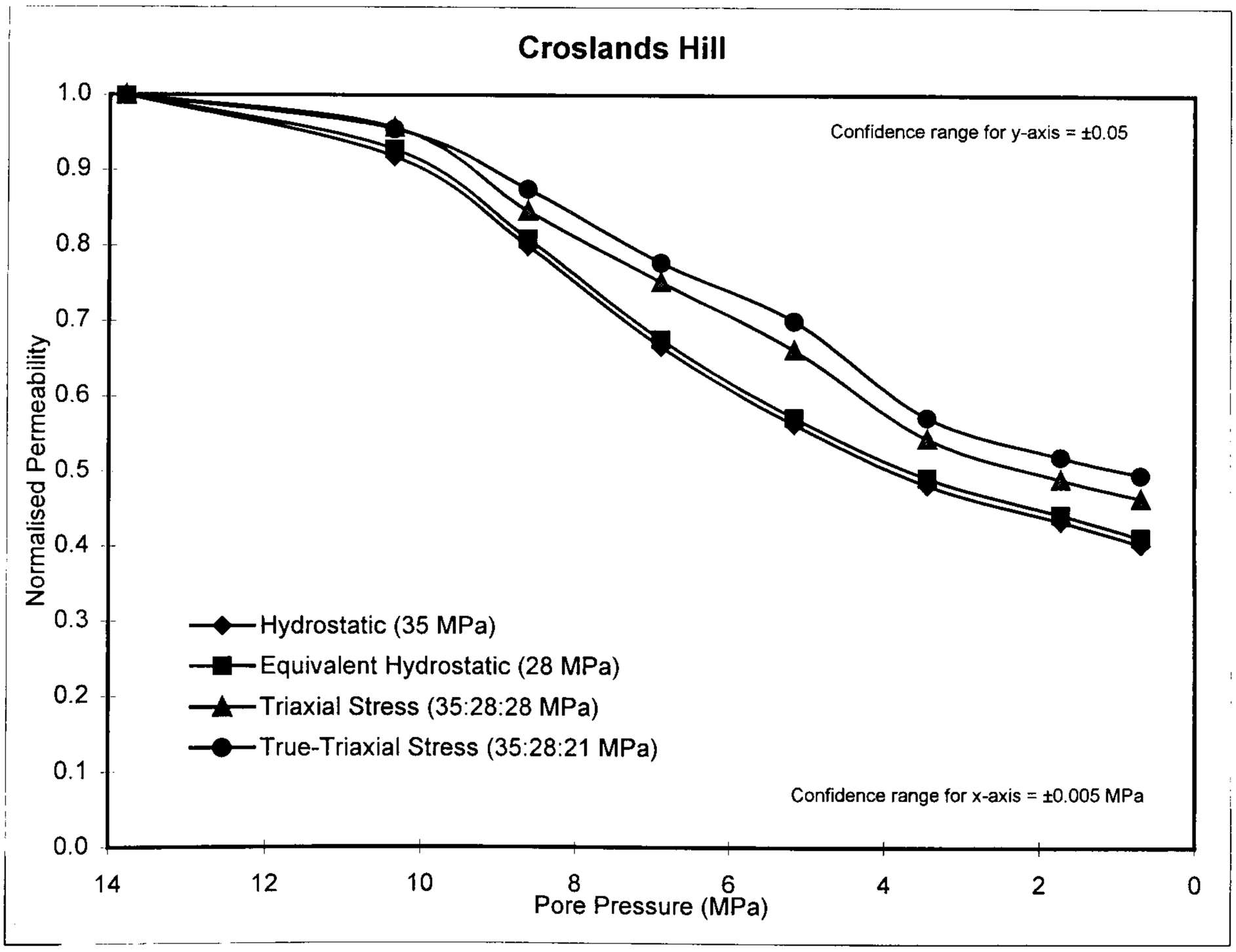

Figure 4.3 Effect of pore pressure on permeability (Croslands Hill)

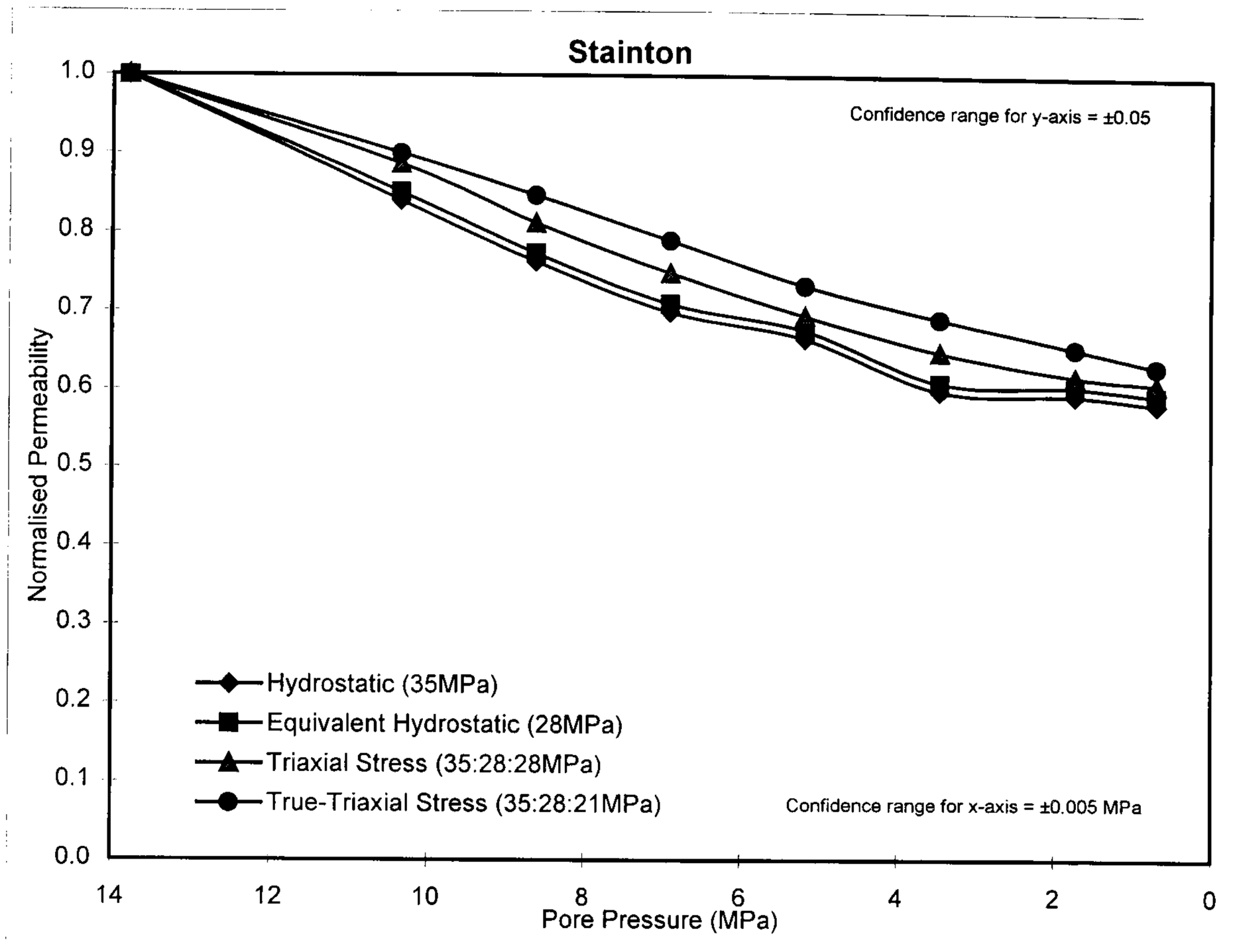

Figure 4.4 Effect of pore pressure on permeability (Stainton)

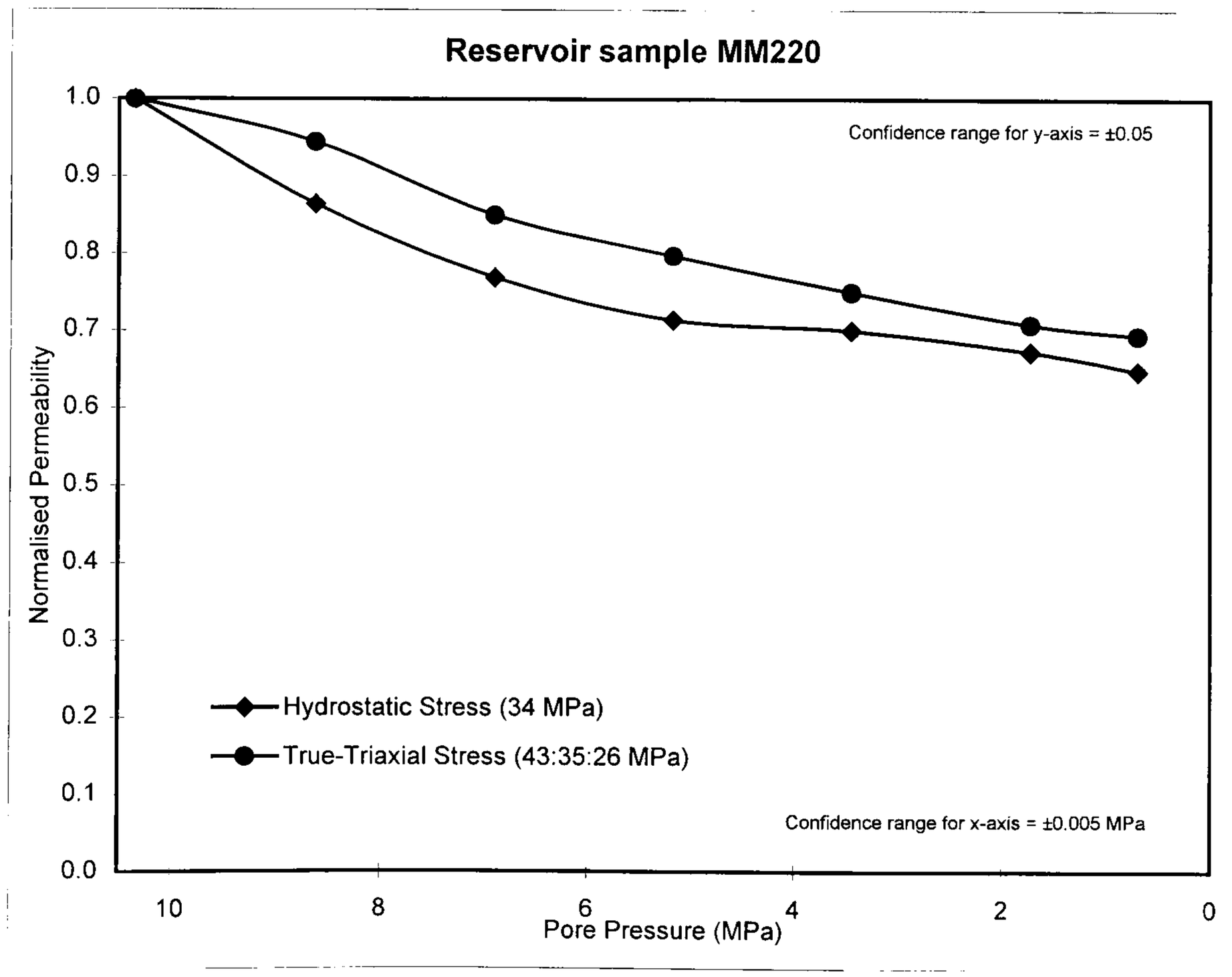

Figure 4.5 Effect of pore pressure on permeability (reservoir sample)

4.3 Permeability Hysteresis Under Hydrostatic and True Triaxial Stresses

Hysteresis is the incompleteness in recovery of any property during loading and unloading cycles. The equilibrium states reached in one direction can be different from those approached in another. For example, permeability hysteresis may be caused by frictional sliding inside the rock, opening of cracks, uneven distribution of stress, failure of internal texture, fines migration, rearranging of pore structure, mobilisation of fine grains and an increase of tortuosity due to collapse of pore space. In addition, microcracks are preferentially oriented with respect to the maximum stress direction.

The effects of hysteresis on permeability are illustrated in Figures 4.8 through 4.12, which show normalised permeability as a function of stress for different stress-states involving loading and unloading cycles. The results show similar trends for all the samples tested. As stress increases the permeability decreases and during unloading permeability increases with decreases of stress for all the rocks tested. Al-Harthy *et al.,* (1998b) observed that permeability hysteresis was more significant under hydrostatic stress and less pronounced under true triaxial stress. The following observations were made from the samples tested :

The hysteresis is more significant under hydrostatic stresses than under true triaxial stresses. The time of relaxation seems to be longer under hydrostatic stress due to principal stresses of equal magnitude being applied around the pore space, while in an anisotropic stress field the principal stresses are unequal. In addition, the maximum stress in an anisotropic stress field will tend to cause connected passages to be compressed greater in a direction of maximum stress as shown in Figure 4.6. Increased grain-grain contact along the direction of maximum stress can prevent pore collapse and reduce further deformation and hence cause the change of permeability to be smaller in an anisotropic stress field than in a hydrostatic stress field. Microscopic grain orientation which can occur due to deposition and compaction processes as shown in Figure 4.7, might cause less change in permeability under true triaxial stress. The grains will be subjected to less stresses in the horizontal direction compared to the vertical direction while under hydrostatic stress the grains will be

subjected to the same stress in all directions. Even under hydrostatic stress, anisotropic permeability might be induced if the grains are themselves anisotropic due to them compressing more in one direction than another. Furthermore rocks are not linearly elastic, and their behaviour is controlled by grain-grain contact and cement bonds between grains. The fact that rock samples are not always linearly elastic can be seen in Figures 3.8 and 3.9 which show these particular stress strain curves. Also, these samples did not return to their original state even though they were only subjected to a relatively small stress. Grain contacts and cement bonds are different in different directions, and rock deformation depends on the stress anisotropy which can alter cement bonds and grain-grain contacts.

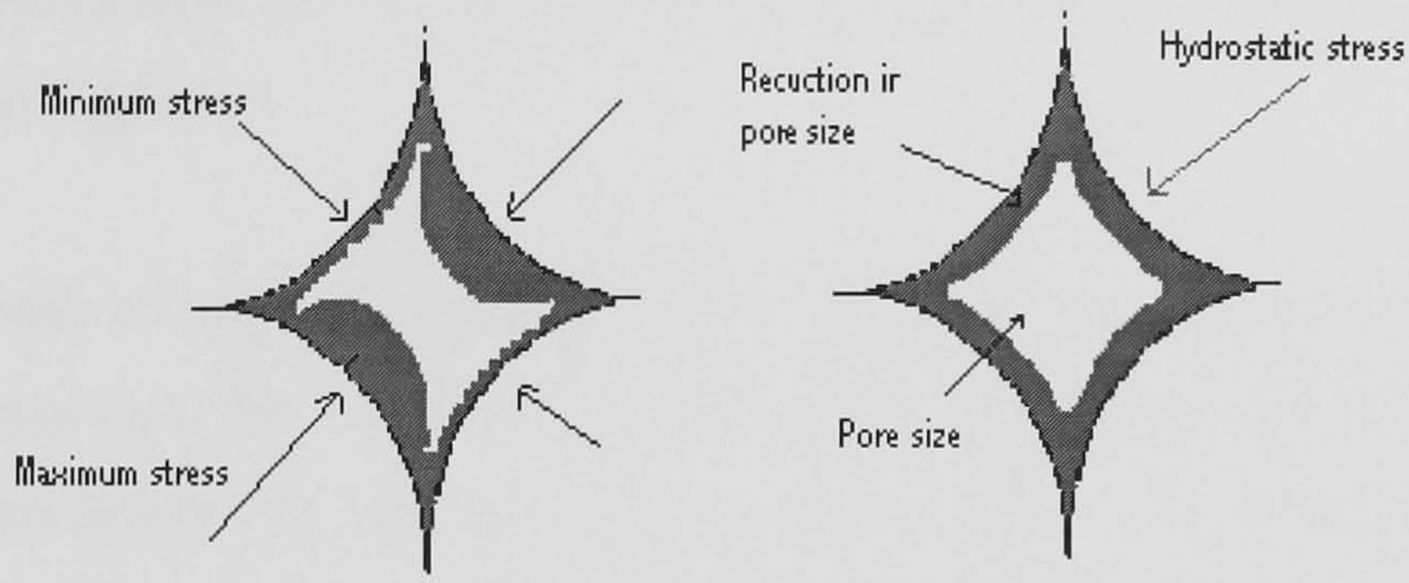

(a) Deviatoric (b) Hydrostatic

Figure 4.6 Schematic illustration showing pore space subjected to three principal stresses

Figure 4.6 shows a schematic of a cross section through a pore space subjected to three principal stress under (a) deviatoric and (b) hydrostatic stresses. It illustrates that the pore space remaining after comparable stresses are applied is larger under the true triaxial stress than under the hydrostatic stress. This can also explain why permeability is higher under true triaxial stress.

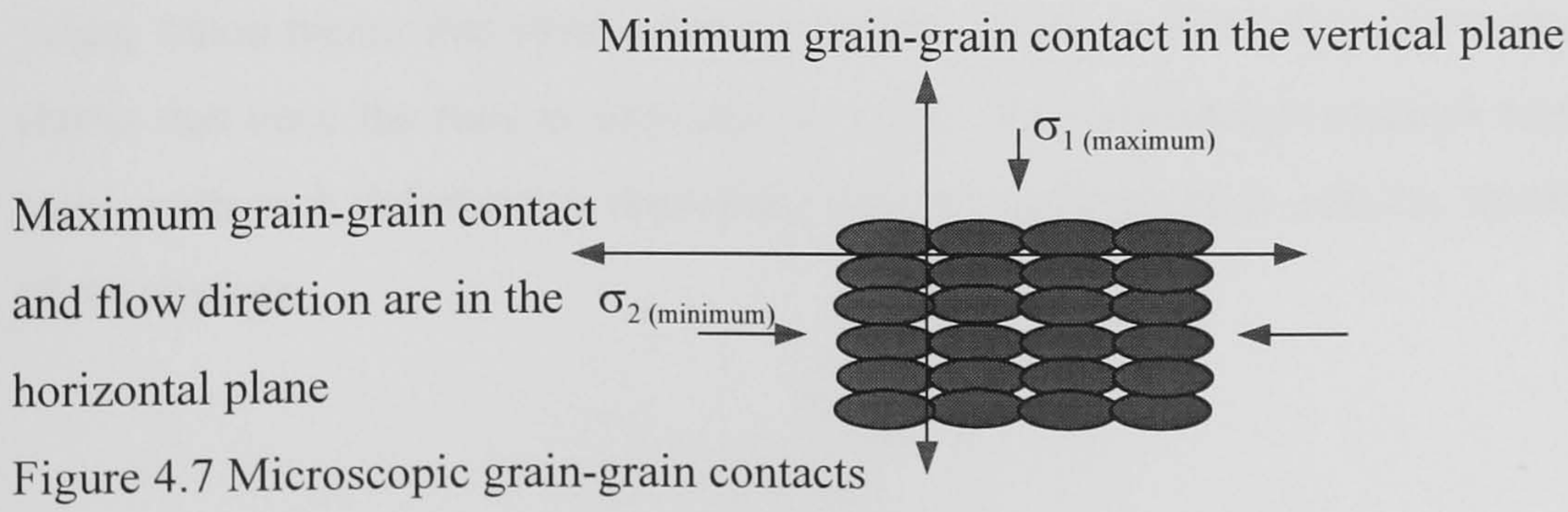

Figure 4.7 Microscopic grain-grain contacts

Figure 4.7 shows schematically the microscopic grain orientation during deposition and compaction. The grain orientation will affect the pores and connected passages when subjected to different stress states and stress paths, either in anisotropic stress fields or under hydrostatic stress. Grain contact is greater in one direction than the other and this would cause hysteresis to be less pronounced under true triaxial stress.

Under true triaxial stress, the maximum stress acts along the direction of maximum grain-grain contact, whilst the minimum stress acts along the direction of minimum (and weakest) grain-grain contact. In contrasts, under hydrostatic loading equal stress is applied on the rock in all directions which can lead to more deformation and possibly pore structure collapses along the direction of weakest grain-grain contact as illustrated in Figure 4.7.

In the majority of cases, as hydrostatic stress increases, the normalised permeability value is lower than the corresponding value under true triaxial stress. This may be due to higher degrees of compaction and rearrangement of the grains into a tighter structure, which may lead to underestimates of permeability when measurements are performed under hydrostatic stresses.

The degree of reduction of normalised permeability with increase in stress is larger under hydrostatic than under true triaxial stress. This could be explained by sand grains being packed closer to each other under hydrostatic stress. In addition, increased tortuosity due to collapse of pore space can be caused by the magnitude of stress applied under hydrostatic loading.

Regardless of stress state, the normalised permeability did not return to its initial value, which means that permeability hysteresis occurs in both states of stress. This shows that once the rock is subjected to stress, some permanent changes may take place, with rock deformation depending on both the magnitude and the distribution of the stresses.

During unloading cycle under hydrostatic stress, (see Figures 4.8 and 4.9) the permeability decreased first then increased with decreasing stress. This might be due to some permanent pore structure collapse and resulting fines migration which might block pores passages and reduce permeability. This may also be due to stress not reaching equilibrium at the end of loading cycle. King *et al.* (1997) observed the influence of changes in the intermediate principal stress on the transport properties (permeability). They also observed during cracking cycle, at higher stress levels there is tendency of decrease in permeability then increase sharply as the stress level is further increased.

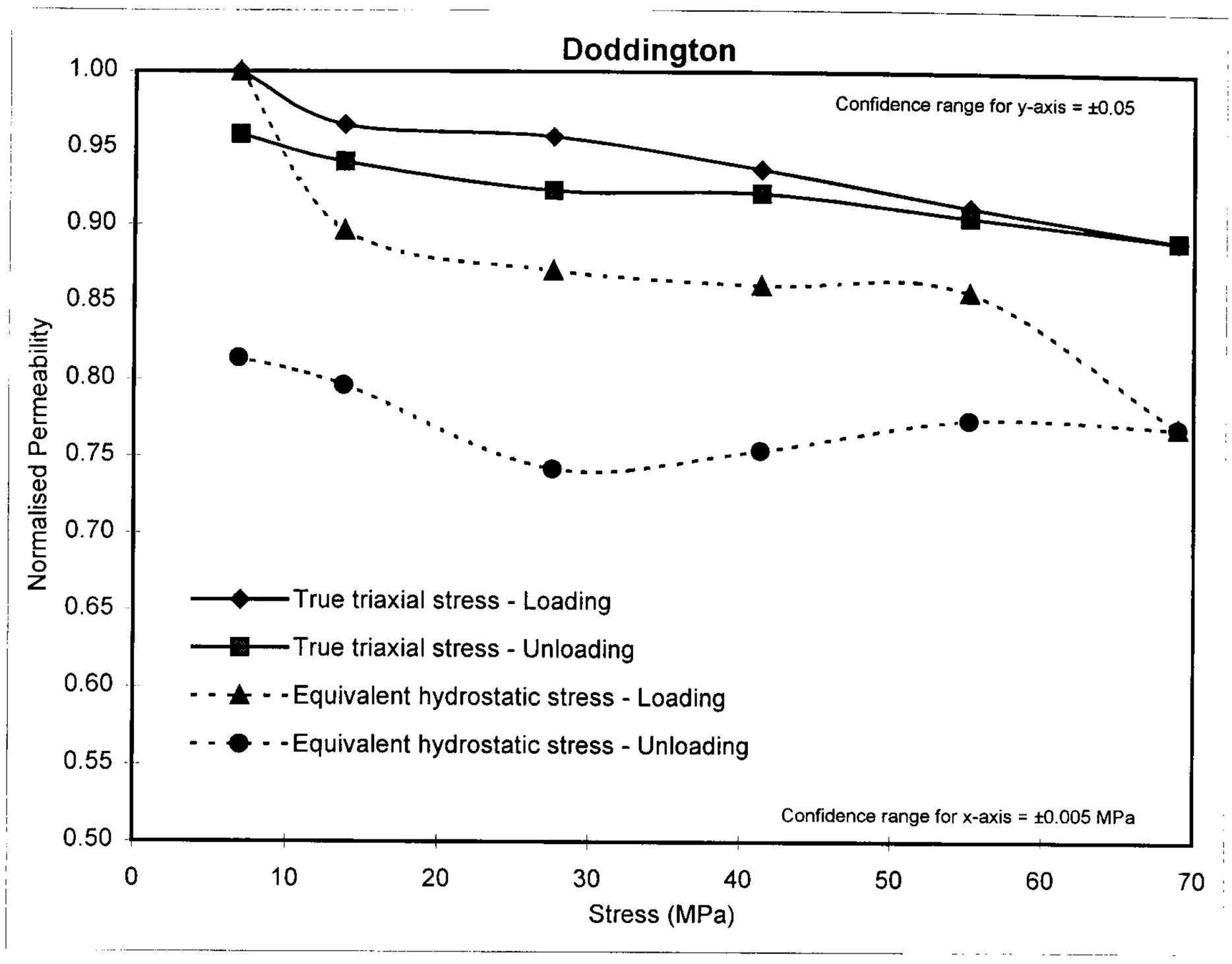

Figure 4.8 Effect of hysteresis on permeability (Doddington)

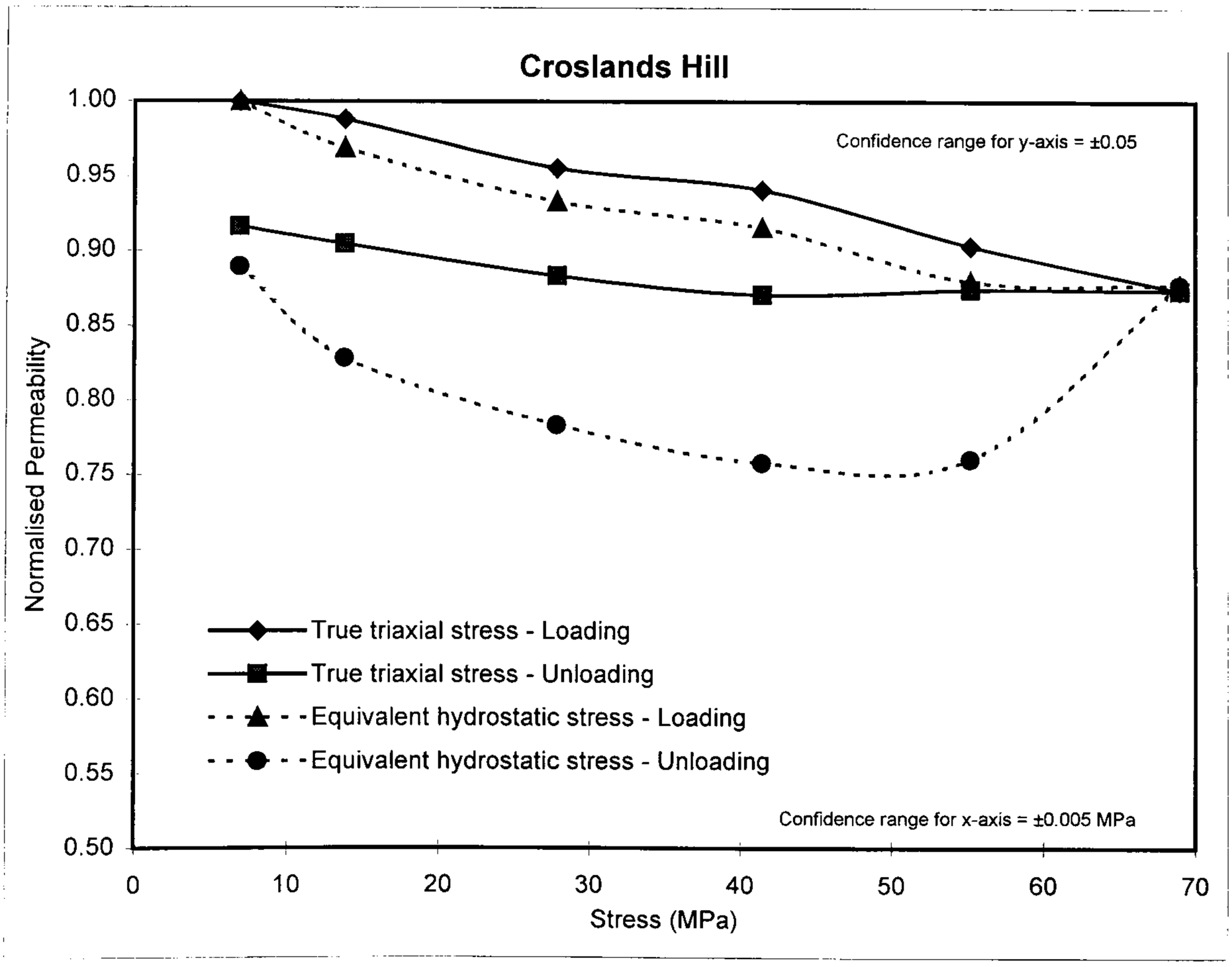

Figure 4.9 Effect of hysteresis on permeability (Croslands Hill)

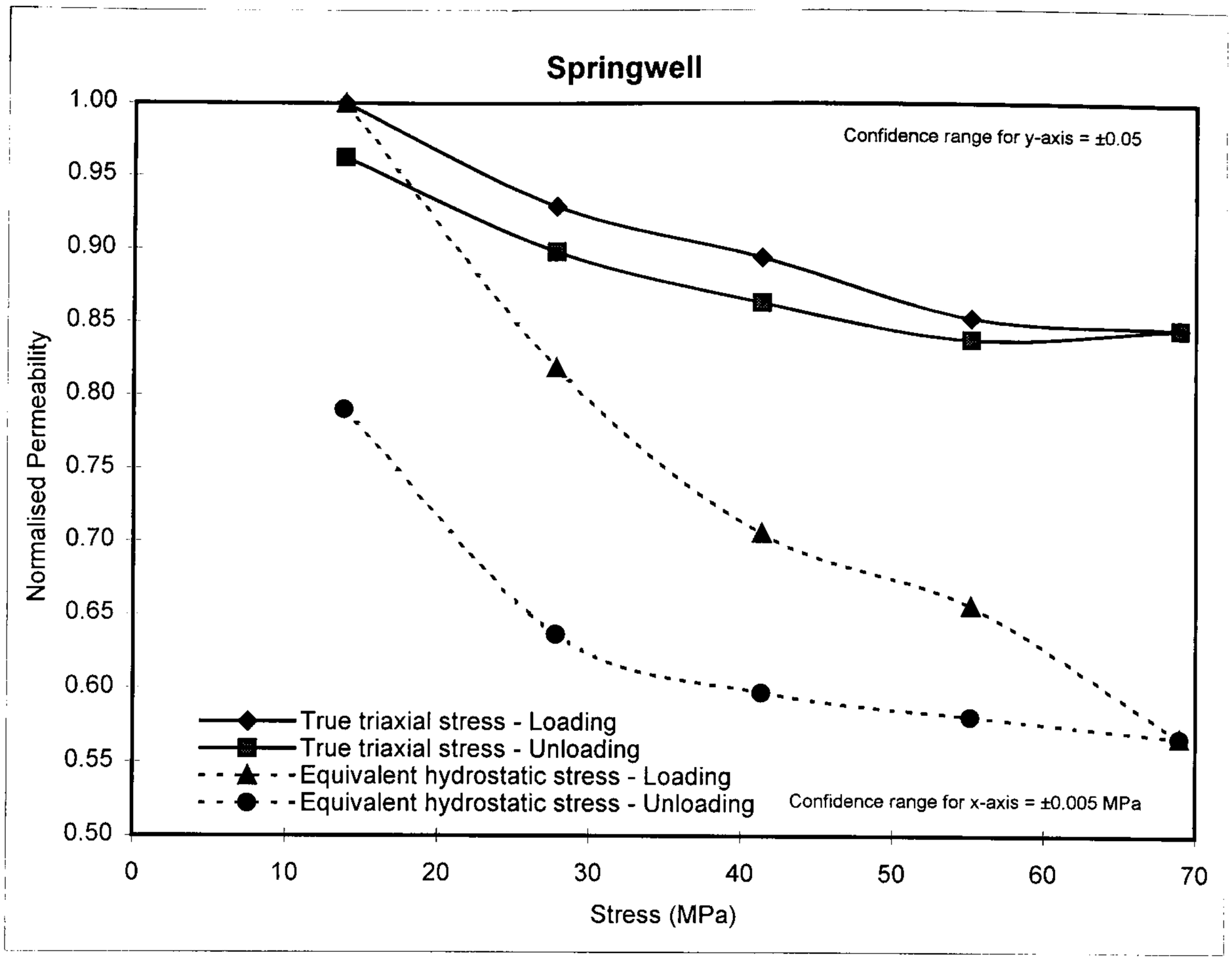

Figure 4.10 Effect of hysteresis on permeability (Springwell)

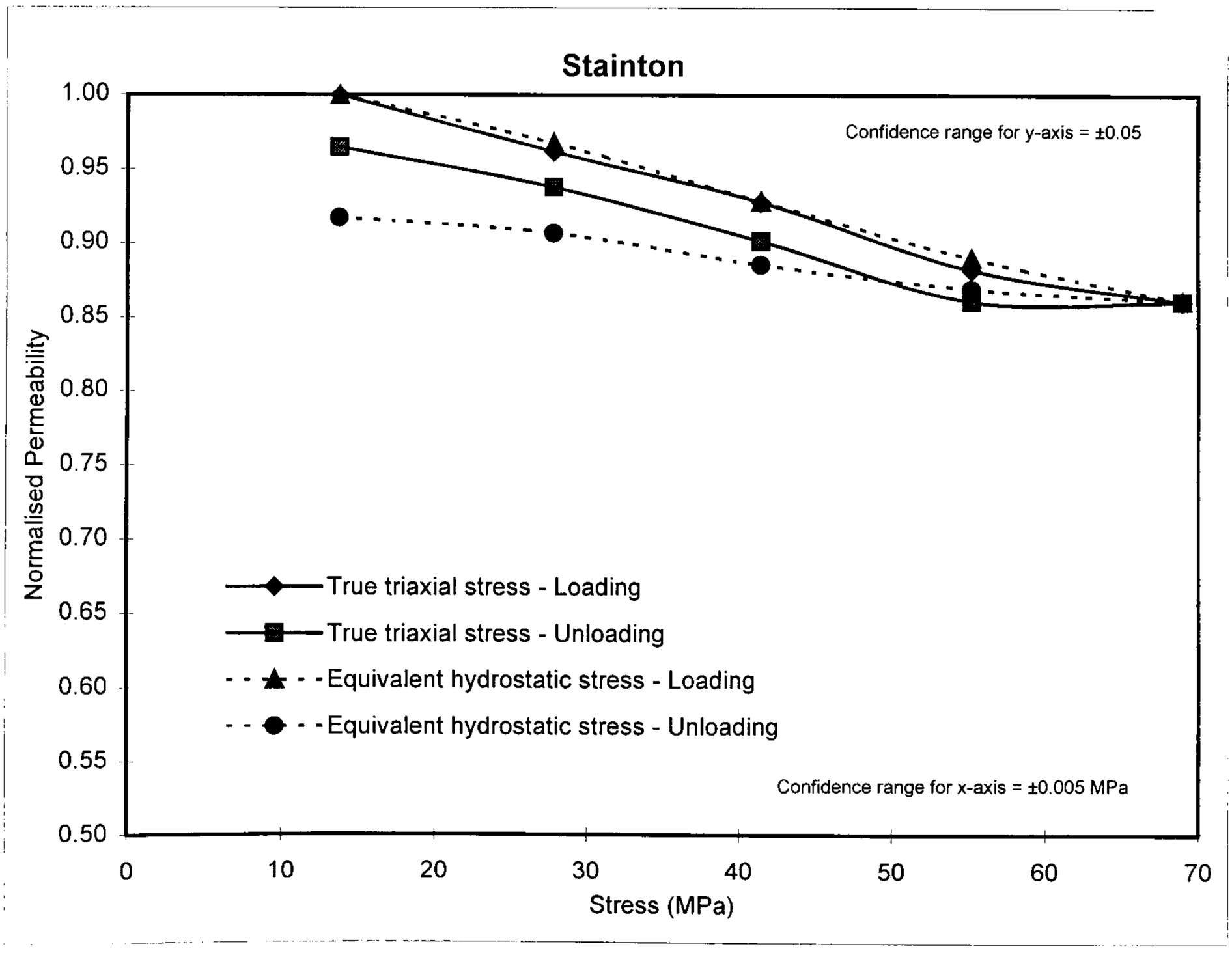

Figure 4.11 Effect of hysteresis on permeability (Stainton)

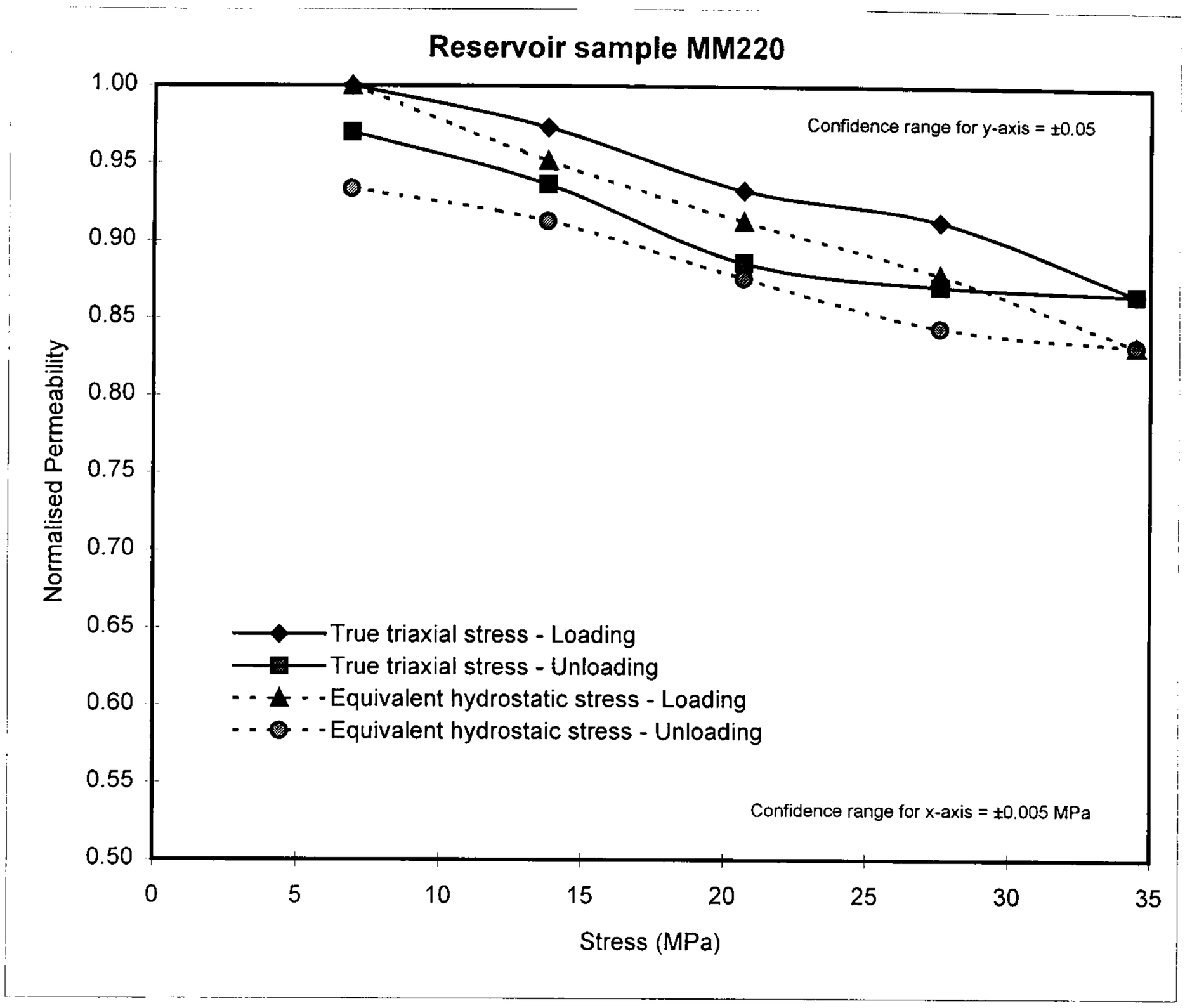

Figure 4.12 Effect of hysteresis on permeability (reservoir sample)

4.4 Effect of Stress on Permeability

The effects of stress on permeability is illustrated in Tables 4.1 through 4.5, which show values of normalised permeability determined for hydrostatic and true triaxial stresses during loading and unloading. The results for four outcrop samples and one reservoir sample indicate, in general, that under true triaxial stress there is less reduction in normalised permeability than under a comparable equivalent hydrostatic stress. The maximum permeability reduction under hydrostatic stress for most of the samples varies between 14% to 43%, while under true triaxial loading the variation is between 11% to 15%. The permeability reduction due to different stress states reflect processes by which pore bodies and throats can deform. The pore fluid pathways are closed off due to steady compaction of the rock and by loss of porosity as the stress is increased. The permeability reduction is related to the amount and strength of intergranular cementation, as seen in SEM pictures (see appendix A).

Each sample showed different trends of permeability reduction, but the reduction of permeability with increase of stress is gradual regardless of stress states. However, in the case of Springwell sandstone there is a sharp decrease in permeability with stress, whereas permeability hysteresis is more pronounced. This could be explained by a similar argument as used to explain permeability hysteresis, i.e., grain-grain contacts are stronger, and hence there is less compression on the pores and connected passages. In other words, grain contact is stronger in one direction than other, and this causes the normalised permeability to be less under true triaxial stress. Hence the change in permeability is less significant in anisotropic stress fields than in hydrostatic stress fields.

The above results have important implications in special core analysis. Currently, it is common practice to convert true triaxial stresses *in situ* to equivalent hydrostatic stresses for laboratory convenience. The conversion is usually based on a simple average of all three principal stresses (i.e., $\sigma = (\sigma_1 + \sigma_2 + \sigma_3)/3$). The results from this research indicate that this approximation can lead to significant errors in measured transport properties such as permeability. It is recommended that some true triaxial experiments are to be performed for stress sensitive reservoirs (e.g., tight,

overpressured, naturally fractured) to determine the petrophysical properties accurately, and to provide more reliable factors for routine hydrostatic data.

Table 4.1 Values of normalised permeability under different stress states (Doddington)

	Hydrostatic		True Triaxial (σ_1:σ_2:σ_3 = 1:0.8:0.6)	
Stress	Kn (Loading) K_o = 2390 mD	Kn (Unloading)	Kn (Loading) K_o = 1840 mD	Kn (Unloading)
6.90	1.00	0.81	1.00	0.96
13.80	0.90	0.80	0.97	0.94
27.80	0.87	0.74	0.96	0.92
41.40	0.86	0.75	0.94	0.92
55.20	0.86	0.77	0.91	0.91
69.00	0.77	0.77	0.89	0.89

Table 4.2 Values of normalised permeability under different stress states (Croslands Hill)

	Hydrostatic		True Triaxial (σ_1:σ_2:σ_3 = 1:0.8:0.6)	
Stress	Kn (Loading) K_o = 13.6 mD	Kn (Unloading)	Kn (Loading) K_o = 13.4 mD	Kn (Unloading)
6.90	1.0	0.89	1.00	0.92
13.80	0.97	0.83	0.99	0.90
27.80	0.93	0.78	0.96	0.88
41.40	0.92	0.76	0.94	0.87
55.20	0.88	0.76	0.90	0.87
69.00	0.88	0.88	0.87	0.87

Table 4.3 Values of normalised permeability under different stress states (Springwell)

	Hydrostatic		True Triaxial (σ_1:σ_2:σ_3 = 1:0.8:0.6)	
Stress	Kn (Loading) K_o = 19.7 mD	Kn (Unloading)	Kn (Loading) K_o = 17.1 mD	Kn (Unloading)
13.80	1.00	0.79	1.00	0.96

27.80	0.82	0.64	0.93	0.90
41.40	0.71	0.60	0.89	0.86
55.20	0.66	0.58	0.85	0.84
69.00	0.57	0.57	0.85	0.85

Table 4.4 Values of normalised permeability under different stress states (Stainton)

	Hydrostatic		True Triaxial (σ_1:σ_2:σ_3 = 1:0.8:0.6)	
Stress	Kn (Loading) K_o = 114 mD	Kn (Unloading)	Kn (Loading) K_o = 145 mD	Kn (Unloading)
13.80	1.00	0.92	1.00	0.96
27.80	0.97	0.91	0.96	0.94
41.40	0.93	0.89	0.93	0.90
55.20	0.89	0.87	0.88	0.86
69.00	0.86	0.86	0.86	0.86

Table 4.5 Values of normalised permeability under different stress states (reservoir sample)

	Hydrostatic		True Triaxial (σ_1:σ_2:σ_3 = 1:0.8:0.6)	
Stress	Kn (Loading) K_o = 438 mD	Kn (Unloading)	Kn (Loading) K_o = 600 mD	Kn (Unloading)
6.90	1.00	0.93	1.00	0.97
13.80	0.95	0.91	0.97	0.94
20.70	0.91	0.88	0.93	0.89
27.60	0.88	0.84	0.91	0.87
34.50	0.83	0.83	0.87	0.87

In summary, the change of permeability under anisotropic stress fields can be explained as follows :

1. Different stress states cause different degrees of pore deformation. Hydrostatic loading has shown more change in pore deformation and transport properties.
2. Permanent deformation may occur when a rock is subjected to stress. The extent

of this deformation depends on rock type and magnitude of stress.

3. Strengths of grain boundary contacts for each rock are different, thus the reduction of permeability varies between different rocks.
4. During deposition of sand particles and as a consequence of subsequent changes such as cementation, bonds between grains are weaker in some parts and stronger in others. If weak parts are subjected to higher stress then there will be more closure of pores and connected passages due to deformation and pore structure collapses. This will cause the permeability to decrease. This suggests that there could be a relationship between microscopic scale heterogeneity and the effects of stress path on the sample.

4.5 Summary

Experimental investigations involving analogue materials and borehole samples from reservoir depths have been carried out under various stress conditions. The following conclusions are made based on the results obtained in this study :

1. The effects of pore pressure on permeability under different stress-conditions have indicated significant stress- and stress-path dependence.
2. There are reductions to permeability as pore pressure decreases and effective stress increases.
3. The results show that permeability is dynamic during production, i.e., permeability changes with pore pressure.
4. The hysteresis effect is more significant under hydrostatic stresses and less pronounced under true triaxial stresses.
5. Permeability hysteresis is more pronounced in low permeability samples.
6. The results for the samples tested indicate, in general, that under true triaxial stress there is less reduction in permeability than under a comparable hydrostatic stress.
7. There is a greater degree of reduction in low permeability samples than in high permeability samples.
8. The experimental results have illustrated the importance of applying realistic and true triaxial stresses, and elevated pore pressures when measuring permeabilities of sedimentary rocks in the laboratory.

CHAPTER 5

PERMEABILITY AND RESISTIVITY ANISOTROPY, AND PORE VOLUME CHANGE

5.1 Introduction

Permeability and resistivity of reservoir rocks change with scale of observation and with direction of fluid and current flow. The presence of fractures can enhance permeability and resistivity anisotropy in hydrocarbon reservoirs and, in addition, *in situ* stress anisotropy can influence the anisotropy of transport properties. Traditional/routine laboratory measurements of permeability and resistivity are carried out in one direction along the core plug axis which does not take into account the anisotropy of rock properties. Furthermore, laboratory measurements of petrophysical properties, including pore volume deformation, are often carried out under simulated burial conditions which involve equivalent hydrostatic stress or sometimes anisotropic triaxial loading in which two of the principal stresses are equal. However, permeability and resistivity may vary in three principal directions, and pore volume change may differ under different stress states.

The reason for ignoring anisotropy in many cases is perhaps due to the perception that the effect is negligible, and the cost involved in characterising it is prohibitive. However, many reservoir rocks categorised as homogeneous and isotropic show some degree of anisotropy. To consider a detailed study of anisotropy behaviour in the reservoir there should be justification in terms of improvements of final reservoir description and performance predictions in field development planning.

Anisotropy may be attributed to the following reasons:

- Packing and orientation of sand grains and laminations perpendicular to vertical direction. Lake (1988) and Ayan *et al.* (1994) suggested that heterogeneity is the major source of anisotropy and that severe anisotropy is the result of local heterogeneity.

- During sand deposition, the long axis of the grains align parallel to the direction of maximum velocity. The greatest cross-sectional area of the grains lies in a horizontal plane and causes permeability in the vertical direction different from those in the horizontal directions.
- Regional stress fields usually induce oriented microcracks.
- Cross bedding is the alternate layering of sands of differing grain sizes and/or textures which can also influence the anisotropy.
- Grain orientation, grain size, cementation, packing, sorting and grain size variation may cause permeability anisotropy.
- Depositional environments, such as channel deposits in cross bedded sands, may also account for anisotropy.

In addition, anisotropy may also be attributed to periodical layering which causes changes in sediment type and which produces beds of varying materials or grain sizes. At the grain pore scale, movements of grains during deposition of sediments are influenced by gravity. Grains tend to align in the direction of least resistance to the movement of air or water during deposition. During transport, grains undergo sorting (i.e., separation by shape, weight or size and gravity segregation). This causes different types of grain alignments and packing, and causes anisotropy. Thus anisotropy is governed by variations in materials and variation in arrangement and grain size. Compaction by overburden pressure can cause fracturing, or plastic deformation, orientation of grains, or flattening of point contacts. At a larger scale, fractures either open or fill to form zones with different transport properties to the surrounding rock, again causing anisotropy.

This investigation focuses on core scale anisotropy caused by grain orientation and small scale laminations. This chapter presents laboratory measurements of principal permeabilities and resistivities of outcrop and reservoir sandstone rocks under hydrostatic and true triaxial stresses. Measurements of permeability and resistivity were carried out in the three principal directions using cubic rock samples at low and high stresses. Also presented are measurements of pore volume change under hydrostatic and true triaxial stresses. The main objectives of the work were to

investigate directional and stress dependence of transport properties under realistic stress states.

5.2 Directional Permeability and Resistivity

5.2.1 Introduction

The production of oil and gas in many hydrocarbon reservoirs is affected by heterogeneity and/or anisotropy in the structure of the reservoirs. One of the purposes of this study was to show that even at smaller scales, anisotropic behaviour should still be recognised since values of permeability and resistivity may differ significantly in different directions. The recognition of anisotropy in the early stage of a full field development plan can lead to better predictions of field performance in designing water floods, controlling gas or water coning and steam processes. Ignoring resistivity anisotropy may lead to wrong estimations of hydrocarbon saturation and oil initially in place.

A novel method for measuring directional permeability and resistivity on a cubic sample under realistic true triaxial stress has been developed and used in this study. A series of experiments were conducted on selected reservoir and outcrops sandstone samples, i.e., reservoir sample MM220, St. Bees sandstone and Springwell sandstone. Samples of each material were subjected to true triaxial and equivalent hydrostatic stresses. At low stresses the samples were subjected to an equivalent hydrostatic stress of 6.9 MPa and a true triaxial stress in the ratio of 1:0.8:0.6 for the major:intermediate:minor stresses (i.e., 8.6:6.9:5.2 MPa). At high stresses the samples were subjected to a hydrostatic stress of 34.5 MPa and a true triaxial stress in the same ratios (i.e., 43.1:34.5:25.9 MPa).

A 5% NaCl solution was used as the flowing fluid in the permeability and resistivity measurements. The permeability and resistivity anisotropies at low and high stresses were calculated and all resistivity data were corrected to a common temperature by using ARPS equation (Worthington *et al.,* 1990).

5.2.2 Directional Permeability

Due to the depositional environment of hydrocarbon reservoir rocks there is often evidence of permeability anisotropy. Water breakthrough during production in the early stage of a reservoir life is usually one of the first indications of permeability anisotropy. Vertical permeability anisotropy is the ratio between horizontal and vertical permeabilities (i.e., K_x/K_z or K_y/K_z) while horizontal permeability anisotropy is the ratio between horizontal permeabilities (i.e., K_x/K_y). In most hydrocarbon reservoirs, horizontal anisotropy is assumed to be an order of magnitude smaller than vertical anisotropy. Fractures or grain orientation due to depositional environment can cause horizontal permeability anisotropy, while vertical permeability anisotropy is caused by cross bedding and shales. Inaccurate knowledge of directional permeability can have an important effect on planning reservoir development, especially for fluid injection operations. Permeability anisotropy is especially important for designing horizontal wells.

Traditional measurements of permeability anisotropy in the laboratory involve taking several plugs in different directions from a single core, and measuring permeability along the different core axes (Dullien, 1979 and Bernabe, 1992). However, this analysis using different plugs can be influenced by the combined effects of anisotropy and heterogeneity, since permeability may vary from point to point.

In routine permeability measurements, plugs are only taken in two principal axes (i.e., vertical and horizontal), and not in three principal axes. This does not allow the correct representation of permeability anisotropy in all three principal directions on the same samples. Therefore, this study has focused on measurements of permeability in three principal directions to allow vertical permeability anisotropy (between minimum and maximum horizontal and vertical directions x, y and z) and horizontal permeability anisotropy (variations with direction in horizontal plane x and y directions) to be determined from single cubic samples.

Tables 5.1 through 5.6 show three principal permeabilities and vertical and horizontal anisotropies under different stress states for one reservoir sample and two outcrop

samples. The results show clearly that there is strong permeability anisotropy between the two horizontal and vertical directions. In addition, there is also permeability anisotropy between the maximum (x) and minimum (y) horizontal directions. The reservoir sample shows a vertical permeability anisotropy (i.e., K_x/K_z or K_y/K_z) of between 15 and 40 depending on the stress applied. There is also a difference of between 10 and 15 in vertical permeability anisotropy depending on which horizontal direction is considered (either maximum x or minimum y). The two horizontal directions (i.e., K_x/K_y) show a permeability anisotropy of around 1.7 under different stresses. The reservoir samples are from an oil field in the South of Oman. The reservoir rock is Lower Carboniferous sandstone. There is clear horizontal lamination observed at whole core scale and the cubic sample scale.

The two outcrop samples show vertical permeability anisotropy of between 1.2 and 2.1 depending on the sample and stresses applied. There is also a difference of between 0.2 and 0.8 in vertical permeability anisotropy depending on which horizontal direction is considered. The two horizontal directions show permeability anisotropy of 1.1 to 1.6 relative to one another for the outcrop samples. Close visual and petrographic examination of the two outcrop samples indicate that St. Bees has a bedding structures and Springwell appears homogeneous at the core scale. The degree of permeability anisotropy from 1.30 to 1.96 for the Springwell sample is attributed to the microscale grain orientation effect caused by the sedimentation process. The anisotropic behaviour of St. Bees may be caused by the combined effects of lamination and microscopic grain orientation.

Based on the data measured along the three principal directions, there is clearly a presence of anisotropic behaviour in these sandstone samples. The anisotropy between vertical and horizontal properties shows that there is more severe anisotropy between vertical and horizontal directions than between the two horizontal directions. Anisotropic behaviour may have important implications for petrophysical evaluations, especially in horizontal wells and reservoir engineering calculations. For example, horizontal wells should be oriented orthogonally to the maximum horizontal permeability to achieve maximum inflow potential. An optimised

horizontal well orientation will increase a well's performance, reduce the number of wells needed to drain the entire reservoir, and improve a water flood performance if horizontal injection and production wells are used.

The effect of stress on permeability anisotropy does not show a clear trend for all samples tested. However, for the reservoir samples, permeability anisotropy under hydrostatic and true triaxial stress showed a slight decrease with increasing stress. This may be explained as variable grain packing and cementing along different directions. Both horizontal and vertical permeabilities decrease with applied stress, with the higher permeability decreasing more significantly probably because of the direction of weakest or loosest grain packing. For two outcrop samples, Springwell and St. Bees, there was no clear trend of change to permeability anisotropy as the stress was increased.

When permeability anisotropy at ambient conditions was compared to that at high stresses the results showed that for the outcrop sample there was no significant change in permeability anisotropy with stress. For the reservoir sample, permeability anisotropy was lower at ambient conditions than at a high stresses. Based on the measured permeability anisotropy, no definite conclusions can be drawn regarding stress dependency of anisotropy, and more investigation is required.

The effect of stress states on permeability show clearly that permeability reduction under true triaxial stress was less than that under hydrostatic at both low and high stresses.

In summary, it is well known that vertical permeability and horizontal permeabilities of reservoir rocks can differ appreciably. However, the variation of permeability in the horizontal plane is not widely recognised. This difference can have significant impact on the prediction of production performance, especially for horizontal wells and enhanced oil recovery.

Table 5.1 Directional permeability and anisotropy under different stress states (Reservoir sample MM220 from South of Oman)

Reservoir sample MM220 Under Equivalent Hydrostatic Stress at 6.9 MPa

Directions	K (mD)	K_x/K_z or K_y/K_z (vertical anisotropy)	K_x/K_y (horizontal anisotropy)
X	438	25.8	1.73
Y	254	14.9	
Z	17.0		

Reservoir sample MM220 Under True Triaxial Stress at 8.6:6.9:5.2 MPa

Directions	K (mD)	K_x/K_z or K_y/K_z (vertical anisotropy)	K_x/K_y (horizontal anisotropy)
X	600	40.0	1.68
Y	358	23.9	
Z	15.0		

Reservoir sample MM220 Under Equivalent Hydrostatic Stress at 34.5 MPa

Directions	K (mD)	K_x/K_z or K_y/K_z (vertical anisotropy)	K_x/K_y (horizontal anisotropy)
X	366	24.0	1.67
Y	220	14.7	
Z	15.0		

Reservoir sample MM220 Under True Triaxial Stress at 43.1:34.5:25.9 MPa

Directions	K (mD)	K_x/K_z or K_y/K_z (vertical anisotropy)	K_x/K_y (horizontal anisotropy)
X	521	37.2	1.71
Y	304	21.7	
Z	14.0		

Table 5.2 Directional permeability and anisotropy under different stress states (St. Bees sandstone)

St. Bees Under Equivalent Hydrostatic Stress at 6.9 MPa

Directions	K (mD)	K_b/K_c or K_a/K_c (vertical anisotropy)	K_b/K_a (horizontal anisotropy)
A	188	1.52	1.19
B	224	1.28	
C	147		

St. Bees Under True Triaxial Stress at 8.6:6.9:5.2 MPa

Directions	K (mD)	K_b/K_c or K_a/K_c (vertical anisotropy)	K_b/K_a (horizontal anisotropy)
A	216	1.50	1.11
B	239	1.36	
C	159		

St. Bees Under Equivalent Hydrostatic Stress at 34.5 MPa

Directions	K (mD)	K_b/K_c or K_a/K_c (vertical anisotropy)	K_b/K_a (horizontal anisotropy)
A	159	1.59	1.33
B	212	1.20	
C	133		

St. Bees Under True Triaxial Stress at 43.1:34.5:25.9 MPa

Directions	K (mD)	K_b/K_c or K_a/K_c (vertical anisotropy)	K_b/K_a (horizontal anisotropy)
A	168	1.46	1.20
B	201	1.22	
C	138		

Table 5.3 Directional permeability and anisotropy under different stress states (Springwell sandstone)

Springwell Under Equivalent Hydrostatic Stress at 6.9 MPa

Directions	K (mD)	K_c/K_b or K_a/K_b (vertical anisotropy)	K_c/K_a (horizontal anisotropy)
A	8.24	1.57	1.19
B	6.28	1.31	
C	9.84		

Springwell Under True Triaxial Stress at 8.6:6.9:5.2 MPa

Directions	K (mD)	K_c/K_b or K_a/K_b (vertical anisotropy)	K_c/K_a (horizontal anisotropy)
A	9.00	1.96	1.52
B	6.98	1.29	
C	13.7		

Springwell Under Equivalent Hydrostatic Stress at 34.5 MPa

Directions	K (mD)	K_c/K_b or K_a/K_b (vertical anisotropy)	K_c/K_a (horizontal anisotropy)
A	7.37	1.50	1.13
B	5.55	1.33	
C	8.33		

Springwell Under True Triaxial Stress at 43.1:34.5:25.9 MPa

Directions	K (mD)	K_c/K_b or K_a/K_b (vertical anisotropy)	K_c/K_a (horizontal anisotropy)
A	7.99	2.14	1.59
B	5.96	1.34	
C	12.7		

Table 5.4 Directional permeability and anisotropy under hydrostatic stress (Reservoir sample MM220 from South of Oman)

Reservoir sample MM220 Under Equivalent Hydrostatic Stress at 6.9 MPa

Directions	K (mD)	K_x/K_z or K_y/K_z (vertical anisotropy)	K_x/K_y (horizontal anisotropy)
X	70.7	16.4	NA
Y	NA	NA	
Z	4.30		

Table 5.5 Directional permeability and anisotropy at ambient (Reservoir sample MM220 from South of Oman)

Reservoir sample MM220 Ambient Stress

Directions	K_{air} (mD)	K_{liquid} (mD)	$(K_x/K_z)_{air}$ or $(K_x/K_z)_{Liquid}$
X	80.0	18.0	1.54
Z	52.0	12.0	1.50

Table 5.6 Directional permeability and anisotropy at ambient (St. Bees)

St. Bees Ambient Stress

Directions	K_{air} (mD)	K_{liquid} (mD)	$(K_b/K_c)_{air}$ or $(K_b/K_c)_{Liquid}$
B	220	127	1.26
C	175	92.0	1.38

5.2.3 Directional Resistivity

A rock is considered to be electrically isotropic if the same value of resistivity is measured irrespective of the direction of measurements. Conversely, the rock is electrically anisotropic if the resistivity measured in one direction is different than that measured in other two principal directions. In electrical anisotropy, resistivity depends on the direction of current flow in the rock. The effect of anisotropy on resistivity logs depends on the angle between the borehole and formation and the tool configurations. With the increase in horizontal well drilling over the last ten years, electrical anisotropy has become the focus of research and development in the oil industry (Soares and Countinho, 1997). The difference in resistivities in horizontal and vertical wells are caused by variations in reservoir quality, nearby layers, resistivity anisotropy, and borehole and invasion effects (Bonnie, 1993). Resistivity anisotropy is caused by microscale grain orientation, laminations as well as heterogeneities at various larger scales. Lovell *et al.* (1994 and 1997) reported the technique of electrical resistivity imaging of cores using four electrode contact measurements to provide a link between core electrical imaging and petrophysical properties and heterogeneity. They also demonstrated that by using numerical modelling, the borehole images respond to fine scale resistivity changes, which suggests that the quantitative resistivity core images can be related directly to the downhole images, particularly involving thin beds and small scale heterogeneities.

Electrical resistivity measurements on reservoir rocks are widely used to estimate porosity and water saturations by using two empirical Archie's equation (see Equation 2.16). In this type of measurement, electrical resistivity is measured in one direction on core samples cut parallel or perpendicular to visible bedding planes at neighbouring locations. However, electrical resistivity often varies in different directions. If the hydrocarbon bearing formation has a horizontally layered structure with thinly laminated sand/shale sequences, or in a clean sand with thin cemented streaks or fractures, resistivity in the vertical direction can be different from that in the horizontal direction. For an anisotropic formation, electrical resistivity will depend on the direction of measurements. Therefore, in well logging measurements, the formation resistivity will depend on the angle between the current flow and the

lamination. In this type of approach the third principal direction is ignored and only considers two principal directions are considered during measurements.

Anisotropy depends very much on the scale of observation. The total anisotropy of a formation is a combination of macroscopic and microscopic anisotropies. Macroscopic anisotropy can occur in a sequence of parallel rock layers, each with different electrical properties. The layers can range from fine to coarse in scale, and sometimes they can be clearly visible to the eye. Microscopic anisotropy is caused by preferred orientation or alignment of the fabric of the rock itself. For vertical wells with horizontal bedding perpendicular to the wellbore, which is usually the case, the logging tool (e.g., laterolog) measures the resistivity parallel to the bedding. However, there are many instances where bedding is inclined relative to the wellbore, in which case measured resistivity data may be high because of anisotropy. For horizontal wells, the resistivity data measured may be significantly higher than the true pay interval value. This may lead to erroneous estimations of hydrocarbon in place if uncorrected resistivities are used to estimate porosities and water saturations.

Traditionally, to identify electrical resistivity anisotropy (i.e., R_x/R_z), only maximum horizontal and vertical resistivities are measured. The third minimum horizontal resistivity is assumed to be same as the maximum horizontal resistivity. This study investigates electrical resistivity in three principal directions, which allows the vertical resistivity anisotropy (i.e., variations between the minimum or maximum horizontal and vertical directions x, y and z) and horizontal resistivity anisotropy (i.e., variations in the horizontal plane x and y) to be calculated from the same sample. Anisotropy coefficient is defined as square root of ratio of maximum resistivity to minimum value.

Tables 5.7 to 5.12 show three principal resistivities, and anisotropy and resistivity anisotropy coefficients under different stress states for one reservoir and two outcrop sandstone samples. The results clearly show that there is strong electrical resistivity anisotropy between the horizontal and vertical z directions. In addition, there is also resistivity anisotropy between maximum (x) and minimum (y) horizontal directions

for Springwell sandstone (see Table 5.9). The reservoir sample (see Table 5.7) exhibits a vertical electrical resistivity anisotropy of around 1.6 depending on the stresses applied. There is also a very small difference in vertical electrical resistivity anisotropy depending on which horizontal direction it is compared to. No horizontal electrical resistivity anisotropy was observed. The resistivity anisotropy coefficient is around 1.3 which shows anisotropy behaviour is strong.

The two outcrop samples exhibit vertical electrical resistivity anisotropy of between 1.11 and 1.27, depending on stress applied. Only one of the outcrop samples (Springwell) showed a difference, which ranged from 0.07 to 0.24 in vertical anisotropy depending on which horizontal direction was used for comparison. Only one of the outcrop samples (i.e., Springwell sandstone) showed horizontal resistivity anisotropy, which ranged from 1.07 to 1.13. The electrical resistivity anisotropy coefficient ranged from 1.11 to 1.24, indicating clear anisotropy behaviour.

Although the occurrence of electrical anisotropy is well documented, the horizontal principal resistivity anisotropy has been largely ignored in formation evaluation, possibly because of a lack of experimental data or because few techniques for evaluating it have been reported. In very strongly anisotropic formations the effects of anisotropy in the horizontal plane can actually be greater than those in the vertical plane. In this study anisotropy in resistivity was seen in both horizontal and vertical planes.

Formation factor and cementation exponent also showed this directional dependency (see Table 5.7 through 5.9). For the reservoir sample, the formation factor varied from 20 to 36, and the cementation factor varied from 1.85 to 2.20. For one of the outcrop samples (St. Bees sandstone) the formation factor varied from 16 to 22, and for another (Springwell sandstone) it varied from 31 to 45. The cementation factor varied from 2.03 to 2.25 for both outcrop samples depending on the stress applied.

However, stress does not seem to have a clear effect on anisotropy in the samples tested, except for the reservoir sample which exhibits a slight increase of anisotropy

with stress. For the two outcrop samples no clear change of electrical resistivity anisotropy was observed as the stress increased, probably because both the horizontal and vertical electrical resistivities are decreasing similarly with increasing stress. When resistivity anisotropy at ambient conditions is compared to that at high stresses, it is seen that both the outcrop and reservoir samples exhibit only small changes. Thus, based on the data obtained, no definite conclusions can be drawn regarding stress dependency of resistivity anisotropy. Clearly, further investigation is required.

The effect of stress on electrical resistivity is slightly different under true triaxial and hydrostatic stresses. There is an increase in electrical resistivity as the stresses increase, and formation factor and cementation exponent also increase with stress.

Permeability anisotropy varies with the size of pore throats and the interconnectivity of pores in successive layers, whereas electrical anisotropy depends on the distribution of the conducting phase in the pore spaces and variations of mineralogy. Although for these samples clay content is very low as indicated in appendix A.

Table 5.10 shows principal resistivities, anisotropy, and the electrical resistivity anisotropy coefficient under hydrostatic stresses for one reservoir sandstone sample. The results clearly show that there is strong permeability and strong electrical resistivity anisotropy between the horizontal (x) and vertical (z) directions.

Table 5.7 Directional resistivity, anisotropy and anisotropy coefficient under different stress states - (Reservoir sample MM220 South of Oman)

Reservoir sample MM220 Under Equivalent Hydrostatic Stress at 6.9 MPa

Directions	r@20°C (Ω)	R (Ω-m)	F	m	R_Z/R_X or R_Z/R_Y (vertical anisotropy)	R_X/R_Y (horizontal anisotropy)	$\lambda=(R_Z/R_X)^{0.5}$ (anisotropy coefficient)
X	73.3	3.0	20.5	1.86	1.63	1.04	1.28
Y	72.1	2.9	20.1	1.85	1.69		
Z	120.9	4.9	33.7	2.16			

Reservoir sample MM220 Under True Triaxial Stress at 8.6:6.9:5.2 MPa

Directions	r@20°C (Ω)	R (Ω-m)	F	m	R_Z/R_X or R_Z/R_Y (vertical anisotropy)	R_X/R_Y (horizontal anisotropy)	$\lambda=(R_Z/R_X)^{0.5}$ (anisotropy coefficient)
X	68.7	2.8	19.2	1.82	1.68	1.00	1.30
Y	68.9	2.8	19.2	1.82	1.68		
Z	114.9	4.7	32.0	2.13			

Reservoir sample MM220 Under Equivalent Hydrostatic Stress at 34.5 MPa

Directions	r@20°C (Ω)	R (Ω-m)	F	m	R_Z/R_X or R_Z/R_Y (vertical anisotropy)	R_X/R_Y (horizontal anisotropy)	$\lambda=(R_Z/R_X)^{0.5}$ (anisotropy coefficient)
X	80.7	3.3	22.5	1.91	1.58	1.00	1.26
Y	80.6	3.3	22.5	1.91	1.58		
Z	128.8	5.2	35.9	2.20			

Reservoir sample MM220 Under True Triaxial Stress at 43.1:34.5:25.9 MPa

Directions	r@20°C (Ω)	R (Ω-m)	F	m	R_Z/R_X or R_Z/R_Y (vertical anisotropy)	R_X/R_Y (horizontal anisotropy)	$\lambda=(R_Z/R_X)^{0.5}$ (anisotropy coefficient)
X	77.3	3.1	21.6	1.89	1.61	1.00	1.27
Y	76.8	3.1	21.4	1.88	1.61		
Z	124.0	5.0	34.6	2.18			

Table 5.8 Directional resistivity, anisotropy and anisotropy coefficient under different stress states - (St. Bees sandstone)

St. Bees Under Equivalent Hydrostatic Stress at 6.9 MPa

Directions	r@20°C (Ω)	R (Ω-m)	F	m	R_c/R_b or R_c/R_a (vertical anisotropy)	R_a/R_b or (horizontal anisotropy)	$\lambda=(R_c/R_a)^{0.5}$ (anisotropy coefficient)
A	60.4	2.4	16.8	2.05	1.13	1.00	1.06
B	59.6	2.4	16.6	2.04	1.13		
C	67.3	2.7	18.8	2.13			

St. Bees Under True Triaxial Stress at 8.6:6.9:5.2 MPa

Directions	r@20°C (Ω)	R (Ω-m)	F	m	R_c/R_b or R_c/R_a (vertical anisotropy)	R_a/R_b or (horizontal anisotropy)	$\lambda=(R_c/R_a)^{0.5}$ (anisotropy coefficient)
A	58.9	2.4	16.4	2.04	1.13	1.00	1.06
B	58.1	2.4	16.2	2.03	1.13		
C	66.3	2.7	18.5	2.12			

St. Bees Under Equivalent Hydrostatic Stress at 34.5 MPa

Directions	r@20°C (Ω)	R (Ω-m)	F	m	R_c/R_b or R_c/R_a (vertical anisotropy)	R_a/R_b or (horizontal anisotropy)	$\lambda=(R_c/R_a)^{0.5}$ (anisotropy coefficient)
A	69.8	2.8	19.5	2.16	1.14	1.00	1.07
B	69.8	2.8	19.5	2.16	1.14		
C	79.3	3.2	22.1	2.25			

St. Bees Under True Triaxial Stress at 43.1:34.5:25.9 MPa

Directions	r@20°C (Ω)	R (Ω-m)	F	m	R_c/R_b or R_c/R_a (vertical anisotropy)	R_a/R_b or (horizontal anisotropy)	$\lambda=(R_c/R_a)^{0.5}$ (anisotropy coefficient)
A	67.4	2.7	18.8	2.13	1.11	0.96	1.07
B	68.2	2.8	19.0	2.14	1.15		
C	77.5	3.1	21.6	2.24			

Table 5.9 Directional resistivity, anisotropy and anisotropy coefficient under different stress states - (Springwell sandstone)

Springwell Under Equivalent Hydrostatic Stress at 6.9 MPa

Directions	r@20°C (Ω)	R (Ω-m)	F	m	R_b/R_c or R_b/R_a (vertical anisotropy)	R_a/R_c or (horizontal anisotropy)	$\lambda=(R_b/R_c)^{0.5}$ (anisotropy coefficient)
A	130.6	5.3	36.4	2.11	1.27	1.10	1.13
B	151.1	6.1	42.2	2.19	1.15		
C	118.5	4.8	33.0	2.05			

Springwell Under True Triaxial Stress at 8.6:6.9:5.2 MPa

Directions	r@20°C (Ω)	R (Ω-m)	F	m	R_b/R_c or R_b/R_a (vertical anisotropy)	R_a/R_c or (horizontal anisotropy)	$\lambda=(R_b/R_c)^{0.5}$ (anisotropy coefficient)
A	127.5	5.2	35.6	2.09	1.24	1.13	1.11
B	141.3	5.7	39.4	2.15	1.10		
C	114.5	4.6	31.9	2.03			

Springwell Under Equivalent Hydrostatic Stress at 34.5 MPa

Directions	r@20°C (Ω)	R (Ω-m)	F	m	R_b/R_c or R_b/R_a (vertical anisotropy)	R_a/R_c or (horizontal anisotropy)	$\lambda=(R_b/R_c)^{0.5}$ (anisotropy coefficient)
A	140.1	5.7	39.1	2.15	1.27	1.10	1.13
B	162.6	6.6	45.3	2.23	1.16		
C	127.9	5.2	35.7	2.09			

Springwell Under True Triaxial Stress at 43.1:34.5:25.9 MPa

Directions	r@20°C (Ω)	R (Ω-m)	F	m	R_b/R_c or R_b/R_a (vertical anisotropy)	R_a/R_c or (horizontal anisotropy)	$\lambda=(R_b/R_c)^{0.5}$ (anisotropy coefficient)
A	134.3	5.4	37.5	2.12	1.24	1.07	1.11
B	154.1	6.3	43.0	2.20	1.17		
C	125.2	5.1	34.9	2.08			

Table 5.10 Directional resistivity, anisotropy and anisotropy coefficient under hydrostatic stress - (Reservoir sample MM220 from South of Oman)

Reservoir sample MM220 Under Equivalent Hydrostatic Stress at 6.9 MPa

Directions	r@20°C (Ω)	R (Ω-m)	F	m	R_Z/R_X or R_Z/R_Y (vertical anisotropy)	R_X/R_Y (horizontal anisotropy)	$\lambda=(R_Z/R_X)^{0.5}$ (anisotropy coefficient)
X	51.0	2.1	14.2	1.63	2.19	NA	1.48
Y	NA	NA	NA	NA	NA		
Z	114.6	4.6	32.0	2.13			

Table 5.11 Directional resistivity, anisotropy and anisotropy coefficient at ambient - (Reservoir sample MM220 from South of Oman)

Reservoir sample MM220 Ambient Stress

Directions	r (Ω)	r@20°C (Ω)	R (Ω-m)	F	m	R_Z/R_X	$\lambda=(R_Z/R_X)^{0.5}$
X	84.1	98.3	1.67	11.5	1.48	1.42	1.20
Z	92.0	108.0	2.37	16.3	1.69		

Table 5.12 Directional resistivity, anisotropy and anisotropy coefficient at ambient - (St. Bees)

St. Bees Ambient Stress

Directions	r (Ω)	r@20°C (Ω)	R (Ω-m)	F	m	R_c/R_b	$\lambda=(R_c/R_b)^{0.5}$
B	210.0	245.4	3.66	25.2	2.35	1.11	1.05
C	239.0	279.3	4.05	27.9	2.45		

Tables 5.13 and 5.14 summarise permeability anisotropy and conductivity anisotropy for different samples under hydrostatic and true triaxial stress states. The results show that maximum electrical anisotropy is only around 1.6, but that maximum permeability anisotropy is much greater at around 37.2. This may be due to the fact that permeability is controlled by the size of pore throats and interconnectivity of pores, whilst electrical conductivity is controlled by the distribution of the conducting phase. Of the samples studied, St. Bees sandstone, had the smallest conductivity anisotropy and the largest porosity. Therefore, the assumption that electricity and fluid flow follow the same paths is clearly in question, especially when permeability barriers are present. Difference in permeability and resistivity anisotropy may be due to pore throats close down to such diameters that fluid flow through them stops because the pressure of the fluids are insufficient to overcome the capillary pressure associated with small apertures. These small apertures are still electrically connected and contribute to the overall electrical conductivity of the sample but do not contribute to permeability.

Tables 5.15 and 5.16 show permeability anisotropy and square of formation factor anisotropy for different samples under hydrostatic and true triaxial stress states. The relation proposed by Wyllie and Spangler (1952), which states that permeability and formation factor along two perpendicular principal axis direction are related, is as follows :

$$\frac{K_1}{K_2} = \left(\frac{F_2}{F_1}\right)^2$$

where :

K_1 = principal permeability in horizontal direction,

K_2 = principal permeability in vertical direction,

F_1 = principal formation factor in horizontal direction,

F_2 = principal formation factor in vertical direction,

The results from this research show that this relation does not hold for the reservoir samples tested, but it is valid for the two outcrop samples tested in this research.

Table 5.13 Permeability and conductivity anisotropy of different samples under hydrostatic stress state

Equivalent Hydrostatic Stress at 34.5 MPa

Sample	Directions	K (mD)	Conductivity (1/Ω-m)	K_x/K_z or K_y/K_z	C_x/C_z or C_y/C_z
Reservoir	X	366	0.303	24.0	1.58
sample	Y	220	0.303	14.7	1.58
MM220	Z	15.0	0.192		
St. Bees	X (A)	159	0.357	1.20	1.14
	Y (B)	212	0.357	1.59	1.14
	Z (C)	133	0.313		
Springwell	X (A)	7.37	0.175	1.33	1.16
	Z (B)	5.55	0.152	1.50	1.27
	Y (C)	8.33	0.192		

Table 5.14 Permeability and conductivity anisotropy of different samples under true triaxial stress state

True Triaxial Stress at 43.1:34.5:25.9 MPa

Sample	Directions	K (mD)	Conductivity (1/Ω-m)	K_x/K_z or K_y/K_z	C_x/C_z or C_y/C_z
Reservoir	X	521	0.323	37.2	1.61
sample	Y	304	0.323	21.7	1.61
MM220	Z	14.0	0.200		
St. Bees	X (A)	168	0.370	1.22	1.15
	Y (B)	201	0.357	1.46	1.11
	Z (C)	138	0.323		
Springwell	X (A)	7.99	0.185	1.34	1.17
	Z (B)	5.96	0.159	2.14	1.24
	Y (C)	12.7	0.196		

Table 5.15 Permeability and square of formation factor anisotropy of different samples under hydrostatic stress state

Equivalent Hydrostatic Stress at 34.5 MPa

Sample	Directions	K (mD)	F	K_x/K_z or K_y/K_z	$(F_z/F_x)^2$ or $(F_z/F_y)^2$
Reservoir	X	366	22.5	24.0	2.55
sample	Y	220	22.5	14.7	2.55
MM220	Z	15.0	35.9		
St. Bees	X (A)	159	19.5	1.20	1.28
	Y (B)	212	19.5	1.59	1.28
	Z (C)	133	22.1		
Springwell	X (A)	7.37	39.1	1.33	1.34
	Z (B)	5.55	45.3	1.50	1.60
	Y (C)	8.33	35.7		

Table 5.16 Permeability and square of formation factor anisotropy of different samples under true triaxial stress state

True Triaxial Stress at 43.1:34.5:25.9 MPa

Sample	Directions	K (mD)	F	K_x/K_z or K_y/K_z	$(F_z/F_x)^2$ or $(F_z/F_y)^2$
Reservoir	X	521	21.6	37.2	2.57
sample	Y	304	21.4	21.7	2.61
MM220	Z	14.0	34.6		
St. Bees	X (A)	168	18.8	1.22	1.32
	Y (B)	201	19.0	1.46	1.29
	Z (C)	138	21.6		
Springwell	X (A)	7.99	37.5	1.34	1.31
	Z (B)	5.96	43.0	2.14	1.52
	Y (C)	12.7	34.9		

5.4 Pore Volume Change

Pore volume change at zero pore pressure was measured under hydrostatic and true triaxial stresses. Electrical resistance was also measured during the pore volume change measurements. The cumulative pore volume deformations and normalised pore volume deformations (cumulative pore volume collected/total sample pore volume) are illustrated in Figures 5.1 through 5.6 for hydrostatic and true triaxial stresses. The results show that cumulative squeeze-out increases with stress due to pore volume compression. From the data measured, there was more change under hydrostatic stress than compared to a comparable true triaxial stress. When cumulative squeeze-out is normalised against total pore volume, the results show only a small pore volume difference for both hydrostatic and true triaxial stresses (see Figures 5.4 to 5.6).

Figures 5.7 through 5.15 show resistivity, formation factor and cementation exponent for different samples under hydrostatic and true triaxial stresses during pore volume change measurements. It can be seen that resistivity, formation factor and cementation exponent all increase with stress. Clearly there was sharp increase from at lower stress up to 6.9MPa, meaning that greatest change occurs when a sample is first subjected to stress. Note that a conformance correction has been applied to take into account squeeze out between the platens and the sample when the first confining pressure is applied. The results also show that there is little difference in resistivity, formation factor and cementation exponent when the sample is under hydrostatic and true triaxial stresses.

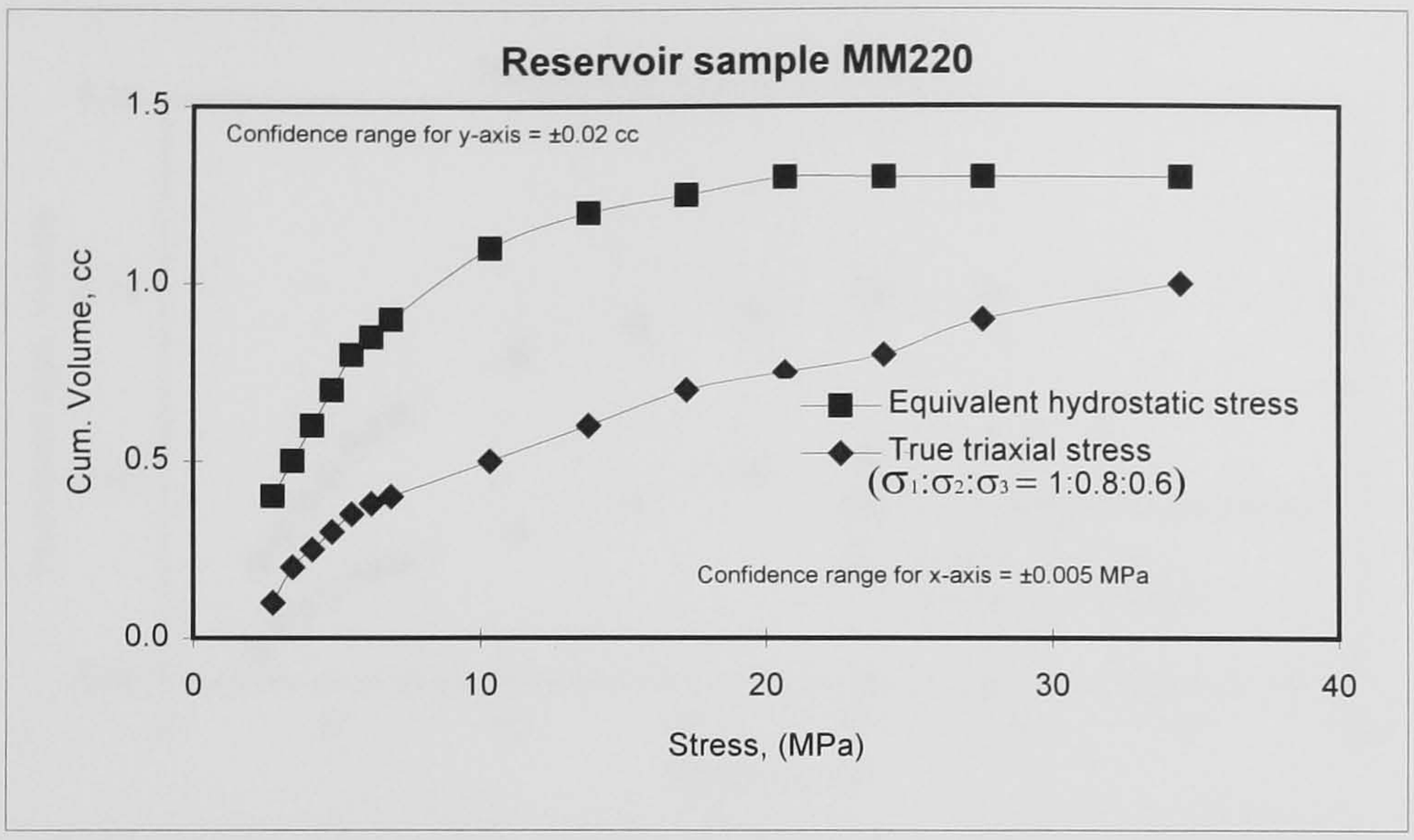

Figure 5.1 Pore volume change versus stress (reservoir sample)

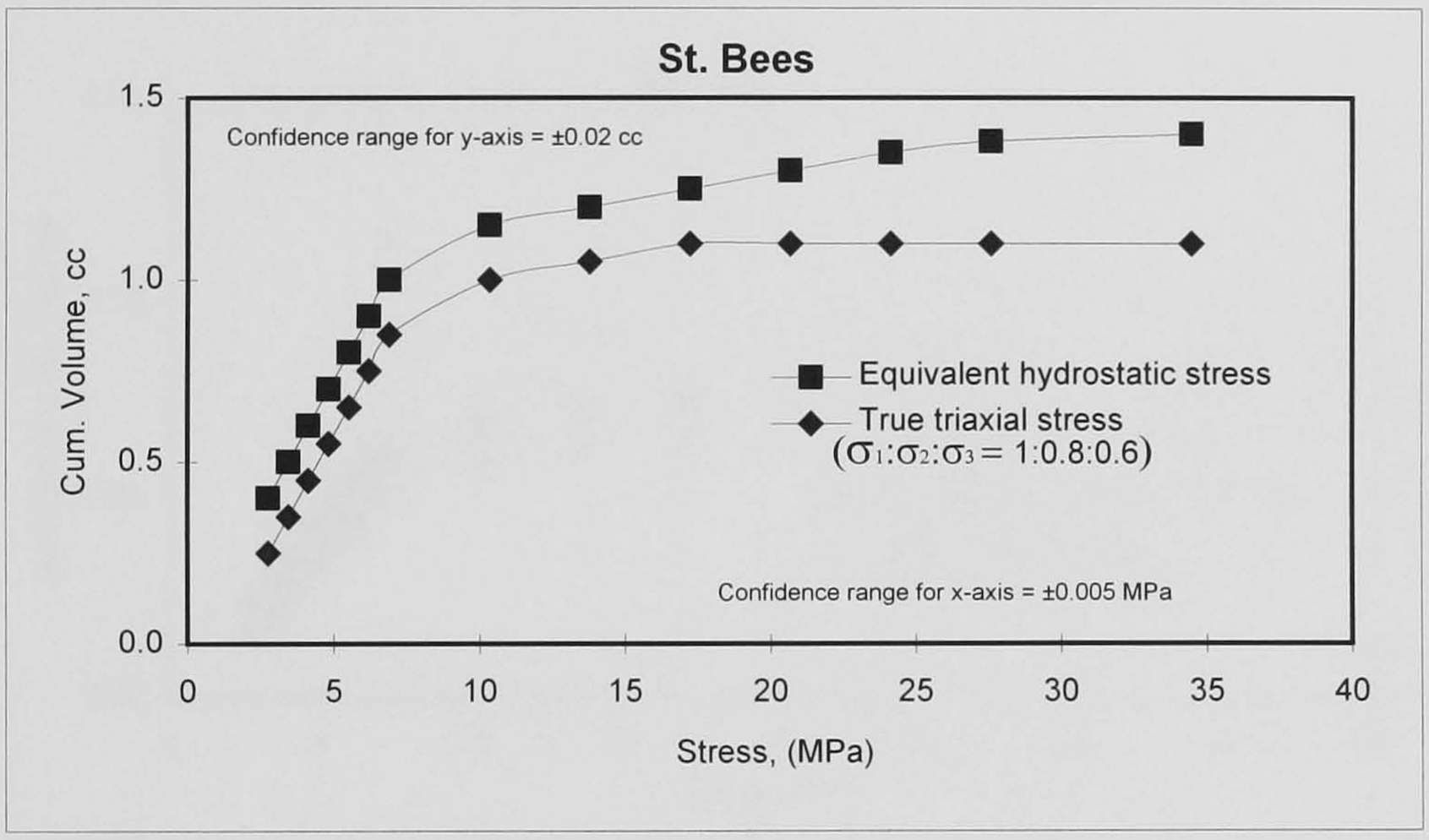

Figure 5.2 Pore volume change versus stress (St. Bees)

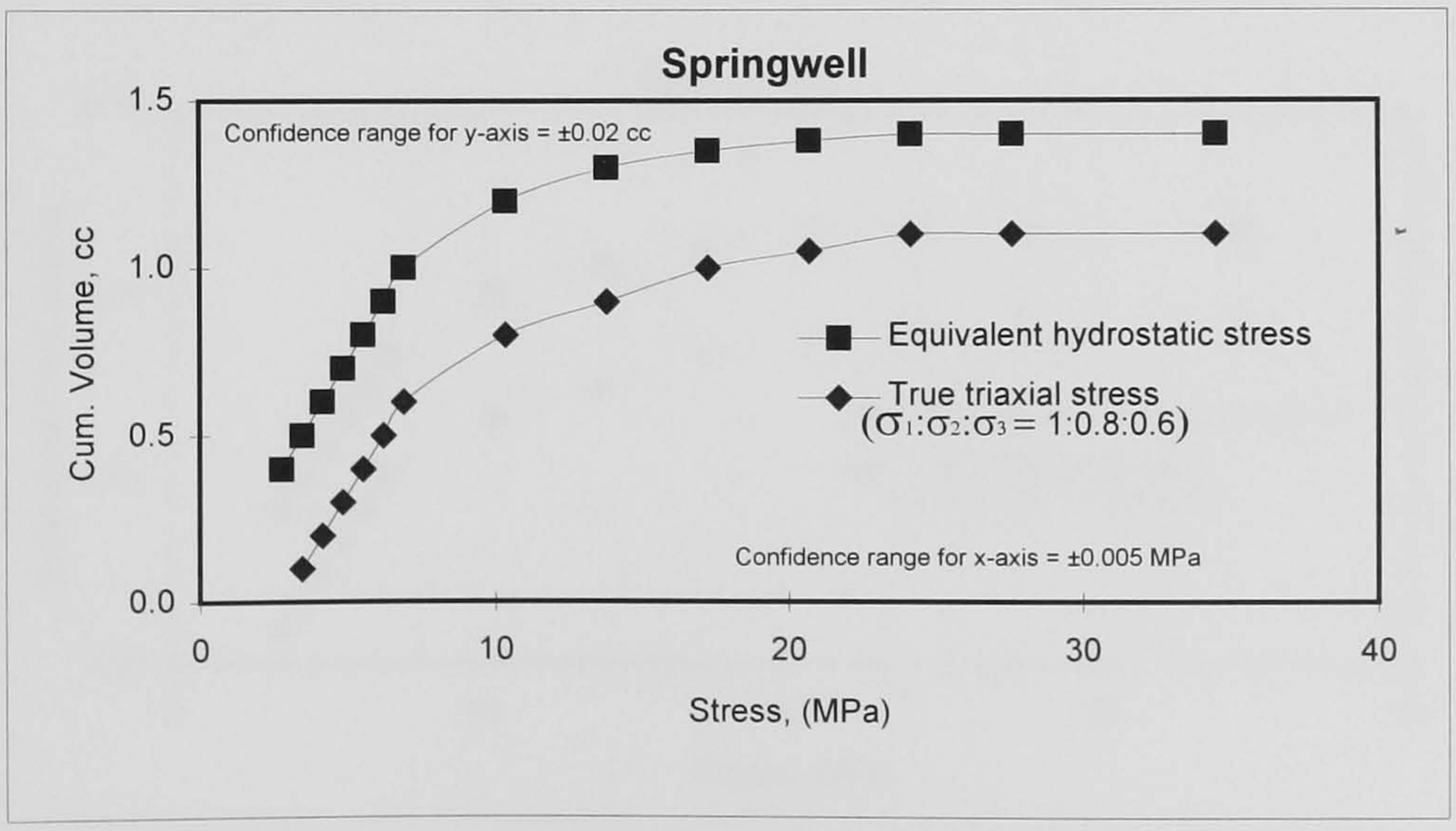

Figure 5.3 Pore volume change versus stress (Springwell)

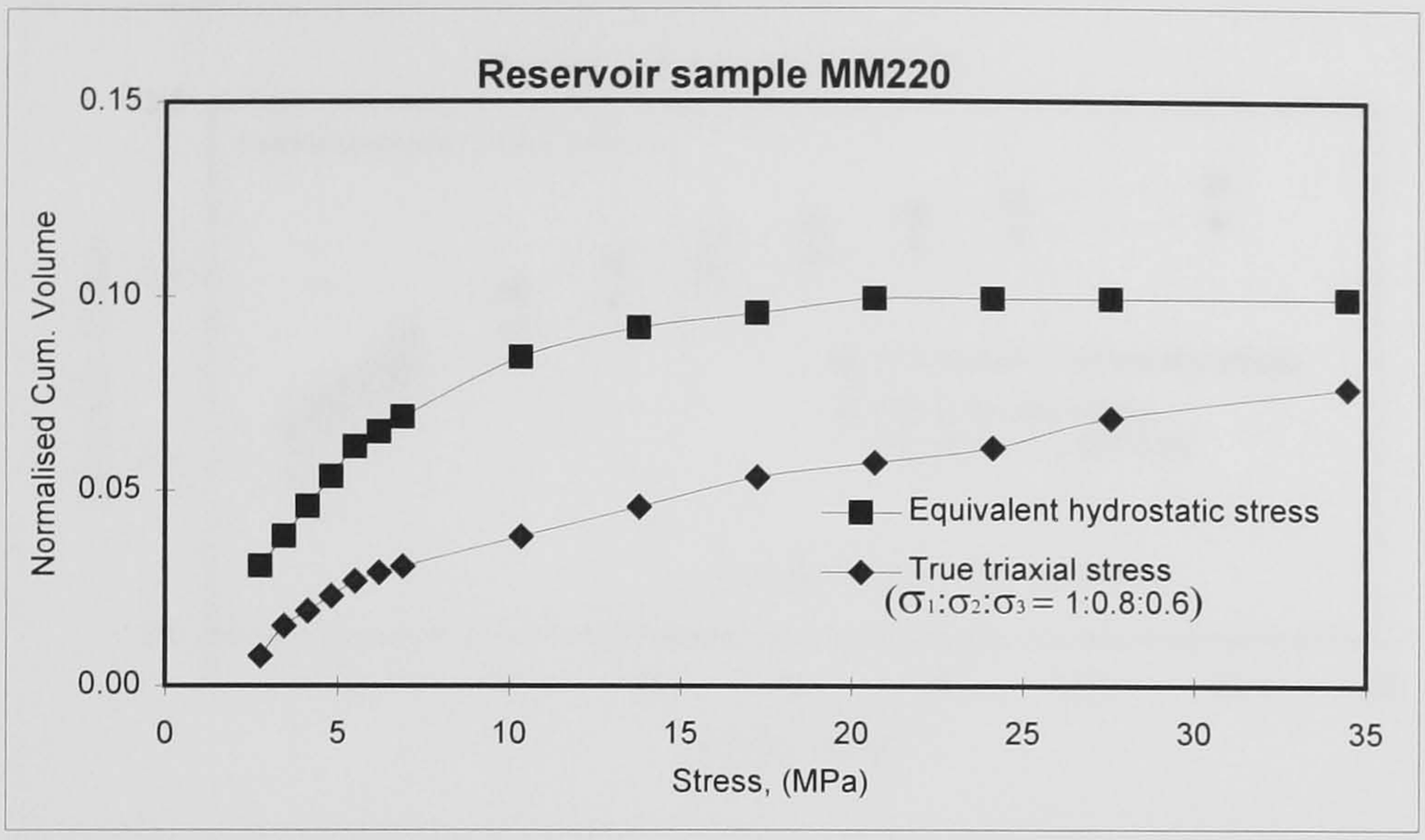

Figure 5.4 Normalised pore volume change versus stress (reservoir sample)

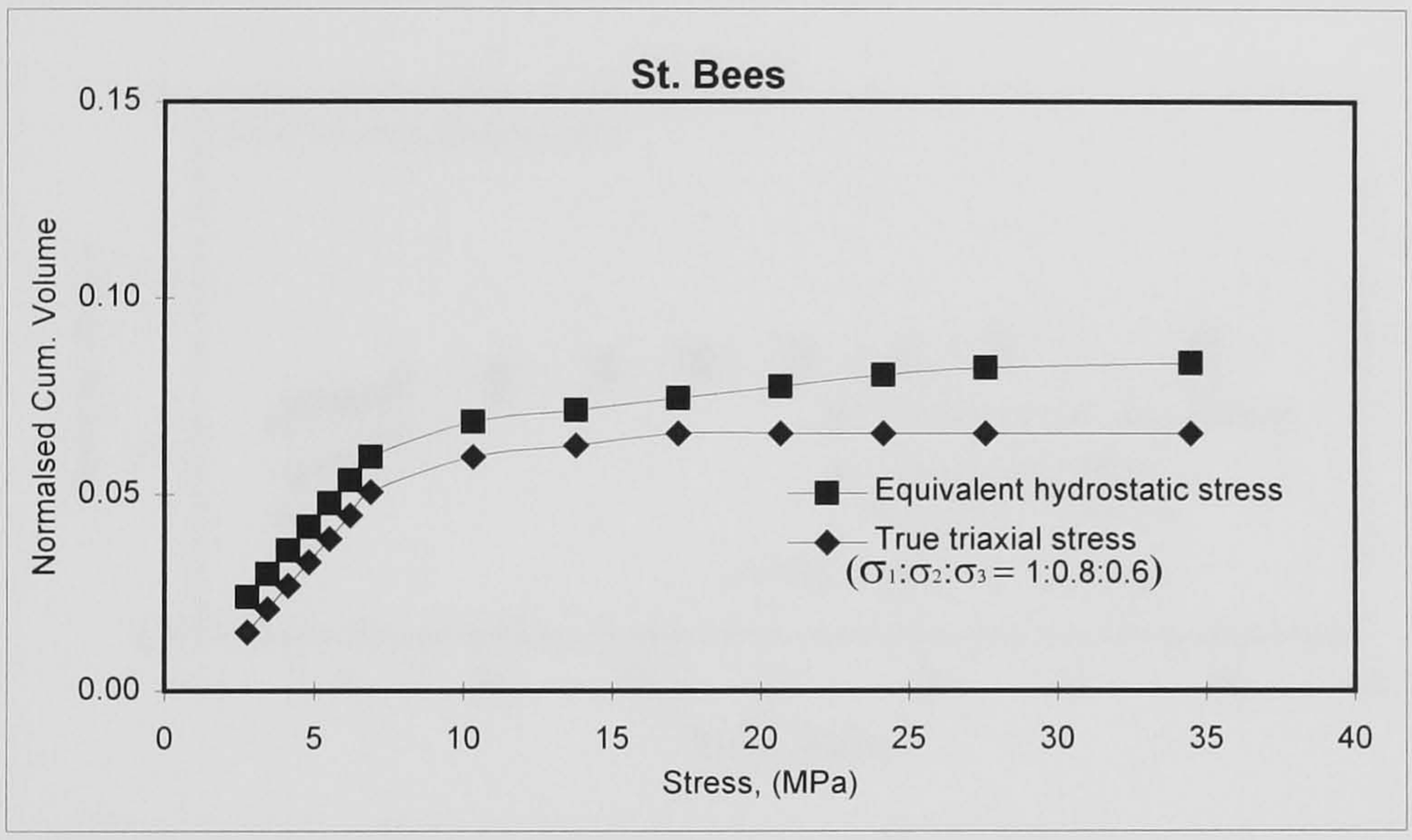

Figure 5.5 Normalised pore volume change versus stress (St. Bees)

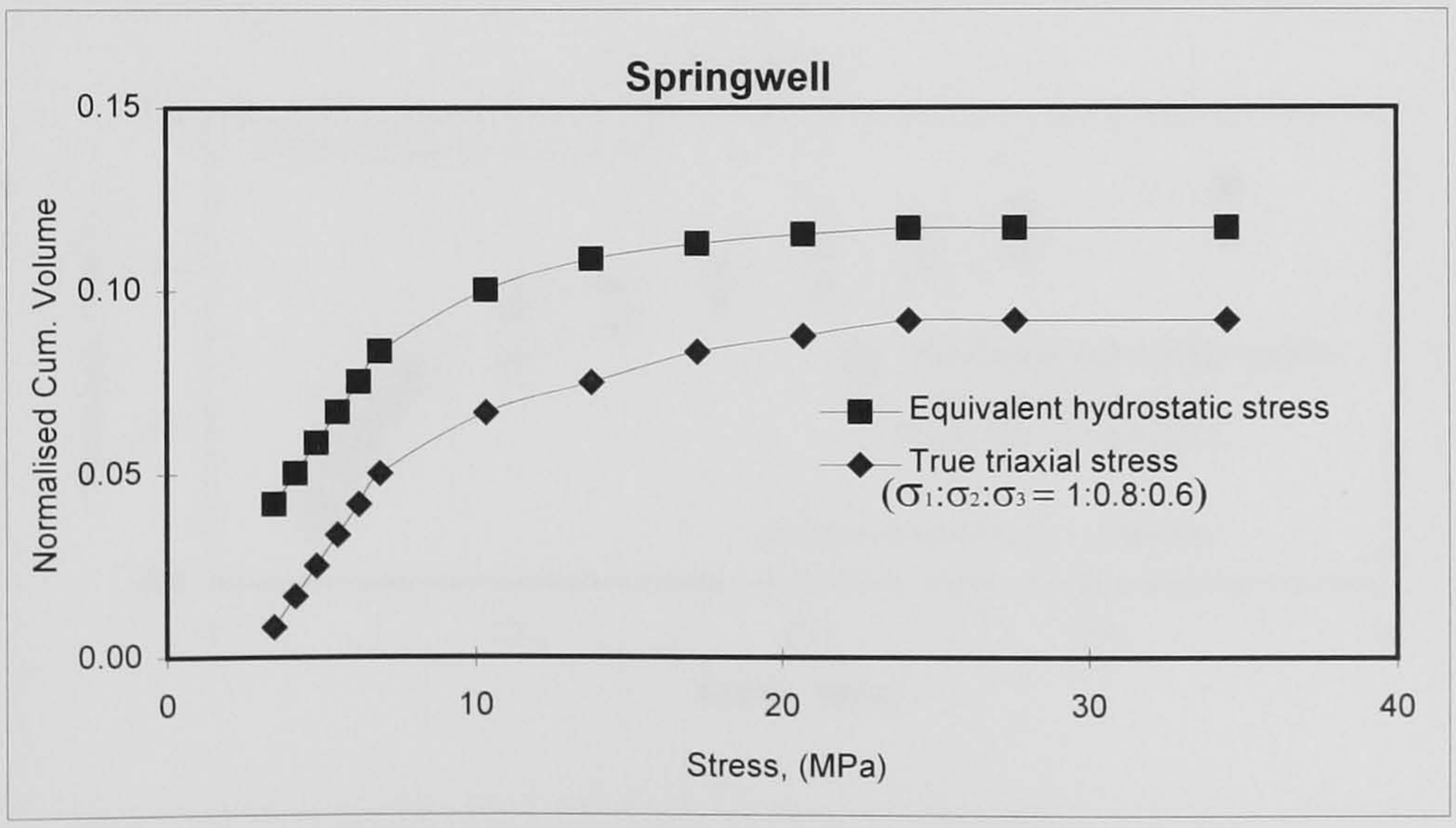

Figure 5.6 Normalised pore volume change versus stress (Springwell)

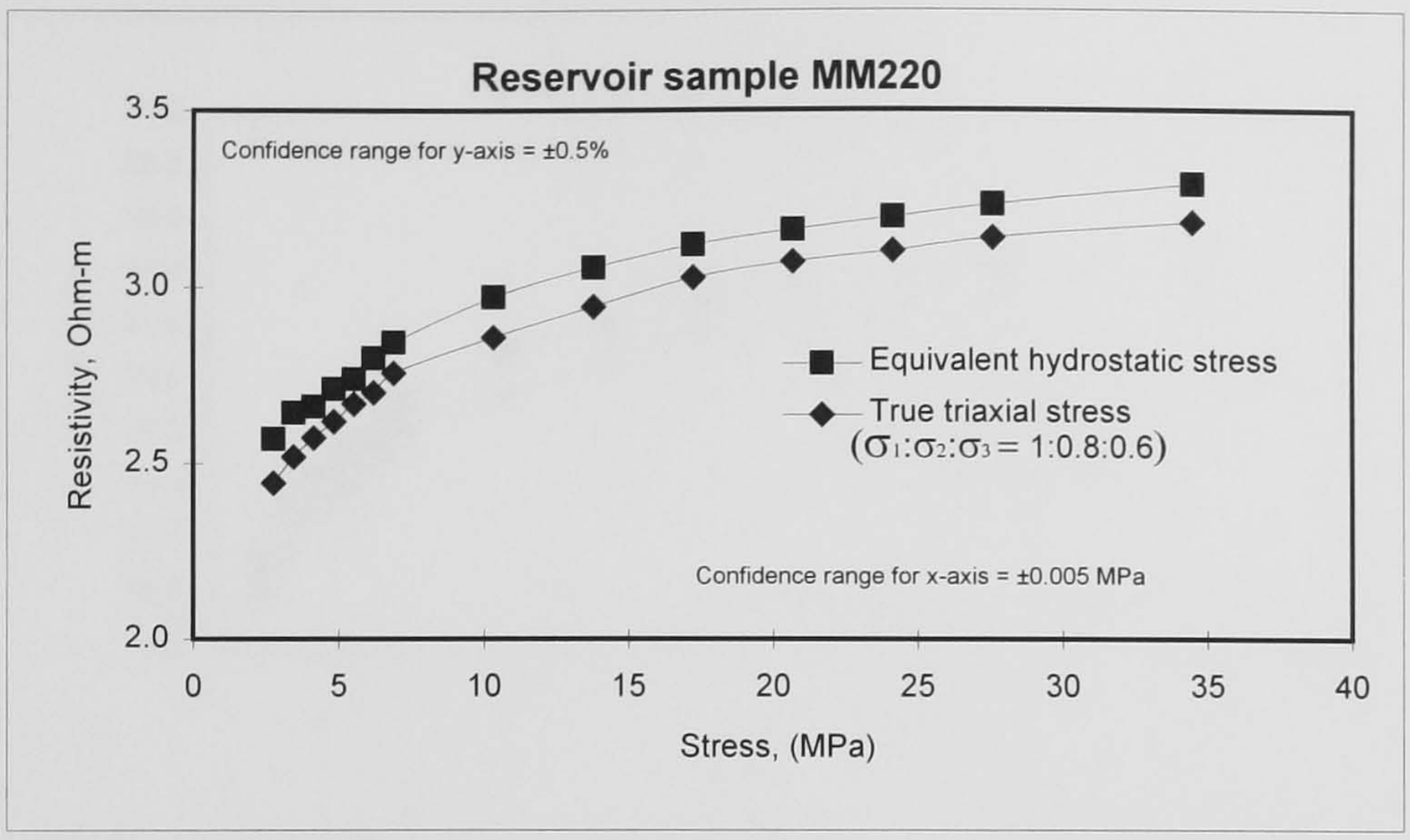

Figure 5.7 Resistivity versus stress (reservoir sample)

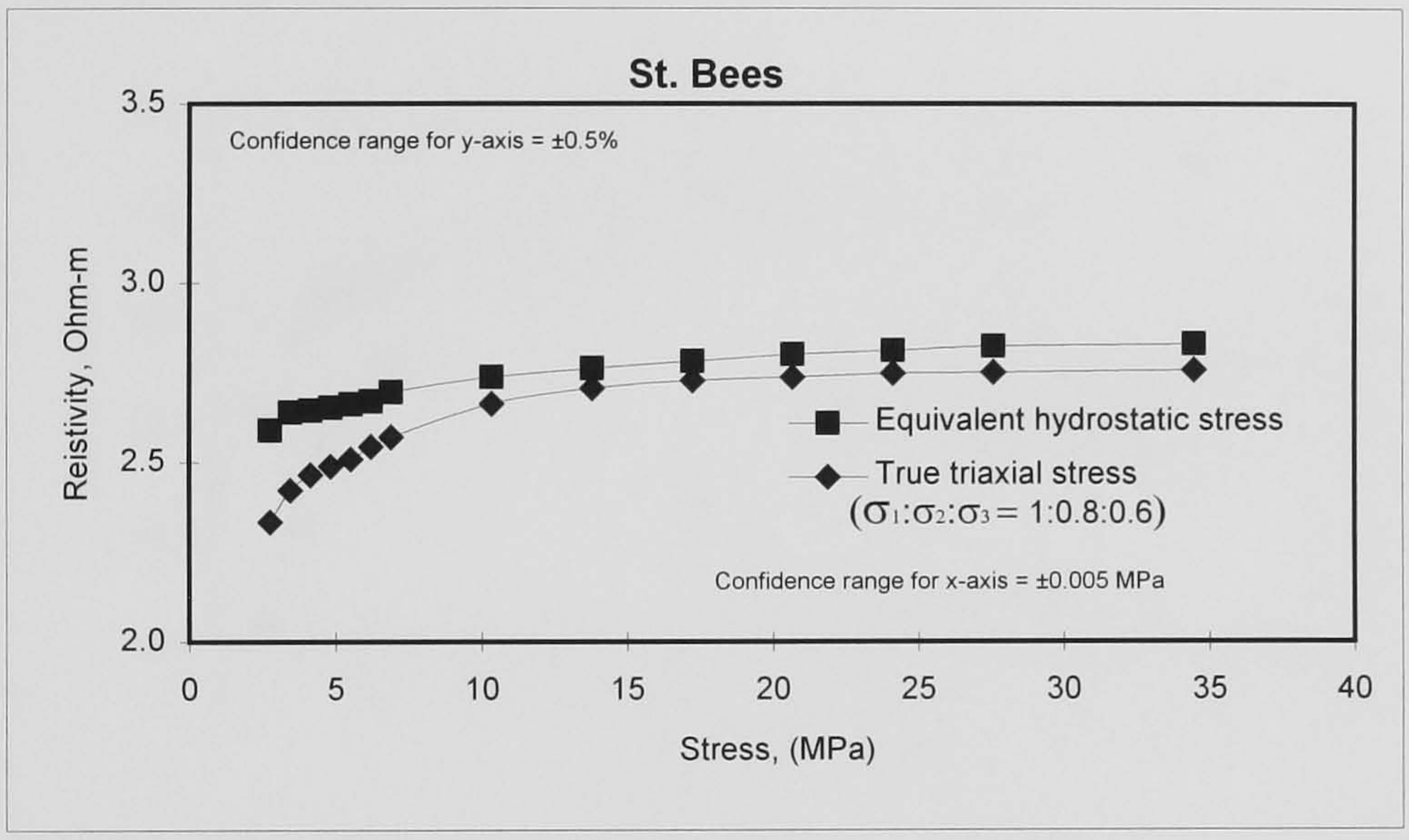

Figure 5.8 Resistivity versus stress (St. Bees)

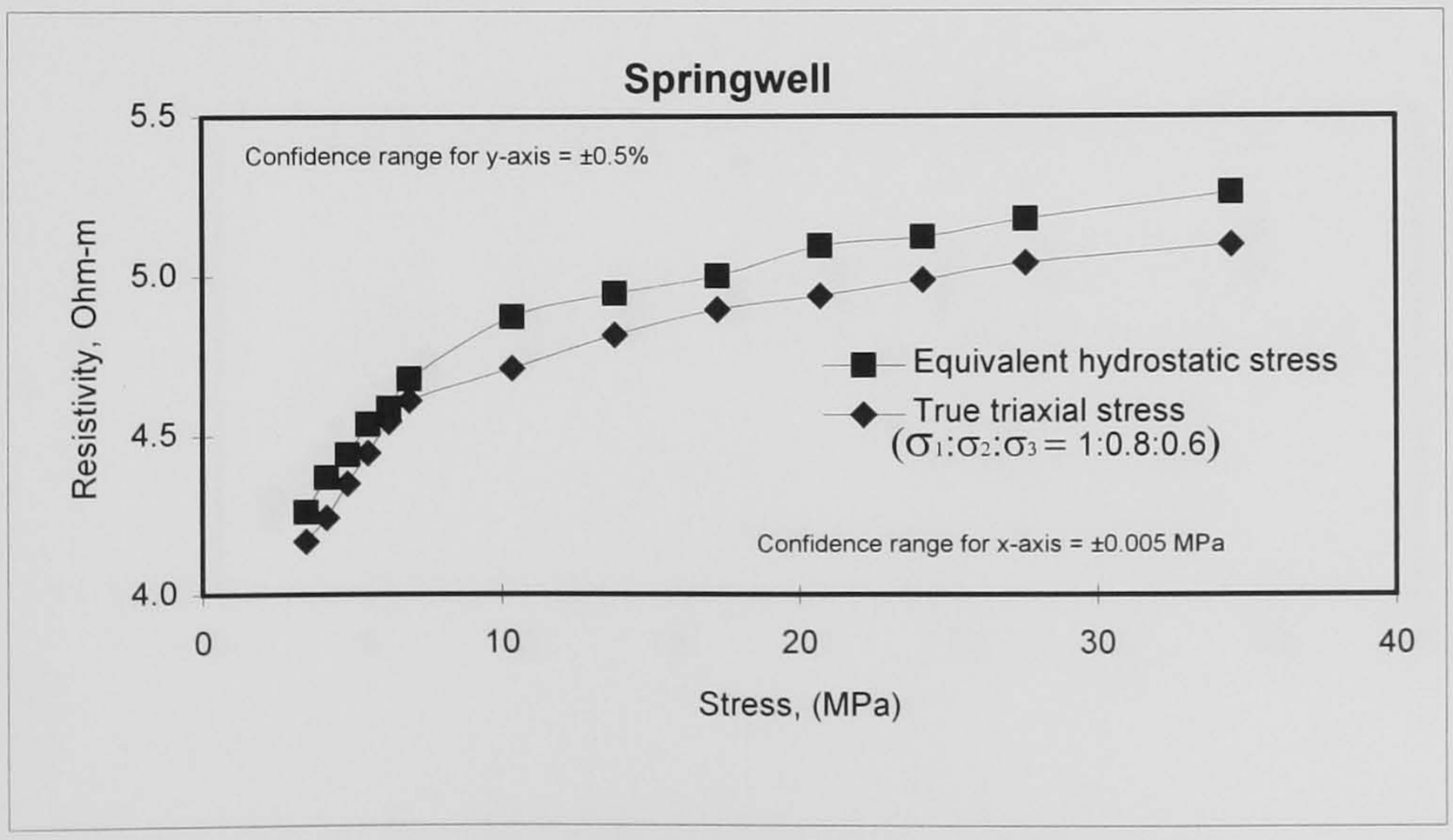

Figure 5.9 Resistivity versus stress (Springwell)

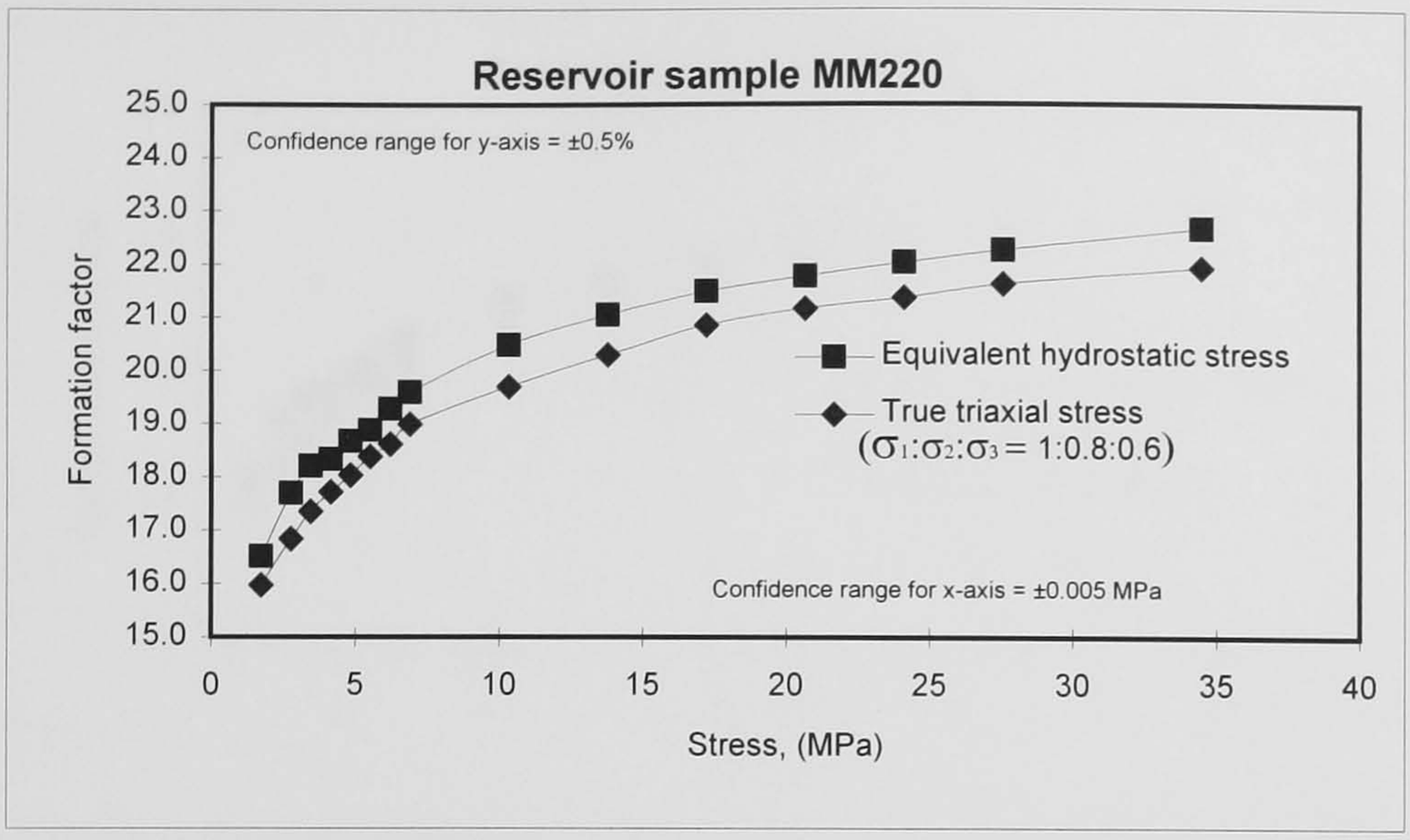

Figure 5.10 Formation factor versus stress (reservoir sample)

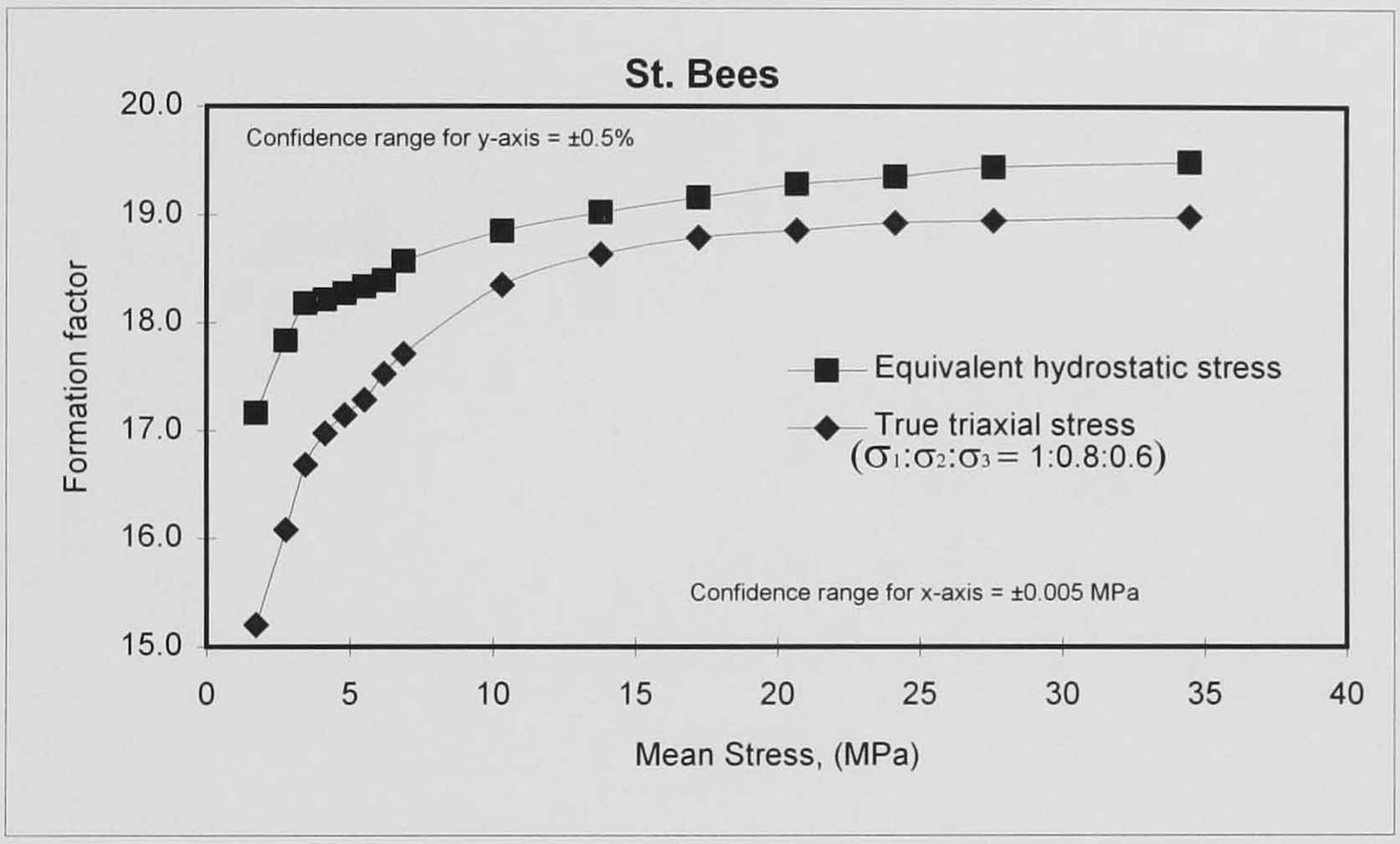

Figure 5.11 Formation factor versus stress (St. Bees)

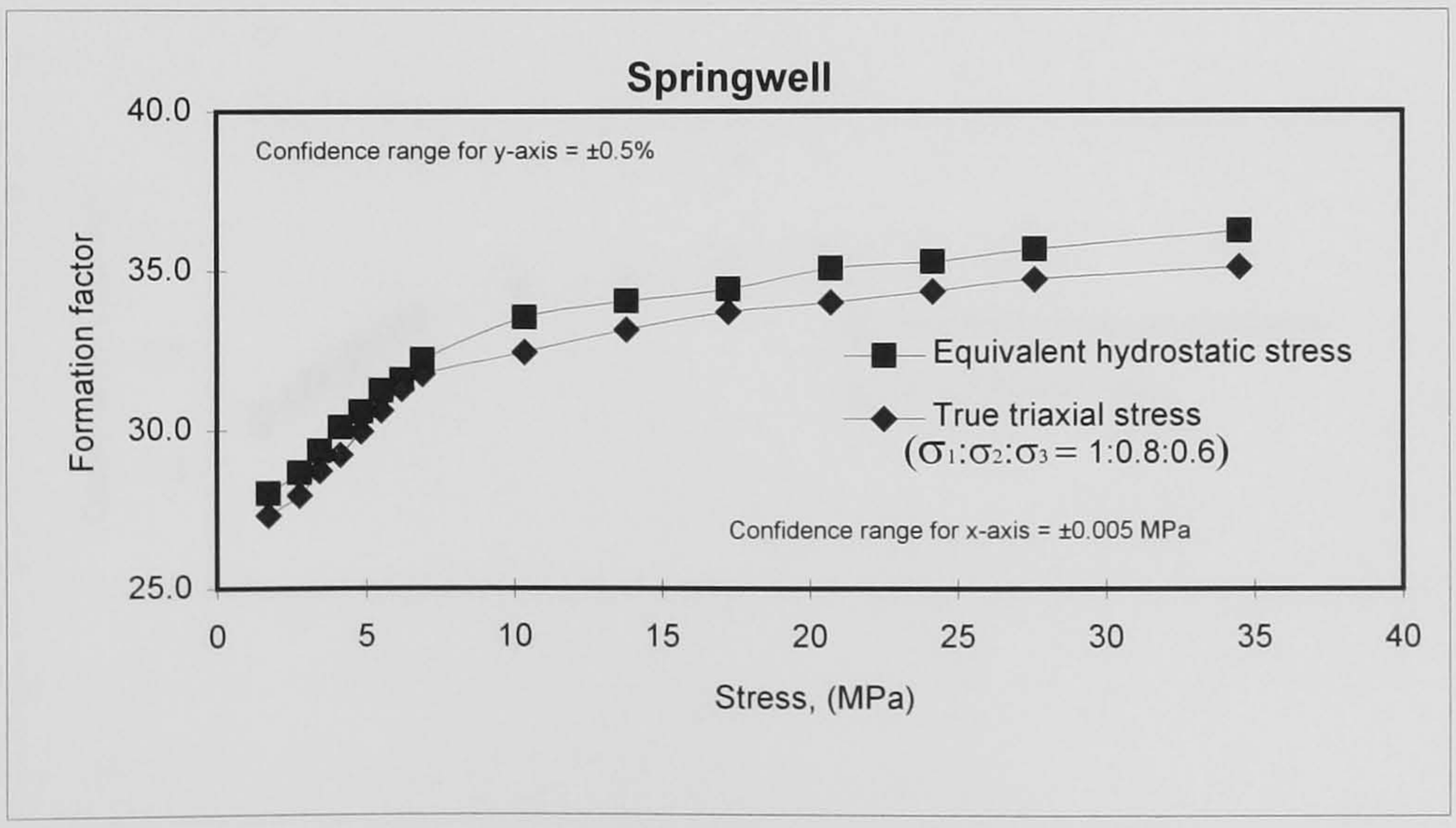

Figure 5.12 Formation factor versus stress (Springwell)

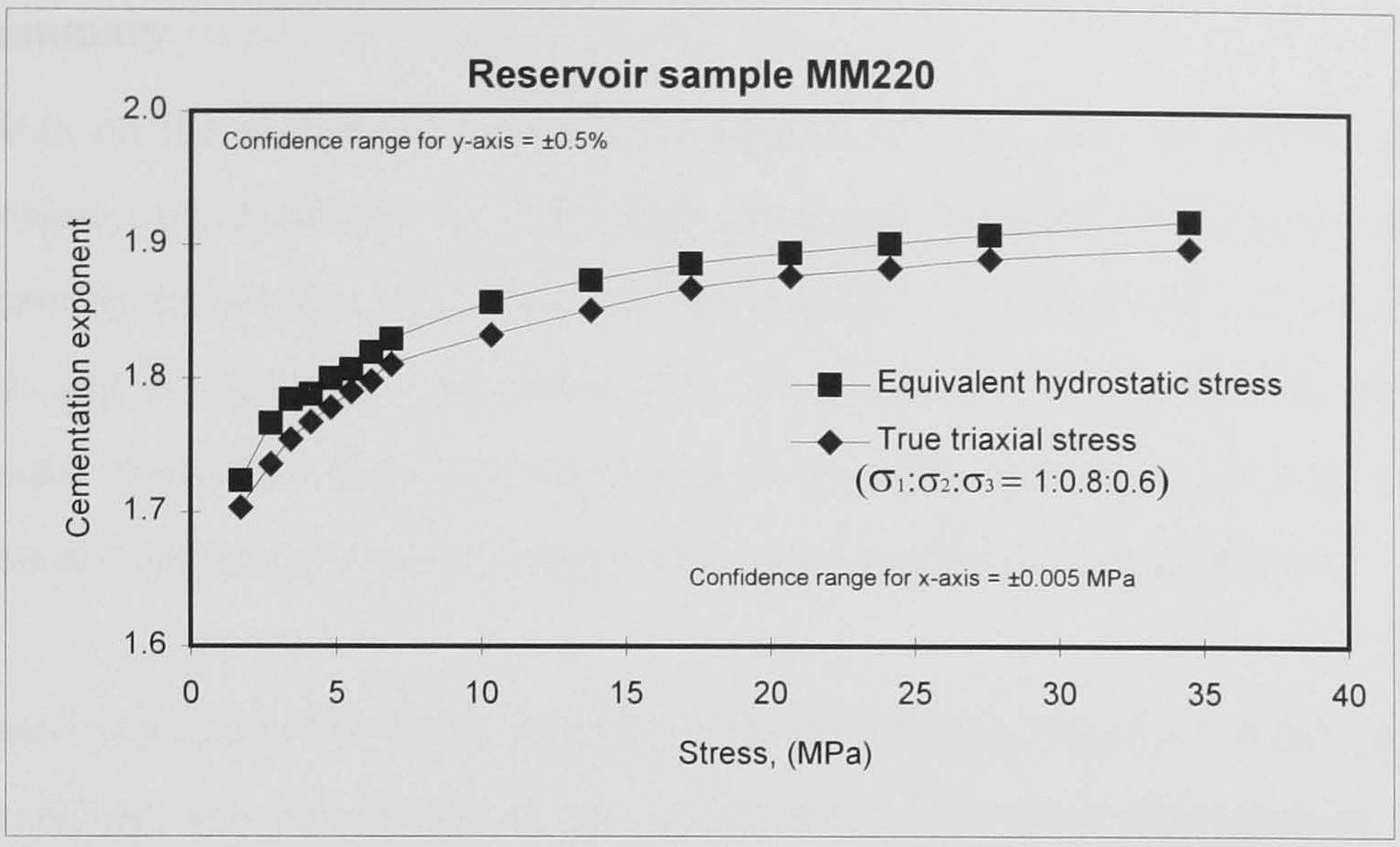

Figure 5.13 Cementation exponent versus stress (reservoir sample)

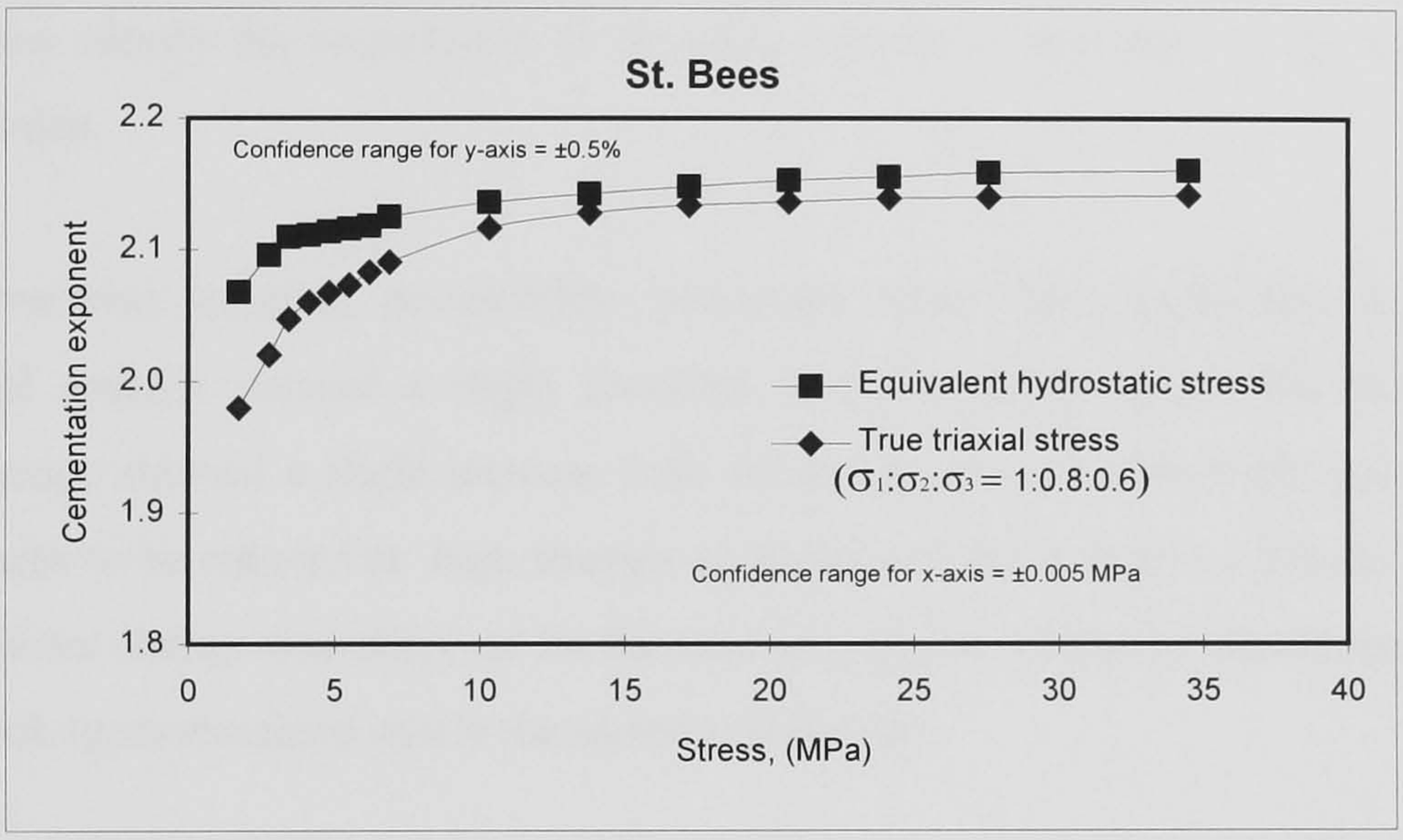

Figure 5.14 Cementation exponent versus stress (St. Bees)

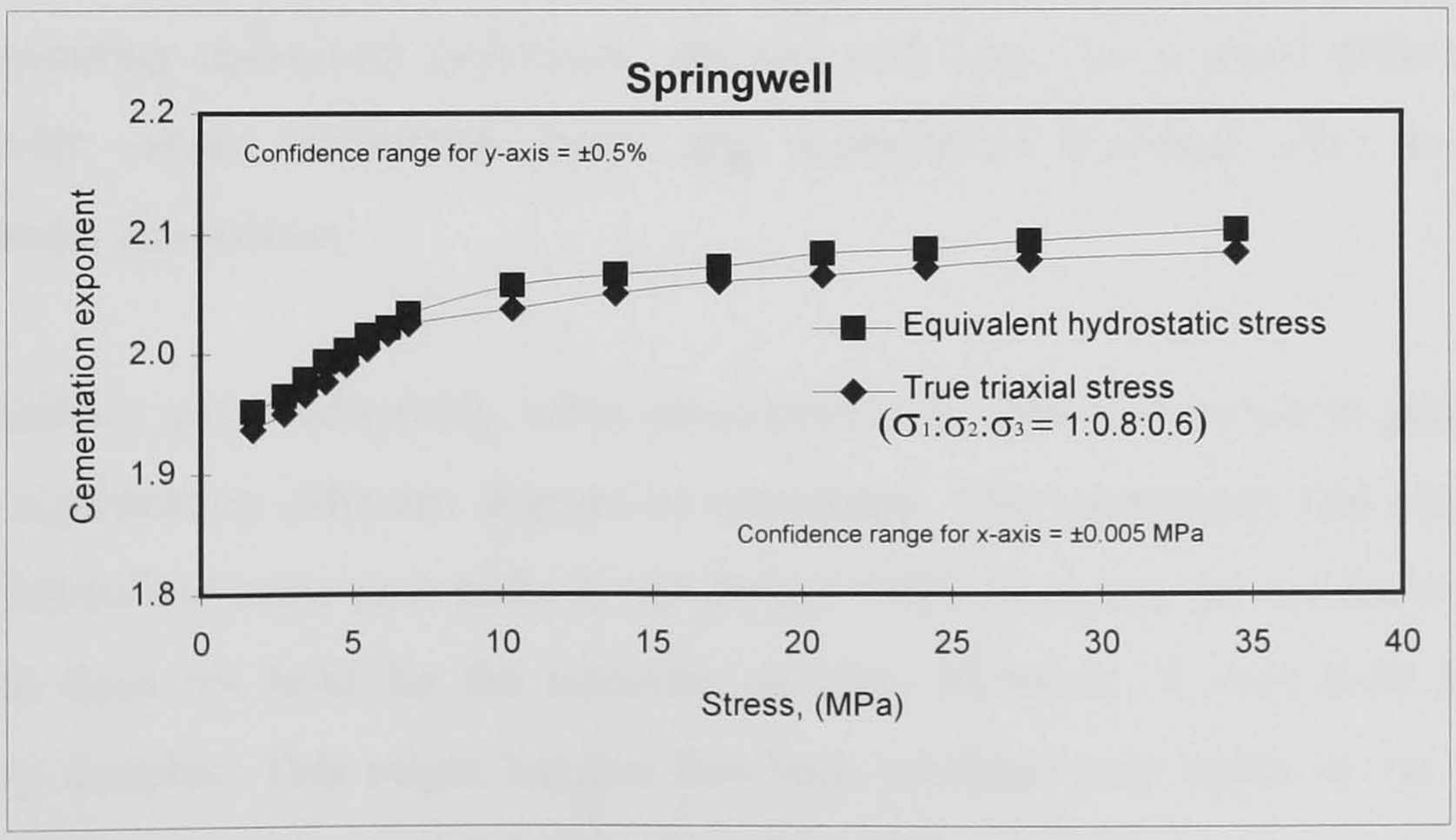

Figure 5.15 Cementation exponent versus stress (Springwell)

5.5 Summary

The tests on the samples (i.e., reservoir sample, St. Bees and Springwell) showed high degrees of anisotropy for both permeability and resistivity. Different values of permeability anisotropy were observed depending on which horizontal direction is used during the calculation. In addition, there was also permeability anisotropy in the horizontal directions. There was no electrical resistivity anisotropy between the two horizontal directions except in the case of a single sample (i.e., Springwell).

A novel procedure has been developed for the measurement of three principal permeabilities and resistivities in the same sample. The main advantage is that all measurements are performed on a single sample, and therefore, it has been possible to show clearly the importance of the third principal component of the transport properties.

For reservoir samples, permeability anisotropy under both hydrostatic and true triaxial stresses showed a slight decrease with increasing stress. The resistivity anisotropy showed a slight increase with increasing stress. Permeability anisotropy was seen to be reduced at high stresses in the case of the reservoir samples, and no significant change was observed for the outcrop samples. Electrical anisotropy for all the rock types remained nearly the same at all stresses.

The permeability values were found to be higher under true triaxial stresses than at corresponding equivalent hydrostatic stresses, and there was a small difference in resistivity values. Formation factor and cementation exponent also show the directional dependency.

Permeability and conductivity, often considered to be analogue transport properties, show significantly different degrees of anisotropy. The assumption that electricity and fluid follow same pore paths is not always valid. Based on the results here, this relation does not hold for the reservoir samples. However, it does hold for two outcrop samples. This might suggest that such relations only holds in the special cases, for example clean sand samples, i.e., free of clay minerals.

There was more pore volume change under hydrostatic than under true triaxial stress, whilst resistivity, formation factor and cementation exponent showed little difference. As the stress increased, resistivity, formation factor and cementation exponent also increased.

Overall, the results show the importance of measuring directional transport properties under different stress conditions. The improved knowledge of directional permeability, resistivity and pore volume change will lead to more realistic predictions of future performance in hydrocarbon reservoirs.

CHAPTER 6

EFFECT OF TRUE TRIAXIAL STRESS ON CAPILLARY PRESSURE CURVES AND ELECTRICAL PROPERTIES

6.1 Introduction

Capillary pressure is a fundamental input for predictions of hydrocarbon in place and fluid displacement behaviour. It reflects rock and fluid interactions and controls hydrocarbon saturation and trapping characteristics. The balance between gravity and capillary forces governs the initial fluid distribution and equilibrium in the reservoir.

Most core analysis studies only measure capillary pressure curves in the drainage cycle. In this study we use the term drainage to mean oil displacing brine and imbibition to mean brine displacing oil. The drainage capillary pressure is therefore the difference in oil and brine pressure measured as function of brine saturation at capillary equilibrium. There is hysteresis between the drainage and imbibition curves, which is caused by the difference in the fluid distribution in the pore network during wetting phase saturation decreases and increases. The drainage and imbibition curves may be used as an indication of wettability of a core, and for estimating the irreducible non wetting phase saturation.

These capillary pressure curves should mimic different processes occurring during the history of the reservoir. For example, displacement of water by oil during the primary oil migration (drainage), and displacement of oil during water flooding and enhanced oil recovery (imbibition).

Routine laboratory measurements of capillary pressure are usually undertaken by mercury porosimetry. Mercury penetrates the pore network of a clean dry rock sample in pressure steps from vacuum up to 200 MPa. Mercury is the non wetting phase and the mercury vapour is the wetting phase. The volume of mercury intruded with each increment pressure rise is measured and a pressure curve is determined.

However, this method is destructive and imposes very high pressures into the pores, which can damage pore structures. Also, the conditions at which the measurements are performed may not be representative of reservoir conditions.

In this study the porous plate method has been used since it gives the full capillary pressure curves for both drainage and imbibition, and the test is representative in terms of stress states and wettability in the reservoir. Also, uniform saturation distributions can be achieved using this method, and the test can mimic oil migration from source rocks, and water flooding or EOR processes.

In this study capillary pressure curves have been determined, for the first time, under realistic and true triaxial stresses as well as under hydrostatic stresses, using the porous plate method. This chapter presents these laboratory measurements of capillary pressure and electrical properties on sandstones containing two fluid phases.

A series of experiments were conducted on outcrop and reservoir samples (i.e., Croslands Hill and Clashach sandstones, and reservoir samples IM and 1L from the North Sea). First, the tests were conducted on the two reservoir samples at ambient and high hydrostatic stresses, and drainage capillary pressure curves were determined. Secondly, the outcrop samples were tested under a hydrostatic stress of 34.5 MPa and true triaxial stresses in the ratio of 1:0.8:0.6 (i.e., 43.1:34.5:25.9 MPa). In this test both the drainage and imbibition capillary pressure curves were determined under stresses. The resistivity index for different saturations were also determined. These experiments were designed to study the effect of hydrostatic stresses, and to compare the results between true triaxial stress and its equivalent hydrostatic stress.

6.2 Capillary Pressure Curves

During laboratory measurements of capillary pressure curves it is common practice to measure rock properties without necessarily taking into account the stress effects, even though the properties at reservoir conditions might differ significantly from those measured under laboratory conditions. Most core analysis laboratory

measurements of capillary pressure are done by mercury porosimetry or centrifuge techniques. However, neither of these techniques duplicates *in situ* conditions. In the mercury injection process, it is necessary to use appropriate factors to convert the measured capillary pressure curves into those for an oil/water system. With the centrifuge technique it is debatable whether or not the high forces causing desaturation in the centrifuge represent reservoir displacement mechanisms, since they can cause uneven saturation distribution. In addition, the data obtained by both methods use normally unstressed samples to describe the matrix at *in situ* stress. Thus the question remains whether or not routine capillary pressure data from such measurements can be realistically extrapolated to *in situ* stress conditions and into two phase fluid flow reservoir simulations. This thesis investigates capillary pressure curves under realistic true triaxial stress.

Figure 6.1 shows the drainage capillary pressure curves of two duplicate reservoir samples 1L and 1M measured at ambient and hydrostatic stresses. All the data points were recorded when capillary pressure equilibrium had been achieved. The plot shows capillary pressure against brine saturation at every equilibrium point, as indicated by no further change occurring to resistivity or brine volume. For the early measurements at low capillary pressure (i.e., 0 to 5 psi), equilibrium for each capillary pressure point took an average of one to two weeks. However, for high capillary pressures, around five to seven days were sufficient, due to the use of highly permeable capillary membranes/ceramic discs.

A comparison of the drainage capillary pressure curves at ambient and hydrostatic stresses shows that the drainage capillary pressure increases with stress. The curve at ambient shows less irreducible brine saturation compared to that measured at high stress. The lower volume of water retained within the pore structure during the desaturation process may be simply due to the fact that the pore bodies and throats are less compressed at lower stress compared to at high stress. This causes a change in pore size distribution of the rock. This argument can be supported by the Laplace equation, (see Equation 2.9) which describes how capillary pressure increases with decreasing pore radii. Hence, any increase in capillary pressure with stress is mainly

due to the reduction in pore sizes. In addition, the curve at ambient conditions may be misleading in qualitative reservoir descriptions. In contrast, the curves measured at the stressed states may give better reservoir descriptions, with measurements performed under true triaxial stresses being expected to give the most representative data.

Figure 6.2 shows the capillary pressure curves versus brine saturation for Clashach outcrop sandstone under realistic hydrostatic and true triaxial stresses. The curve for the true triaxial stress state shows less irreducible brine saturation compared to that measured under equivalent hydrostatic stress. This may be because pores are less compressed under true triaxial stress. Based on these measurements, even though both are at high stress, it might be expected that capillary pressure curves might be different depending on the states of stress applied during measurements. This might have an implication on irreducible brine saturation from the capillary pressure curve and hence on the calculation of oil in place.

Figure 6.3 shows the full capillary pressure curves for Clashach sample (i.e., for drainage, imbibition and secondary drainage) measured at hydrostatic stress (34.5 MPa). These curves mimic different displacement processes, with the drainage curve representing how oil migrates into reservoir rocks from source rocks and the imbibition curve mimicing a water flood process. Oil displacing brine drainage leaves an irreducible water saturation of around 28%. Reducing capillary pressure to zero allows brine to spontaneously imbibe into the rock. Brine saturation increases to 45% during spontaneous imbibition, indicating a water wet tendency. Forced imbibition drives the oil saturation to 44%, indicating that the total oil recovered represents 28% of the total pore volume. Secondary drainage results in the same irreducible brine saturation as primary drainage, indicating that the fluids follow the same paths once the primary and secondary curves overlap, which indicate there is no wettability change.

Figure 6.4 shows the drainage capillary pressure curve for Croslands Hill sandstone under hydrostatic stress. The shape of drainage curve indicates that the sample is well

sorted and has uniform pore size. However, the irreducible brine saturation is high, this may be due to low permeability of the sample. The data from mercury capillary pressure of duplicate sample shows similar behaviour. Figure 6.2 shows small entry pressure and lower irreducible water compared to Figure 6.4. This may be due to the permeability value being high. Due to the long time taken when using the porous plate method, measurements on a comparable duplicate sample could not be completed under true triaxial stresses within the time frame of this research. In fact, few previous studies have looked at the effect of stress on capillary pressure curves, so it remains that further work is needed to gain a better insight into the mechanisms of how stress affects capillary pressure curves.

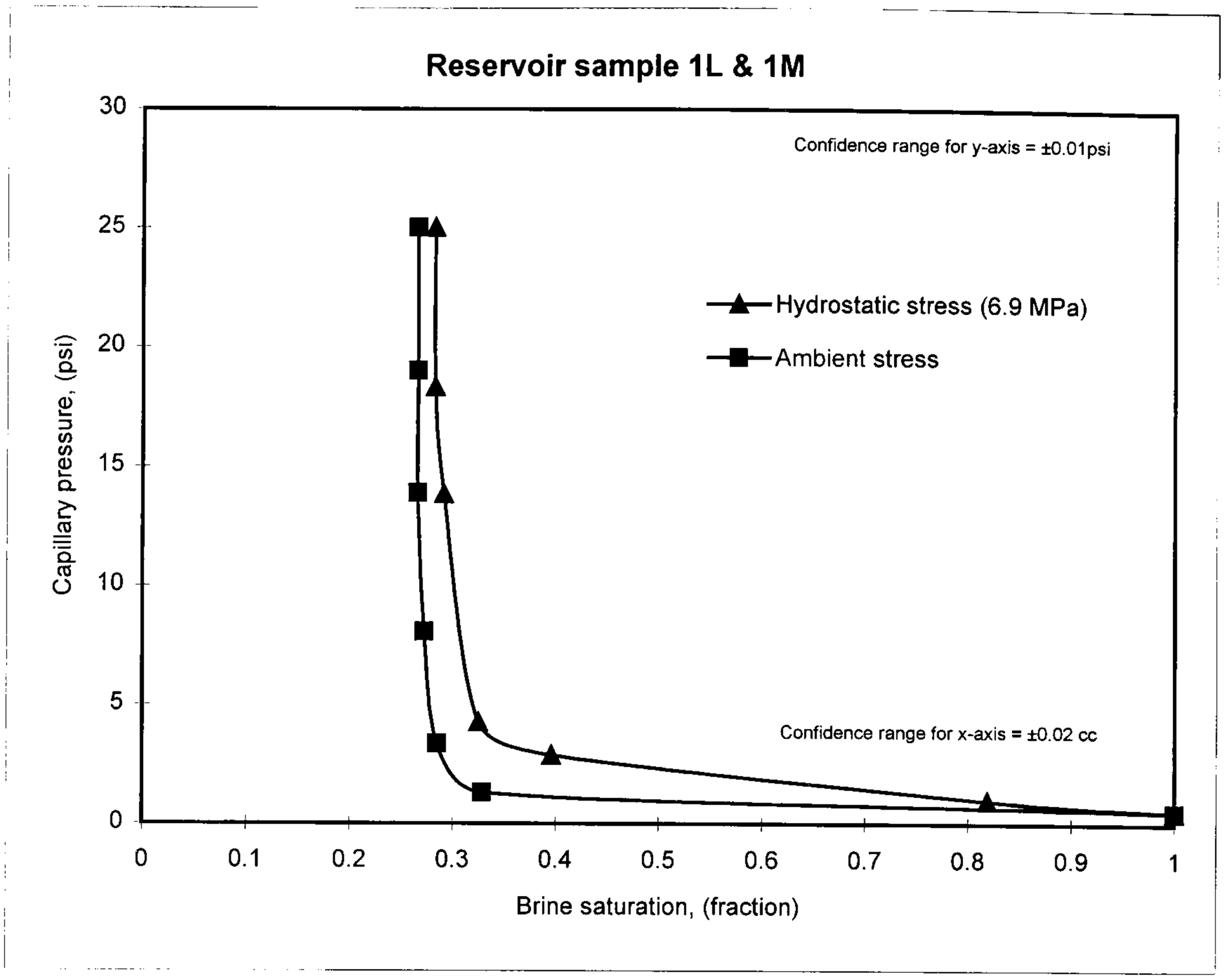

Figure 6.1 Capillary pressure curves at ambient and hydrostatic stress (North Sea oil field 1L & 1M)

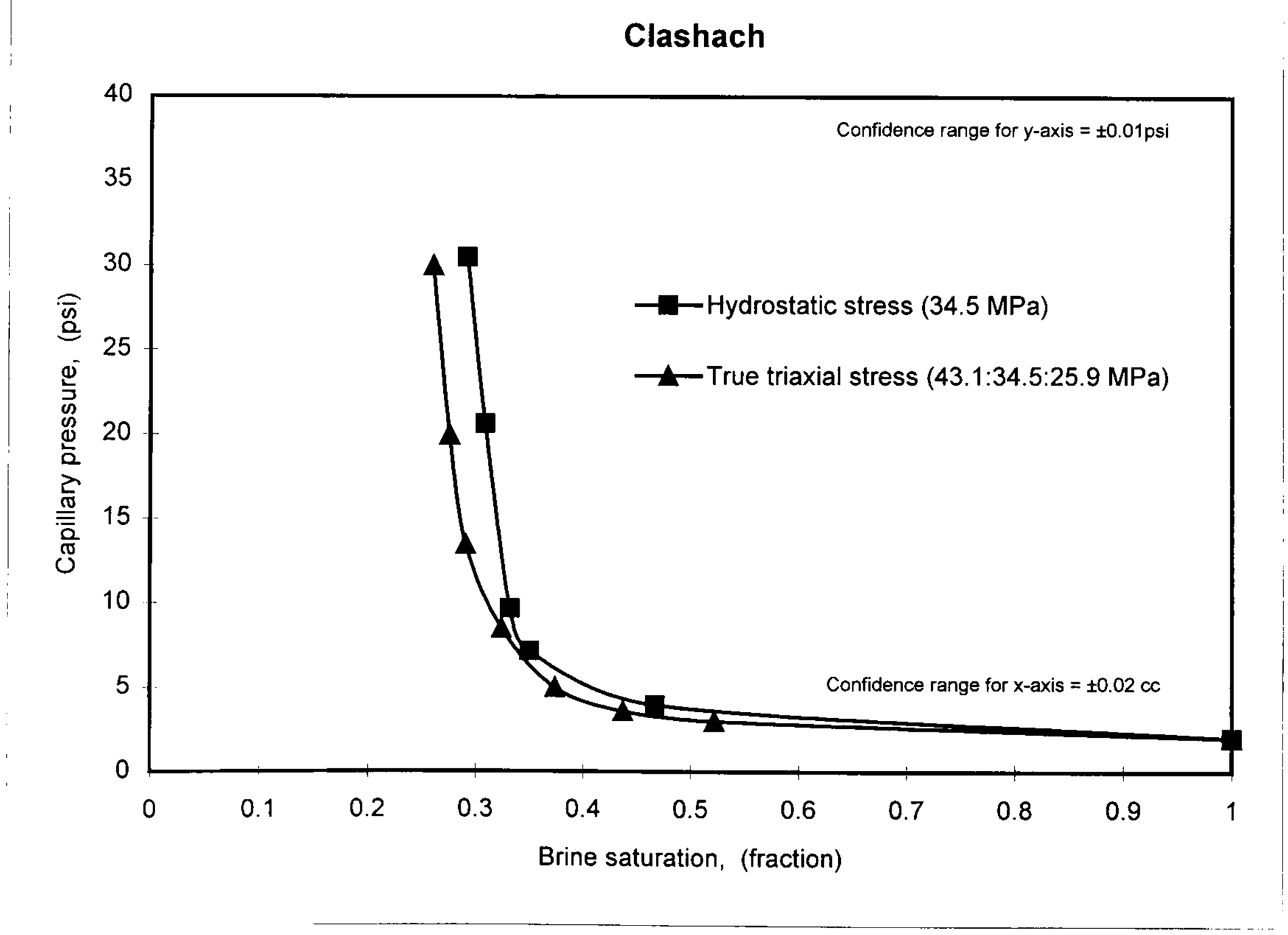

Figure 6.2 Capillary pressure curves under hydrostatic and true triaxial stresses (Clashach)

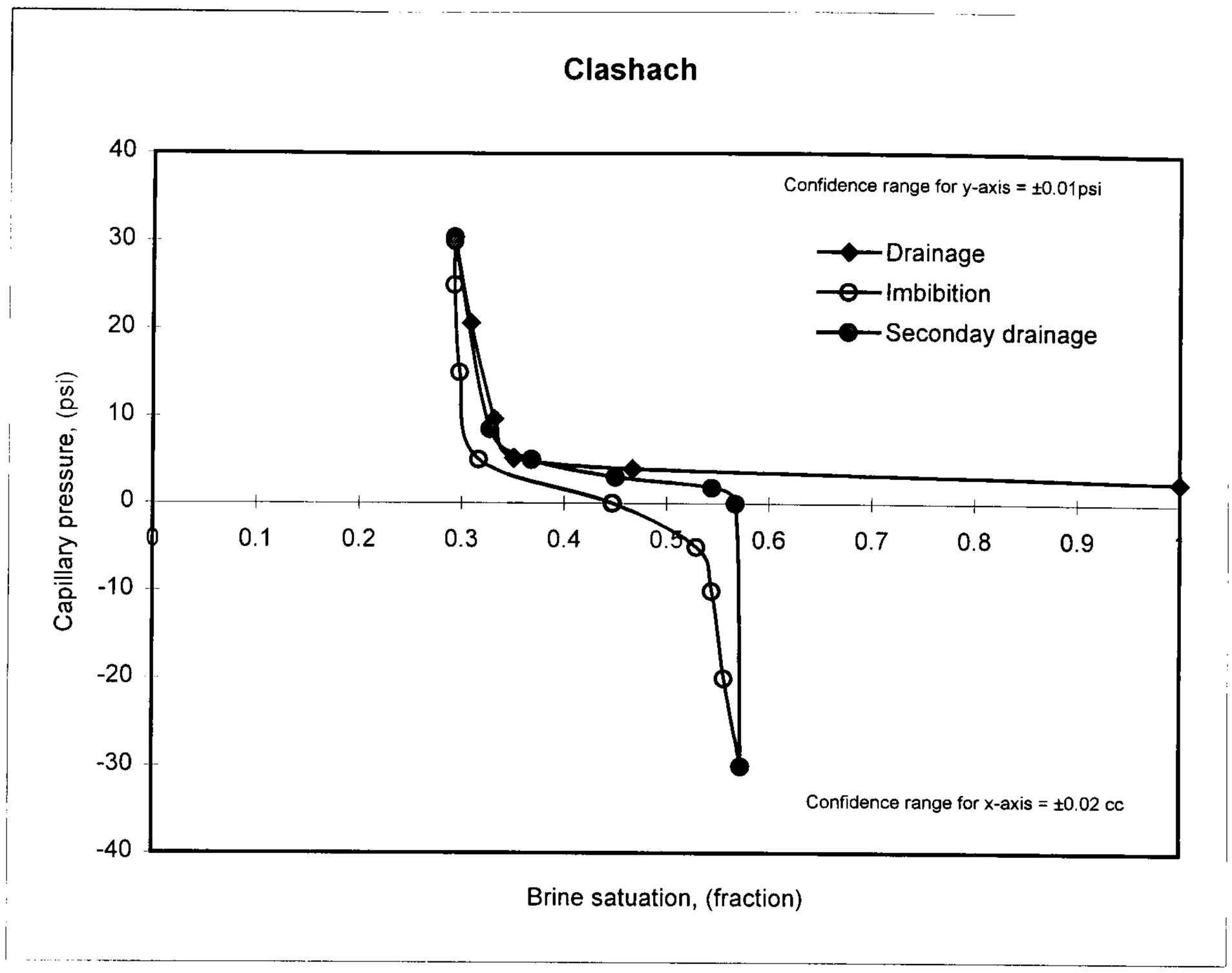

Figure 6.3 Capillary pressure curves at hydrostatic stress of 34.5 MPa (Clashach)

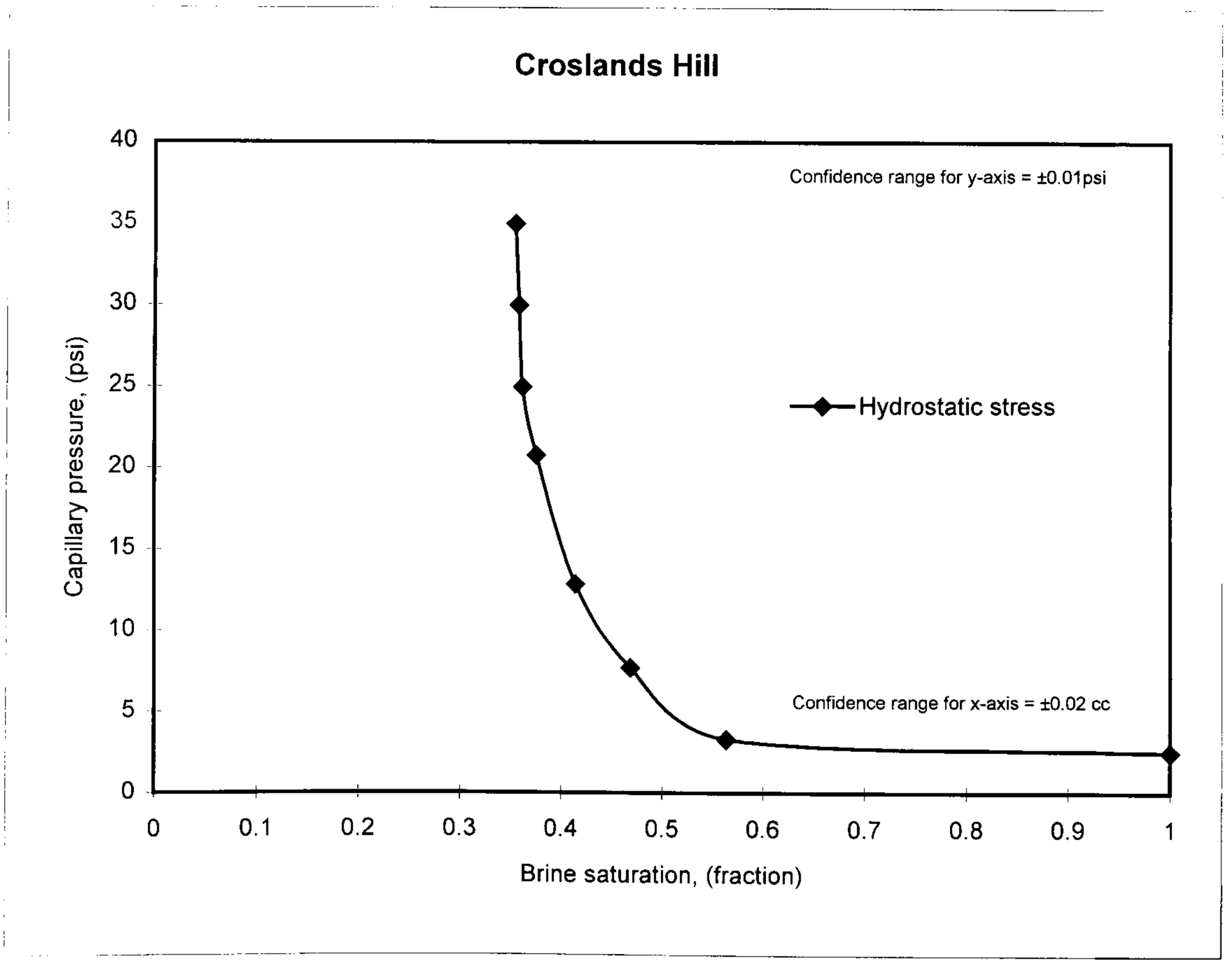

Figure 6.4 Capillary pressure curve at stress of 34.5 MPa (Croslands Hill)

6.3 Electrical Properties of Oil/Brine/Rock Systems

During laboratory measurements of electrical properties of reservoir rocks it is important to design tests that mimic the relevant displacement processes occurring during the history of a reservoir. Relationships of resistivity index against brine saturations depend on magnitude and orientation of the stress. Thus conditions in laboratory measurements should be as close as possible to those encountered *in situ*.

Any increase of resistivity caused by a hydrocarbon displacing brine depends not only on the saturation but also on how the fluids are distributed in the pore spaces. The pore fluid distribution is related to factors such as wettability, pore size distribution and saturation history. When pores are reduced in size there are changes to the length and cross sectional areas of conductive paths, and hence changes to resistivity. Hydrocarbon reservoir rocks experience considerable stress from three main sources; the burial depth induces stress by vertical loading, lateral stresses occur due to geological deformation and lateral confinement, and pore pressures occur due to hydrostatic fluid columns and overpressures. When cores are brought to the surface and to atmospheric pressure the stress is released and the rock begins to relax. This causes changes to the pore structure, and hence changes occur to rock characteristics including electrical properties. The effects of stress on the resistivity index at various saturations have rarely been investigated by previous researchers due to experimental difficulties and the long time periods involved in such measurements.

Little previous work is reported for resistivity indices at stress of various sandstone and limestone rocks, as compared to studies on formation factor and cementation factor. Granville (1959) and Jing *et al.* (1993) concluded that the saturation exponent increases with confining pressure, whilst others (e.g., Longeron *et al.,* 1986, and Lewis *et al.,* 1988) have concluded that saturation exponent decrease slightly with increase confining pressure. To date no publication is available on the effect of true triaxial stress on resistivity index versus saturation.

In this study electrical properties were investigated under different elevated stresses. The experimental results of rock samples fully and partially saturated by brine and under stress have been analysed and presented. Formation factor, cementation factor and saturation exponent have been calculated (see Equation 2.16). All measurements were recorded under hydrostatic and true triaxial stresses, and corrected to a temperature of 20°C. The capillary desaturation processes were achieved by using a water wet ceramic porous disk at one end of the samples and an oil wet porous ceramic disk at the other end as described in Chapter 3.

Figure 6.5 shows double logarithmic plots of resistivity index versus brine saturation under true triaxial and comparable hydrostatic stresses. The saturation exponent is calculated by forced linear regression based on the Archie equation (see Equation 2.16). The results show that for Clashach the saturation exponent at hydrostatic stress is larger than that at true triaxial stress. This is probably due to greater compression of the pores at hydrostatic stress, which leads to reduced pore sizes and increased tortuosity of the current flow. This will have an implication on calculation of water saturation and hence on log calibration.

Table 6.1 shows formation factor, cementation factor and saturation exponent for Clashach under true triaxial and equivalent hydrostatic stresses. The results show that under hydrostatic stress all the electrical properties are higher compared to those at true triaxial stress.

Table 6.1 Electrical properties under true triaxial and equivalent hydrostatic stresses (Clashach)

Stress	Formation factor, F	Cementation factor, m	Saturation exponent, n
Equivalent Hydrostatic (35 MPa)	88.0	1.94	2.20
True triaxial (43:35:26)	66.0	1.81	1.50

Figure 6.6 shows the resistivity index versus brine saturation under hydrostatic stress for two displacement processes, i.e., drainage and imbibition. The result shows that there is a phase dependent hysteresis which is also encountered in the corresponding capillary pressure measurements. The resistivity index versus brine saturation relationship was first determined by desaturating the fully brine saturated core sample until irreducible brine saturation was achieved, then the brine was introduced to the rock sample at different capillary pressure levels. Figure 6.7 shows the resistivity index versus brine saturation under realistic hydrostatic stress for Croslands Hill outcrop material. The values of the saturation exponents are in good agreement with results obtained by previous researchers (Elashahab, 1995).

In summary, there is a difference of capillary pressure and electrical properties under hydrostatic and true triaxial stresses. This may be due to the more significant changes in pore geometry and pore size distribution under hydrostatic stress and hence more tortuous brine phase leading to higher resistivity. As it can be seen in Table 6.1 the value of m is higher under hydrostatic than under true triaxial stress.

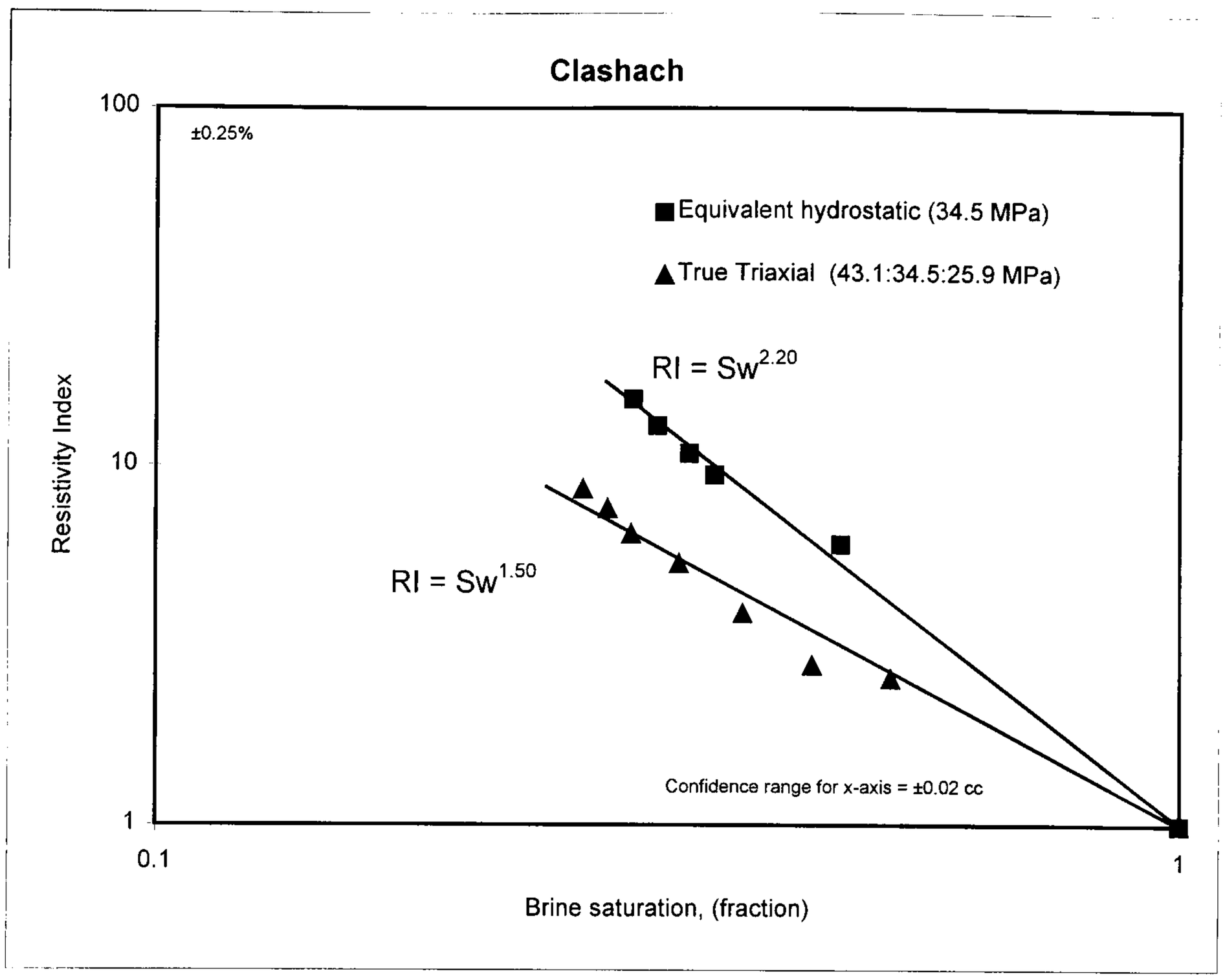

Figure 6.5 Resistivity index vs brine saturation under hydrostatic and true triaxial stresses (Clashach)

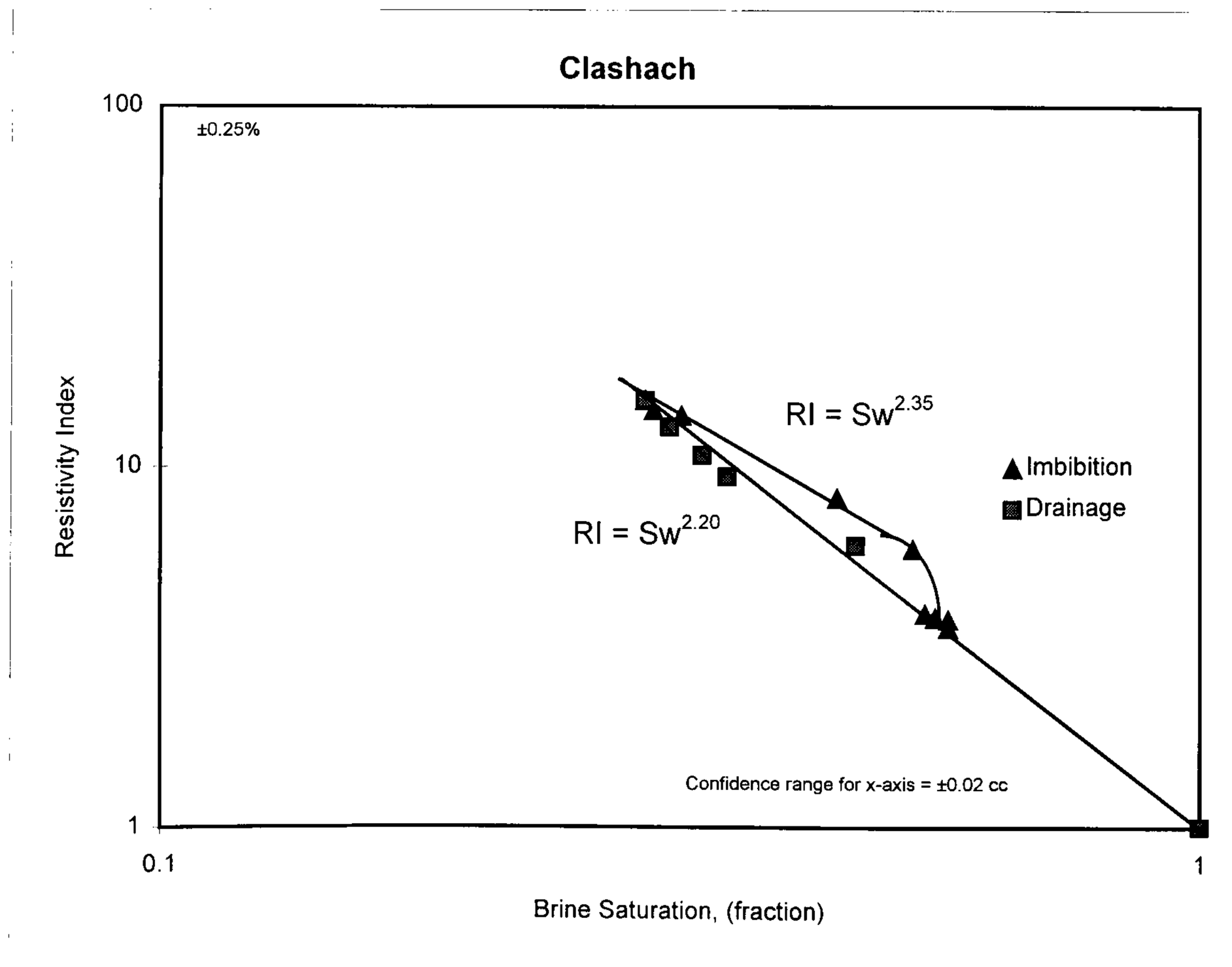

Figure 6.6 Resistivity index vs brine saturation at stress of 34.5 MPa (Clashach)

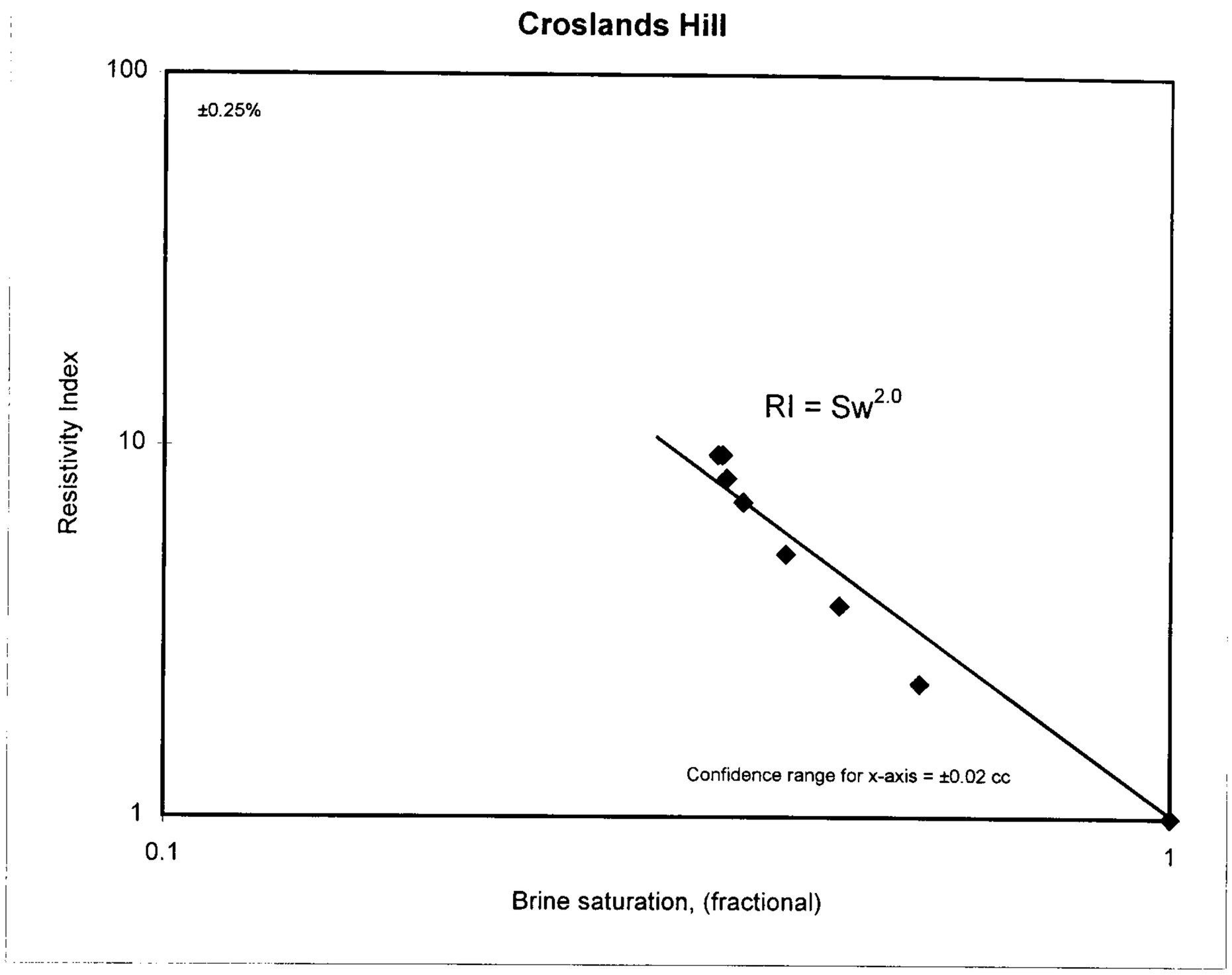

Figure 6.7 Resistivity index vs brine saturation at stress of 34.5 MPa (Croslands Hill)

6.4 Summary

The capillary pressure curves measured at ambient conditions showed lower capillary pressure and lower irreducible brine saturations compared to those at elevated stresses. Such data at ambient conditions may be misleading and can lead to wrong reservoir interpretations. Examples of this would be errors in estimates of initial fluid distributions in a reservoir, or errors in predictions of flood front movements under the influence of viscous, gravitational and capillary forces (Archer and Wall, 1986). In addition, representative capillary pressure curves are important in determining the transition zones and irreducible water saturation for hydrocarbon reservoirs, and during initialisation procedures in reservoir simulation.

Capillary pressure curves under true triaxial stresses showed lower capillary pressure and less irreducible brine saturation compared to those at comparable hydrostatic stresses. The data obtained at ambient and high hydrostatic stresses indicated the curves to be moving upwards, giving higher irreducible brine saturation as stress increased. In comparison, the curves obtained under true triaxial and their comparable hydrostatic stresses indicated the curves moving down and giving lower irreducible saturations. One common practice when simulating reservoir conditions during measurements of capillary pressure is to use equivalent hydrostatic stresses, but it is evident from this research that this might overestimate the value of irreducible brine saturation. However, due to time restrictions, only a limited number of measurements could be performed in this project and clearly more experimental work is needed to confirm this observation.

The measurements of electrical properties showed that values of formation factor, cementation factor and saturation exponent are higher under hydrostatic stresses than at comparable true triaxial stresses. Furthermore, phase dependent hysteresis (i.e., difference in oil displacing water and water displacing oil) was seen between the curves for the two different displacement processes, i.e., between drainage and imbibition.

CHAPTER 7

RESERVOIR ENGINEERING APPLICATIONS

7.1 Introduction

The predictions of reservoir performance using reservoir simulators require the input of representative rock properties. There is the need to know under which conditions such data have been measured, especially if one is attempting to study the uncertainty of the development. In fact, rock properties should always be measured under conditions as close as possible to those encountered in the reservoir, and therefore it is essential that laboratory studies are representative of real conditions in the field.

Since this project investigated rock properties under representative reservoir conditions (i.e., elevated pore pressure, true triaxial stress, dynamic permeability changes with pore pressure decline, permeability and resistivity anisotropy, and two phase conditions) it was appropriate to use these data to assess their impact on reservoir performance predictions. Therefore this chapter incorporates the experimental results into an Eclipse 100 Simulator (Schlumberger GeoQuest, Eclipse 100 98A Manual, 1998) to quantify the effects of petrophysical properties on the performance of model reservoirs.

Having collected data which could characterise the reservoir, the next step was to predict its performance under various production schemes. However, despite the fact that the simulator is one of the most robust used in the oil industry, the version used in this research can not handle all these effects directly, so could only be used indirectly to demonstrate what impact the data would have on reservoir engineering calculations relating to the production life of the imaginary reservoir.

Firstly, the changes in permeability with pore pressure were modelled to mimic the dynamic permeability changes during reservoir production. Permeability was initially considered to be constant during the production life, then was taken to change as pore

pressure declined. For example, if production was to be modelled over a period of one year, simulations runs were conducted for intervals of 1-4 months, each using different permeabilities whilst maintaining equilibrium in the reservoir. The results presented are based on a month time scale for updating stress dependent reservoir properties.

Secondly, the effect of stress states on permeability were incorporated into the simulator, using the data obtained in the laboratory under conditions of true triaxial or hydrostatic stresses.

Thirdly, the effect of anisotropy on permeability was investigated for a horizontal well. The three principal permeabilities were used to demonstrate production performance in two horizontal directions, x and y. Pressure maintenance was then imposed by the addition of a horizontal injection well, and the simulation was repeated.

All simulations showed significant differences in production and other performance indicators. Full details of the models can be found in appendix C.

7.2 Permeability

7.2.1 Description of the Base Model

The base reservoir model in this study had a grid block system of 50x50x10 (x,y and z) (see Figure 7.1). Each grid block was a cube of 50 feet in dimension. The reservoir was taken to be homogeneous with a porosity of 17% and a base permeability of 77 mD. After the base case simulation, permeability was varied based on the decline of pore pressure for both the near wellbore and far-field regions. The reservoir contained two phase oil and water, at an initial reservoir pressure of 4800 psi, and at a constant solution gas-oil ratio. The model was first run assuming natural depletion with one vertical well at its centre. The total production time was set at one year with one month time steps. The production well had bottom hole pressure control in which the bottom hole flowing pressure was set to be constant.

In the second part of the study the base reservoir model (see Figure 7.2) had the same grid block system, but the size of each grid block was 100 feet so that greater horizontal movement of fluid could be considered. The reservoir was again homogeneous with a porosity of 17% and permeabilities of 600, 358 and 15 mD in three principal directions x, y and z. The model was first run to simulate pressure maintenance, with one well at one corner acting as an injector and a second well at the centre acting as a producer. The production well had bottom hole pressure control, and the injection rate was controlled and its bottom hole pressure maintained. Full details of the models used in these studies are given in appendix C.

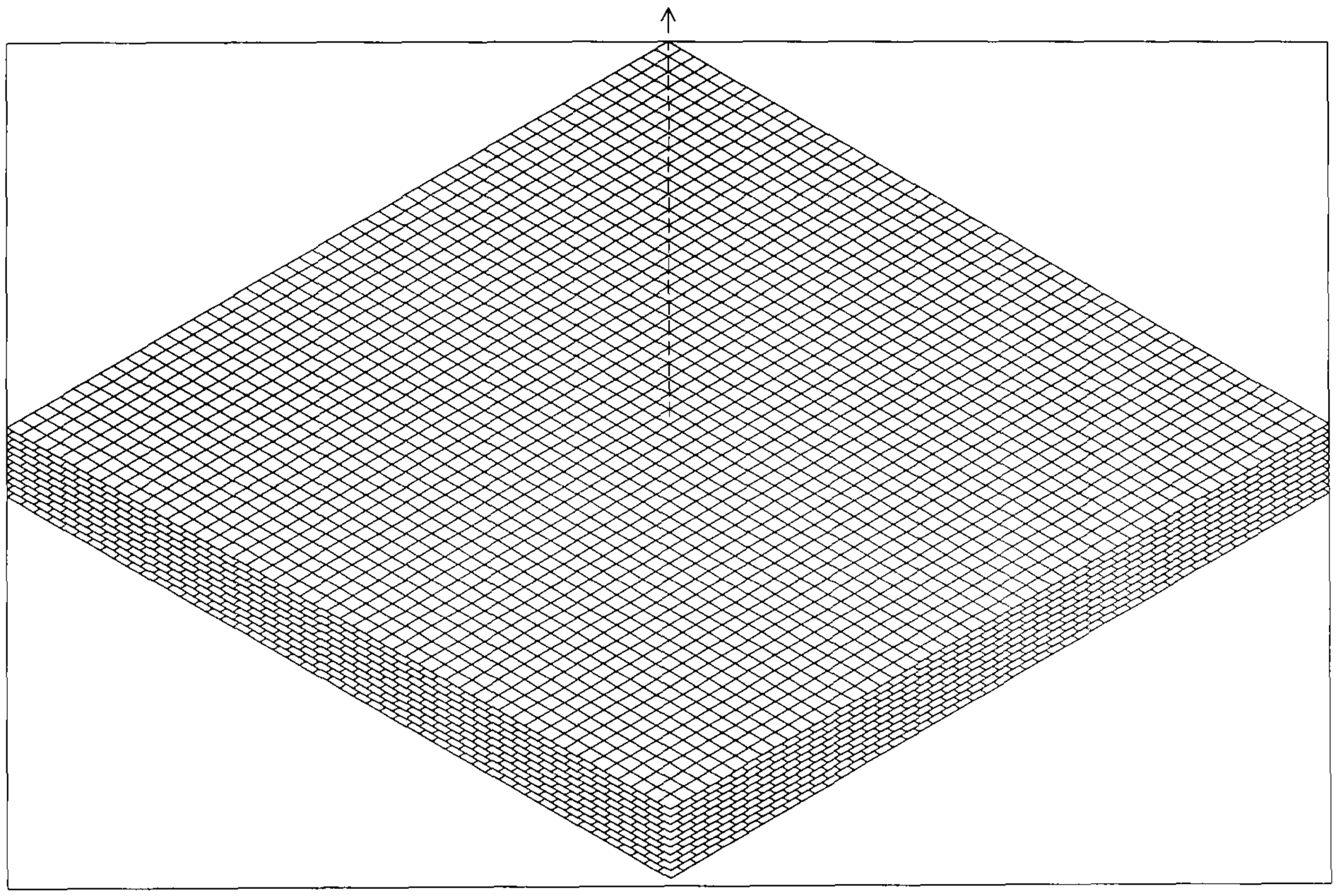

Figure 7.1 Base model used in natural depletion

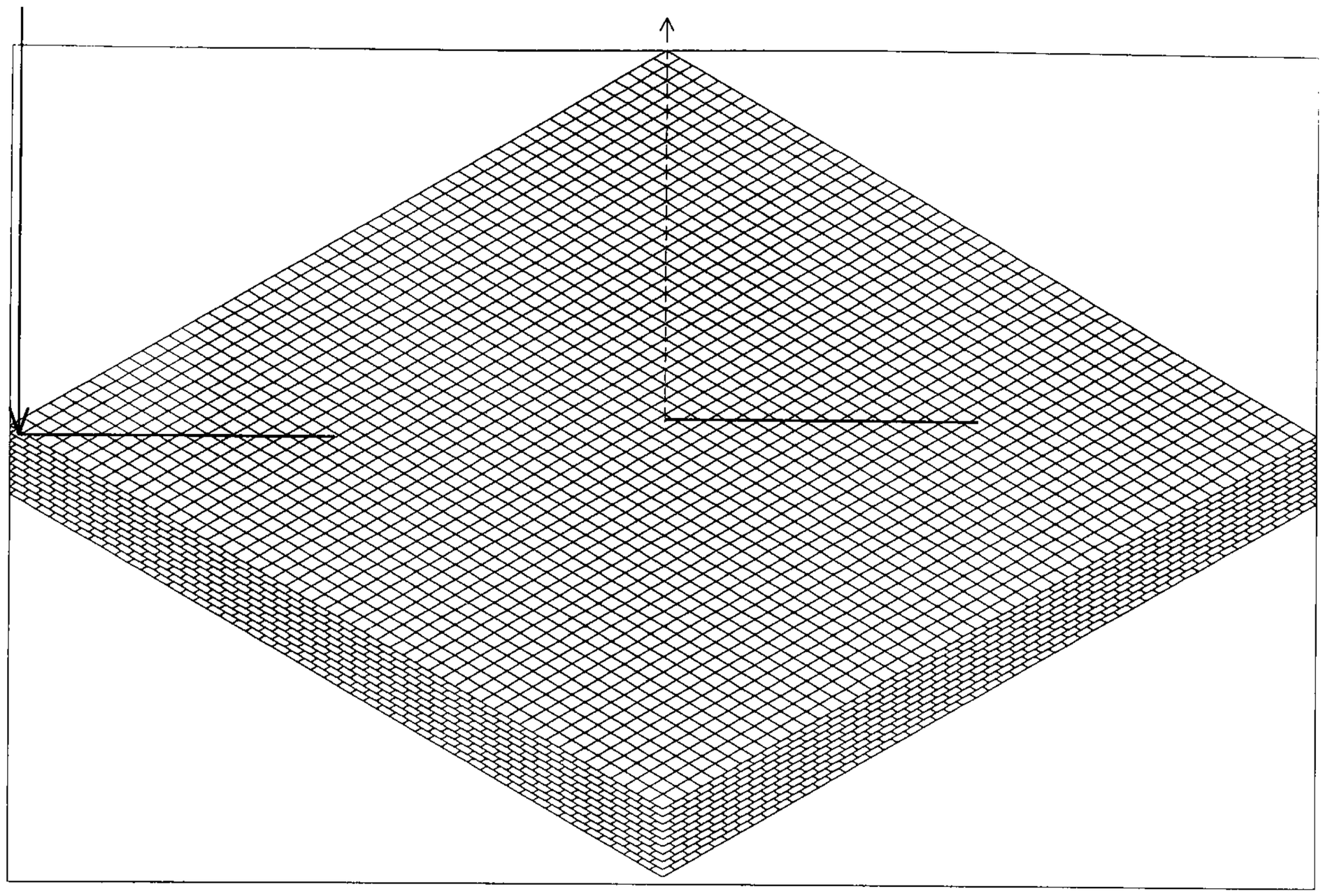

Figure 7.2 Base model used in pressure maintenance

7.2.2 Pore Pressure and Stress Effects

The production of hydrocarbons from petroleum reservoirs is accompanied by significant pressure drops around wellbores and, often, in the far-field. Clearly there will be a greater pressure drop around the wellbore, so the implication of this is that permeability will be reduced more in the near wellbore region compared to that in the far-field.

Therefore, in this part of the investigation, permeability was taken to be constant around the field, then a production induced dynamic change in permeability from the wellbore to the far-field was simulated, as pore pressure declined. The experimental data obtained from the research was also incorporated into the model.

Figures 7.3 and 7.4 show the field oil production and average pressure corresponding to constant permeability around the field. Permeability was also considered constant throughout the production time, as is common practice during most reservoir performance predictions. However, different degrees of reduction in permeability

were then introduced, i.e., 30% and 60% 90% from the original values of permeability. The results show a clear decrease in production as the permeability changes. As might be expected, such changes in permeability can be either constant or dynamic, i.e., changing with production. At 60% reduction there is a decrease of 26% in field oil production after one year compared to the base case, which would be very significant in terms of field economics. However, this part only shows the effect of constant changes in permeability fieldwide.

Figures 7.5 and 7.6 show the oil production and average pressure with changing permeability and changing pore pressure around the field. In this study, permeability was considered to change only once as the production progressed. The model was set for one year, and the simulation runs were interrupted and restarted after one month. At each pause, permeability was changed and reservoir equilibrium was maintained. The results show that there is decrease in oil production. This simulation shows that if you consider permeability changing once then this may lead to erroneous predictions and show that there is more reduction in oil production. At 60% permeability reduction there is a decrease of around 10% in total oil production. However, during production, permeability should change according to the rate of pore pressure decline, therefore a more realistic case, involving changing permeability with the amount of depletion, was simulated.

Figures 7.7 and 7.8 show oil production and average pressure for the simulation of continuously changing permeability and pore pressure. The model was set for one year, and simulation runs were stopped and restarted twice within the year; first month with permeability 77 mD, then four months at 30% reduction in permeability, then seven months at 60% reduction in permeability. The results were a decrease of 7%, in oil production compared to the base case, but a smaller reduction than seen in the previous simulations (see Figures 7.5 and 7.6). The runs were repeated with 40% and 80% reduction in permeability, which resulted in as much as 16% reduction to total oil production. In summary, as might be expected, there was less decrease in total production with the continuous permeability changes as compared to the reservoir having constant permeability changes.

Figures 7.9 and 7.10 show the field production and average pressure with continuously changing permeability and pore pressure using the data from the hydrostatic and true triaxial stress experiments. Here, permeability differences between true triaxial and hydrostatic stresses were 16%, and the simulation data show there is a more significant decrease in total production under hydrostatic stress than under a state of true triaxial stress, i.e., a decrease of around 12% from the base case compared to 7% .

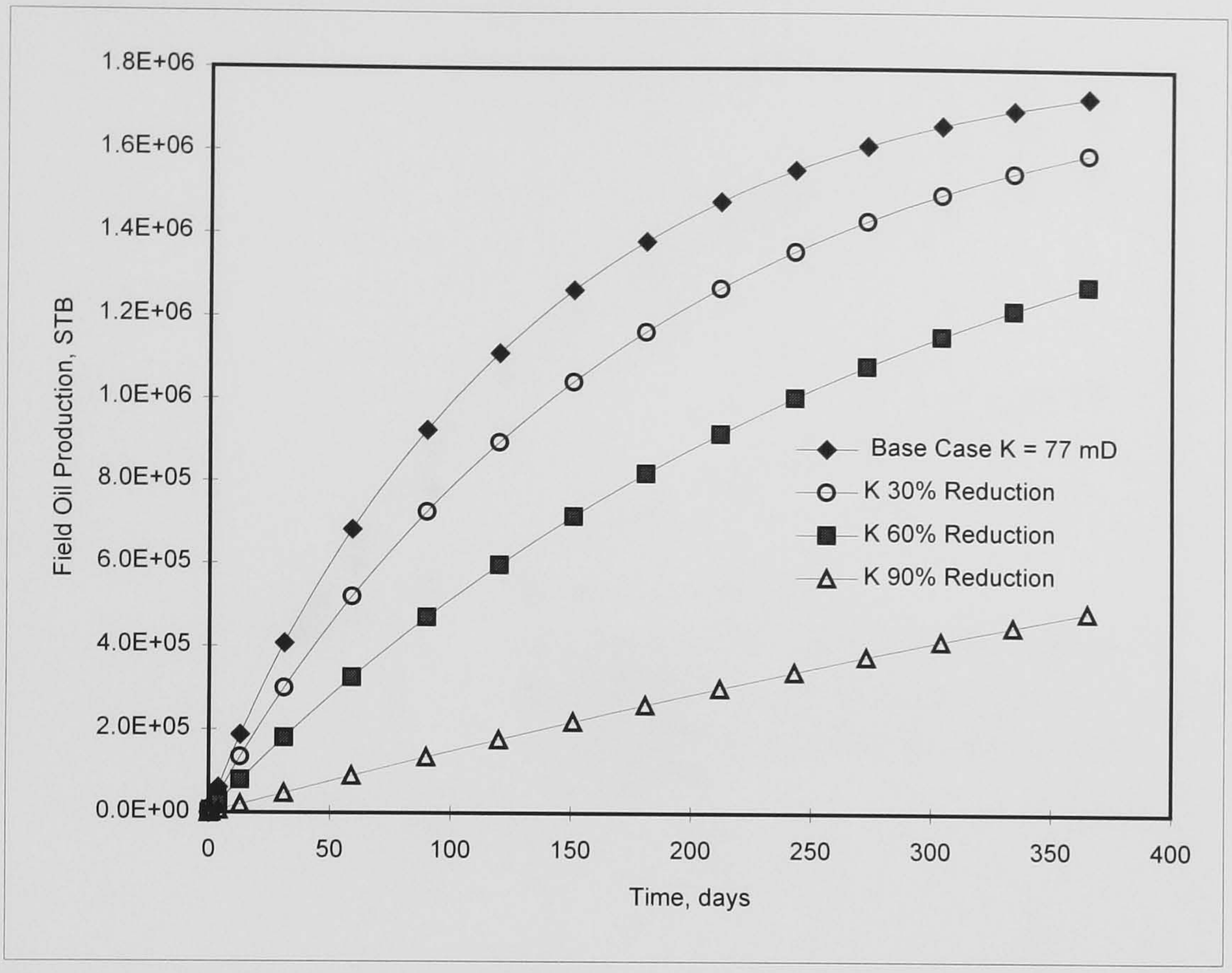

Figure 7.3 Field oil production versus time showing the effects of permeability reductions

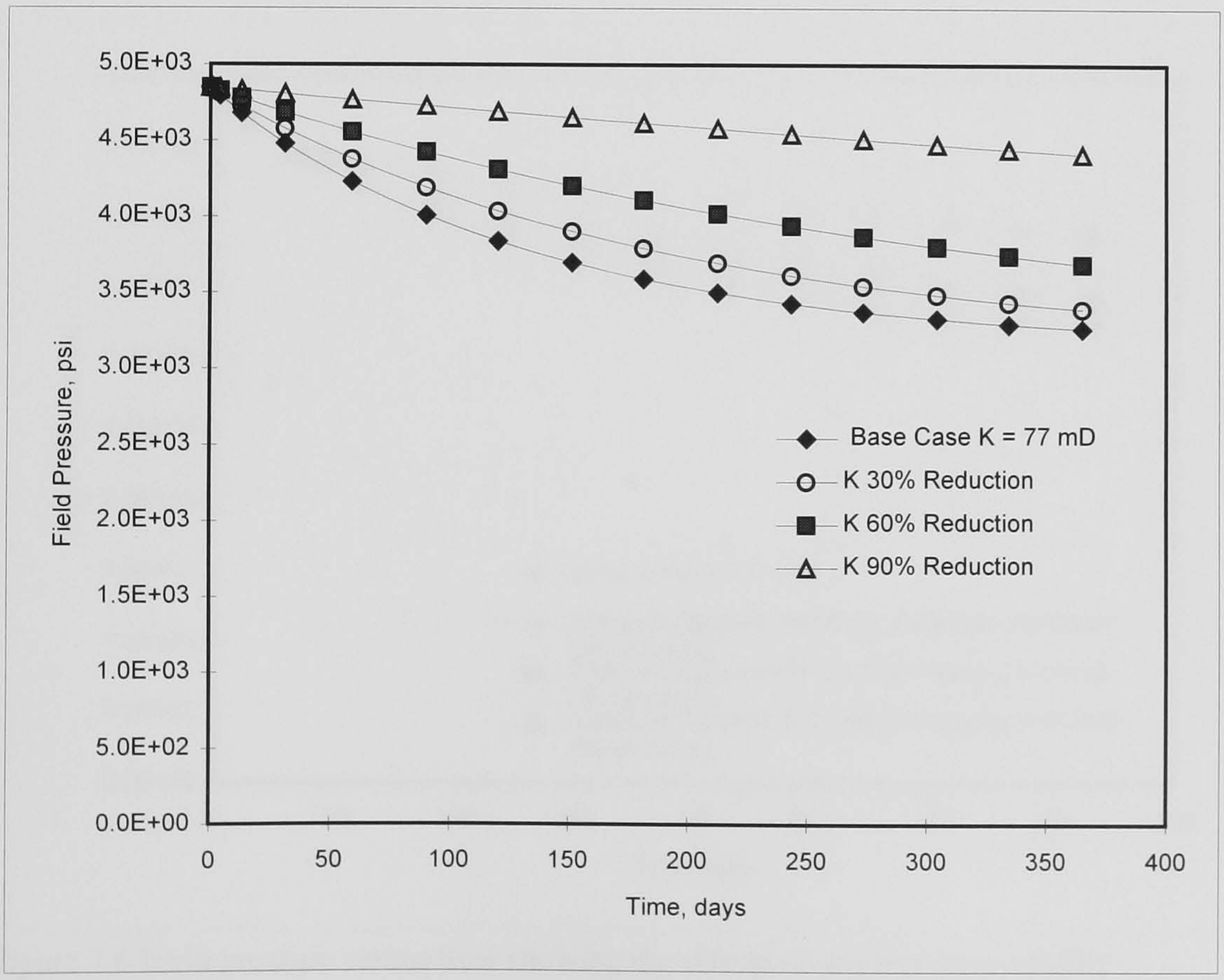

Figure 7.4 Field pressure versus time showing the effects of permeability reductions

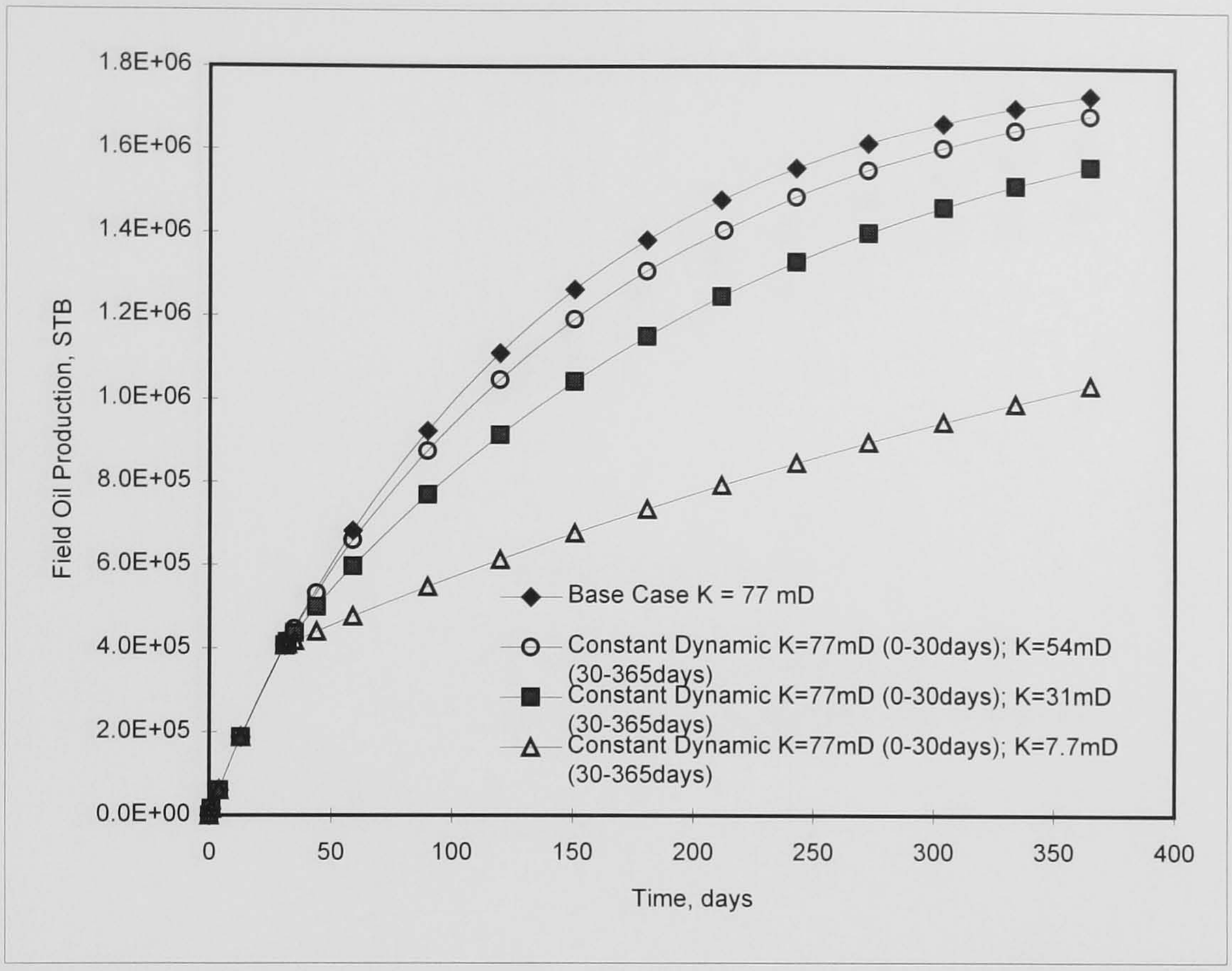

Figure 7.5 Field oil production versus time showing the effects of one step permeability reductions

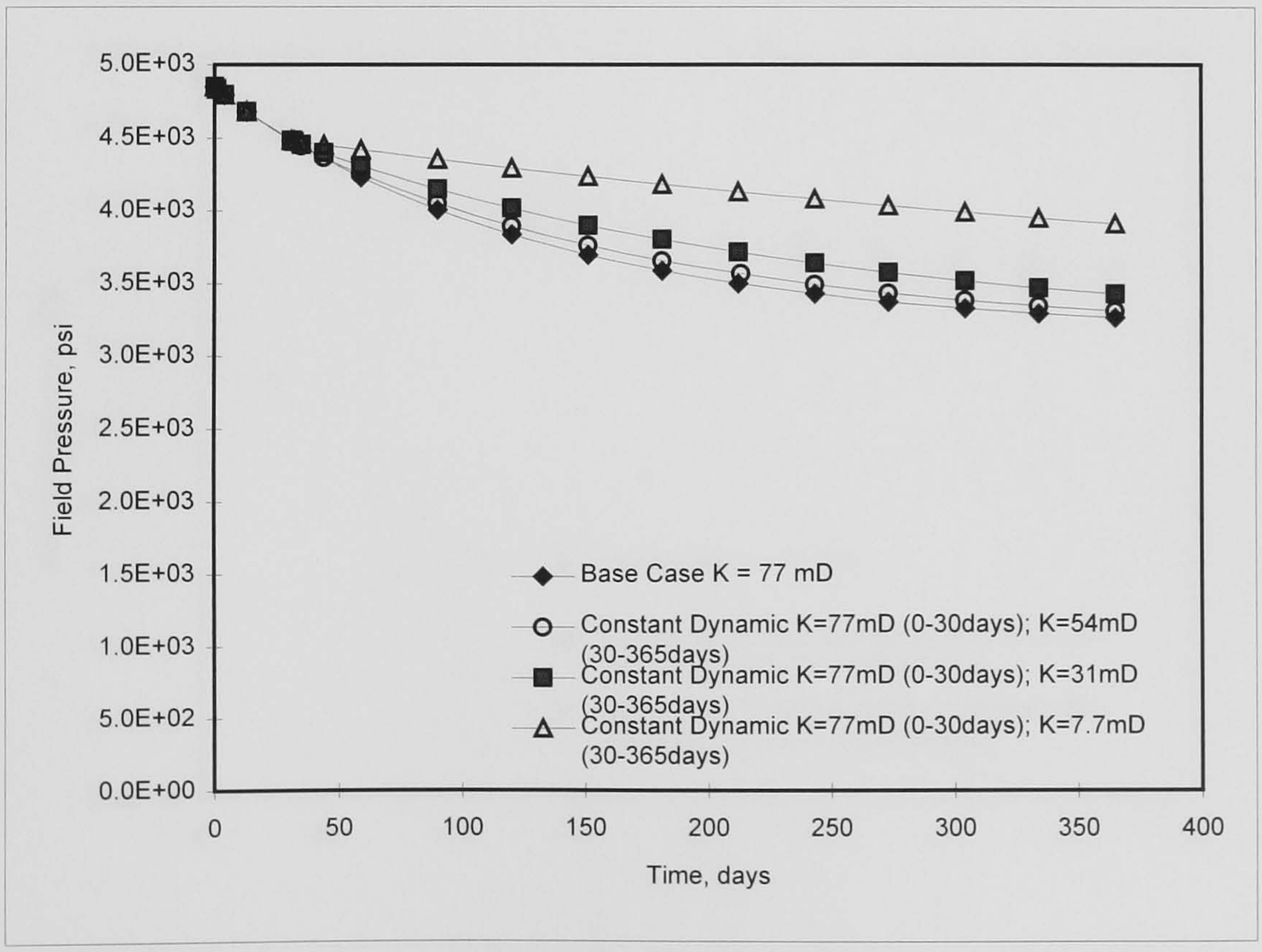

Figure 7.6 Field pressure versus time showing the effects of one step permeability reductions

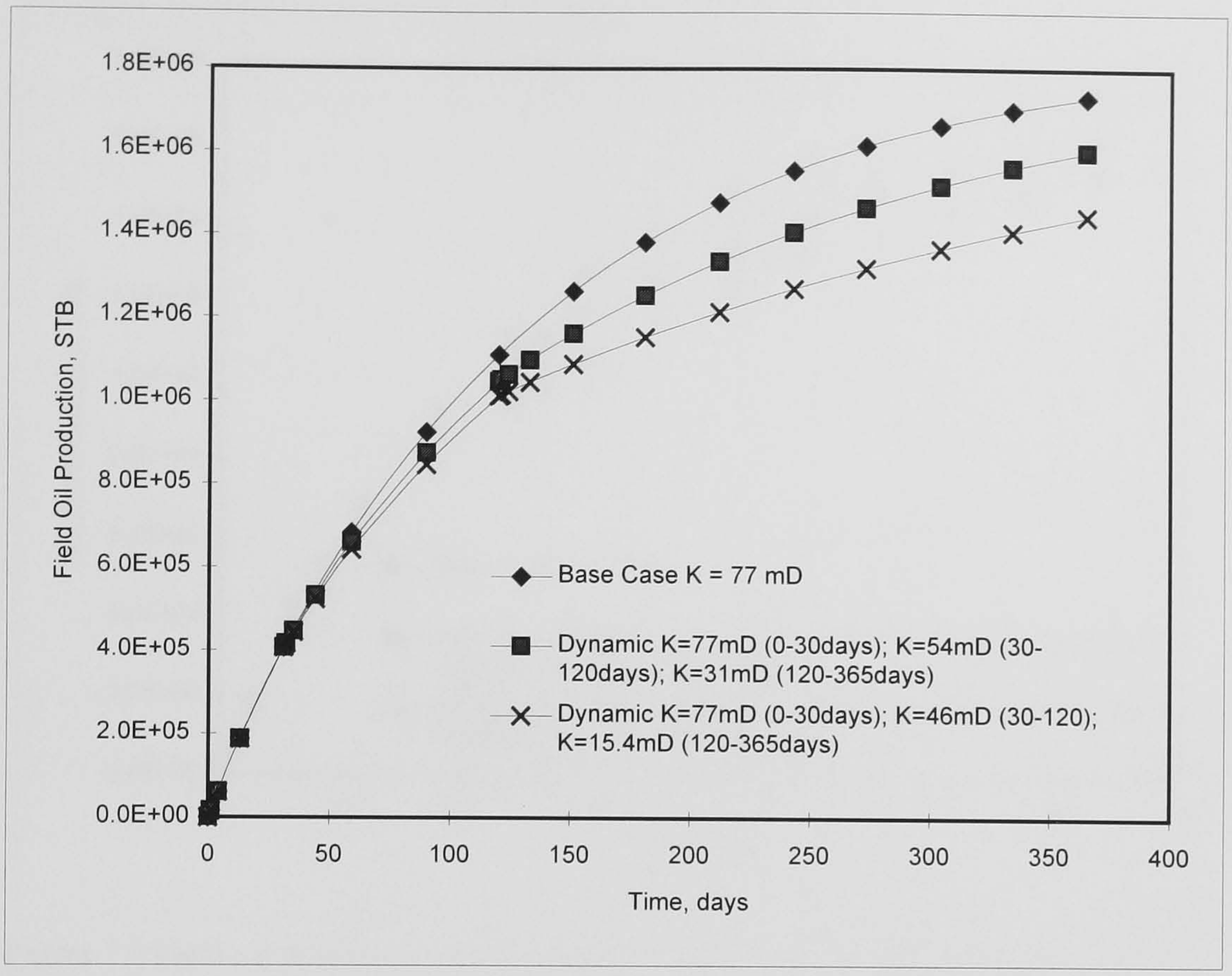

Figure 7.7 Field oil production versus time showing the effects of three steps permeability reductions

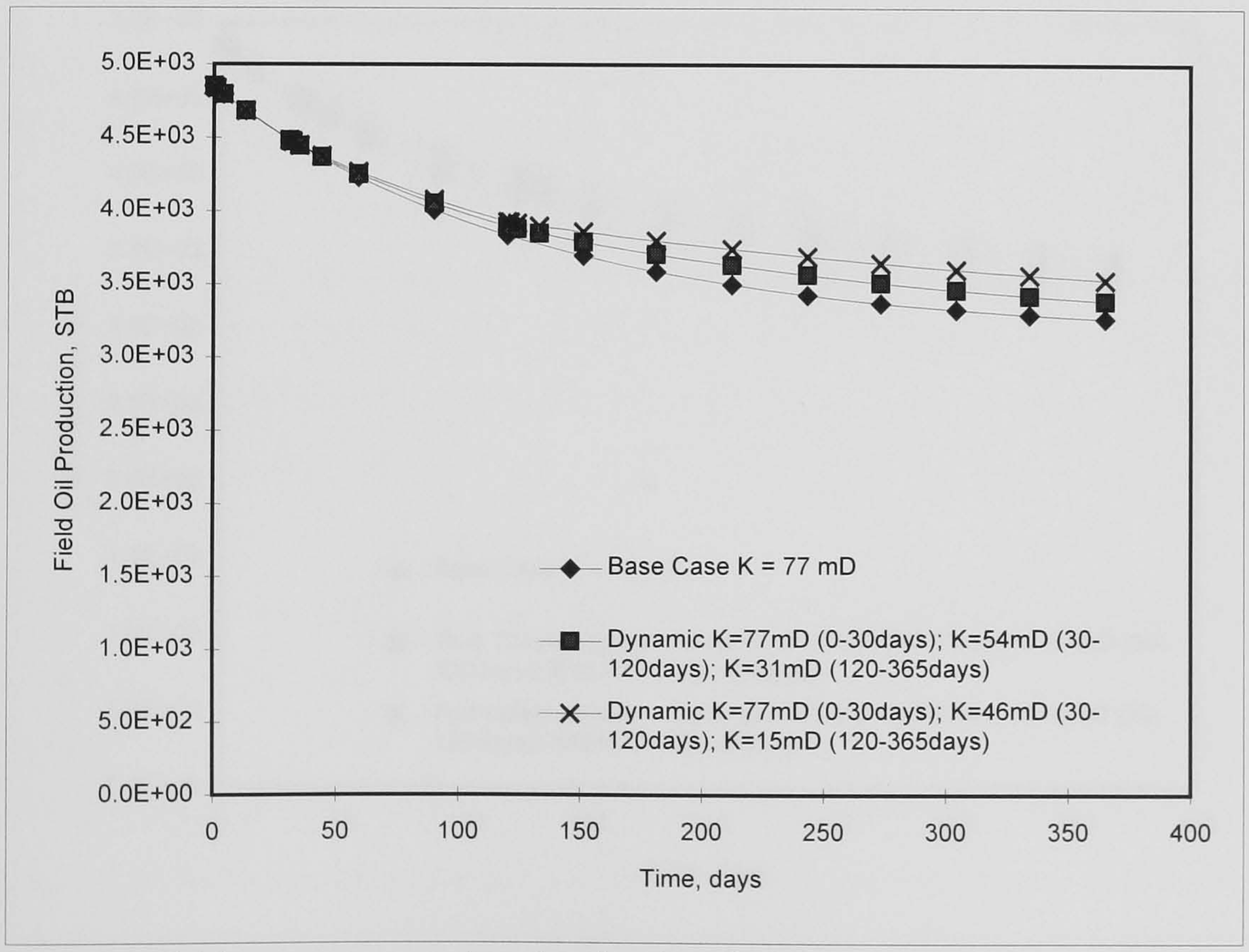

Figure 7.8 Field pressure versus time showing the effects of three steps permeability reductions

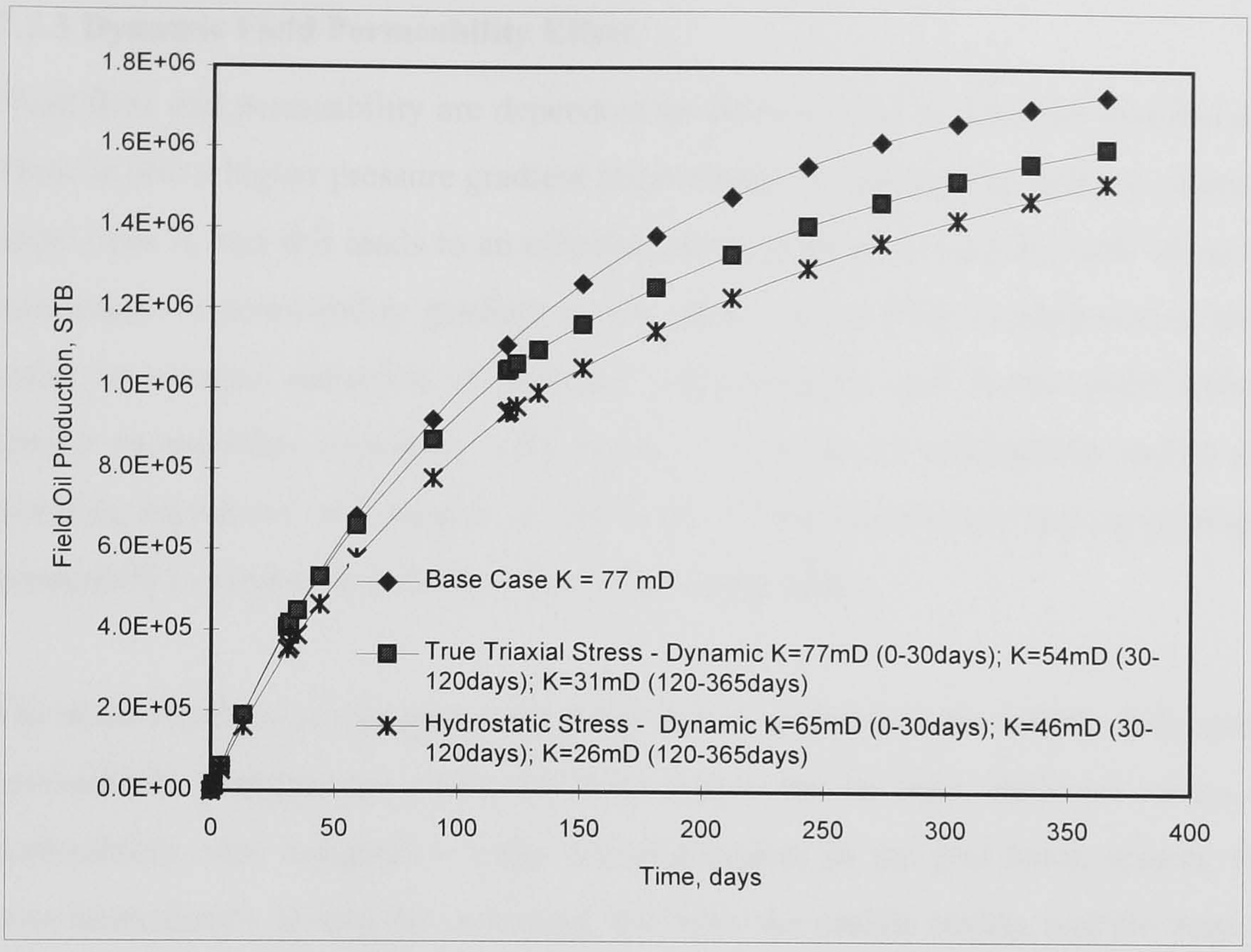

Figure 7.9 Field oil production versus time showing the effects of three steps permeability reductions at different stress states

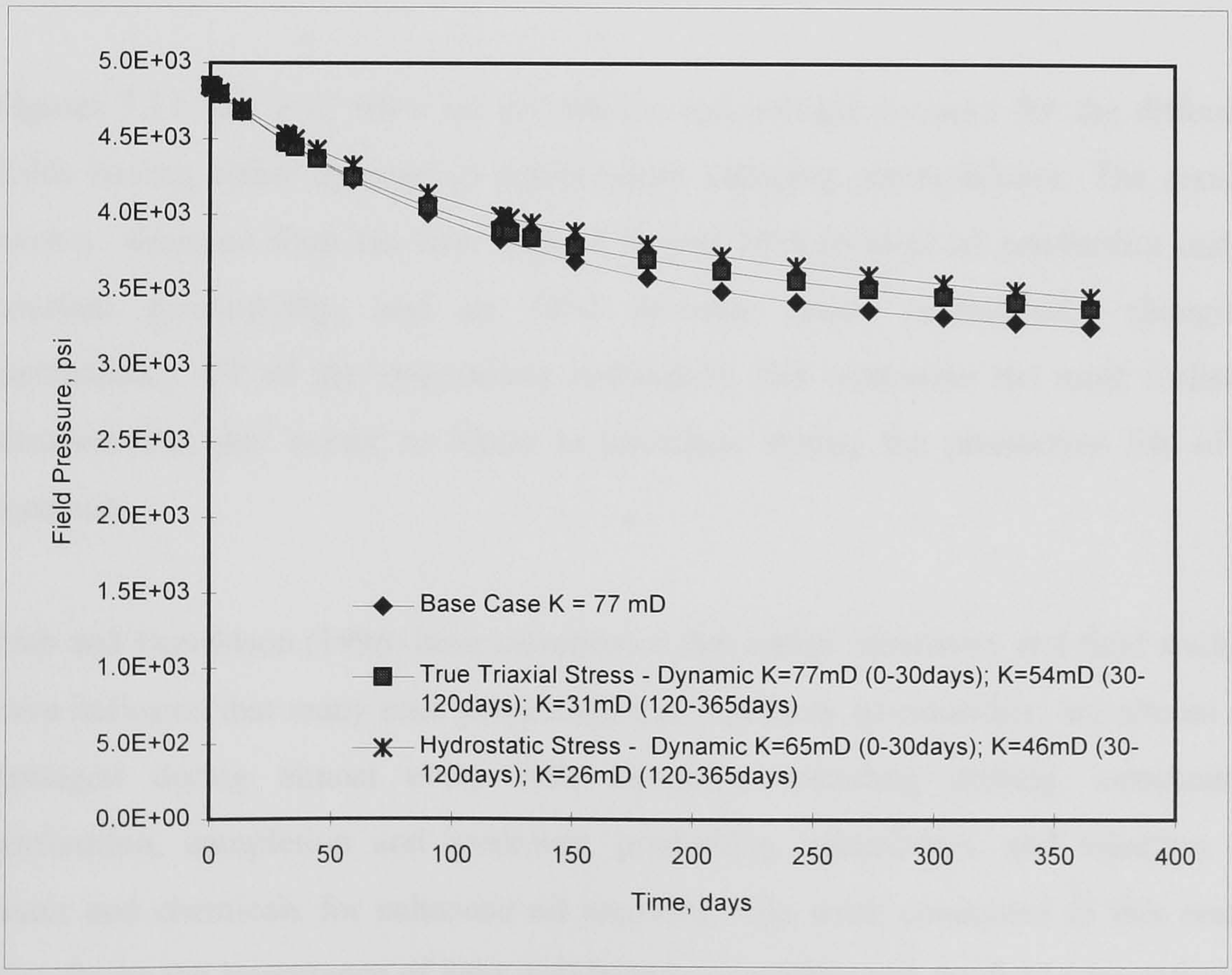

Figure 7.10 Field pressure versus time showing the effects of three steps permeability reductions at different stress states

7.2.3 Dynamic Field Permeability Effect

Fluid flow and permeability are dependent on pressure and on pressure distribution. There is also a higher pressure gradient in proximity to a producing well than there is away from it, and this leads to an effective stress gradient around the well which in turn causes a permeability gradient in the same region. Such a phenomenon may result in unequal reduction of principal permeabilities, and hence could induce greater permeability anisotropy. The amount of change in permeability and in the resulting anisotropy will depend on the level of stress anisotropy and on principal permeability orientation relative to that of the stress field.

The main objective of this part of the study was to understand the effects of dynamic permeability changes near to the well bore and in the far field. Different values of permeability were assigned to three different regions in the grid block system; the zone immediately around the producing wellbore, the middle region, and the zone at furthest distance from the well, with the permeability increasing with distance from the well location.

Figures 7.11 and 7.12 show oil production and average pressure for the different fields having either constant or continuously changing permeabilities. The results were a decrease from the base case of around 10% in total oil production under constant permeability, and an 18% decrease under continuously changing permeability. Of all the simulations undertaken, this represents the most realistic situation that one would be likely to encounter during the production life of a reservoir.

Tiab and Donaldson (1996) have commented that earlier laboratory and field studies have indicated that many rock properties, and especially permeability, are altered or damaged during almost every field operation including drilling, cementing, perforation, completion and workover, production, stimulation, and injection of water and chemicals for enhanced oil recovery. The work conducted in this study also shows the importance of near well bore permeability and far field permeability, and demonstrates how dynamic permeability changes can occur with depletion.

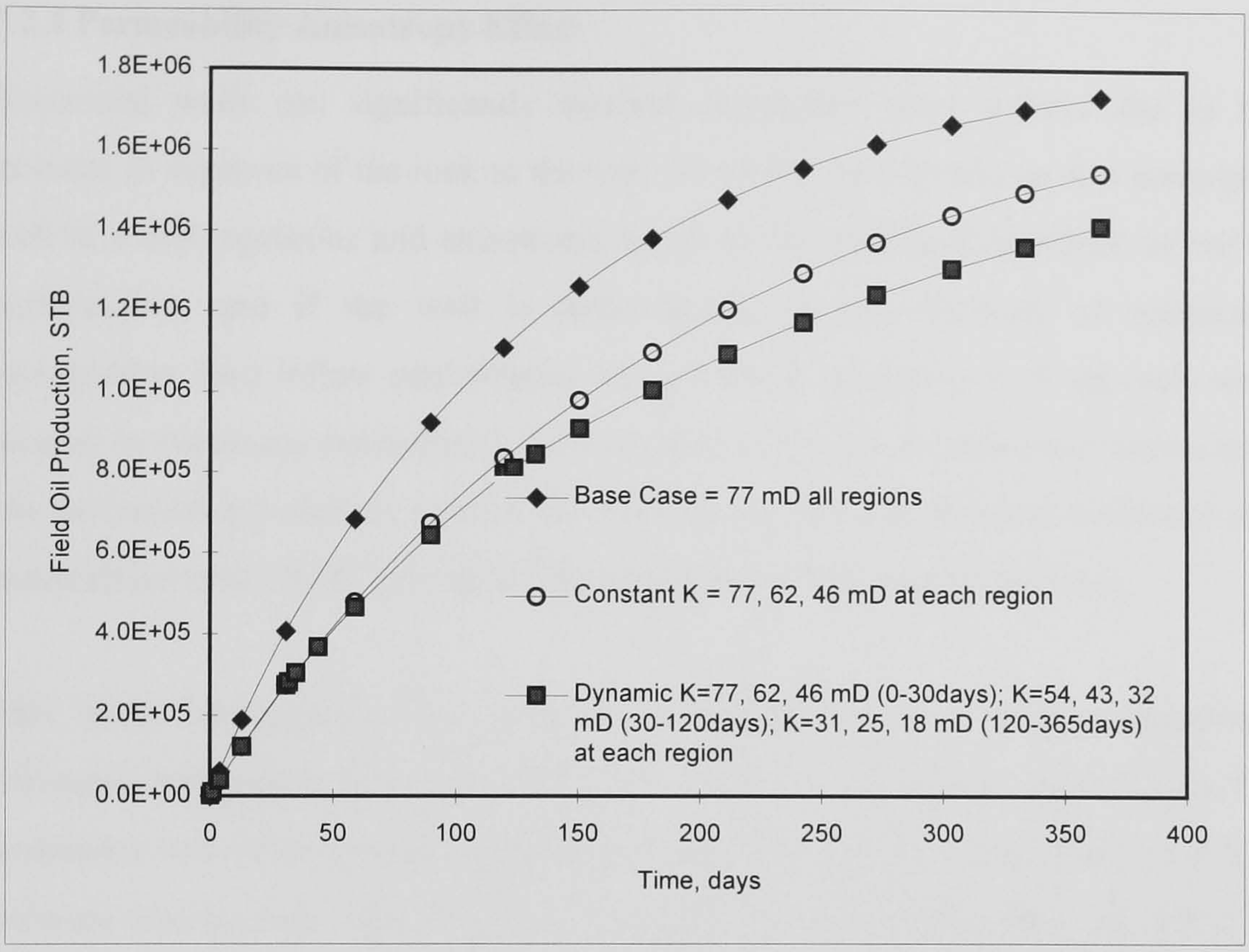

Figure 7.11 Field oil production versus time showing the effects of different regions with three steps permeability reductions

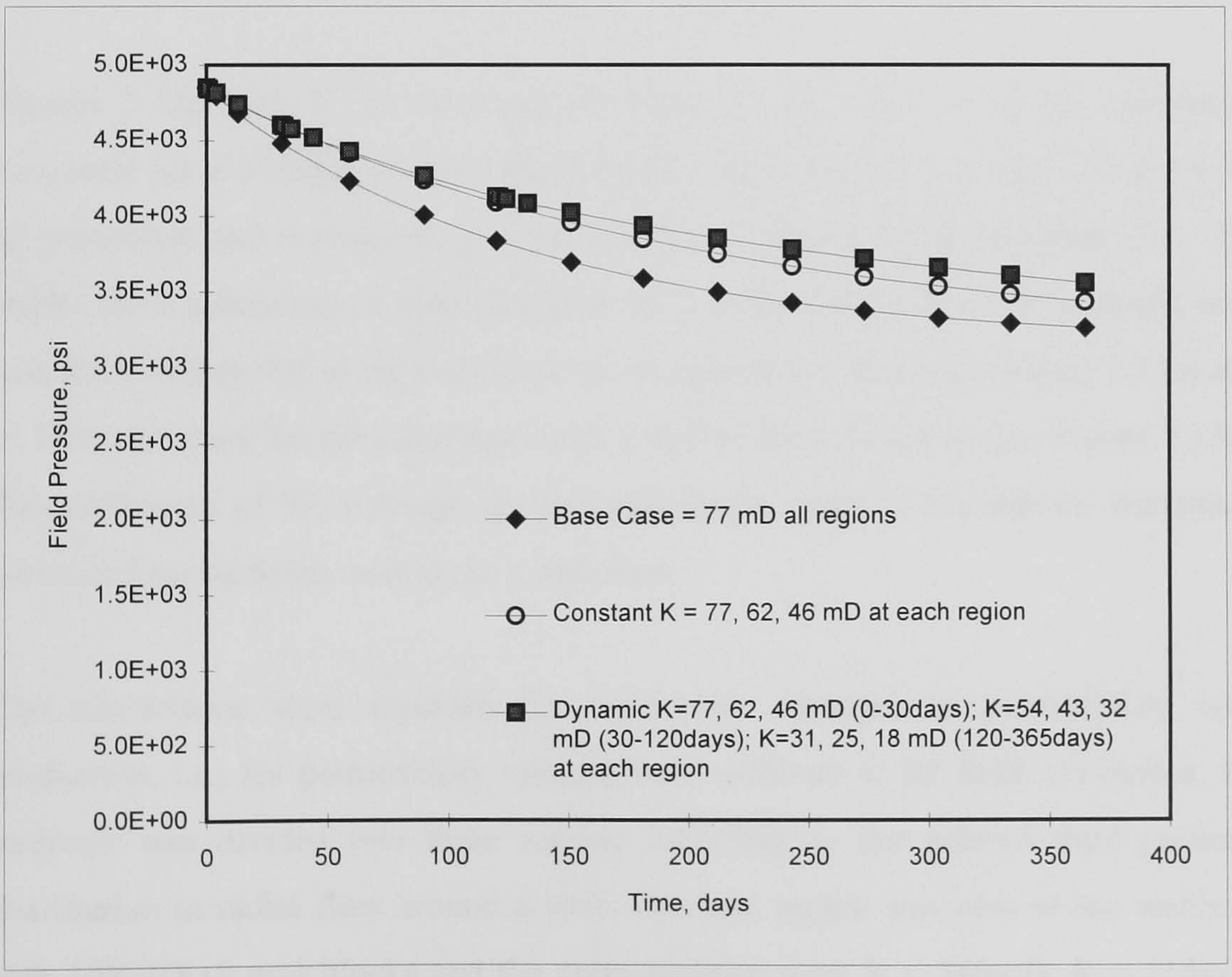

Figure 7.12 Field pressure versus time showing the effects of different regions with three steps permeability reductions

7.2.4 Permeability Anisotropy Effect

Horizontal wells can significantly increase production from a field due to the increase in exposure of the rock to the well. However, the orientation of a horizontal well in a heterogeneous and anisotropic reservoir can significantly affect the well's performance, and if the well is perpendicular to the direction of maximum permeability then inflow performance will be better compared to if the well were parallel to maximum permeability. During permeability characterisation studies only one horizontal (x) and the vertical (z) permeability are usually used, and only one permeability ratio (K_v/K_h) is usually incorporated into the field simulations.

This study investigated three principal permeabilities (i.e., vertical, maximum horizontal and minimum horizontal) and their effect on production performance in a horizontal well with natural depletion of the field, and later with water injection pressure maintenance. The purpose of this study was to demonstrate the effect of permeability anisotropy on reservoir production performance, using the directional permeability data obtained from the experimental work.

Figures 7.13a and 7.13b show the illustrations of wellbore in the maximum horizontal (x) and minimum horizontal (y) directions. Figures 7.14 and 7.15 show the oil production and average pressure for isotropic and anisotropic permeabilities. The results show a decrease of approximately 13% of production from the isotropic base case for a well drilled in the y direction in an anisotropic field, (see Figure 7.13b) and an 18% reduction for the same field with a well in the x direction (see Figure 7.13a). This difference of 5% between the two anisotropic cases is because the maximum horizontal permeability was in the x direction.

The simulations were repeated for field wide changes in permeability with production, i.e., for permeability varying from wellbore to far field. As before, the reservoir was divided into three regions according to the general fluid pressure distribution in radial flow around a well. The first region was near to the wellbore with 10X10X10 grid blocks and the permeabilities were K_x= 360mD, K_y= 215mD, and K_z= 15mD. The second region was at the middle, between region I and far field

with grid blocks up to 30X30X10 and the permeabilities were K_x= 420mD, K_y= 251mD, and K_z= 15mD. The third region was outside region II and the permeabilities K_x= 600mD, K_y= 358mD, and K_z= 15mD. The results of the simulation are shown in Figures 7.16 and 7.17. With the well in the x direction the result was a decrease of around 28% in field production compared to the base case, with only a 21% reduction occurring for the well along the y direction.

Figures 7.18 and 7.19 show the oil production and average pressure during pressure maintenance for the anisotropic case with permeability varying from wellbore to far field. The results show that there is a decrease of 30% from the production in the base case when the well is in the x direction, (see Figure 7.13a) compared to only 24% for the well in the y direction (see Figure 7.13b). Clearly, permeability anisotropy coupled with well orientation has a significant effect on well performance prediction. In addition, such permeability anisotropy will impact upon water flood schemes and breakthrough time.

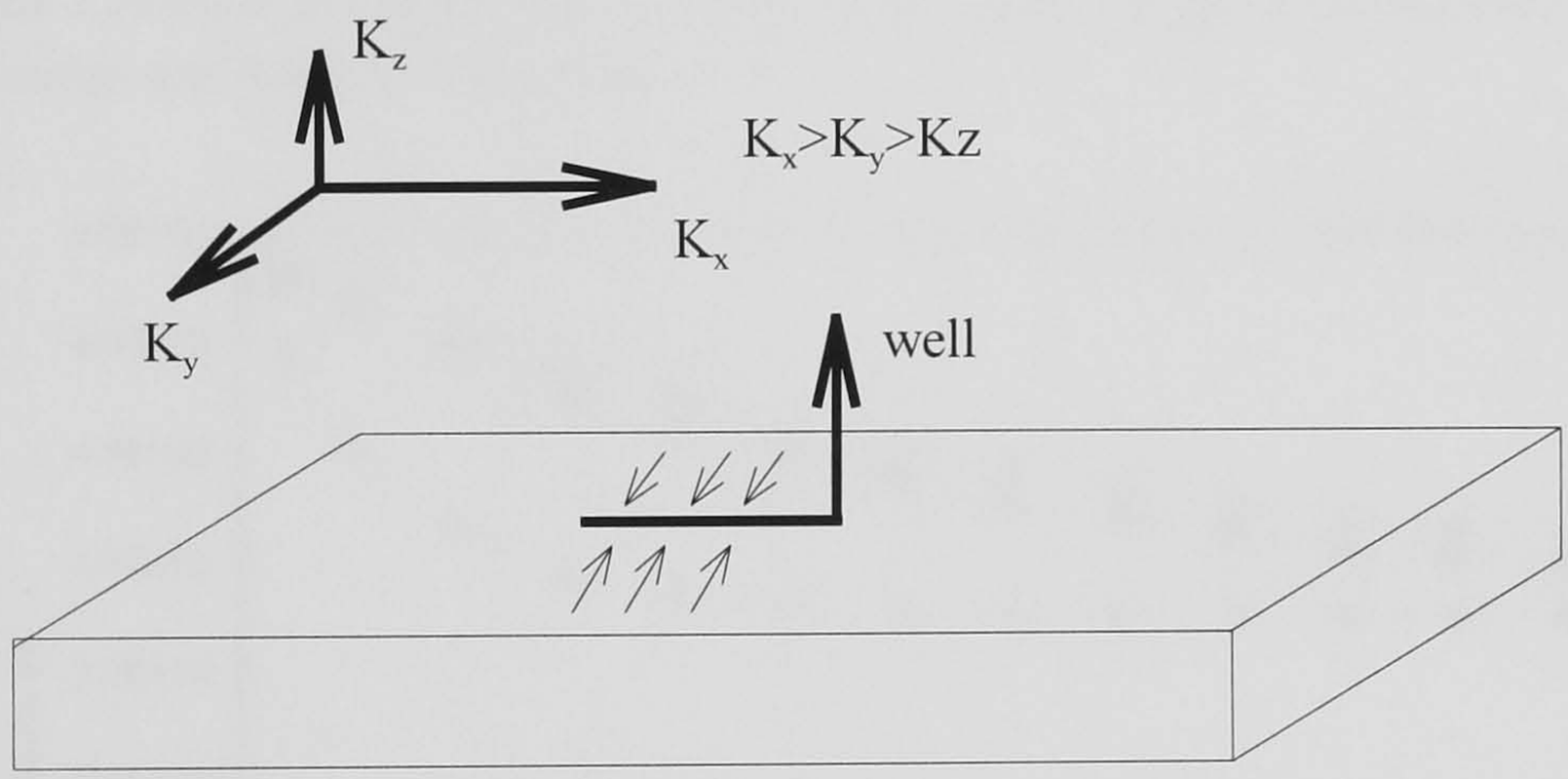

Figure 7.13a Wellbore direction in x-direction

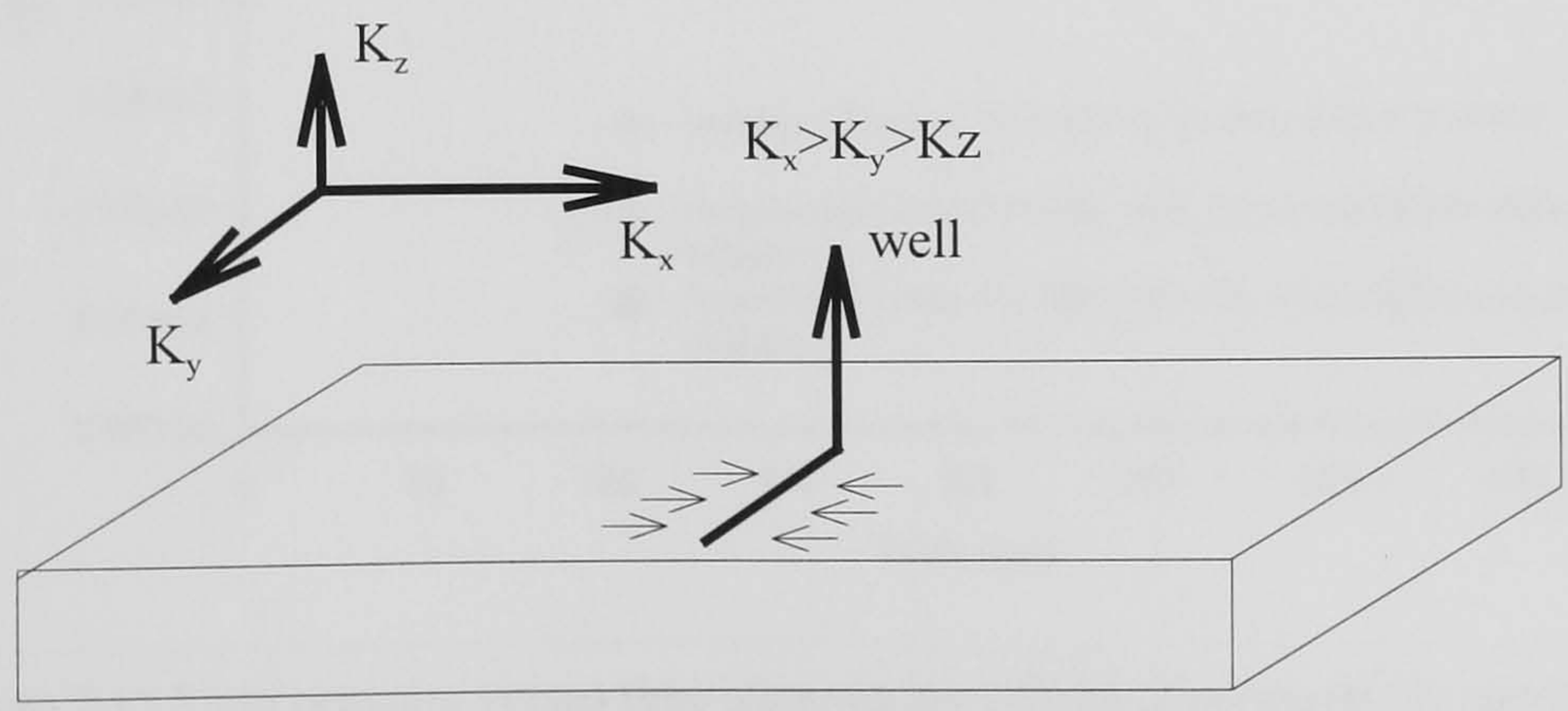

Figure 7.13b Wellbore direction in y-direction

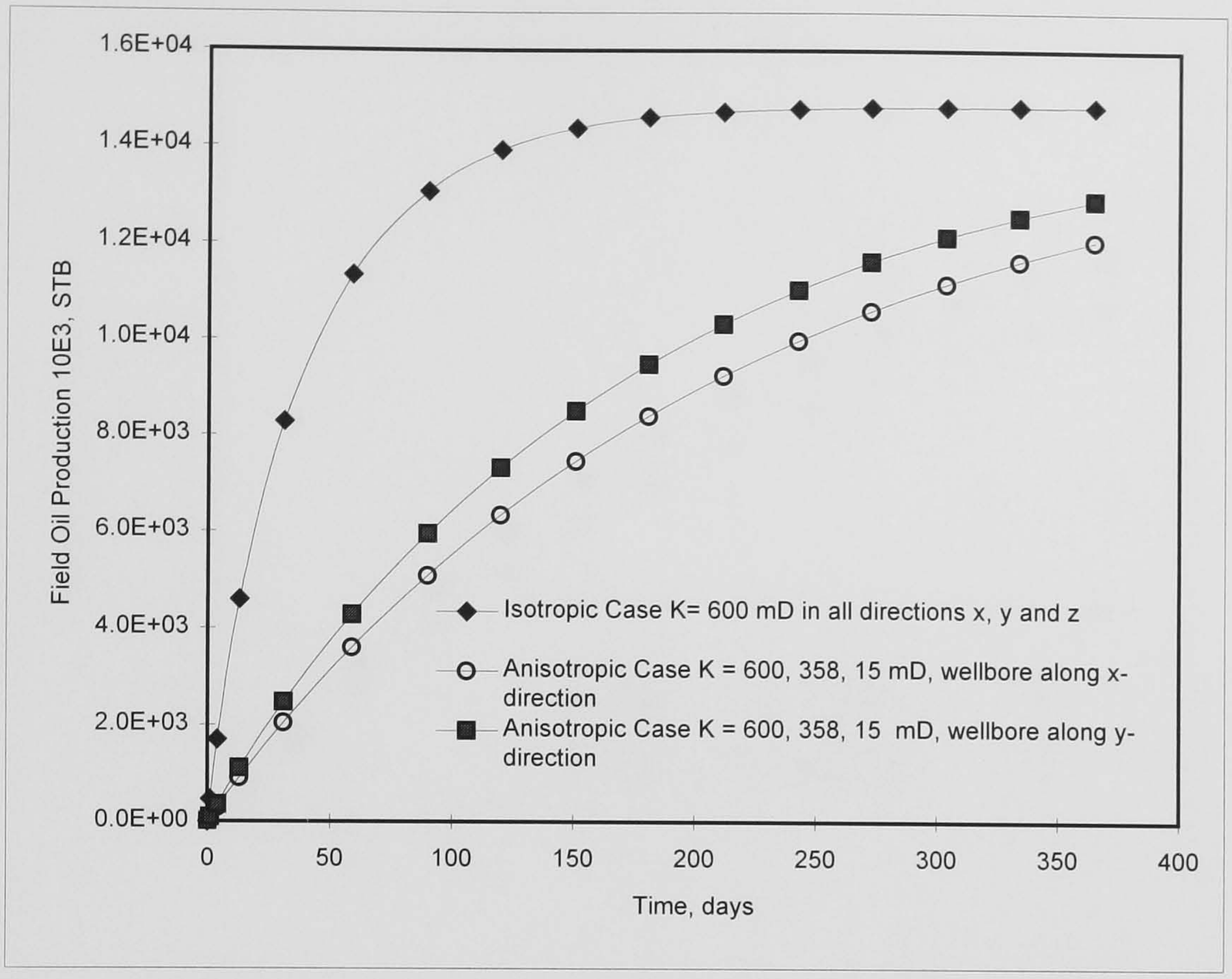

Figure 7.14 Field oil production versus time showing the effects of permeability anisotropy and wellbore orientation

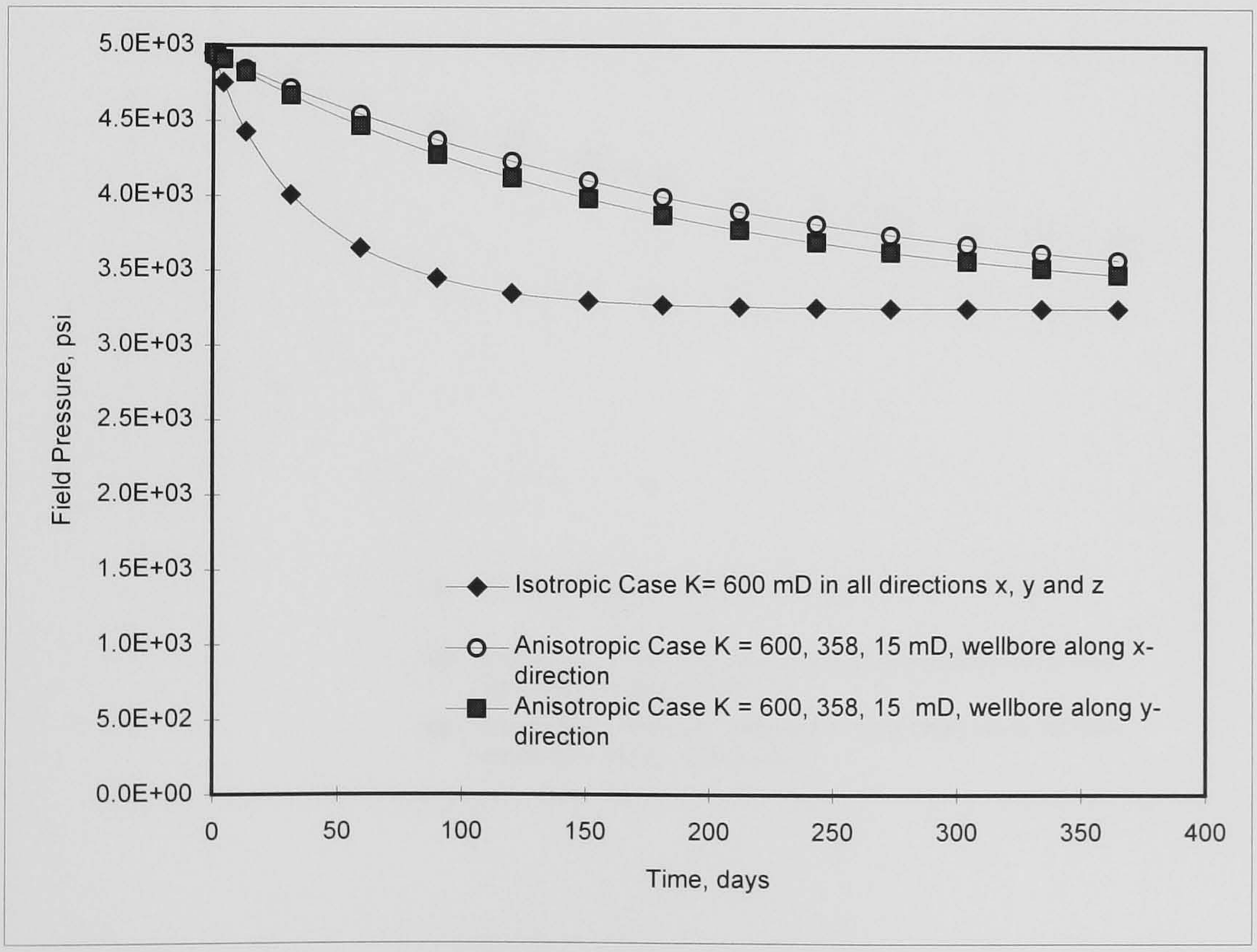

Figure 7.15 Field pressure versus time showing the effects of permeability anisotropy and wellbore orientation

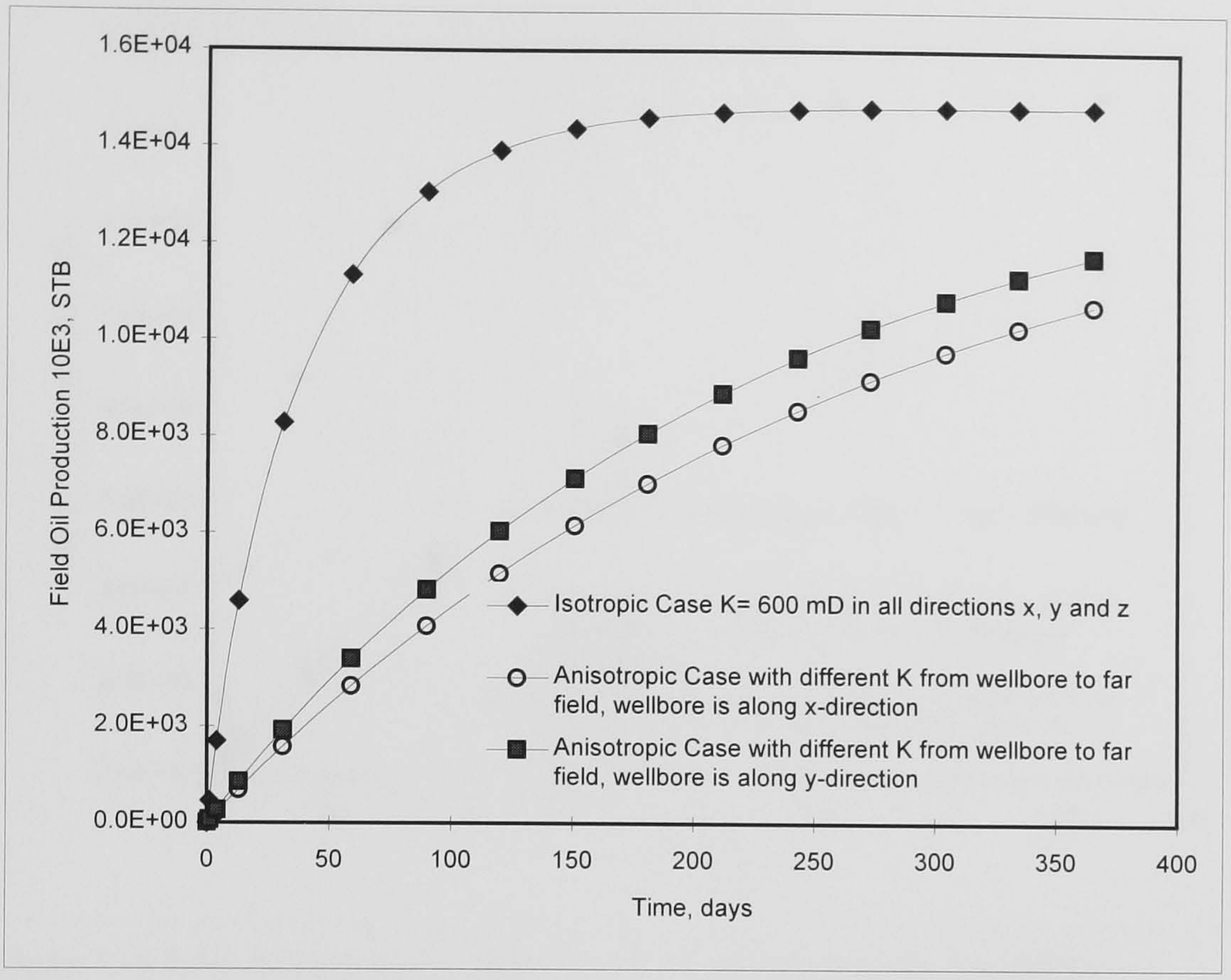

Figure 7.16 Field oil production versus time showing the effects of permeability anisotropy, wellbore orientation and regional permeability change

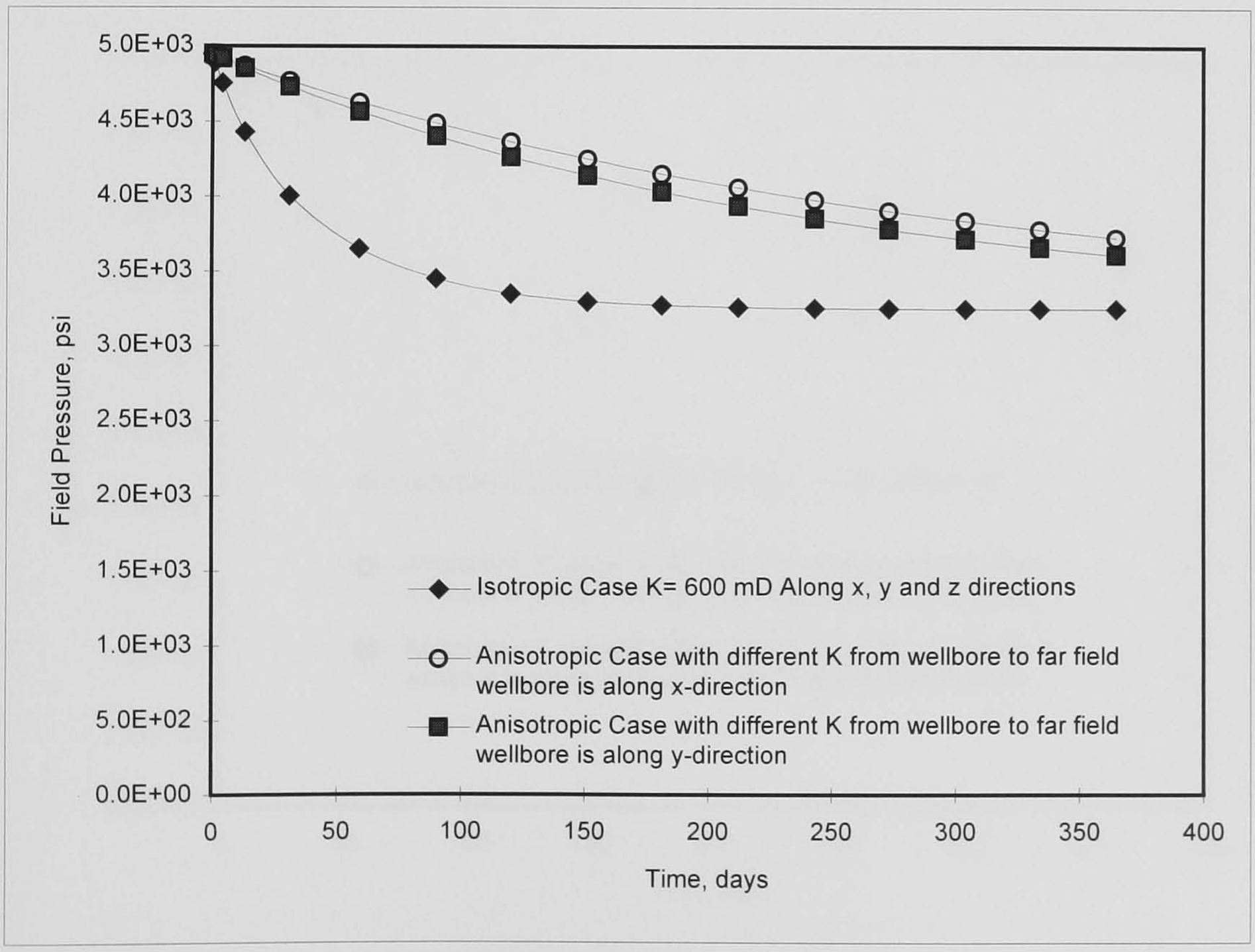

Figure 7.17 Field pressure versus time showing the effects of permeability anisotropy, wellbore orientation and regional permeability change

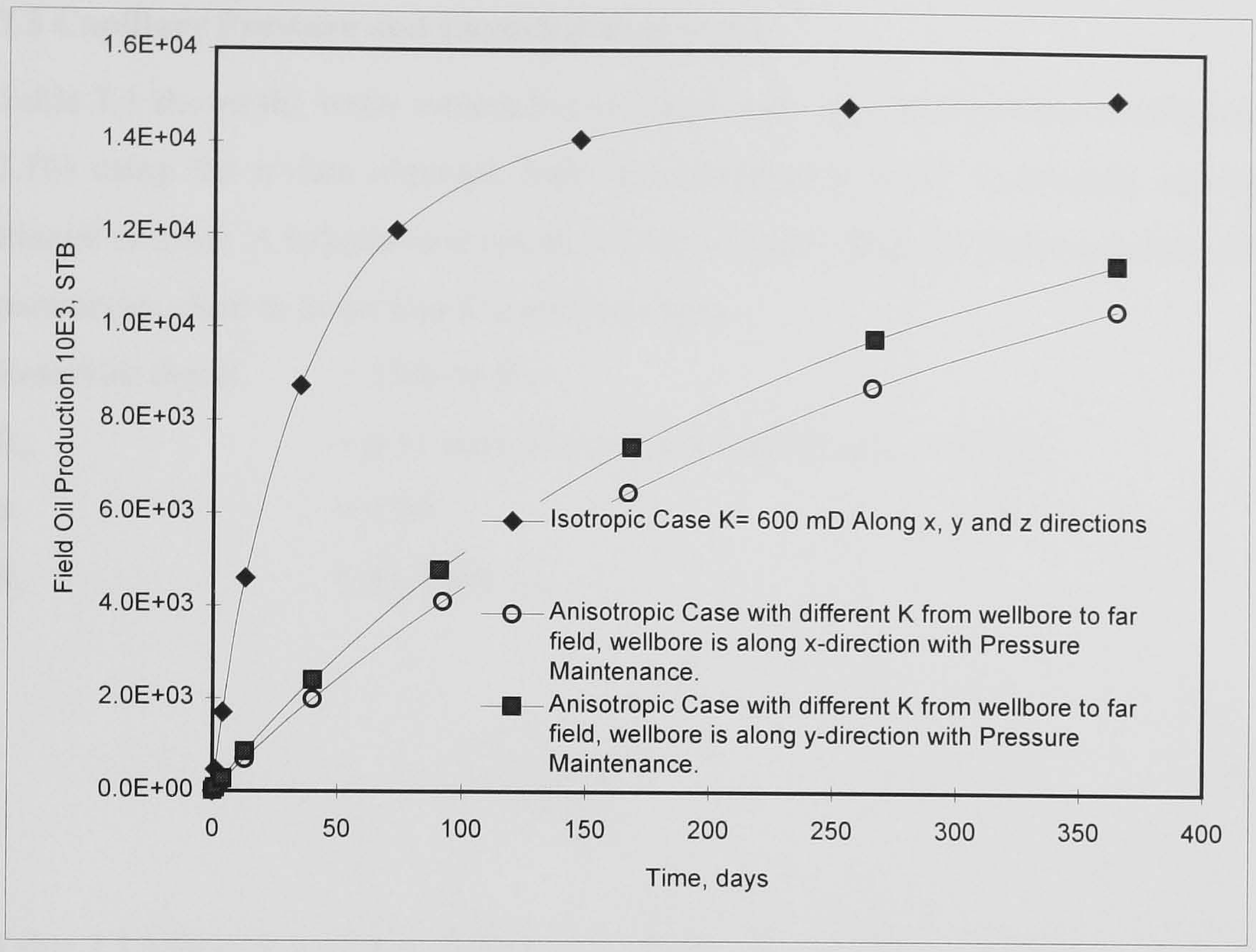

Figure 7.18 Field oil production versus time showing the effects of permeability anisotropy, wellbore orientation and regional permeability change with pressure maitenance

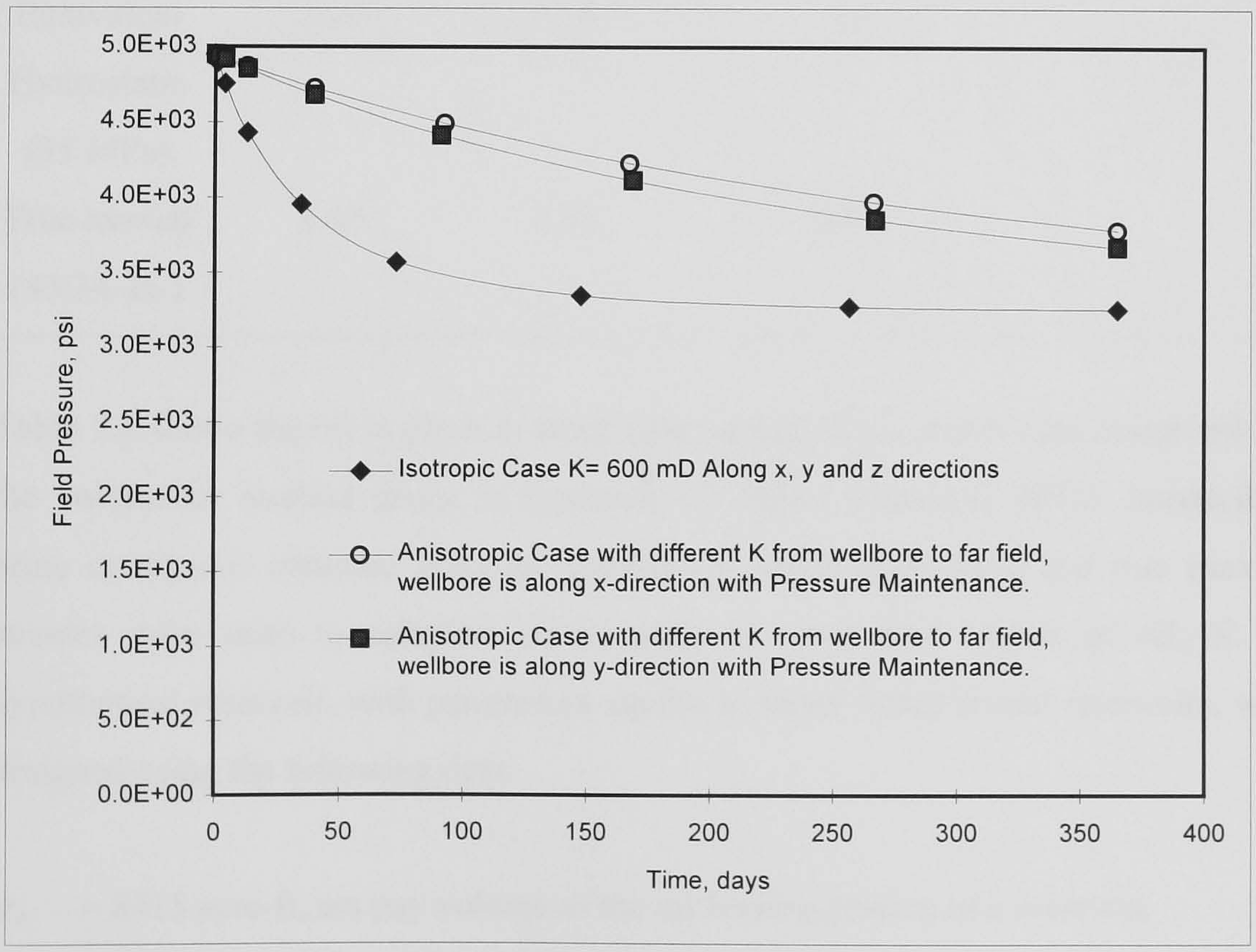

Figure 7.19 Field pressure versus time showing the effects of permeability anisotropy, wellbore orientation and regional permeability change with pressure maitenance

7.3 Capillary Pressure and Electrical Properties

Table 7.1 shows the water saturation calculated from Archie Equation (see Equation 2.16) using the n data obtained from the experiments under hydrostatic and true triaxial stresses. A hypothetical reservoir was designed using the following data, with parameters close to those found in real reservoirs :

Reservoir depth = 2500 m SS

R_w = 0.11 ohm.m (Reservoir temperature = 99.4°C

ϕ = 0.20

R_t = 68.7 ohm.m

$$S_w = \left(\frac{R_w}{\varphi^m R_t} \right)^{\frac{1}{n}} \tag{7.1}$$

Table 7.1 Effect of stress on parameter n and computed brine saturation

Stress	Saturation exponent, n	Cementation factor, m	Brine saturation Sw (%)	Saturation change dSw (%)
Equivalent Hydrostatic (35 MPa)	2.20	1.94	22.2	12.7
True triaxial (43:34:26.)	1.50	1.81	9.50	

Table 7.2 shows the oil in place in stock-tank barrels of oil, and N was calculated by the volumetric method given in Equation 7.2 below (Bradley, 1992). Irreducible brine saturations obtained from the experiment under hydrostatic and true triaxial stresses were used to calculate oil in place in stock-tank barrels of oil, N. A hypothetical reservoir, with parameters similar to those found in real reservoirs, was designed using the following data:

V_O = 8415 acre-ft, net pay volume of the oil bearing portion of a reservoir

B_O = 1.2, oil formation volume factor

7758 = number of barrels per acre-foot

ϕ = 0.20

$$N = \frac{7758 V_o \phi (1 - S_{iw})}{B_o} \tag{7.2}$$

Table 7.2 Effect of stress on irreducible brine saturation during OIP calculation

Stress	Irreducible brine saturation Sw_i (%)	Oil in place, N (STB)	OIP change dN (%)
Equivalent Hydrostatic (35 MPa)	29.9	$7.63 X10^6$	
			5.0
True triaxial (43:35:26)	26.2	$8.03 X10^6$	

The results from Table 7.1 show a saturation difference of 11.3% between hydrostatic and true triaxial stresses. Therefore, the use of hydrostatic stress during laboratory measurements would result in an underestimate of the oil in place. The results from Table 7.2 show a difference of 5% in the estimation of the oil in place between hydrostatic and true triaxial stress.

7.4 Summary

In summary, the direct application of the experimental data on reservoir performance can be summarised as follows :

1. Simulation results show that the permeability reduction due to changes in the stress states and pore pressure can give significantly different estimates of production.
2. The permeability of a deforming porous medium varies with time since the reservoir pressure varies with time.
3. Stress-sensitive permeability will have a significant effect on the production characteristics of certain reservoirs. Simulation results show that when the permeability variation was taken into account, calculated flow rates may be considerably lower than when the permeability was assumed to be constant.

4. The effect of well orientation on reservoir performance prediction has been analysed. For an isotropic reservoir (K_x=K_y=K_z), the production results will be different than if an anisotropic reservoir is considered.
5. Such anisotropic characteristics can be used in a simple reservoir simulation to demonstrate the expected changes for a producing reservoir. A significant change was predicted when considering the recovery of oil from horizontal wells in a waterflood as opposed to vertical wells. Hence, properly placed horizontal wells (i.e., horizontal wellbore perpendicular to the maximum horizontal permeability) can enhance oil recovery in designing oil recovery projects.

CHAPTER 8

CONCLUSIONS AND RECOMMENDATIONS

8.1 Introduction

In this research the effects of pore pressure, stress magnitude, stress path, hysteresis, and anisotropy on permeability have been investigated using a new true triaxial stress loading system. In addition, capillary pressure and electrical properties have also been investigated. The experimental data have been used in a numerical simulation study to demonstrate some direct applications of this work in reservoir engineering.

The laboratory measurements were undertaken on outcrop and reservoir sandstone samples, including 40 mm cubic and 38 mm diameter cylindrical samples. The equipment used included a hydrostatic high pressure multi-sample cell and a true triaxial loading system.

The research covered the following six aspects :

1. Additional features were incorporated into the true triaxial stress loading system, by adding high pore pressure and two phase flow measurements capabilities.
2. Measurements of permeability were conducted at high pore pressures and under true triaxial, triaxial and hydrostatic stresses.
3. Measurements of permeability hysteresis were made under different stresses.
4. Measurements of pore volume deformation, directional permeability and electrical properties in three principal directions were made under true triaxial and hydrostatic stresses.
5. Measurements of capillary pressure and electrical properties were undertaken under true triaxial and hydrostatic stresses.
6. The experimental data were incorporated into a reservoir simulator to evaluate the impact on reservoir engineering applications.

The remaining part of this chapter presents the main findings and conclusions from this research work, and some recommendations for further investigations.

8.2 Conclusions

8.2.1 Experimental Techniques

The modified true triaxial stress loading system has been used successfully to measure permeability under realistic high pore pressures and true triaxial stresses. The permeability and electrical properties of the three principal directions have been measured successfully at the same time using single cubic samples. A range of petrophysical rock properties have been studied in the laboratory under realistic true triaxial stresses and pore pressures. The combination of high pore pressure and cubic true triaxial samples has been successfully achieved.

8.2.2 Pore Pressure, Hysteresis and Stress Effects on Permeability

The effects of pore pressure and stress on permeability have been shown to be significant. Permeability increases with pore pressure and decreases with increase in effective stress and have indicated stress path dependence. The hysteresis effects are more significant under hydrostatic stresses, and are rather less pronounced under true-triaxial stresses. Low permeability samples show more permeability hysteresis than high permeability samples, and under true triaxial stresses there is less reduction in permeability than that seen under comparable hydrostatic stresses. Pore pressure was found to have a larger effect on permeability than did the hysteresis and stress effects.

The experimental results have illustrated the importance of applying realistic and true triaxial stresses and elevated pore pressure when measuring permeability on laboratory samples.

8.2.3 Permeability and Resistivity Anisotropy, and Pore Volume Deformation

A high degree of anisotropy in permeability and resistivity has been observed in the outcrop and reservoir samples. However, whilst different horizontal directions showed dramatically different values of permeability they did not exhibit the same degree of difference in electrical resistivities. Therefore, although permeability and conductivity are both considered to be transport properties they exhibit different degrees of anisotropy and are functions of different processes and mechanisms. Under hydrostatic stress, pore volume deformations were found to be greater than those seen under comparable true triaxial stresses. Resistivity, formation factor and cementation exponent were all found to increase with stress, under both hydrostatic and true triaxial conditions.

8.2.4 Capillary Pressure and Electrical Properties

The capillary pressure curves measured at ambient conditions showed lower irreducible brine saturations compared to those determined at elevated stresses. The capillary pressure curves at true triaxial stresses showed lower capillary pressures and irreducible brine saturations compared to those at comparable equivalent hydrostatic stresses. Electrical measurements for formation factor, cementation factor and saturation exponent all revealed higher values under hydrostatic stresses compared to those under true triaxial stresses. Hysteresis between two different displacement processes (i.e., drainage and imbibition) was also seen, although more experiments are needed to confirm the effects of true triaxial stress on capillary pressure curves and resistivity index against saturation.

8.2.5 Reservoir Engineering Applications

As pore pressure declines during production there are dynamic permeability changes within a reservoir, (i.e., permeability decreasing with pore pressure depletion). This process was simulated and shown to have an impact on reservoir performance predictions. Such behaviour is usually neglected in reservoir performance predictions, and permeability is often considered to be constant throughout the producing life of a field. This study demonstrates the importance of considering

permeability changes with pore pressure, and consequently production induced permeability variation from wellbore to far field. Furthermore production in an anisotropic permeability field can vary between horizontal wells drilled in different directions.

8.2.6 General Conclusion

The measurements made in this study have demonstrated that differences are induced by the application of true triaxial and comparable hydrostatic stresses. The studies of variations of permeability with pore pressure and stress also highlighted some effects of different stress paths, and permeability hysteresis was shown to be stress state dependent.

The research demonstrated how anisotropy in permeabilities and resistivities can be measured, and also how such behaviour can have a significant effect on horizontal well performance. The application of experimental data to a simple reservoir simulation was performed, and the impact of the experimental results was demonstrated in terms of reservoir production performance.

The studies into the effects of stress on capillary pressure curves showed that irreducible brine saturation and capillary pressure under true triaxial stresses were lower than those at comparable equivalent hydrostatic stresses. Less changes in the cementation factors, formation factors and saturation exponents were also observed under true triaxial stresses.

Permeability and electrical conductivity measurements should be carried out under true triaxial stresses and elevated pore pressures if one is concerned with stress-sensitive (e.g., low permeability, fractured or highly compressible) reservoirs.

8.3 Recommendations

The following areas are recommended for future experimental studies and numerical modelling :

1. Further detailed petrographic (SEM and thin section) analyses are recommended to understand the nature of stress effect and its influence on petrophysical properties.
2. Further two phase relative permeability, capillary pressure and electrical resistivity studies under conditions of true triaxial stress are needed to investigate in depth how stress, hysteresis and anisotropy affect rock properties when multi-phases are present.
3. Further in depth experimental studies are needed to address the effects of anisotropy, pore pressure and hysteresis on transport properties for a wide range of stress sensitive reservoirs such as carbonate formations.
4. The development of a robust and coupled 3D and multi-phase stress sensitive fluid flow simulator is needed in order to incorporate the true triaxial stress effects and dynamic permeability in reservoir flow simulations.

REFERENCES AND BIBLIOGRAPHY

Aasum, Y., Kasap, E., and Kelkar, M.: 'Analytical upscaling of small-scale permeability using full tensor', SPE 25913, presented at the SPE Rocky Mountain Regional/Low Permeability Symposium held in Denver , Colorado, USA (1993), 679-692.

Adams, A.: 'Stress-sensitive permeability in a high-permeability sandstone reservoir - the Kuparuk field', SPE 11718, presented at the California Region Meeting held in Ventura, California, USA (1983), 479-486.

Adamson, A.: 'Physical Chemistry of Surfaces', 5th edition. Wiley-Interscience publication, John Wiley&Sons, Inc. NY, Chichester, Brisbane, Toronto, Singapore (1990).

Addis, M.A., Choi, X. and Gunning, J.: 'The influence of the reservoir stress depletion response on the lifetime considerations of well completion design', SPE 47289, presented at the SPE/ISRM Eurock held in Trondheim, Norway (1998), 1-9.

Ajufo, A.O., Daneshjou, D.H. and Warne, J.D.: 'Capillary pressure characteristics at overburden pressure using the centrifuge method', SPE 26148, presented at the SPE Gas Technology Symposium held in Calgary, Alberta, Canada (1993), 107-117.

Al-Harthy, S.S., Dennis, J.W., Jing, X.D. and Marsden, J.R.: 'Hysteresis, true-triaxial stress path and pore pressure effects on Permeability', SPE 47269, presented at the SPE/ISRM Eurock held in Trondheim, Norway (1998a), 1-9.

Al-Harthy, S.S., Dennis, J.W., Jing, X.D. and Marsden, J.R.: 'Petrophysical properties under true-triaxial stress for hydrocarbon recovery prediction', SPE 39770, presented at the SPE Permian Basin Oil and Gas Recovery Conference, held in Midland, Texas, USA (1998b), 1-6.

Al-Harthy, S.S., Jing, X.D. and Marsden, J.R.: 'Petrophysical properties of reservoir rocks under true triaxial stress', London Petrophysical Society, Dialog, Volume 7, Issue 1 (1999), 5-7.

Al-Harthy, S.S., Jing, X.D. Marsden, J.R. and Dennis, J.W.: 'Petrophysical Properties of Sandstones Under True Triaxial Stresses I: Directional Transport Characteristics and Pore Volume Deformation', SPE 57287, to be presented at the SPE Asia Pacific Improved Oil Recovery Conference, Kuala Lumpur (1999).

Allan, D.: 'Anisotropy calculation from multi-frequency/multi-spacing MWD tools: a new technique', Dialog, Vol. 6 Issue 2, April (1998), 6-9.

Amadei, B. and Stephansson, O.: 'Rock stress and its measurements' Chapman and Hall publishing company (1997).

Amyx, J.W., Bass, D.M. and Whiting, R.L.: 'Petroleum Reservoir Engineering, Physical Properties, McGraw-Hill Book Company, New York (1960).

Andersen, M.A.: 'Predicting reservoir condition pore volume compressibility from hydrostatic stress laboratory data', SPE 14213, presented at the presented at the 60th Annual Technical Conference and Exhibition of the SPE held in Las Vegas, Nevada, USA (1985), 1-7.

Anderson, B., Bryant, I., Luling, M., Spices, B. and Helbig, K.: 'Oilfield anisotropy: Its origins and electrical characteristics', Oilfield Review, Vol. 6 No. 4 (1994), 48-56.

Antoine, J.N.: 'A method to drive dips from bed boundaries in borehole Images', SPE 20540, presented at the presented at the 65th Annual Technical Conference and Exhibition of the SPE held in New Orleans, LA, USA (1990), 121-127.

Archer, J.S. and Wall, CG.: 'Petroleum Engineering: Principles and Practice', Graham and Trotman Ltd, London (1986).

Archie, G.E.: 'Electrical resistivity log as an aid in determining some reservoir characteristics' Trans., AIME, Vol. 146 (1942), 54-62.

Armstrong, Phil., Ireson, D., Chmela, B., Dodds, K., Esmersoy, C., Miller, D., Hornby, B., Colin, S., Schoenberg, M., Leaney, S. and Lynn, H.: 'The promise of elastic anisotropy', Oilfield Review, October (1994).

Auzerais, F.M., Ellis, D.V., Dussan E.B. and Pinoteau, B.J.: 'Laboratory characterisation of anisotropic rocks', SPE 20602, presented at the Annual Technical Conference and Exhibition of the SPE held in New Orleans, LA, USA (1990), 751-758.

Ayan, C., Colley, N., Cowan, G., Ezekwe, E., Wannell, M., Goode, P., Halford, F., Joseph, J., Mongini, A., Obondoko, G. and Pop, J.: 'Measuring permeability anisotropy: The latest approach', Oilfield Review, October (1994), 24-35.

Azeemuddin, M., Roegiers, J.C., Suri, P., Zaman, M. and Kukreti, A.R.: 'Stress-dependency permeability measurement of rocks in a triaxial cell', Rock Mechanics Proceeding of the 35th US Symposium, Ch. 133 (1995), 645-650.

Berumen, S. and Tiab, D.: 'Effect of pore pressure on conductivity and permeability of fractured reservoir' SPE 35694, presented at the Western Region Meeting held in Anchorage, Alaska, USA (1996), 445-460.

Bieber, M.T. and Zamora, M.: 'Measurement and overall characterisation of permeability anisotropy by tracer injection', Revue de L'institut Francais du Petrole, Vol. 51 No. 3 (1996), 333-347.

Biot, M.A.: 'Theory of elasticity and consolidation for a porous anisotropic solid', Journal of Applied Physics, Vol. 26, (1955), 182-197

Bloch, M., Siqueira, A.M., Ferreira, F.H. and Conceicao, J.C.J.: 'Techniques for determining in situ stress directions and magnitudes', SPE 39075, presented at the 5th Latin America and Caribbean Petroleum Engineering Conference and Exhibition held in Rio de Jeneiro, Brazil (1997), 1-13.

Bonnie, J.H.M.: 'Reconciliation of resistivity log readings in vertical and horizontal boreholes', SPE 26431, presented at the Annual Technical Conference and Exhibition of the SPE held in Houston, Texas, USA (1993), 151-160.

Brace, W.F. and Orange, A.S.: 'Electrical resistivity changes in saturated rock under stress', Science, Vol. 153 (1966), 1525-1526.

Brace, W.F., Orange, A.S. and Madden, T.R.: 'The effect of pressure on the electrical resistivity of water-saturated crystalline rocks', Journal of Geophysical Research, Vol. 70 No. 22 (1965), 5669-5678.

Bruno, M.S., Boverg, C.A. and Nakagawa, F.M.: 'Anisotropy stress influence on the permeability of weakly-cemented sandstones', Rock Mechanics as a multidisciplinary science, Proceeding of the 32nd US symposium, Ch. 124 (1991), 375-383.

Buchsteiner, H., Warpinski, N.R. and Economides, M.J.: 'Stress-induced permeability reduction in fissured reservoirs', SPE 26513, presented at the Annual Technical Conference and Exhibition of the SPE held in Houston, Texas, USA (1993), 65-74.

Carnes, P.S.: 'Effect of natural fractures or directional permeability in water flooding', SPE 1423, SPE of AIME (1960), 17-24.

Chen, H.Y., Teufel, L.W. and Lee, R.L.: 'Coupled fluid flow and geomechanics in reservoir study - theory and governing equations', SPE 30752, presented at the SPE Annual Technical Conference and Exhibition held in Dallas, Texas, USA (1995), 507-519.

Chowdiah, P.: 'Influence of water-desaturation technique and stress on laboratory measurement on hydraulic properties of tight sandstones', SPE Formation Evaluation, December (1988), 679-685.

Christoffersen, K.R. and Whitson, C.H.: 'Gas/oil capillary pressure of chalk at elevated pressures', SPE 26673, presented at the 68th Annual Technical Conference and Exhibition of the SPE held in Houston, Texas, USA (1993), 701-716.

Cosse, R.: 'Basic of Reservoir Engineering', Editions Tech., Paris, France (1993).

Crawford, B.R. and Smart, B.G.D.: 'The influence of stress anisotropy on horizontal well performance predicted via special core analysis under true triaxial conditions', SPE 28452, presented at the 69th Annual Technical Conference and Exhibition of the SPE held in New Orleans, LA, USA (1994), 923-935.

Dabbous, M.K., Reznik, A.A., Mody, B.G., Fulton, P.F. and Taber, J.J.: 'Gas-water capillary pressure in coal at various overburden pressures', SPE Journal, October (1976), 261-268.

Daltaban, T.S., Lewis, J.J. and Archer, J.S.: 'Field minipermeameter measurements - Their collection and interpretation', presented at the 5th Annual European Symposium on Improved Oil Recovery, Budapest (1989), 671-682.

Dey, T.N.: 'Permeability and electrical conductivity changes due to hydrostatic stress cycling of Berea and Muddy J sandstone', Journal of Geophysical Research, Vol. 91 No. B1 (1986), 763-766.

Donaldson, E.C., Kendella, R.F., Pavelka, E.A. and Crocker, M.E, 'Equipment and procedures for fluid flow and wettability tests of geological materials', U.S dept. Energy report, Nat. Tech. Info. Sv., Springfield, VA, USA (1980), 1-15.

Duquerroix, J.P.L., Lemouzy, P., Noetinger, B. and Romeu, R.K.: 'Influence of the permeability anisotropy ratio on large-scale properties of heterogeneous

reservoirs', SPE 26612, presented at the Annual Technical Conference and Exhibition of the SPE held in Houston, Texas, USA (1993), 29-40.

Durucan, S., Daltaban, T.S., Shi, J.Q. and Wang, J.M.: 'Numerical modelling and variation of stress and pore pressure dependent dynamic permeability behaviour of coal seams around wellbore', Intergas, Paper No. 9528 (1995), 413-421.

Elashahab, B.: 'An experimental investigation of permeability variations with confining pressure', MSc thesis, Imperial College, London, UK (1990).

Elashahab, B.: 'Effect of wettability, hysteresis and saturation distribution on the electrical properties of rocks at reservoir conditions', PhD thesis, Imperial College, London, UK (1995).

Elashahab, B.M., Jing, X.D. and Archer J.S.: 'Laboratory determination of Archie saturation exponent of various water-wet and oil-wet sandstone rocks at reservoir conditions', Presented at the 2nd Mediterranean Petroleum Conference MPC93, Tripoli, Libya (1993), 221-241.

Farmer, I.: 'Engineering behaviour of rocks', 2nd edition, London, Chapman and Hall (1983).

Farquhar, R.A., Smart, B.G.D., Todd, A.C., Tompkins, D.E. and Tweedie, A.J.: 'Stress sensitive of low permeability sandstones from the Rotliegendes sandstone', SPE 26501, presented at the 68th Annual Technical Conference and Exhibition of the SPE held in Houston, Texas, USA (1993), 851-861.

Fatt, I.: 'Effect of overburden and reservoir pressure on electrical logging formation factor', Bull. of American Assoc. of Petroleum Geologists, Vol. 41 No. 11 (1957).

Firoozabadi, A. and Hauge, J., 'Capillary pressure in fractured porous medium', Journal of Petroleum Technology, June (1990), 784-791.

Firoozabadi, A. and Markeset, T.: 'Laboratory studies in fractured porous medium', Part I, Reinfiltration for gas-liquid system' In Situ, 19(1) (1995), 1-21.

Garrouch, A.A. and Sharma, M.: 'The influence of clay content, salinity, stress, and wettability on the dielectric properties of brine-saturated rocks: 10Hz to 10MHz', Geophysics, Vol. 59 No 6 (1994), 909-916.

Gatens, J.M., Lee, W.J., Hopkins, C.W. and Lancaster, S.A.: 'The effect of permeability anisotropy on the evaluation and design of hydraulic fracture treatments

and well performance', SPE 21501, presented at the SPE Gas Technology Symposium held in Houston, Texas, USA (1991), 211-222.

Glover, P.W.J., Meredith, P.G., Sammonds, P.R. and Murrell, S.A.F.: 'Measurements of complex electrical conductivity and fluid permeability in porous rocks at raised confining pressures,' Eurock, Rotterdam (1994), 29-36.

Gobran, B.D., Brigham, W.E. and Ramey, H.J.: 'Absolute permeability as a function of confining pressure, pore pressure, and temperature', SPE Formation Evaluation, March (1987), 77-84.

Grattoni, C.A. and Dawe R.A.: 'Anisotropy in pore structure of porous media', Powder Technology 85 (1995), 143-151.

Grattoni, C.A. and Dawe R.A.: 'Electrical resistivity anisotropy due to pore scale structure', presented at the international society of core analysis, Stavanger, Norway, SCA-9416 (1994), 1-10.

Grattoni, C.A. and Dawe R.A.: 'Influence of fluid distribution upon electrical resistivity of partially saturated media', presented at the 36th Annual SPWLA June (1995), 1-9.

Gray, D.H. and Fatt, I.: 'The effect of stress on permeability of sandstone cores' SPE Journal, June (1963), 95-100.

Greenkorn, R.A., Johnson, C.R. and Shallenberger, L.K.: 'Directional permeability of heterogeneous anisotropic porous media', SPE Journal, December (1961), 124-132.

Guppy, K.H., Marsden, S.S. and Moris, M.: 'The measurement of directional permeability and the application in thermal recovery projects', SPE 7131, presented at the Regional Meeting of SPE of AIME held in San Francisco, California, USA (1978), 1-8.

Hagiwara, T.: 'A new method to determine horizontal-resistivity in anisotropic formations without prior knowledge of relative dip', SPWLA 37th Annual Logging Symposium, Paper Q (1996), 1-8.

Hagiwara, T.: 'EM log response to anisotropic resistivity in thinly laminated formations with emphasis on 2-MHz resistivity devices', SPE Formation Evaluation, December (1996), 211-217.

Hagiwara, T.: 'Macroscopic anisotropy' Approach to analysis of thinly laminated sand/shale sequences: Sensitivity analysis of sand resistivity estimate and environmental corrections', SPE 38669, presented at the SPE Annual Technical Conference and Exhibition of the in San Antonio, Texas, USA (1997), 275-286.

Hagiwara, T.: 'On the direction of core dielectric constant and conductivity measurements', The Log Analyst, November-December (1986), 26-29.

Hagiwara, T.: 'Response of 2 MHz resistivity devices in thinly laminated formations (Anisotropic resistivity and EM log interpretation)', SPE 28426, presented at the Annual Technical Conference and Exhibition of the SPE held in New Orleans, LA, USA (1994), 667-674.

Hassler, G.L. and Brunner, E.: 'Measurements of capillary pressures in small core samples', Trans. of AIME (1945), 114-123.

Herget, G.: 'Stresses in rock' A. A. Balkema/Rotterdam/Brookfield Publishing Company, Netherlands (1988).

Hettema, M.H.H., Schutjens, P.MT.M., Verboom, B.J.M. and Gussinkio, H.J: 'Production-induced compaction of sandstone reservoirs: The strong influence of field stress', SPE 50630, presented at the 1998 SPE European Petroleum Conference in the Hague, The Netherlands (1998), 1-8.

Hill, D.G.: 'A laboratory investigation of conductivity and dieletrical constant tensors of rocks', PhD thesis, Michigan State University (1969).

Holt, R.M.: 'Permeability reduction induced by a nonhydrostatic stress field', SPE 19595, presented at the 64th Annual Technical Conference and Exhibition of the SPE in San Antonio, Texas, USA (1989), 251-258.

Hopkins C.W.: 'The importance of in situ stress profiles in hydraulic-fracturing applications', Journal of Petroleum Technology, September (1997), 994-948.

Horie, T., Firoozabadi, A. and Ishimoto, K.: 'Laboratory Study of Capillary Interaction in Fractured/Matrix Systems', SPE Reservoir Engineering, August (1990), 353-360.

Hudson, J. and Cooling, C.: 'In situ rock stresses and their measurements in the U.K-Part-I- The current state of knowledge', Int. J. Rock Mech. Min. Sci. & Geomech. Abstr. 25 (1988), 363-270.

Hudson, J.A.: 'Comprehensive Rock Engineering, Principal, Practice and Projects' Volume 3, Rock testing and site characterisation, Pergamon press (1993).

Ioannidis, M.A., Chatzis, I. and Kwiecien, M.J: 'Computed enhanced core analysis for petrophysical properties', Journal of Canadian Petroleum Technology, March (1999), 18-24.

Jaeger, J.C. and Cook, N.G.: 'Fundamentals of rock mechanics', 3rd edition, Chapman and Hall, London (1979).

Jing, X.D., Archer, J.S. and Daltaban, T.S.: 'Laboratory study of the electrical and hydraulic properties of rocks under simulated reservoir conditions', Marine and Petroleum Geology, April (1992), 115-127.

Jing, X.D., Elashahab, B.M. and Archer, J.S.: 'Experimental investigation of the effect of wettability, saturation history and overburden pressure on resistivity index', SPWLA 15th European Formation Evaluation Symposium, Stavanger, Norway (1993), 1-17.

Jones, M. and Mathiesen, E.: 'Pore pressure change and compaction in North Sea chalk hydrocarbon reservoirs', Int. J. Rock Mech. Min. Sci. & Geomech. Abstr. Vol. 30 No. 7 (1993), 1205-1208.

Kennedy, D.W. and Givens, W.W.: 'Method for determining tensor conductivity components of a transversely isotropic core sample of subterranean formation', Patent number 5095273 (1992), 1-10.

Khan, M. and Teufel, L.W.: 'Prediction of production-induced changes in reservoir stress state using numerical model', SPE 36697, presented at the Annual Technical Conference and Exhibition of the SPE held in Denver, Colorado, USA (1996), 1-11

King, M.J.: 'Application and analysis of tensor permeability to crossbedded reservoirs', SPE 26118, presented at the western region meeting, Alaska, USA (1993), 745-746.

King, M.S, Shakeel, A. and Chaudry N.A.: 'Acoustic wave propagation and permeability in sandstones with systems of aligned cracks', Developments in Petrophysics, Geological Society Special Publication, No. 122 (1997), 69-85.

King, M.S., Chaudry, N.A. and Shakeel, A.: 'Experimental ultrasonic velocities and permeability for sandstones with aligned cracks', Int. J. Rock Mech. Min. Sci. & Geomech. Abstr. Vol. 32 No. 2 (1995), 155-163.

Klein, J.D.: 'Induction log anisotropy corrections', The Log Analyst, March-April (1993), 18-27.

Koelman, J.M.V.A., Horst van der, M., Lomas, A.T., Koelemij, A.T. and Bonnie, J.H.M.: 'Interpretation of resistivity logs in horizontal wells an application to complex reservoirs from Oman', SPWLA 37th Annual Logging Symposium, Paper Q (1996), 1-9.

Labastie, A.: 'Capillary continuity between matrix blocks of a fractured reservoir', presented at the 65th Annual Technical Conference and Exhibition of the SPE held in New Orleans, Louisiana, USA (1990), 423-432.

Lachance, D.P. and Andersen, M.A.: 'Comparison of uniaxial strain and hydrostatic stress pore-volume compressibilities in the Nugget sandstone', SPE 11971, presented at the 58th Annual Technical Conference and Exhibition of the SPE held in San Francisco, California, USA (1983), 1-8.

Lake, L.W.: 'The origin of anisotropy', Journal of Petroleum Technology, April (1988), 395-396.

Landrum, B.L. and Crawford, P.B.: 'Effect of directional permeability on sweep efficiency and production capacity', SPE AIME. 219 (1960), 407-411.

Lee, J.: 'Well testing', SPE textbook series Vol. 1, Society of Petroleum Engineers of AIME, New York, Texas, USA (1982).

Lerner, D.B., Dacy, J.M., Raible, C.J., Rathmell, J.J., Swanson, G. and Walls, J.D.: 'SCA Guidelines for sample preparation and porosity measurement of electrical resistivity samples', 'Part II Sample preparation and porosity measurement', The Log Analyst, March -April (1990), 57-63.

Leung, W.F.: 'A tensor model for anisotropy and heterogeneous reservoirs with variable directional permeabilities', SPE 15134, presented at the SPE California Regional Meeting Oakland, California, USA (1986), 405-415.

Leverett, M.C.: 'Capillary behaviour in porous solids', Trans. AIME, Vol. 142 (1941), 152-169.

Lewis, M.G., Sharma, M.M. and Dunlap, H.H.: 'Wettability and stress effects on saturation and cementation exponents', Trans. SPWLA 29th Annual Logging Symposium, Paper K, San Antonio, Texas, USA (1988), 1-23.

Longeron, D.G., Argaud, M.J. and Bouvier, L.: 'Resistivity index and capillary pressure measurements under reservoir conditions using crude oil', presented at the 64th Annual Technical Conference and Exhibition of the SPE held in San Antonio, Texas, USA (1989), 187-200.

Longeron, D.G.: 'Effect of overburden pressure, nature and microscopic distribution of the fluids on electrical properties of rock samples', SPE 15383, presented at the 61st Annual Technical Conference and Exhibition, held in New Orleans, LA, USA (1986), 194-201.

Lorenz, J.C.: 'Stress-sensitive reservoirs', Journal of Petroleum Technology, January (1999), 61-63.

Lovell, M.A., Harvey, P.K., Jackson, P.D., Ball, J.K., Ashu, A.P., Flint, R.F and Gunn, D.: 'Electrical resistivity core imaging: towards a 3-dimensional solution', SPWLA 35th Annual Logging Symposium, Paper JJ (1994), 1-6.

Lovell, M.A., Harvey, Williams, C.G., P.K., Jackson, A.P., Flint, R.C and Gunn, D.A.: 'Electrical resistivity core imaging: a petrophysical link to borehole images', Log Analyst, November-December (1997), 45-53.

Maerefat, N.I., Baldwin, B.A., Chaves, A.A., LaTorraca G.A. and Swanson, B.F.: 'SCA Guidelines for sample preparation and porosity measurement of electrical resistivity samples', 'Part IV Guidelines for saturating and desaturating cores plugs during electrical measurements', The Log Analyst, March-April (1990), 68-75.

Mahmood, A. and Nurmi, R.: 'Fractures in the basement', Middle East Well Evaluation Review, No 14 (1993), 26-43.

Mahmood, S.M., Maerefat, N.L., and Chang, M.M.: 'Laboratory measurements of electrical resistivity at reservoir conditions', SPE Formation Evaluation, September (1991), 291-300.

Manrique, J.F., Kasap, E. and Georgi, D.: 'Effects of heterogeneity and anisotropy on probe measured permeabilities', SPE Journal, March (1997), 16-23.

Marcus, H.: 'The permeability of a sample of an anisotropic porous medium', Journal of Geophysical Research, Vol. 67 No. 13 (1962), 5215-5225.

Marsden, J.R.: 'Personal communication', Imperial College of Science, Technology and Medicine, University of London (1996).

Michelis, P.: 'A true triaxial cell for low and high pressure experiments', Int. Journal of Rock Mech. Min. Sci. and Geomech. Abstract, Vol. 22 No. 3 (1985), 183-188.

Moran, J.H., and Gianzero, S.: 'Effects of formation anisotropy on resistivity-logging measurements', Geophysics, Vol. 44 No. 7 (1979), 1266-1286.

Morita, N., Gray, K.E., Srouji, F.A.A. and Jogi, P.N.: 'Rock-property changes during reservoir compaction', SPE Formation Evaluation, September (1992), 197-205.

Morita, N., Whitfill, D.L., Nygaad, O. and Bale, A.: 'A quick method to determine subsidence, reservoir compaction, and in situ stress induced by reservoir depletion', SPE 17150, presented at the Formation Damage Control Symposium held in Bakersfield, California, USA (1988), 73-84.

Morrow, C.A., Bo-Chong, Z. and Byerlee, J.D.: 'Effective pressure law for permeability of Westerly granite under cyclic loading', Journal of Geophysical Research, Vol. 91 No. B3 (1986), 3870-3876.

Myer, L.R., Cook-Polet, A.M., Pyrak-Nolte, L.J. and Marone, C.: 'Mercury porosimetry studies on a natural fracture', Presented at the 4th Annual International Conference on High Level Radioactive Waste Management held in Las Vegas, Nevada, USA, Vol. 1 (1993), 2017-2022.

Nelson R A.: 'Fractured reservoirs: tuning knowledge into practice', Journal of Petroleum Technology, April (1987), 407-414.

Nelson R A.: 'Geological analysis of naturally fractured reservoir,' Gulf Publishing Company, Book division, Houston, London, Paris, Tokyo (1985).

Nelson, R.A and Handin, J.W.: 'Experimental study of fracture permeability in porous rocks', AAPG, Vol. 61 No. 2 (1977), 227-236.

Oilfield Review.: 'Formation anisotropy: Reckoning with its effects', Oilfield Review 2 No 1 (1990), 16-23.

Omar, A.E. and El-Gassier, M.M.: 'Permeability and rock resistivity hysteresis of sandstones', Journal of Engineering, King Saudi University, Vol. 12 (2) (1986), 287-300.

Omoregie, Z.S.: 'Factors affecting the equivalent of different capillary pressure measurement techniques', SPE 15384, presented at the 61st Annual Technical Conference and Exhibition of the SPE held in New Orleans, LA, USA (1986), 1-15.

Osorio, R.G., Chen, H.Y. and Teufel, L.W.: 'Fully coupled fluid-flow/geomechanics simulation of stress-sensitive reservoirs', SPE 38023, presented at the Symposium on Reservoir Simulation held in Dallas, Texas, USA (1997), 321-322.

Osorio, R.G., Chen, H.Y. and Teufel, L.W.: 'Numerical simulation of coupled fluid-flow/geomechanical behaviour of tight gas reservoirs with stress-sensitive permeability', SPE 39055, presented at the SPE 5th Latin American and Caribbean Petroleum Engineering Conference and Exhibition, held in Rio de Janeiro, Brazil (1997), 1-15.

Ostensen, R.W.: 'The effect of stress-dependent permeability on gas production and well testing', SPE Formation Evaluation, June (1986), 227-235.

Parsons, R.W.: 'Directional permeability effects in developed and unconfined five spots', Journal of Petroleum Technology, April (1972), 487-494.

Peffer, J., O'Callaghan, A. and Pop, J.: 'In situ determination of permeability anisotropy and its vertical distribution - A case study', SPE 38942, presented at the SPE Annual Technical Conference and Exhibition held in San Antonio, Texas, USA (1997), 341-351.

Perez, J.M., Poston, S.W. and Edwards, C.M.: 'The Permeability of micro-fractures on oil recovery from low-permeability reservoirs', SPE 25857, presented at the SPE Rocky Mountain Regional/Low Permeability Reservoirs Symposium held in Denver, Colorado, USA (1993), 165-175.

Puri, R. and Seidle, J.P.: 'Measurement of stress-dependent permeability of coal and its influence on coalbed methane production', In Situ, Vol. 16 No 3 (1992), 183-202.

Rasmus, J.C.: 'A summary of the effect of various pore geometries and their wettabilities on measured and in-situ values of cementation and saturation exponents', The Log analyst, March-April (1987), 152-164.

Rauen, A. and Soffel, H.C.: 'Determination of electrical resistivity, its anisotropy and heterogeneity on drill cores: a new method', Geophysics Prospecting, Vol. 43 (1995), 283-298.

Read, M.D. and Meredith, P.G and Murrell, S.A.: 'Permeability measurement techniques under hydrostatic and deviatoric stress conditions', Rock at great Depth, Maurry and Fourmaintraux (eds), Balkema, Rotterdam (1989), 211-217.

Reitsma, S.: 'Laboratory measurement of capillary pressure-saturation relationships in a rock fracture', Water Resources Research, Vol. 30 No. 4 (1994), 865-878.

Rhett, D.W. and Teufel, L.W.: 'Effect of reservoir stress path on compressibility and permeability of sandstones', SPE 24756, presented at the 67th Annual Technical Conference and Exhibition of the SPE in Washington DC, USA (1992), 965-972.

Rhett, D.W. and Teufel, L.W.: 'Stress path dependence of matrix permeability of North Sea sandstone reservoir rock', Rock Mechanics, Tillerson and Wawersik (eds) Rotterdam (1992), 345-353.

Ritter, L.C. and Drake, R.L.: 'Pore size distribution in porous material', Industrial and Engineering Chem. Fund., Vol. 17 (1945), 782-786.

Rose, W.: 'A new method to measure directional permeability', Journal of Petroleum Technology, May (1982), 1142-1144.

Rose, W.: 'A note on the role played by sediment bedding in causing permeability anisotropy', Journal of Petroleum Technology, February (1983), 330-333.

Rose, W.: 'Discussion of paper by H. Marcus - The permeability of a sample of an anisotropic porous medium', Journal of Geophysical Research, Vol. 68 No. 16 (1963), 4881-4883.

Rose, W.: 'Laboratory measurements of directional permeability trends', Project 61031 Special Core Analysis Report prepared for US Dept. of Energy under Contract No. DE-AC19-78BC00042 (1982).

Rose, W.: 'Permeability anisotropy in low permeability formations', SPE/DOE 10810, presented at the Unconventional Gas Recovery Symposium, held in Pittsburgh, PA, USA (1982), 195-202.

Ruistuen, H., Teufel, L.W. and Rhett, D.: 'Influence of reservoir stress path on deformation and permeability of weakly cemented sandstone reservoirs', SPE 36535, presented at the SPE Annual Technical Conference and Exhibition held in Denver, USA (1996), 463-470.

Runge, R.J. and Hill, D.G.: 'The role of anisotropy in ULSEL', SPWLA 12th Annual Logging Symposium, Paper J (1971),1-23.

Samaroo, B.H. and Guerrero, E.T.: 'The effect of temperature on drainage capillary pressure in rocks using a modified centrifuge', SPE 10153, presented at the 56th Annual Fall Technical Conference and Exhibition of the SPE held in San Antonio, Texas, USA (1981), 1-12.

Saner, S., Amabeoku, M. and Kassami, M.: 'Formation resistivity response to loading and unloading confining pressure', Journal of Petroleum Science and Engineering, Vol. 16 (1996), 169-179.

Sayers, C.M., Van Munster, J.G. and King, M.S.: 'Stress-induced ultrasonic anisotropy in Berea sandstone', Int. J. Rock Mech. Min. Sci. & Geomech. Abstr. Vol. 27 No. 5 (1990), 429-436.

Scheidegger, A E.: 'The physics of flow through porous media', University of Toronto Press (1957).

Schlumberger GeoQuest, .: 'Eclipse 100 98A reference manual' (1998).

Schlumberger, C., Schlumberger, M. and Leonardon, E.G.: 'Some observations concerning electrical measurements in anisotropic media, and their interpretation', Trans. AIME, Vol. 110 (1934), 159-182.

Schlumberger.: 'Log interpretation principal/applications', Schlumberger education services (1989).

Schutjens, P.M.T.M., Blanton, T.L., Martin, J.W., Lehr, B.C. and Baaijens, M.N.: 'Depletion-induced compaction of an overpressured reservoir sandstone: an experimental approach', SPE 47277, presented at the SPE/ISRM Eurock held in Trondheim, Norway (1998), 1-13.

Schutjens, P.M.T.M., Ruig, de H., Sayers, C.M., Munster, van J.G. and Whitworth, J.L.: 'Production-induced compaction of the Brent field: an experimental approach', SPE Formation Evaluation, June (1996), 99-107.

Settari, A. and Mourits, F.M.: 'A coupled reservoir and geomechanical simulation system', SPE Journal, September (1998), 219-226.

Sharma, M.M., Garrouch, A. and Dunlap, H.F.: 'Effects of wettability, pore geometry and stress on electrical conduction in fluid-saturated rocks', The Log Analyst, September-October (1991), 511-526.

Sharma, M.M.: 'Petrophysics class notes', The University of Texas at Austin (1995).

Smart, B.G.D. and Crawford, B.R.: 'An innovative new cell for testing rock core under true triaxial stress states', Society of Core Analysis, Conference Paper 9320 (1993), 1-12.

Smart, B.G.D.: 'A true triaxial cell for testing cylindrical rock specimens', Int. Journal of Rock Mech. Min. Sci. and Geomech. Abstract, Vol. 32 No. 3 (1995), 269-275.

Soares, G.F. and Coutinho, M.R.: 'Identification of the electrical anisotropy on cretaceous turbiditics reservoirs through log simulation in horizontal wells', SPE 39012, presented at the 5th Latin American and Caribbean Petroleum Engineering Conference and Exhibition held in Rio de Janeiro, Brazil (1997), 1-9.

Sondenaa, E., Bratteli, F., Kolltveit, K. and Norman, H.P.: 'A Comparison between pressure data and saturation exponent obtained at ambient conditions and at reservoir conditions', SPE 19592, presented at the 64th Annual Technical Conference and Exhibition of the SPE held in San Antonio Texas, USA (1989), 213-225.

Sondenaa, E., Bratteli, F., Norman, H.P. and Kolltveit, K.: 'The effect of reservoir conditions and wettability on electrical resistivity', SPE 22991, presented at the SPE Asia-Pacific Conference held in Perth, Western Australia (1991), 401-415.

Stesky, R M., 'Electrical conductivity of brine-saturated fractured rock', Geophysics Vol. 51 No. 8 (1986), 1585-1593.

Swanson, B.F.: 'Microporosity in reservoir rocks: Its measurement and influence on electrical resistivity', The Log Analysts, November-December (1985), 42-52.

Takahashi, M., Koidei, H. and Sugita, Y.: 'Three principal stress effects on permeability of Shirahama sandstone', International Congress on Rock Mechanics - Proceedings, Vols. 2 Ch. 189 (1995), 729-732.

Teeuw, D.: 'Prediction of formation compaction from laboratory compressibility data', SPE Journal, September (1971), 263-271.

Teufel, L.W. and Rhett, D.W.: 'Failure of Chalk during waterflooding of the Ekofisk field,' SPE 24911, presented at the 67th Annual Technical Conference and Exhibition of the SPE held in Washington DC, USA (1992), 565-574.

Teufel, L.W. and Rhett, D.W.: 'Geomechanical Evidence for shear failure during production of the Ekofisk field,' SPE 22755, presented at the 66th Annual Technical Conference and Exhibition of the SPE held in Dallas, Texas, USA (1991a), 905-912.

Teufel, L.W., Rhett, D.W. and Farrell H.E.: 'Effect of reservoir depletion and pore pressure drawdown on in situ and deformation in the Ekofisk field, North Sea' Rock Mechanics as a multidisiplinary science, Proceeding of the 32nd US symposium, Ch. 124 (1991b), 63-72.

Teufel, L.W., Rhett, D.W., Farrell H.E. and Lorenz J.C.: 'Control of fractured reservoir permeability by spatial and temporal variations in stress magnitude and orientation', SPE 26437, presented at the Annual Technical Conference and Exhibition of the SPE held in Houston, Texas, USA (1993), 1-11.

Tiab, D. and Donaldson, E.C.: 'Petrophysics, theory and practice of measuring reservoir rock and fluid transport properties,' Gulf Publishing Company, Houston (1996).

Van Golf-Racht, T.D.: 'Fundamental of fractured reservoir engineering', Elsevier Scientific Publishing Company, Amsterdam, Oxford, New York (1982).

Wade, J.M., Hough, E.V. and Pedersen, S.H.: 'Practical methods employed in determining anisotropy for optimisation of a planned waterflood of the Eldfisk', SPE 48961, presented at the Annual Technical Conference and Exhibition of the SPE held in New Orleans, LA, USA (1997), 49-63.

Wang, J.T., Daltaban, T.S. and Archer, J.S.: 'The role of permeability tensors in modelling fluid flow in fractured reservoir', OSEA 92214, presented at the 9th Offshore South East Asia Conference held in Singapore (1992a), 541-551.

Wang, J.T., Daltaban, T.S. and Archer, J.S.: 'The use of permeability tensor in modelling heterogeneous and fractured flow media', SPE 24503, presented at the 5th Abu Dhabi Petroleum Conference held in Abu Dhabi, UAE (1992b), 1-11.

Wannell, M., Colley, N. and Halford, F.R.: 'The use of new technology to determine permeability anisotropy', SPE 26801, presented at the Offshore European conference held in Aberdeen, UK (1993), 489-495.

Wardlaw, N.C. and Taylor, R.P.: 'Mercury capillary pressure curves and the interpretation of pore structure and capillary behaviour in reservoir rocks', Bull. Can. Petrol. Geol., Vol. 24 No. 2 (1976), 225-262.

Warpinski, N.R. and Teufel, L.W.: 'Determination of the effective-stress law for permeability and deformation in low permeability rocks', SPE 20572, presented at

the 65th Annual Technical Conference and Exhibition of the SPE held in New Orleans, LA, USA (1990), 453-464.

Western Atlas International.: 'Fundamentals of rock properties', Core laboratories Manual (1992).

Widarsono, B.: 'In situ determination using differential strain analysis and ultrasonic shear-wave splitting', PhD thesis, Imperial College, London, UK (1996).

Winsauer, W.O., Shearin, A.M., Masson, P.H. and Williams, M.: 'Resistivities of brine saturated sands in relation to pore geometry', Bulletin AAPG, 1952, 36, 253-277

Worthington, A.E., Hedges, J.H. and Pallat, N.: 'SCA Guidelines for sample preparation and porosity measurement of electrical resistivity samples', 'Part I Guidelines for preparation of brine and determination of brine resistivity for the use in electrical measurements', The Log Analyst, January-February (1990), 20-28.

Worthington, P.F.: 'The influence of formation anisotropy upon resistivity-porosity relationships', presented at the 22nd Annual Logging Symposium, June (1981), 1-25.

Worthington, P.F.: 'Estimation of intergranular permeability from well logs', Dialog, 3(3), (1995), 7-10.

Wyllie, R.J. and Spangler, M.B.: 'Application of electrical resistivity measurements to problem of fluid flow in porous media', Bulletin of the American Association of Petroleum Geologists, Vol. 36 No. 2 (1952), 359-403.

Yassir, N.A. and Bell, J.S.: 'Abnormally high fluid pressures and associated porosities and stress regimes in sedimentary basins', SPE Formation Evaluation, March (1996), 5-10.

Zaafran, Z.M.: 'Studying the effect of sandstone anisotropy on the quantitative interpretation of resistivity sounding and logging', SPWLA 22nd Annual Logging symposium, Paper BB (1981), 1-13.

Zimmerman, R.W., 'Compressibility of sandstones', Elsevier Science Publishing B.V., Netherlands (1991).

Zoback, M.D, and Byerlee, J.D.: 'Effect of high-pressure deformation of Ottawa sand', AAPGB, Vol. 60 No. 9 (1976), 1531-1542.

Zoback, M.D, and Byerlee, J.D.: 'Permeability and effect stress', AAPGB, Vol. 59 (1975), 154-160.

APPENDICES

APPENDIX A

Doddington

Doddington sandstone is from Doddington Hill quarry in Northumberland, and is a Carboniferous fell sandstone with fine-medium grains, pink in colour, and highly porous and permeable.

Kair: 2700 mD
Porosity: 23.52%
Quartz: 98%
Feldspar: 2%
Rock Fragments: 0%
Cement: Kaolinite
Matrix: No
Angularity: angular-sub angular
Sphericity: moderate
Compositional Maturity: super mature
Textural Maturity: mature
Comments: feldspar predominantly microcline with some perthite; long and point contacts

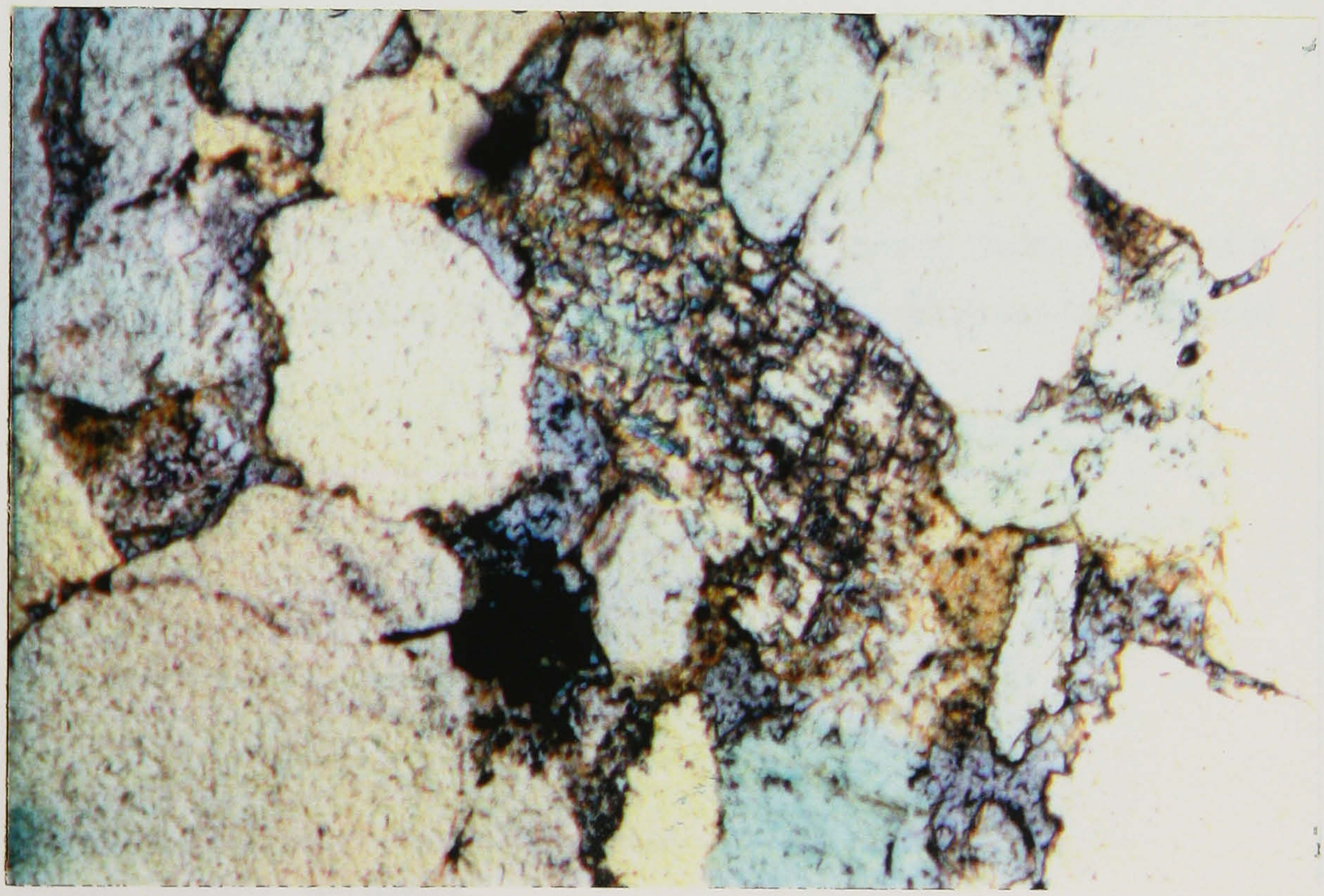

155 microns

Figure A.1 Thin section of Doddington with magnification = 30

Figure A.2 SEM of Doddington with magnification = 780

Croslands Hill

Croslands Hill sandstone is from the Croslands Moor quarry, Huddersfield, and it belongs to the Carboniferous Millstone grit series with fine grains and light brown in colour.

Kair: 14.18 mD
Porosity: 19.22%
Quartz: 85%
Feldspar: 5%
Rock Fragments: 10%
Cement: Kaolinite; occasional syntaxial quartz overgrowth cements
Matrix: No
Angularity: sub angular
Sphericity: moderate
Compositional Maturity: sub mature-mature
Textural Maturity: sub mature
Comments: some corrosion of quartz grains; long and sutured contacts

155 microns

Figure A.3 Thin section of Croslands Hill with magnification = 30

250 microns

Figure A.4 SEM of Croslands Hill with magnification = 780

Springwell

Springwell sandstone is from Springwell quarry near Gateshead, and it belongs to the Carboniferous Middle Coal Measures series, with fine to medium grains and fawn in colour.

Kair: 19.73 mD
Porosity: 16.92%
Quartz: 75%
Feldspar: 5%
Rock Fragments: 20%
Cement: Kaolinite
Matrix: No
Angularity: sub angular
Sphericity: moderate
Compositional Maturity: sub mature
Textural Maturity: sub mature
Comments: point contacts, occasional interpenetrating grains

155 microns

Figure A.5 Thin section of Springwell with magnification = 30

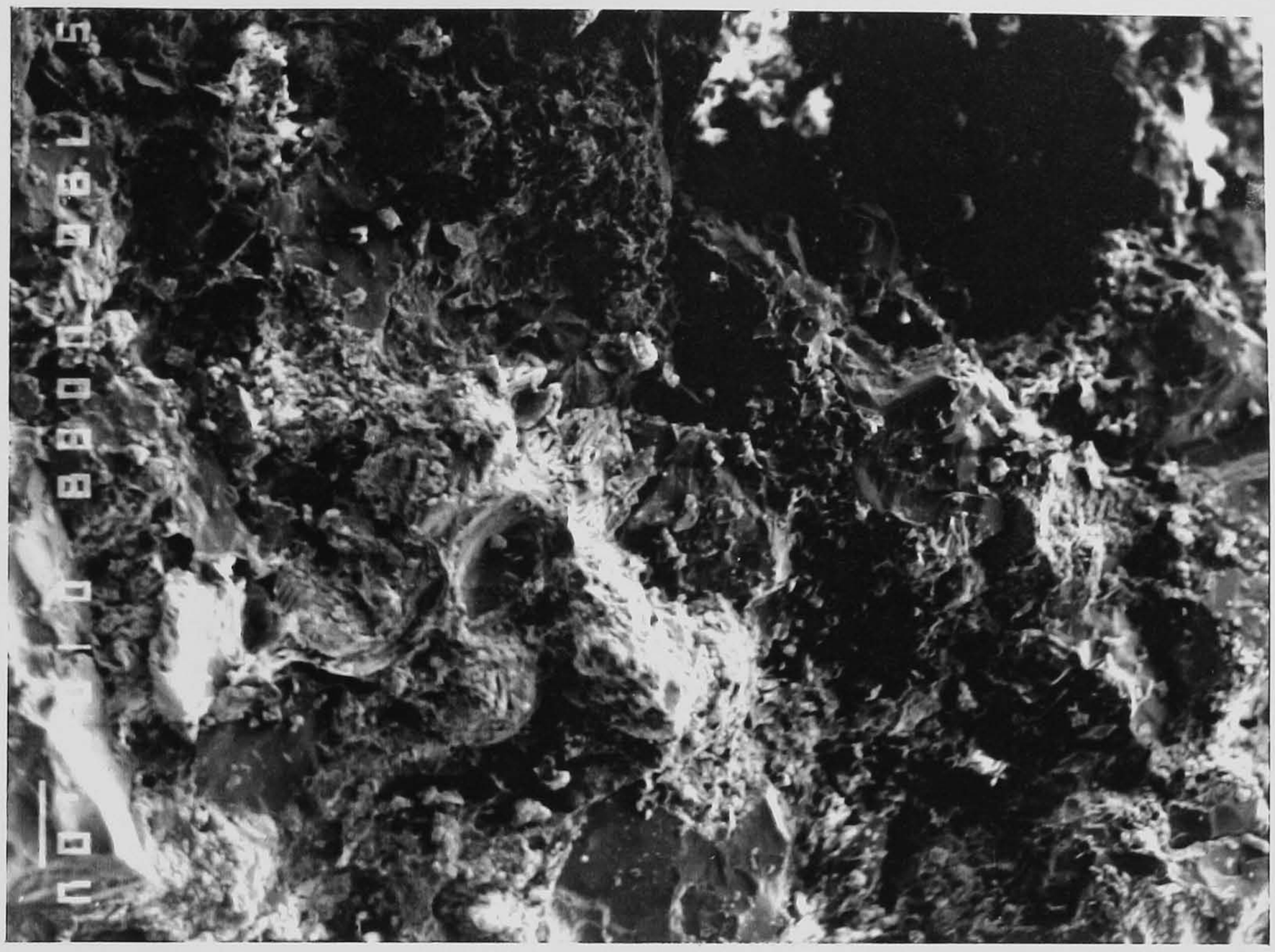

Figure A.6 SEM of Springwell with magnification = 780

Stainton

Stainton is from the Stainton quarry in County Durham and it belongs to Carboniferous limestone series with fine to medium grains and drab pink in colour.

Kair: 116 mD
Porosity: 17.0%
Quartz: 95%
Feldspar: 2%
Rock Fragments: 3%
Cement: Kaolinite (+ some optically unresolvable clays?)
Matrix: No
Angularity: sub-angular
Sphericity: moderate
Compositional Maturity: mature-super mature
Textural Maturity: mature
Comments: grains have long and sutured contacts, with some interpenetrating contacts

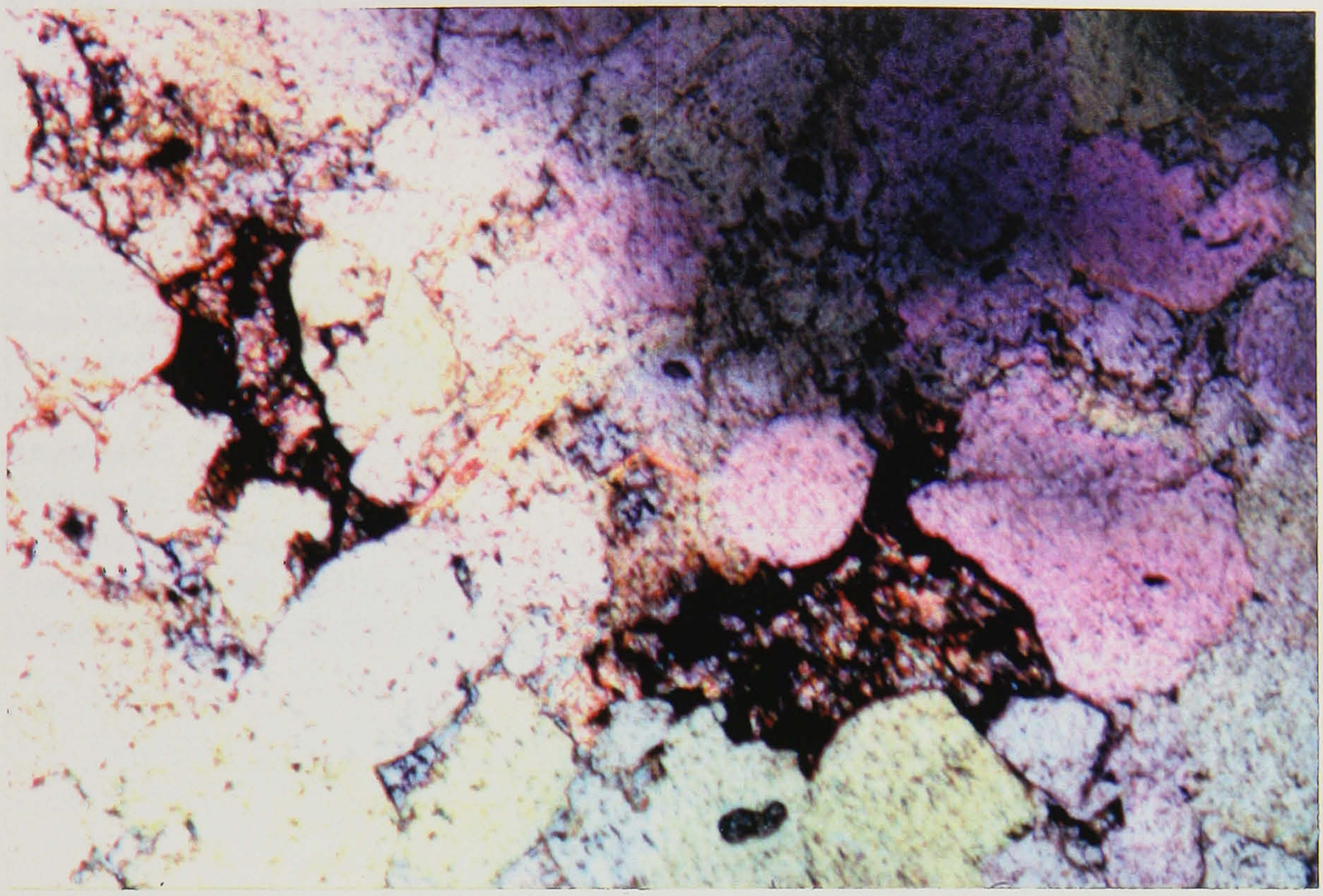

155 microns

Figure A.7 Thin section of Stainton with magnification = 30

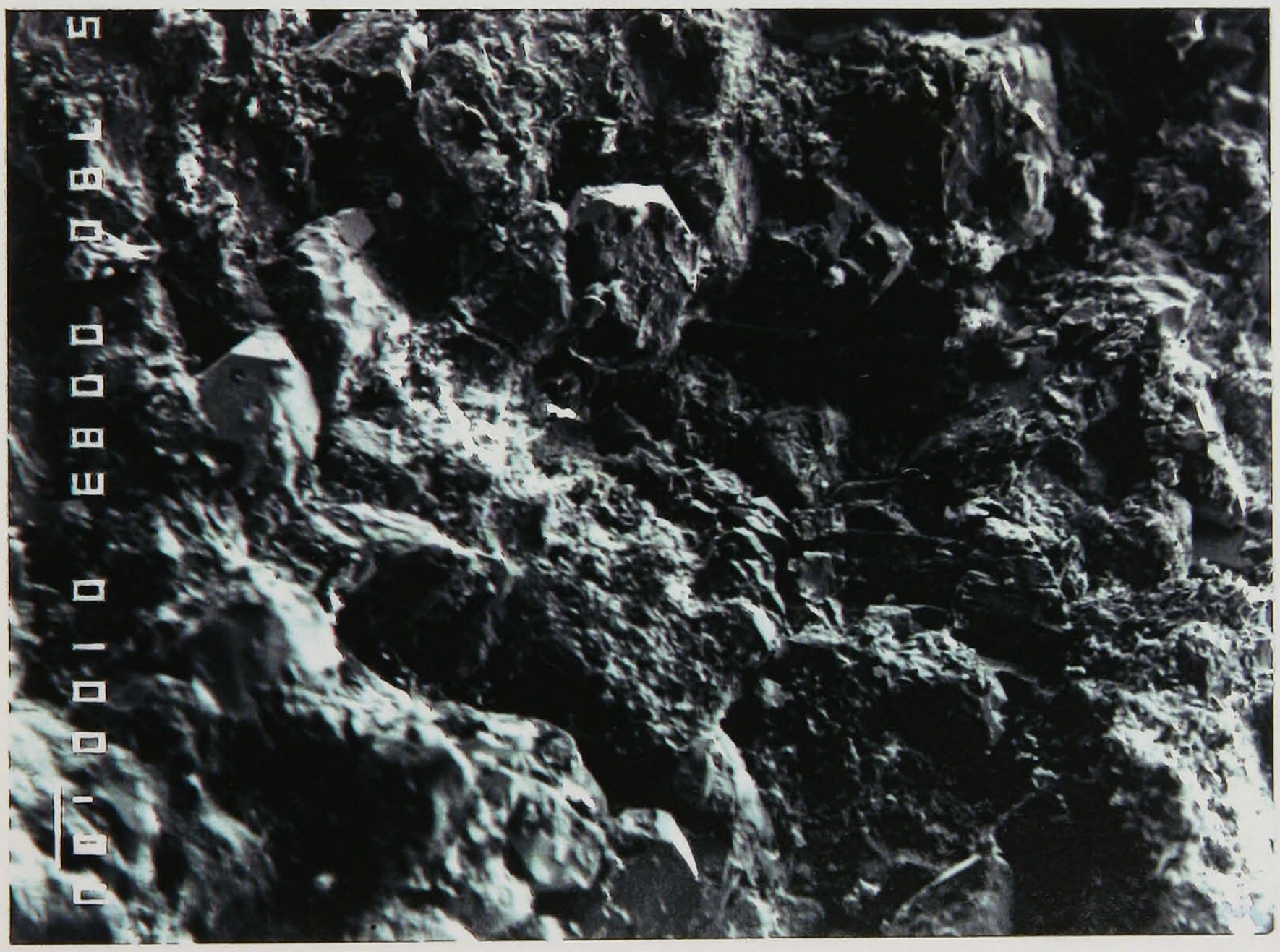

250 microns

Figure A.8 SEM of Stainton with magnification = 780

St. Bees

St. Bees is from the Birkham quarry in Cumbria and it is from the Triassic age, with fine grains and dark red in colour.

Kair: 220 mD
Porosity: 25.54%
Quartz: 90%
Feldspar: 5%
Rock Fragments: 5%
Cement: Calcite, poikilotopic
Matrix: No
Angularity: angular
Sphericity: low
Compositional Maturity: mature
Textural Maturity: sub-mature
Comments: grains floating in cement; occasional point contacts

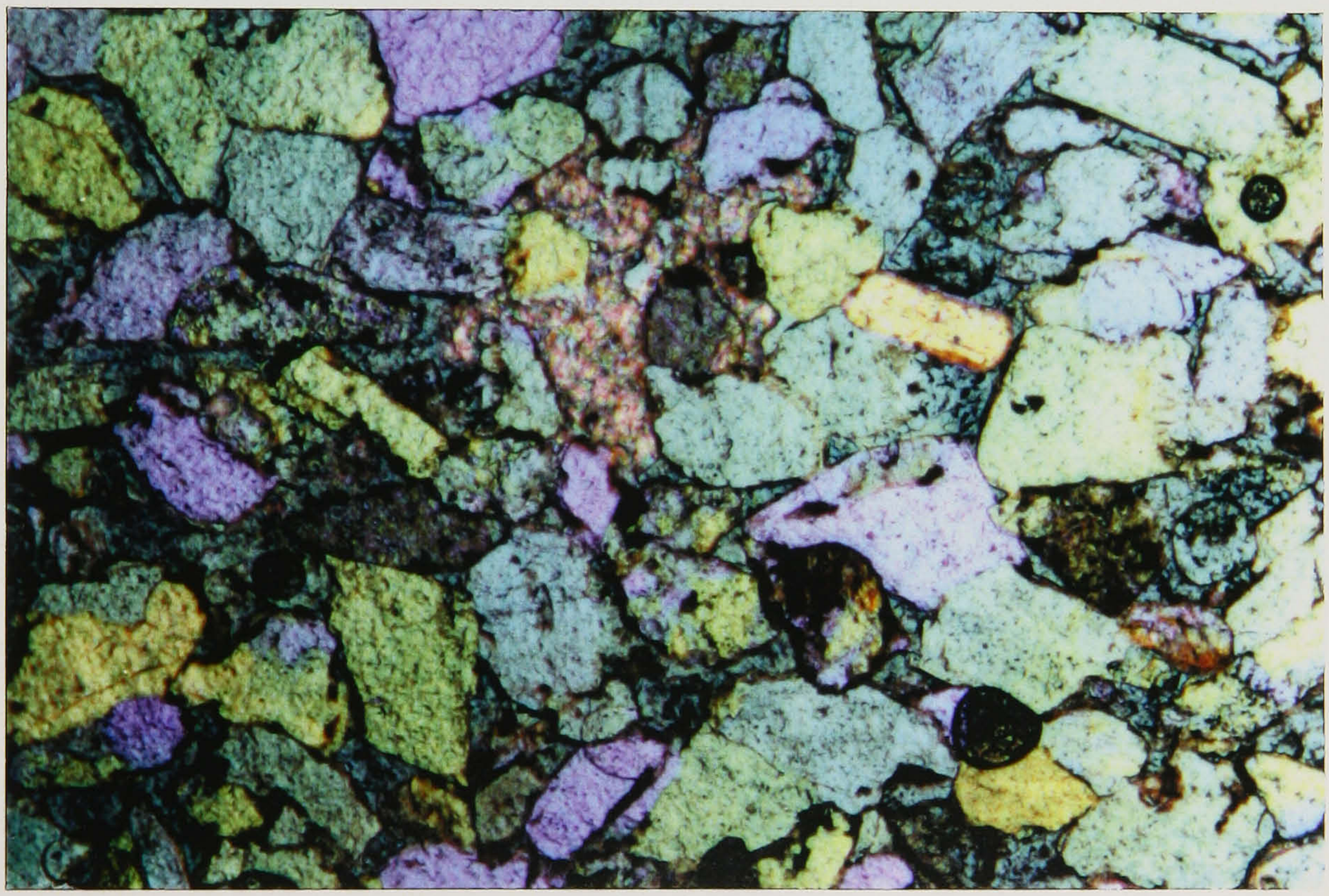

155 microns

Figure A.9 Thin section of St. Bees with magnification = 30

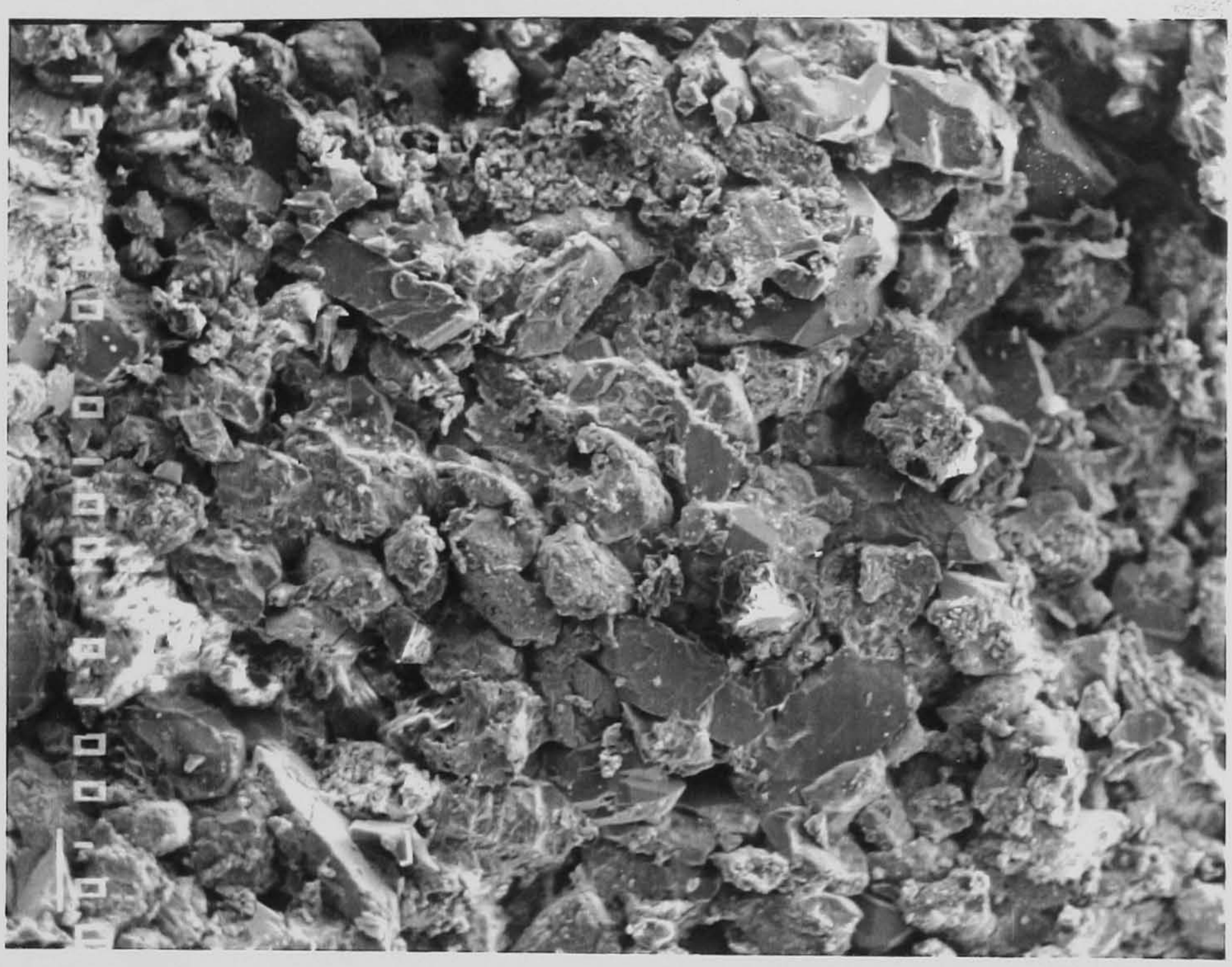

250 microns

Figure A.10 SEM of St. Bees with magnification = 780

Clashach

Clashach is from the Clashach quarry on the Moray coast, North East Scotland, and it is from the Triassic age, with fine well sorted grains and very light brown in colour

Kair: 91 mD
Porosity: 9.91%
Quartz: 95%
Feldspar: 2%
Rock Fragments: 3%
Cement: syntaxial quartz overgrowth cements
Matrix: No
Angularity: sub angular
Sphericity: moderate
Compositional Maturity: mature-super mature
Textural Maturity: mature
Comments: well developed syntaxial overgrowths; 10-15% of quartz is polycrystalline; long and occasional sutured contacts

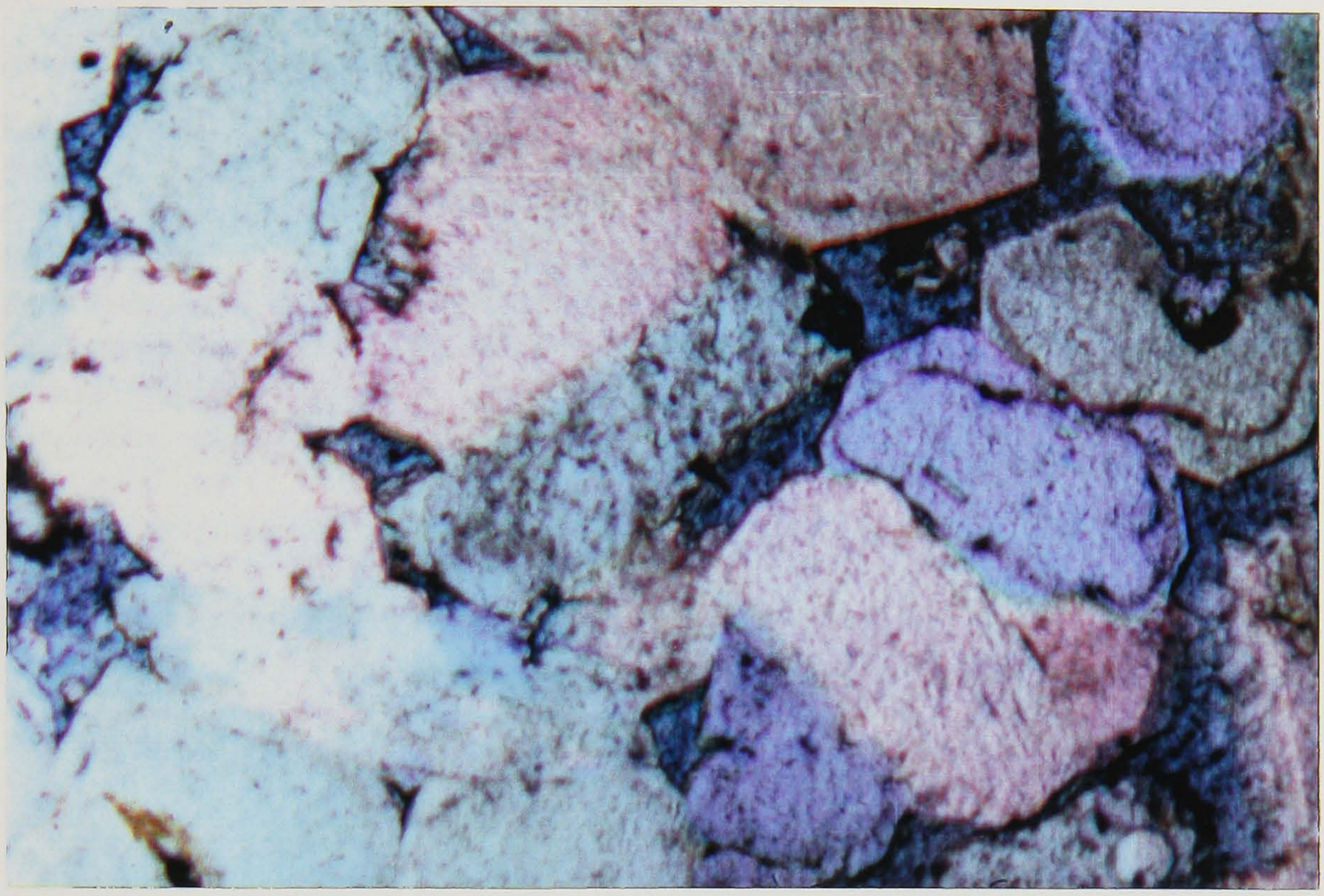

155 microns

Figure A.11 Thin section of Clashach with magnification = 30

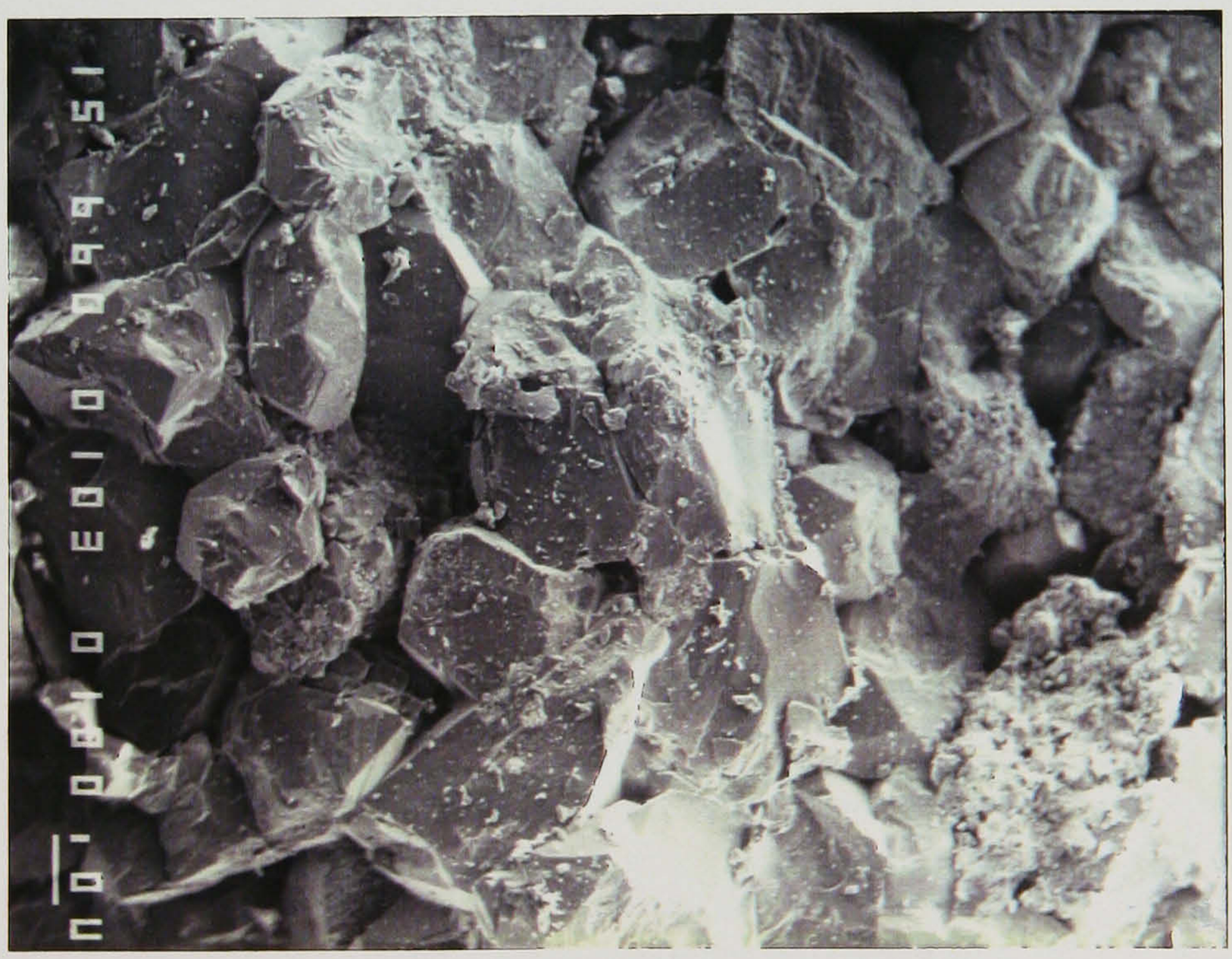

250 microns

Figure A.12 SEM of Clashach with magnification = 780

Reservoir sample (MM220)

MM220 is from an oil field in the South of Oman, from Lower Carboniferous sandstones with fine to medium grains and light brown in colour.

Kair: 830 mD
Porosity: 19.66%
Quartz: 90%
Feldspar: 5%
Rock Fragments: 5%
Cement: Calcite, poikilotopic
Matrix: No
Angularity: angular
Sphericity: low
Compositional Maturity: mature
Textural Maturity: sub mature
Comments: grains floating in cement; occasional point contacts

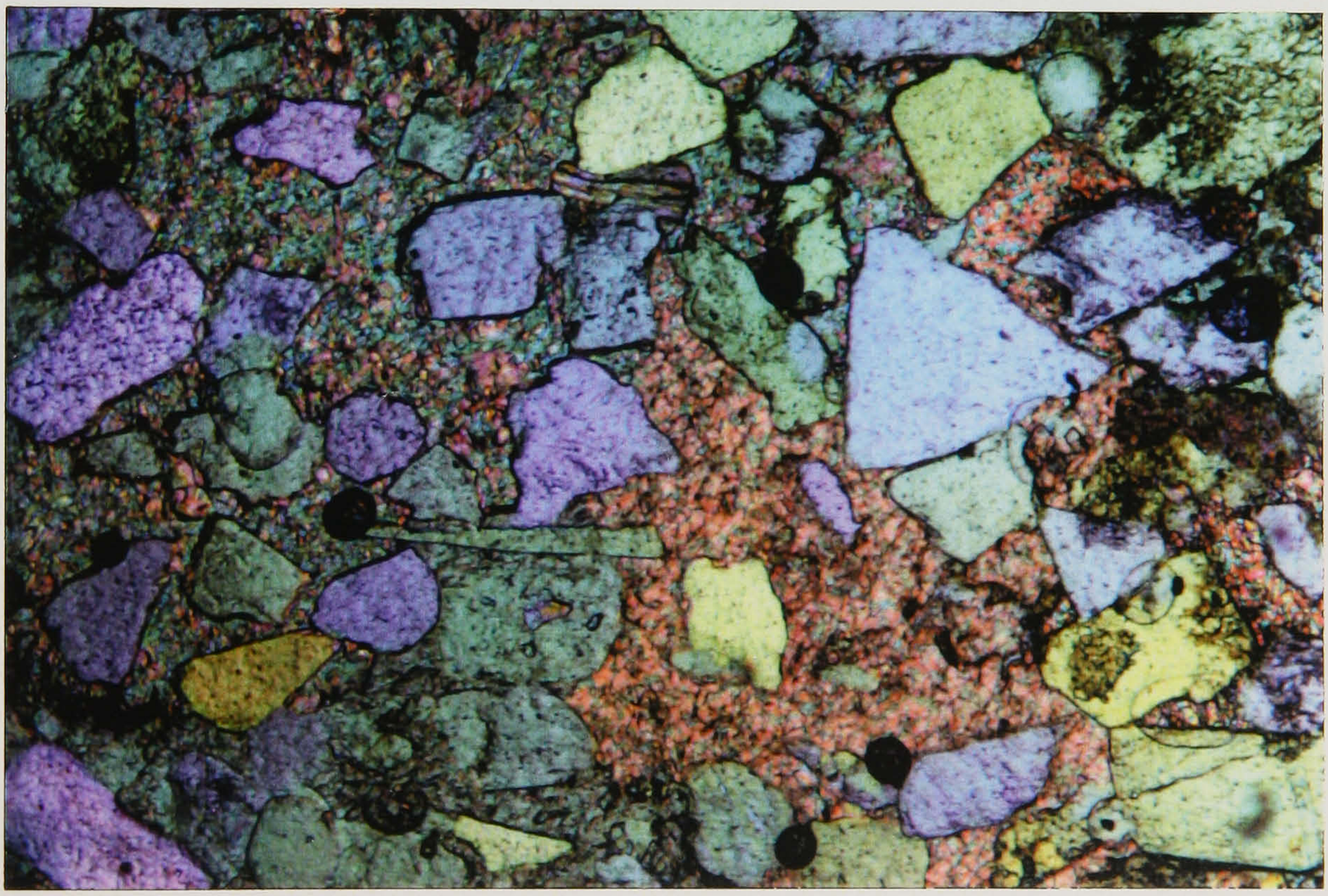

155 microns

Figure A.13 Thin section of reservoir sample (MM220) with magnification = 30

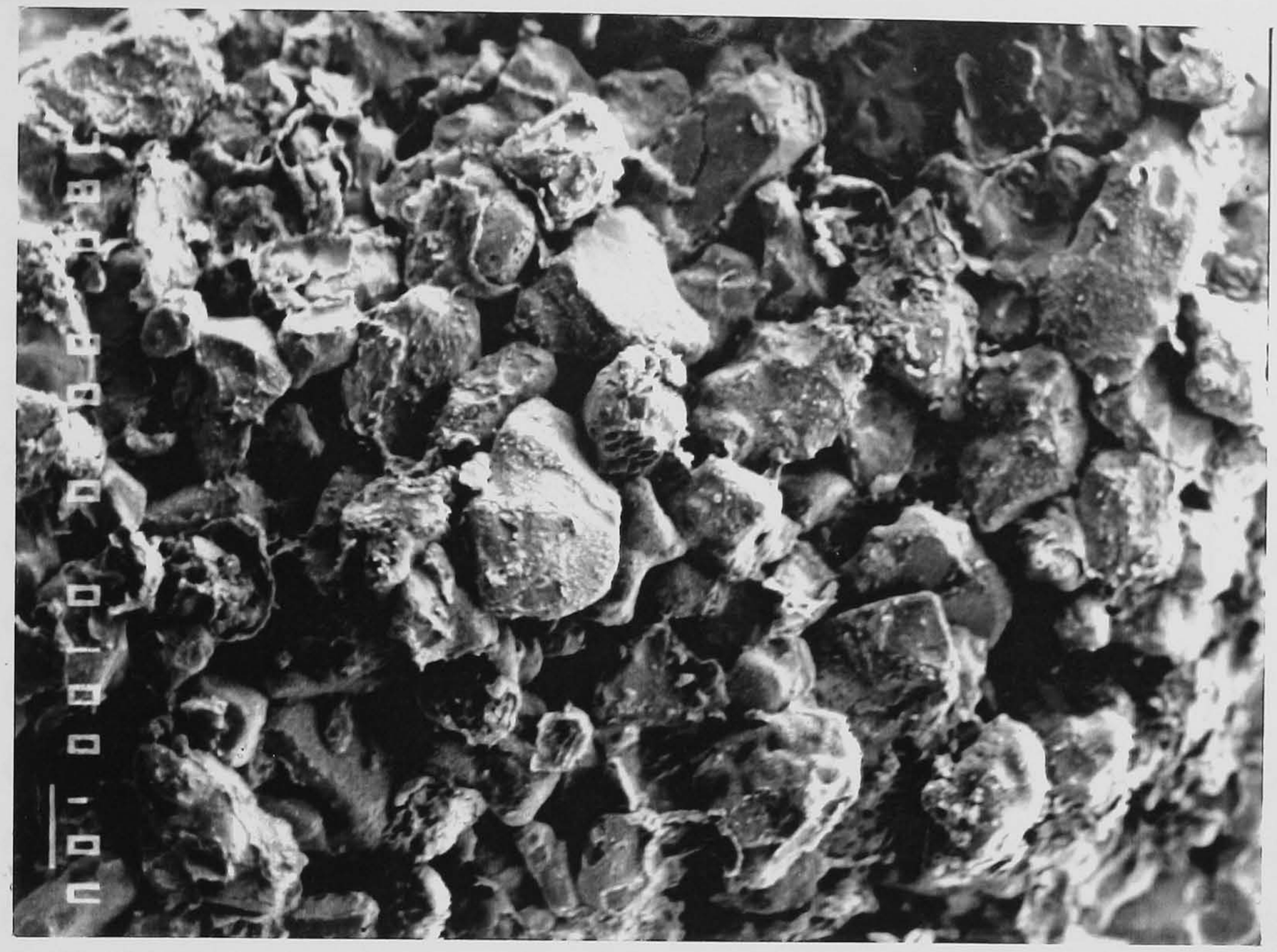

250 microns

Figure A.14 SEM of reservoir sample (MM220) with magnification = 780

Table A.1 Basic rock characterisation

Samples	**Shape**	**Size (cm)**	**Kair (mD)**	ϕ **(%)**	ρ_{grain} **(g/cc)**
Doddington					
D1	cylindrical	3.80x7.02	2700	23.52	2.647
D2 (hysteresis and stress)	cube	4.05	2570		
D3 (hysteresis and stress)	cube	4.05	2557		
Croslands Hill					
CH1 (capillary pressure, RI)	cylindrical	3.79x7.02	14.2	19.22	2.645
CH2 (hysteresis and stress)	cube	4.05	14.2		
CH3 (hysteresis and stress)	cube	4.05	14.2		
CH4 (pore pressure)	cube	4.05	47.9	19.43	2.663
CH5 (pore pressure)	cube	4.05	47.3	19.55	2.642
CH6 (pore pressure)	cube	4.05	47.8	19.27	2.644
Springwell					
SP1	cylindrical	3.79x7.02	19.7	16.92	2.655
SP2 (hysteresis and stress)	cube	4.05	20.4		
SP3 (hysteresis and stress)	cube	4.05	19.2		
SP4 (pore pressure)	cube	4.05	20.3	18.80	2.724
SP5 (pore pressure)	cube	4.05	19.4	18.74	2.718
SP6 (pore pressure)	cube	4.05	19.8	17.27	2.685
SP7 (anisotropy)	cube	4.05	21.0	16.97	2.674
SP8 (anisotropy)	cube	4.05	20.2	17.12	2.669

Samples	Shape	Size (cm)	Kair (mD)	ϕ (%)	ρ_{grain} (g/cc)
Stainton					
ST1	cylindrical	3.8x7.01	116	17.00	
ST2 (hysteresis and stress)	cube	4.05	115		
ST3 (hysteresis and stress)	cube	4.05	150		
ST4 (pore pressure)	cube	4.05	117	17.27	2.613
ST5 (pore pressure)	cube	4.05	119	16.78	2.616
ST6 (pore pressure)	cube	4.05	120	17.25	2.618
St. Bees					
SB1 (anisotropy)	cylindrical	3.80x7.6	220	23.54	2.623
SB2 (anisotropy)	cylindrical	3.80x7.6	175	23.99	2.619
SB3 (anisotropy)	cube	4.05	214	24.39	2.747
SB4 (anisotropy)	cube	4.05	219	25.17	2.773
Clashach					
CL1 (capillary pressure, RI)	cylindrical	3.80x7.0	91	9.91	2.640
CL2 (capillary pressure, RI)	cube	4.05	90	9.93	2.654
Reservoir sample from Oman (MM220-)					
1	cylindrical	3.80x6.0	830	19.66	2.641
2 (hysteresis and stress)	cube	4.05	450		
3 (hysteresis and stress)	cube	4.05	652		
4 (pore pressure)	cube	4.05	361	18.06	2.700
5 (pore pressure)	cube	4.05	370	18.62	2.715
6 (anisotropy)	cube	4.05	1005	19.63	2.611
7 (anisotropy)	cube	4.05	1102	19.48	2.606
8 (anisotropy)	cylindrical	3.71x6.36	80.0	19.16	2.645
9 (anisotropy)	cylindrical	3.74x4.98	52.0	19.13	2.642

Samples	Shape	Size (cm)	Kair (mD)	ϕ (%)	ρ_{grain} (g/cc)
Reservoir sample from North Sea					
1L	cylindrical	3.8x7	880	18.55	2.653
1M	cylindrical	3.8x7	807	18.76	2.672

APPENDIX B

Table B.1 Effect of Pore Pressure on liquid Permeability (Springwell)

Pore Pressure (MPa)	K (mD) Hydrostatic (34.5 MPa)	K (mD) Triaxial (σ_1:σ_2:σ_3=34.5:27.6:27.6)	K (mD) True Triaxial (σ_1:σ_2:σ_3=34.5:27.6:20.7)
0.69	6.09	7.39	8.68
1.72	6.14	7.56	9.91
3.45	6.37	8.07	10.8
5.17	6.47	8.53	13.0
6.90	6.79	9.12	17.8
8.62	9.24	12.8	20.0
10.35	13.0	16.6	22.8
13.79	18.5	20.4	25.0

Table B.2 Effect of Pore Pressure on liquid Permeability (Croslands Hill)

Pore Pressure (MPa)	K (mD) Hydrostatic (34.5 MPa)	K (mD) Triaxial (σ_1:σ_2:σ_3=34.5:27.6:27.6)	K (mD) True Triaxial (σ_1:σ_2:σ_3=34.5:27.6:20.7)
0.69	17.8	21.0	23.5
1.72	19.2	22.2	24.7
3.45	21.4	24.7	27.2
5.17	25.0	30.0	33.3
6.90	29.6	34.1	37.0
8.62	35.5	38.4	41.6
10.35	40.8	43.4	45.4
13.79	44.4	45.4	47.5

Table B.3 Effect of Pore Pressure on liquid Permeability (Stainton)

Pore Pressure (MPa)	K (mD) Hydrostatic (34.5 MPa)	K (mD) Triaxial (σ_1:σ_2:σ_3=34.5:27.6:27.6)	K (mD) True Triaxial (σ_1:σ_2:σ_3=34.5:27.6:20.7)
0.69	27.7	31.2	35.0
1.72	28.2	31.7	36.3
3.45	28.5	33.3	38.4
5.17	31.7	35.7	40.7
6.90	33.3	38.4	43.9
8.62	36.3	41.6	47.0
10.35	39.9	45.4	49.9
12.07	44.4	49.9	53.2
13.79	47.5	51.2	55.5

Table B.4 Effect of Pore Pressure on liquid Permeability (reservoir sample MM220)

Pore Pressure (MPa)	K (mD) Hydrostatic (34.5 MPa)	K (mD) Triaxial (σ_1:σ_2:σ_3=34.5:27.6:27.6)	K (mD) True Triaxial (σ_1:σ_2:σ_3=34.5:27.6:20.7)
0.69	37.0		54.3
1.72	38.4		55.5
3.45	39.9		58.7
5.17	40.7		62.4
6.90	43.9		66.5
8.62	49.3		73.9
10.35	57.0		78.3

Table B.5 Permeability under different stress states (Doddington)

Doddington	Hydrostatic		True Triaxial (σ_1:σ_2:σ_3=1.0:0.8:0.6)	
Mean stress (MPa)	K (Loading) (mD)	K (Unloading) (mD)	K (Loading) (mD)	K (Unloading) (mD)
6.90	2390	1950	1840	1770
13.80	2140	1900	1780	1730
27.80	2080	1780	1760	1700
41.40	2060	1810	1730	1700
55.20	2050	1850	1680	1670
69.00	1840	1840	1640	1640

Table B.6 Permeability under different stress states (Croslands Hill)

Croslands Hill	Hydrostatic		True Triaxial (σ_1:σ_2:σ_3=1.0:0.8:0.6)	
Mean stress (MPa)	K (Loading) (mD)	K (Unloading) (mD)	K (Loading) (mD)	K (Unloading) (mD)
6.90	13.6	12.1	13.4	12.2
13.80	13.2	11.3	13.2	12.1
27.80	12.7	10.7	12.8	11.8
41.40	12.5	10.3	12.6	11.6
55.20	12.0	10.3	12.1	11.7
69.00	11.9	11.9	11.7	11.7

Table B.7 Permeability under different stress states (Springwell)

Springwell	Hydrostatic		True Triaxial (σ_1:σ_2:σ_3=1.0:0.8:0.6)	
Mean stress (MPa)	K (Loading) (mD)	K (Unloading) (mD)	K (Loading) (mD)	K (Unloading) (mD)
13.80	19.7	15.6	17.1	16.4
27.80	16.1	12.5	15.9	15.3
41.40	13.9	11.8	15.3	14.7
55.20	12.9	11.5	14.6	14.3
69.00	11.2	11.2	14.5	14.5

Table B.8 Permeability under different stress states (Stainton)

Stainton	Hydrostatic		True Triaxial (σ_1:σ_2:σ_3=1.0:0.8:0.6)	
Mean stress (MPa)	K (Loading) (mD)	K (Unloading) (mD)	K (Loading) (mD)	K (Unloading) (mD)
13.80	114	104	145	140
27.80	110	103	140	136
41.40	105	101	135	131
55.20	101	98.7	128	125
69.00	98.0	97.8	125	125

Table B.9 Permeability under different stress states (reservoir sample MM220)

MM220	Hydrostatic		True Triaxial (σ_1:σ_2:σ_3=1.0:0.8:0.6)	
Mean stress (MPa)	K (Loading) (mD)	K (Unloading) (mD)	K (Loading) (mD)	K (Unloading) (mD)
6.90	438	409	600	582
13.80	417	400	584	562
20.70	400	384	560	532
27.60	385	370	548	523
34.50	365	365	520	520

Table B.10 Pore volume deformation under different stress states (reservoir sample MM220)

MM220	Hydrostatic		True Triaxial (σ_1:σ_2:σ_3=1.0:0.8:0.6)	
Mean Stress (MPa)	Cum. Volume (cc)	Normalised Cum. Volume	Cum. Volume (cc)	Normalised Cum. Volume
1.72	0.00	0.00	0.00	0.00
2.76	0.40	0.031	0.10	0.007
3.45	0.50	0.038	0.20	0.015
4.14	0.60	0.046	0.25	0.019
4.83	0.70	0.054	0.30	0.023
5.52	0.80	0.061	0.35	0.027
6.21	0.85	0.065	0.38	0.029
6.90	0.90	0.069	0.40	0.031
10.34	1.10	0.084	0.50	0.038
13.79	1.20	0.092	0.60	0.046
17.24	1.25	0.096	0.70	0.054
20.69	1.30	0.099	0.75	0.057
24.14	1.30	0.099	0.80	0.062
27.59	1.30	0.099	0.90	0.069
34.48	1.30	0.099	1.00	0.077

Table B.11 Pore volume deformation under different stress states (St. Bees)

St. Bees	Hydrostatic		True Triaxial (σ_1:σ_2:σ_3=1.0:0.8:0.6)	
Mean Stress (MPa)	Cum. Volume (cc)	Normalised Cum. Volume	Cum. Volume (cc)	Normalised Cum. Volume
1.72	0.00	0.00	0.00	0.00
2.76	0.40	0.024	0.25	0.149
3.45	0.50	0.030	0.35	0.021
4.14	0.60	0.36	0.45	0.027
4.83	0.70	0.042	0.55	0.033

5.52	0.80	0.048	0.65	0.039
6.21	0.90	0.054	0.75	0.045
6.90	1.00	0.060	0.85	0.051
10.34	1.15	0.069	1.00	0.059
13.79	1.20	0.071	1.05	0.062
17.24	1.25	0.074	1.10	0.066
20.69	1.30	0.077	1.10	0.066
24.14	1.35	0.080	1.10	0.66
27.59	1.38	0.082	1.10	0.66
34.48	1.40	0.083	1.10	0.66

Table B.12 Pore volume deformation under different stress states (Springwell)

Springwell	Hydrostatic		True Triaxial (σ_1:σ_2:σ_3=1.0:0.8:0.6)	
Mean Stress (MPa)	Cum. Volume (cc)	Normalised Cum. Volume	Cum. Volume (cc)	Normalised Cum. Volume
1.72	0.00	0.00	0.20	
2.76	0.00	0.00	0.40	
3.45	0.10	0.008	0.50	0.042
4.14	0.20	0.017	0.60	0.050
4.83	0.30	0.025	0.70	0.059
5.52	0.40	0.033	0.80	0.067
6.21	0.50	0.042	0.90	0.075
6.90	0.60	0.050	1.00	0.084
10.34	0.80	0.067	1.20	0.100
13.79	0.90	0.075	1.30	0.109
17.24	1.00	0.084	1.35	0.113
20.69	1.05	0.088	1.38	0.115
24.14	1.10	0.092	1.40	0.117
27.59	1.10	0.092	1.40	0.117
34.48	1.10	0.092	1.40	0.117

Table B.13 Electrical properties under different stress states (reservoir sample MM220)

	Hydrostatic			True Triaxial (σ_1:σ_2:σ_3=1.0:0.8:0.6)		
Mean stress (MPa)	Resistivity (Ohm-m)	Formation factor	Cementation factor	Resistivity (Ohm-m)	Formation factor	Cementation factor
1.72	2.40	16.50	1.72	2.31	15.96	1.70
2.76	2.57	17.69	1.76	2.44	16.83	1.73
3.45	2.64	18.20	1.78	2.51	17.34	1.75
4.14	2.66	18.32	1.79	2.57	17.71	1.76
4.83	2.71	18.67	1.81	2.61	18.03	1.77
5.52	2.74	18.87	1.82	2.66	18.38	1.78
6.21	2.79	19.27	1.83	2.70	18.61	1.79
6.90	2.84	19.59	1.86	2.76	18.99	1.80
10.34	2.97	20.48	1.87	2.86	19.69	1.83
13.79	3.06	21.05	1.89	2.94	20.29	1.85
17.24	3.12	21.49	1.90	3.02	20.84	1.86
20.69	3.16	21.77	1.91	3.07	21.16	1.87
24.14	3.19	22.03	1.92	3.10	21.37	1.88
27.59	3.23	22.67	1.93	3.13	21.62	1.89
34.48	3.29	22.68		3.18	21.92	1.90

Table B.14 Electrical properties under different stress states (St. Bees)

	Hydrostatic			True Triaxial (σ_1:σ_2:σ_3=1.0:0.8:0.6)		
Mean stress (MPa)	Resistivity (Ohm-m)	Formation factor	Cementation factor	Resistivity (Ohm-m)	Formation factor	Cementation factor
1.72	2.49	17.16	2.06	2.20	15.20	1.97
2.76	2.58	17.83	2.09	2.33	16.08	2.02
3.45	2.63	18.18	2.10	2.42	16.69	2.04
4.14	2.64	18.21	2.11	2.46	16.98	2.05
4.83	2.65	18.27	2.11	2.48	17.15	2.06

5.52	2.66	18.33	2.12	2.51	17.29	2.07
6.21	2.67	18.39	2.12	2.54	17.53	2.08
6.90	2.69	18.57	2.13	2.57	17.71	2.09
10.34	2.73	18.85	2.14	2.66	18.35	2.11
13.79	2.76	19.02	2.14	2.70	18.64	2.12
17.24	2.78	19.16	2.15	2.72	18.79	2.13
20.69	2.79	19.28	2.15	2.73	18.85	2.14
24.14	2.81	19.35	2.16	2.74	18.93	2.14
27.59	2.82	19.44	2.16	2.75	18.95	2.14
34.48	2.83	19.49	2.17	2.76	18.99	2.14

Table B.15 Electrical properties under different stress states (Springwell)

	Hydrostatic			True Triaxial (σ_1:σ_2:σ_3=1.0:0.8:0.6)		
Mean stress (MPa)	Resistivity (Ohm-m)	Formation factor	Cementation factor	Resistivity (Ohm-m)	Formation factor	Cementation factor
1.72	4.07	28.01	1.95	3.97	27.32	1.94
2.76	4.16	28.65	1.96	4.06	27.95	1.95
3.45	4.26	29.34	1.98	4.17	28.71	1.97
4.14	4.37	30.09	1.99	4.24	29.22	1.98
4.83	4.44	30.59	2.00	4.35	29.96	1.99
5.52	4.54	31.24	2.02	4.45	30.63	2.00
6.21	4.59	31.58	2.02	4.55	31.30	2.02
6.90	4.68	32.22	2.03	4.61	31.76	2.03
10.34	4.87	33.56	2.06	4.71	32.46	2.04
13.79	4.95	34.07	2.07	4.82	33.18	2.05
17.24	5.00	34.44	2.07	4.90	33.73	2.06
20.69	5.09	35.09	2.08	4.94	34.01	2.07
24.14	5.12	35.28	2.09	4.99	34.36	2.07
27.59	5.18	35.67	2.09	5.04	34.72	2.08
34.48	5.26	36.23	2.10	5.10	35.11	2.08

Table B.16 Capillary Pressure versus saturation under different stress states (reservoir sample 1L & 1M)

Ambient		Hydrostatic (6.9 MPa)	
Saturation (fraction)	Capillary pressure (psi)	Saturation (fraction)	Capillary pressure (psi)
1.00	0.50	1.00	0.50
0.33	1.31	0.82	0.97
0.28	3.35	0.40	2.87
0.27	8.05	0.33	4.25
0.26	13.87	0.29	13.83
0.26	19.00	0.28	18.32
0.26	25.00	0.28	25.00

Table B.17 Capillary Pressure versus saturation under different stress states (Clashach)

Hydrostatic (34.5 MPa)		True Triaxial (σ_1:σ_2:σ_3=43.1:34.5:25.9 MPa)	
Saturation (fraction)	Capillary pressure (psi)	Saturation (fraction)	Capillary pressure (psi)
1.00	2.00	1.00	2.00
0.47	3.95	0.52	3.00
0.35	7.15	0.44	3.58
0.33	9.69	0.38	5.00
0.31	20.65	0.32	8.50
0.29	30.5	0.29	13.50
		0.28	20.00
		0.26	30.00

Table B.18 Capillary Pressure versus saturation under hydrostatic stress (34.5 MPa) (Clashach and Croslands Hill)

Clashach		Croslands Hill	
Saturation (fraction)	Capillary pressure (psi)	Saturation (fraction)	Capillary pressure (psi)
1.00	2.00	1.00	2.5
0.47	3.95	0.56	3.3
0.35	7.15	0.46	7.7
0.33	9.69	0.41	12.87
0.31	20.65	0.38	20.81
0.29	30.5	0.36	20.0
0.29	30.50	0.35	30.0
0.29	25.0	0.35	35.0
0.29	15.0		
0.31	5.0		
0.44	0.0		
0.52	-5.0		
0.54	-10.0		
0.55	-20.0		
0.57	-30.0		
0.57	-30.0		
0.56	0.0		
0.54	1.8		
0.45	3.0		
0.37	5.0		
0.32	8.5		
0.29	30.0		

Table B.19 Resistivity Index versus saturation under different stress states (Clashach)

Hydrostatic (34.5 MPa)		True Triaxial (σ_1:σ_2:σ_3=43.1:34.5:25.9 MPa)	
Saturation (fraction)	Resistivity Index	Saturation (fraction)	Resistivity Index
1.00	1.00	1.00	1.00
0.47	6.07	0.52	2.56
0.35	9.41	0.44	2.79
0.33	10.80	0.38	3.89
0.31	12.92	0.32	5.35
0.29	15.31	0.29	6.46
		0.28	7.59
		0.26	8.59

Table B.20 Resistivity Index versus saturation under hydrostatic stress (34.5 MPa) (Clashach and Croslands Hill)

Clashach		Croslands Hill	
Saturation (fraction)	Resistivity Index	Saturation (fraction)	Resistivity Index
1.00	1.00	1.00	1.00
0.47	6.07	0.56	2.30
0.35	9.41	0.46	3.70
0.33	10.80	0.41	5.13
0.31	12.92	0.38	7.07
0.29	15.31	0.36	8.20
0.29	15.31	0.35	9.47
0.29	14.35		
0.31	13.84		
0.44	8.19		
0.52	5.93		
0.54	3.93		

0.55	3.83
0.57	3.78
0.57	3.58

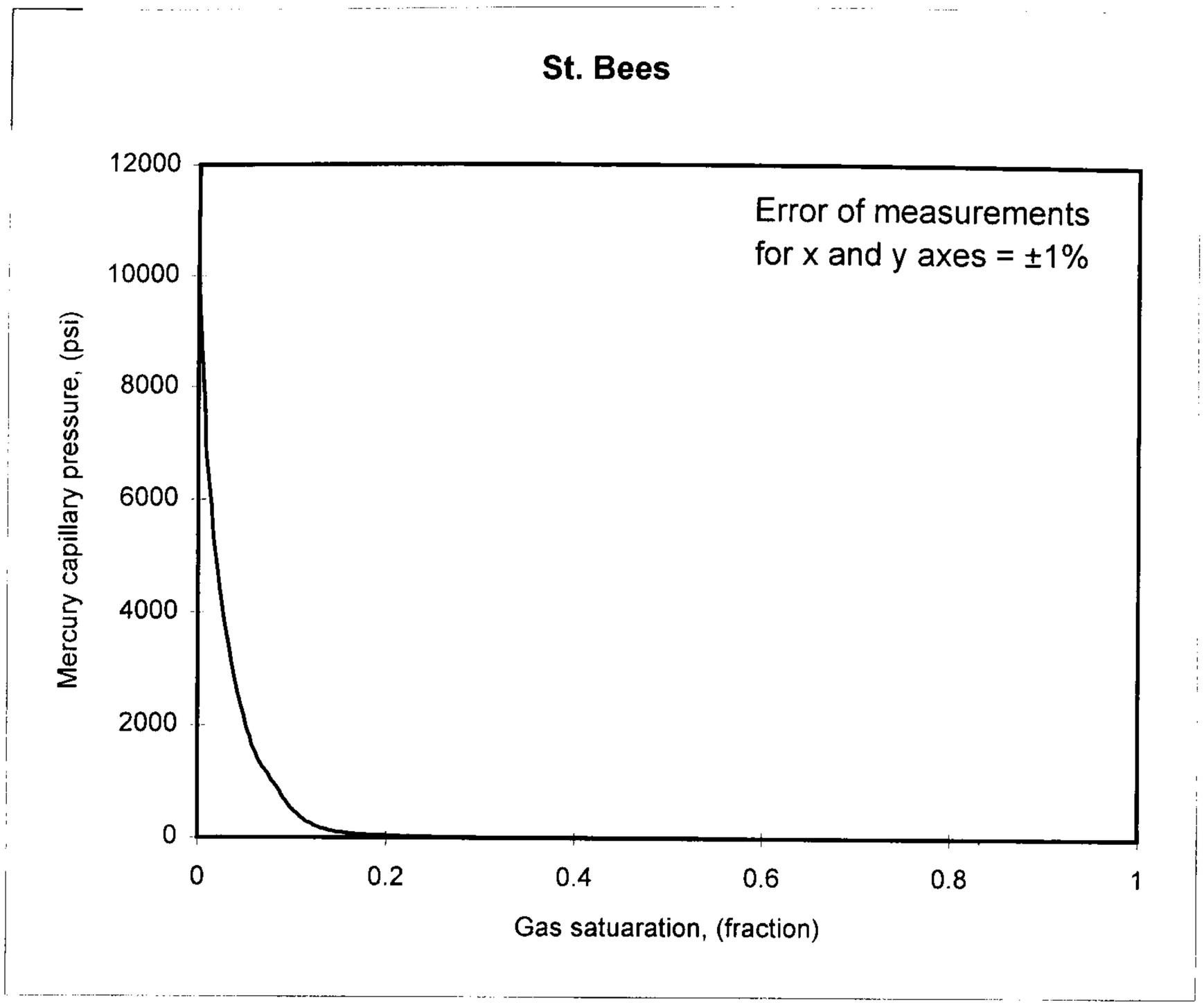

Figure B.1 Mercury capillary pressure curve (St. Bees)

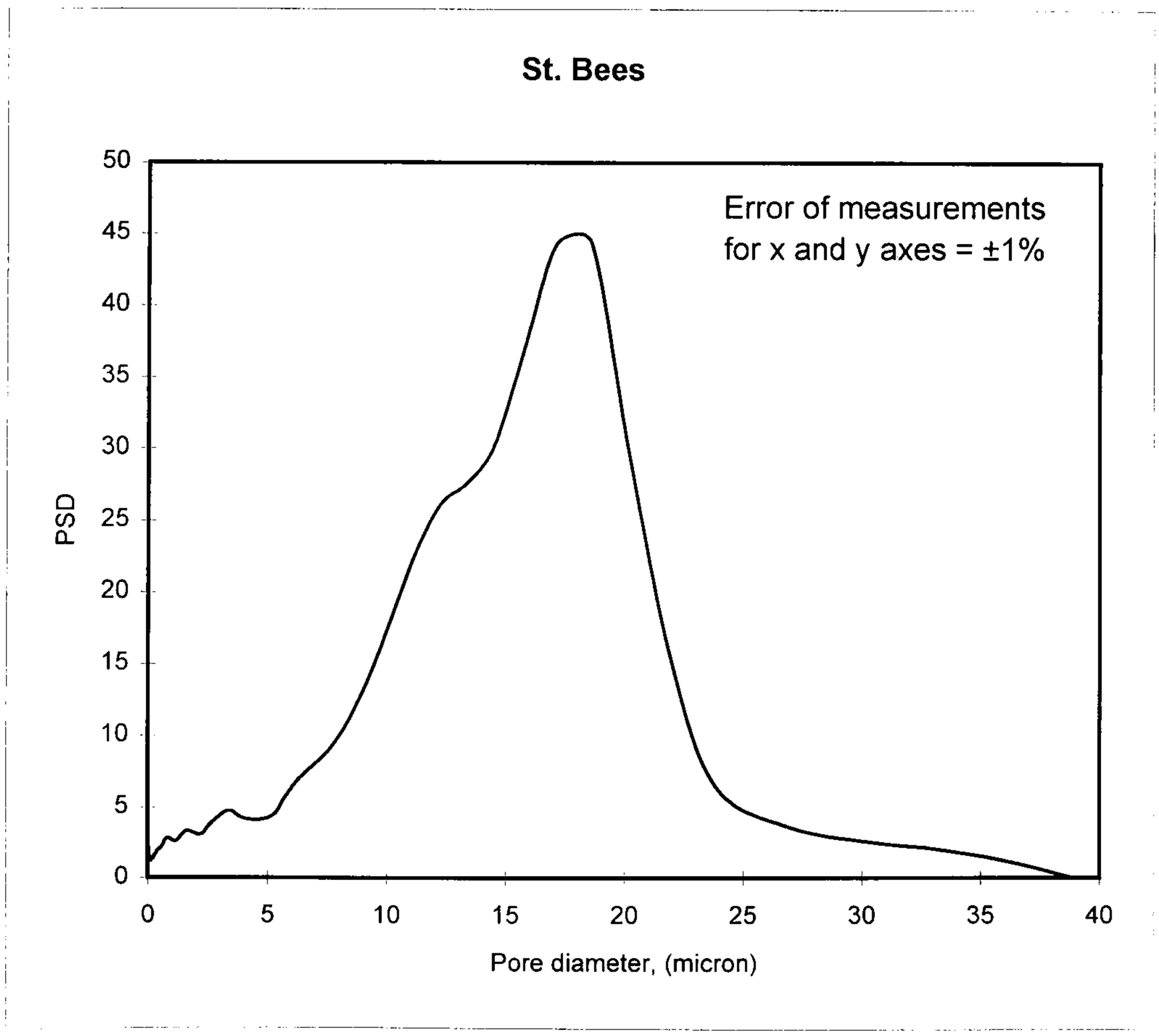

Figure B.2 Pore size distribution (St. Bees)

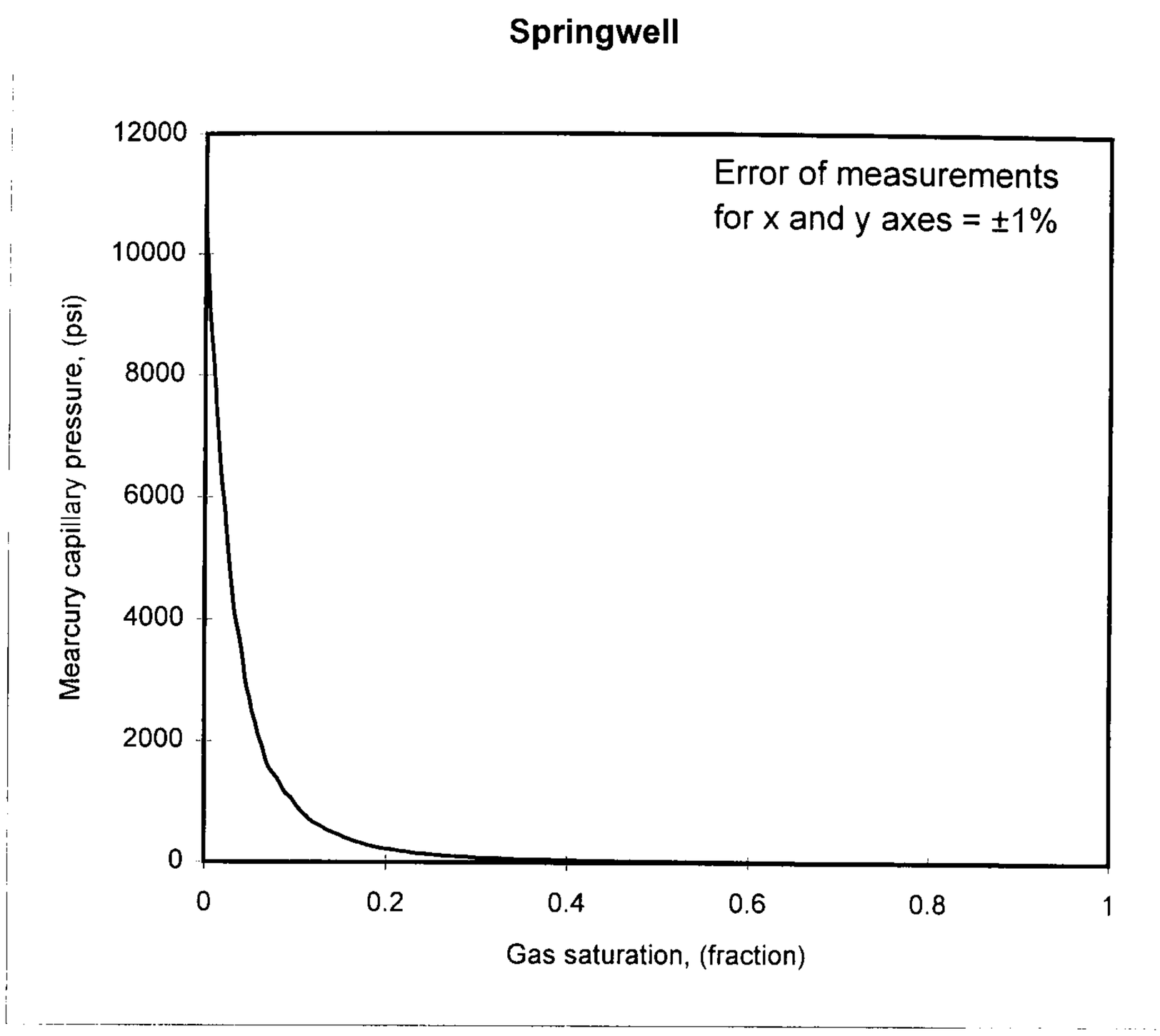

Figure B.3 Mercury capillary pressure curve (Springwell)

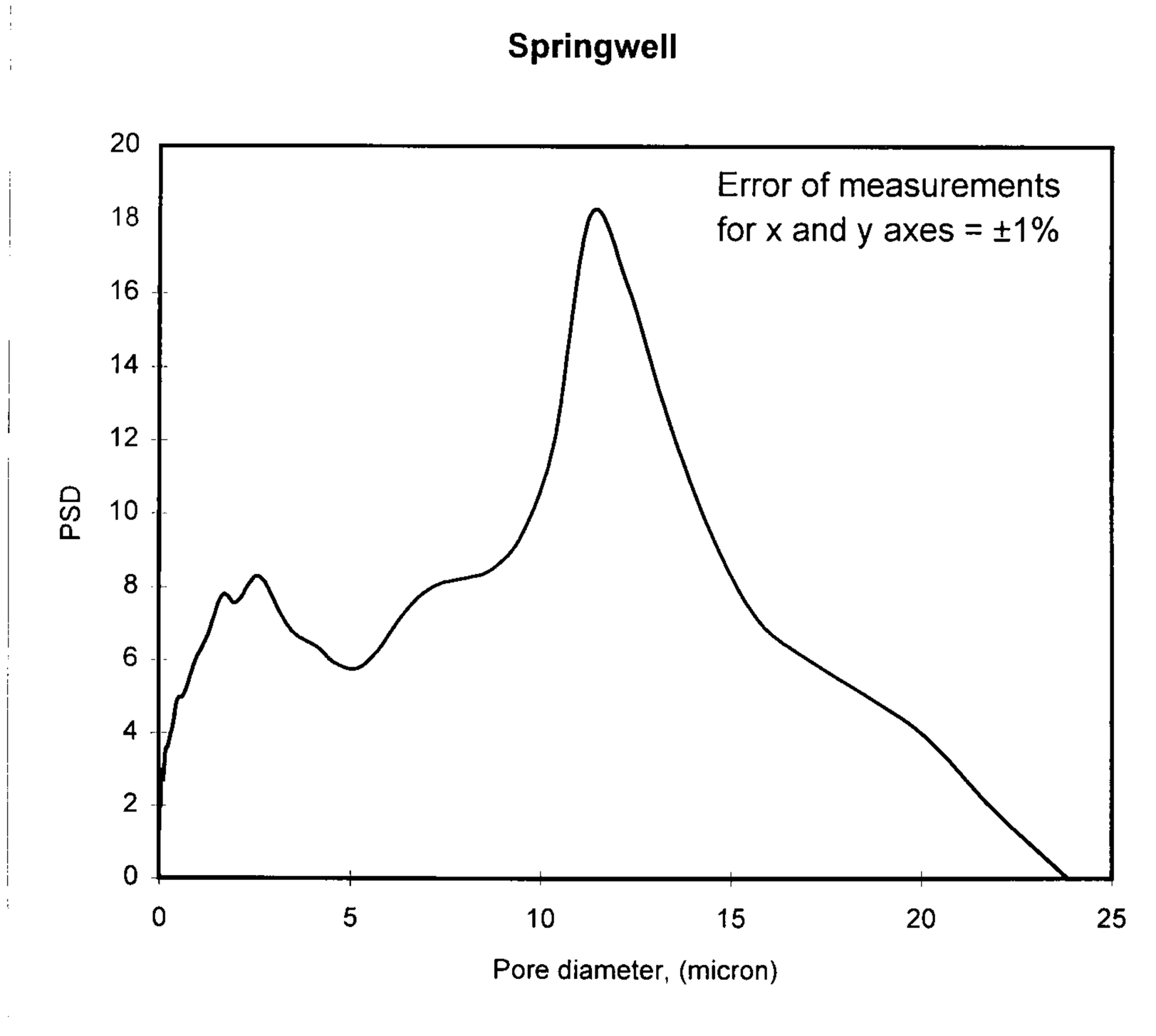

Figure B.4 Pore size distribution (Springwell)

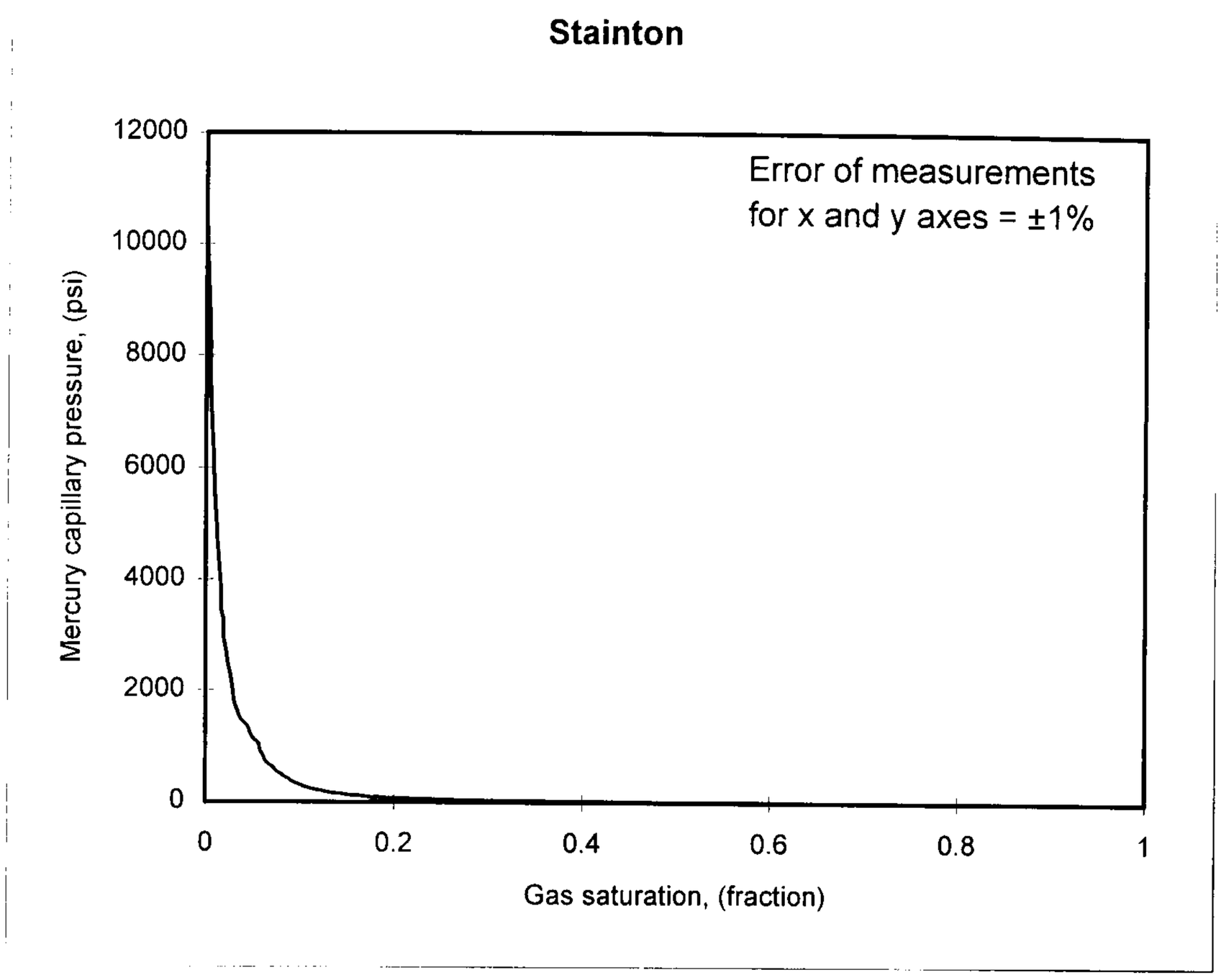

Figure B.5 Mercury capillary pressure curve (Stainton)

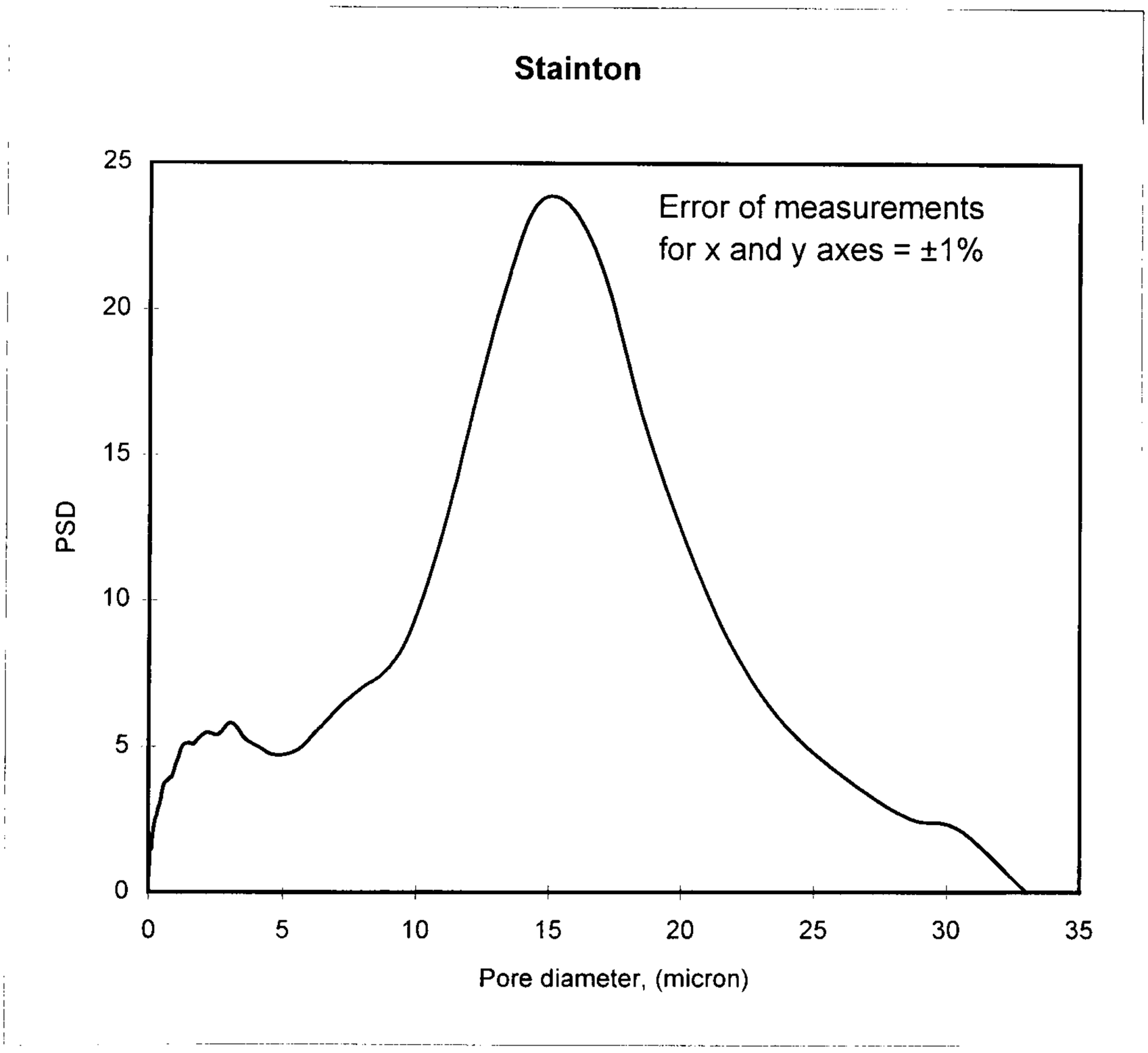

Figure B.6 Pore size distribution (Stainton)

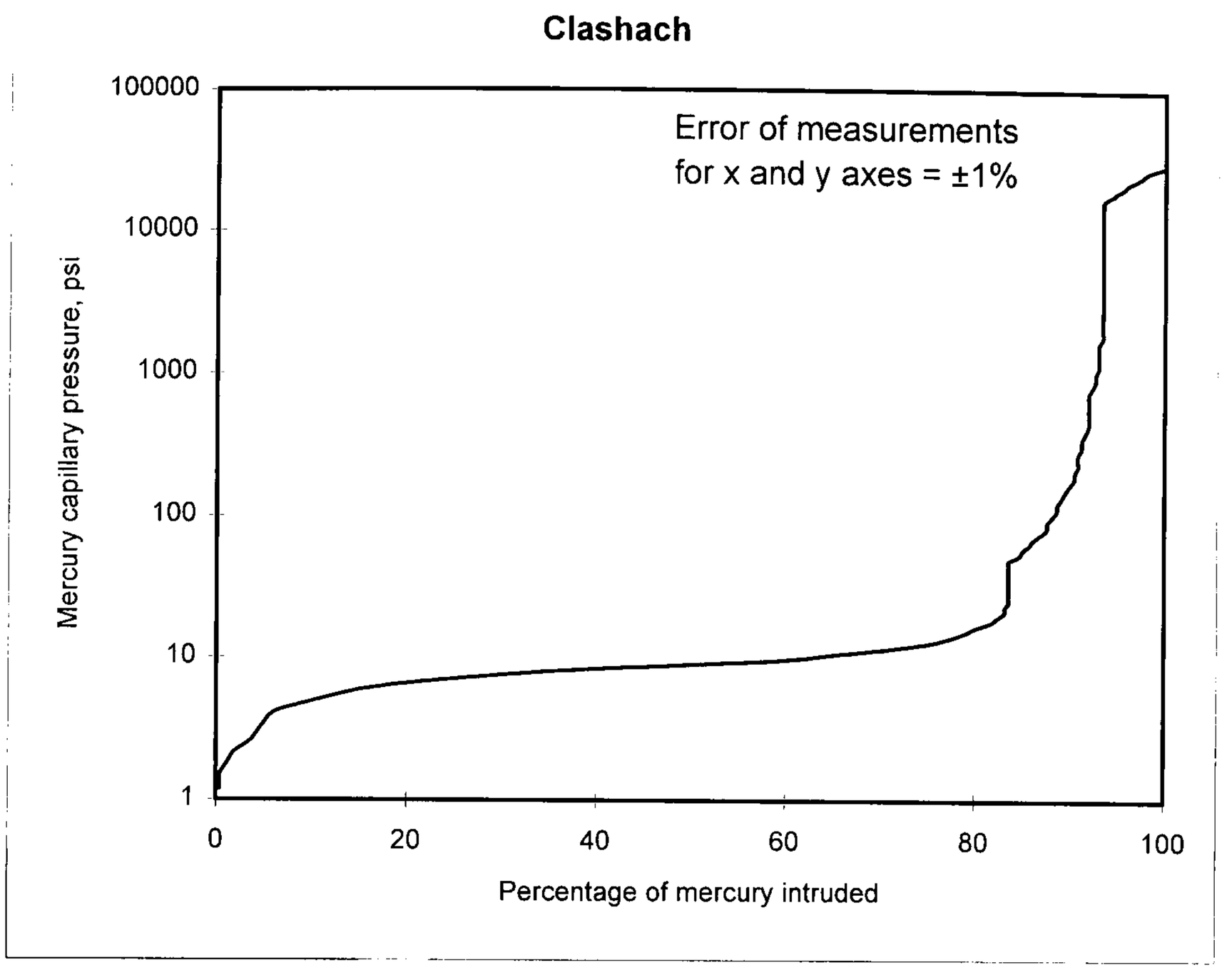

Figure B.7 Mercury capillary pressure curves (Stainton)

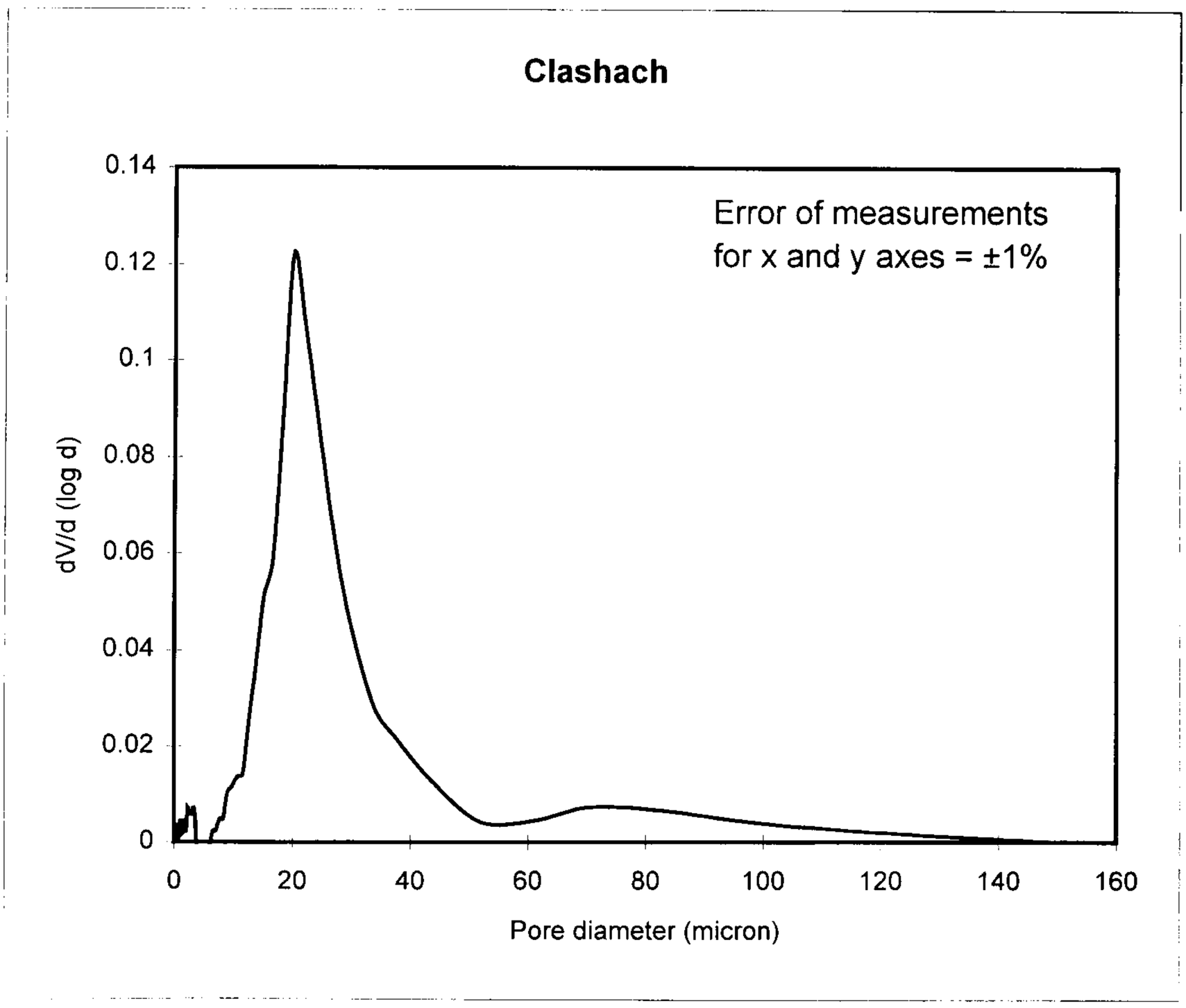

Figure B.8 Pore size distribution (Clashach)

APPENDIX C

Simulation input file first part (without pressure maintenance)

```
-- THIS IS A SIMPLE STUDY OF PORE PRESSURE EFFECT ON
-- PERMEABILITY
-- NATURAL DEPLETION
-- PREPARED BY SAID AL-HARTHY 1/2/99 - BASER.DATA
--
RUNSPEC
TITLE
 PORE PRESSURE STUDY ON PERMEABILITY

DIMENS
   50   50   10 /

OIL

WATER

FIELD

TABDIMS
   1   1  20   20   1   20 /

WELLDIMS
   2   5   1   2 /

START
  1 'JAN' 1998  /

NSTACK
  -1 /

FMTOUT

FMTIN

UNIFOUT

UNIFIN

GRID
```

```
GRIDFILE
 2 /
INIT
--DEBUG
--38*0 1  /

--PSEUDO
EQUALS
'PERMX' 77.0   1  50   1  50  1  10/
'PERMX' 61.6   10 40   10 40  1  10/
'PERMX' 46.2   20 30   20 30  1  10/
'PERMY' 77.0   1  50   1  50  1  10/
'PERMY' 61.6   10 40   10 40  1  10/
'PERMY' 46.2   20 30   20 30  1  10/
/
PERMZ
25000*77.0  /

DXV
  50*50.0 /

DYV
  50*50.0 /

DZ
  25000*50.0 /

TOPS
  2500*4000.0 /


PORO
  25000*0.17 /

RPTGRID
1 1 1 1 1 0 0 0 /

--DEBUG
-- 0 0 1 0 1 0 1  /

PROPS
==================================================================
-- SWAT  KRW  PCOW
SWFN
   .25   .0   35.0
   .30   .02  30.0
   .40   .055 25.0
   .45   .075 20.0
```

```
   .50   .10   15.0
   .55   .13   10.0
   .60   .145   5.0
   .7    1.0   3.0
/

SOF2      1 TABLES   20 NODES IN EACH        FIELD   13:34  5 MAY 85
-- SOIL   KRO
   .30   .000
   .40   .004
   .48   .020
   .50   .036
   .58   .100
   .60   .146
   .68   .330
   .70   .420
   .75   1.000
/

PVTW
 4014.7  1.0  3.03E-06  .5  0.0 /

RSCONST
.8 /
/
PVDO
-- POIL    FVFO     VISCO
  400.0    1.0120    1.160
 1200.0    1.0040    1.164
 2000.0     .9960    1.167
 2800.0     .9880    1.172
 3600.0     .9802    1.177
 4400.0     .9724    1.181
 5200.0     .9646    1.185
 5600.0     .9607    1.190
 8000.0     .9200    2.000 /

ROCK
 4014.7        .30E-05 /

DENSITY
 45.0000  63.0200   .07020 /

RPTPROPS
   2*0 /

REGIONS
==========================================================================
```

```
SATNUM
25000*1 /

SOLUTION
==========================================================================

EQUIL
4250  4850  6000  0   0   0   0   0   0 /

--RPTSOL
-- 'RESTART=2' /

SUMMARY
==========================================================================
RUNSUM

SEPARATE

FOPT

FOPR

FWPT

FWPR

FWCT

FRPV

FPR
/
WBHP
P
/
WOPR
P
/
BPR
25 25 5 /
25 24 5 /
/
WWCT
P
/
SCHEDULE
==========================================================================
```

```
RPTSCHED

 'RESTART=2'  /

WELSPECS
--'I'  'G'   1  1  4000  'WAT'  /
'P'   'G'   25 25 4000  'OIL'  /
/

COMPDAT
--'I      '  1   1   9  10 'OPEN'  0  .0   1.0 /
'P       '  25  25  5  6  'OPEN'  0  .0   1.0 /
/
WCONPROD
-- WELL OPEN/ CNTL  OIL WATER  GAS LIQU  RES  BHP
-- NAME SHUT  MODE RATE  RATE RATE RATE RATE RATE
'P' 'OPEN' 'BHP' 5* 3050 /
/
WCONINJ
--'I' 'WAT' 'OPEN' 'RATE' 190.0 /
/
--TSTEP
--15*120
DATES
1  'FEB' 1998  /
1  'MAR' 1998  /
1  'APR' 1998  /
1  'MAY' 1998  /
1  'JUN' 1998  /
1  'JLY' 1998  /
1  'AUG' 1998  /
1  'SEP' 1998  /
1  'OCT' 1998  /
1  'NOV' 1998  /
1  'DEC' 1998  /
1  'JAN' 1999  /
/

END
```

Simulation input file second part (with pressure maintenance)

```
-- THIS IS A SIMPLE STUDY OF PORE PRESSURE EFFECT ON
-- PERMEABILITY
-- ONE INJECTOR (WATER) AND ONE PRODUCER (OIL + WATER)
-- PREPARED BY SAID AL-HARTHY 1/2/99 - BASER.DATA
--
RUNSPEC
TITLE
 PORE PRESSURE STUDY ON PERMEABILITY

DIMENS
   50   50   10 /

OIL

WATER

FIELD

TABDIMS
   1   1  20   20   1  20 /

WELLDIMS
   2   5   1   2 /

START
   1 'JAN' 1998  /

NSTACK
   -1 /

FMTOUT

FMTIN

UNIFOUT

UNIFIN

GRID
==========================================================================

GRIDFILE
  2  /
INIT
--DEBUG
```

```
--38*0 1  /

--PSEUDO
EQUALS
'PERMX' 77.0   1  50   1  50  1  10/
'PERMX' 61.6   10 40   10 40  1  10/
'PERMX' 46.2   20 30   20 30  1  10/
'PERMY' 77.0   1  50   1  50  1  10/
'PERMY' 61.6   10 40   10 40  1  10/
'PERMY' 46.2   20 30   20 30  1  10/
/
PERMZ
25000*77.0  /

DXV
  50*50.0 /

DYV
  50*50.0 /

DZ
 25000*50.0 /

TOPS
 2500*4000.0 /


PORO
 25000*0.17 /

RPTGRID
1 1 1 1 1 0 0 0 /

--DEBUG
-- 0 0 1 0 1 0 1  /

PROPS
==================================================================

-- SWAT  KRW  PCOW
SWFN
  .25   .0   35.0
  .30   .02  30.0
  .40   .055 25.0
  .45   .075 20.0
  .50   .10  15.0
  .55   .13  10.0
  .60   .145  5.0
```

```
   .7     1.0   3.0
/

SOF2      1 TABLES   20 NODES IN EACH        FIELD   13:34  5 MAY 85
--  SOIL   KRO
   .30   .000
   .40   .004
   .48   .020
   .50   .036
   .58   .100
   .60   .146
   .68   .330
   .70   .420
   .75  1.000
/

PVTW
 4014.7  1.0  3.03E-06  .5  0.0 /

RSCONST
.8 /
/
PVDO
-- POIL    FVFO      VISCO
 400.0     1.0120     1.160
 1200.0    1.0040     1.164
 2000.0     .9960     1.167
 2800.0     .9880     1.172
 3600.0     .9802     1.177
 4400.0     .9724     1.181
 5200.0     .9646     1.185
 5600.0     .9607     1.190
 8000.0     .9200     2.000 /

ROCK
 4014.7        .30E-05 /

DENSITY
 45.0000  63.0200   .07020 /

RPTPROPS
   2*0 /

REGIONS
==================================================================

SATNUM
 25000*1 /
```

```
SOLUTION
==========================================================================

EQUIL
4250  4850  6000  0   0   0   0   0   0 /

--RPTSOL
--  'RESTART=2'  /

SUMMARY
==========================================================================
RUNSUM

SEPARATE

FOPT

FOPR

FWPT

FWPR

FWCT

FRPV

FPR
/
WBHP
P
/
WOPR
P
/
BPR
25 25 5 /
25 24 5 /
/
WWCT
P
/
SCHEDULE
==========================================================================

RPTSCHED
 'RESTART=2'   /
WELSPECS
```

```
--'I'  'G'   1  1  4000  'WAT'  /
'P'   'G'   25 25 4000  'OIL'  /
/

COMPDAT
--'I      '  1  1  9  10 'OPEN'  0  .0  1.0 /
'P       '  25  25  5  6  'OPEN'  0  .0  1.0 /
/
WCONPROD
-- WELL  OPEN/  CNTL   OIL  WATER  GAS  LIQU  RES  BHP
-- NAME  SHUT   MODE  RATE  RATE  RATE  RATE  RATE  RATE
'P' 'OPEN' 'BHP' 5* 3050 /
/
WCONINJ
--'I' 'WAT' 'OPEN' 'RATE' 190.0 /
/
--TSTEP
--15*120
DATES
1  'FEB' 1998  /
1  'MAR' 1998  /
1  'APR' 1998  /
1  'MAY' 1998  /
1  'JUN' 1998  /
1  'JLY' 1998  /
1  'AUG' 1998  /
1  'SEP' 1998  /
1  'OCT' 1998  /
1  'NOV' 1998  /
1  'DEC' 1998  /
1  'JAN' 1999  /
/

END
```